

INFORMATION TO USERS

This manuscript has been reproduced from the microfilm master. UMI films the text directly from the original or copy submitted. Thus, some thesis and dissertation copies are in typewriter face, while others may be from any type of computer printer.

The quality of this reproduction is dependent upon the quality of the copy submitted. Broken or indistinct print, colored or poor quality illustrations and photographs, print bleedthrough, substandard margins, and improper alignment can adversely affect reproduction.

In the unlikely event that the author did not send UMI a complete manuscript and there are missing pages, these will be noted. Also, if unauthorized copyright material had to be removed, a note will indicate the deletion.

Oversize materials (e.g., maps, drawings, charts) are reproduced by sectioning the original, beginning at the upper left-hand corner and continuing from left to right in equal sections with small overlaps.

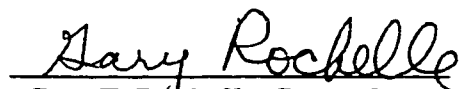
Photographs included in the original manuscript have been reproduced xerographically in this copy. Higher quality 6" x 9" black and white photographic prints are available for any photographs or illustrations appearing in this copy for an additional charge. Contact UMI directly to order.

Bell & Howell Information and Learning
300 North Zeeb Road, Ann Arbor, MI 48106-1346 USA
800-521-0600

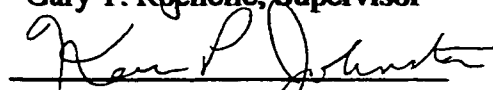
UMI[®]

**Carbon Dioxide Absorption and Solution Equilibrium in Piperazine
Activated Methyldiethanolamine**

**Approved by
Dissertation Committee:**



Gary T. Rochelle, Supervisor



Keith P. Johnston



Kamy Sepahmouri



R. Bruce Eldridge



James E. Critchfield

Carbon Dioxide Absorption and Solution Equilibrium in Piperazine

Activated Methyldiethanolamine

by

Sanjay Bishnoi, B.Sc.; M.S.

Dissertation

Presented to the Faculty of the Graduate School of

The University of Texas at Austin

in Partial Fulfillment

of the Requirements

for the Degree of

Doctor of Philosophy

The University of Texas at Austin

December, 2000

UMI Number: 3004215



UMI Microform 3004215

Copyright 2001 by Bell & Howell Information and Learning Company.

All rights reserved. This microform edition is protected against
unauthorized copying under Title 17, United States Code.

Bell & Howell Information and Learning Company
300 North Zeeb Road
P.O. Box 1346
Ann Arbor, MI 48106-1346

To My Family

Acknowledgements

I wish to express my gratitude to Professor Gary Rochelle for his guidance and support throughout this work. I am always amazed by his quick ability to digest new concepts. He has always fostered a positive research environment and allowed me to solve problems with my own approach and at my own time. I find the most educational part of a Ph.D. is not the numerical or experimental tools learned, but the ability to identify an open ended problem and to spend your time appropriately on the vital parts of the problem. Dr. Rochelle's attitudes towards advising have emphasized this part of my education and allowed me to make many of my own mistakes and have many of my own successes.

I have also had the pleasure of interacting with a great set of individuals in our research group. There have been 7 Ph.D. and 4 M.S. degrees awarded to members of Dr. Rochelle's group during my 4 years here. The exercise of totaling those numbers a few months ago not only reminded me of the help previous students have given me, it also suggested that, perhaps, I had better start writing my dissertation. Drs. Mark Posey, Lingbing Zhao, Chen Shen, Chris Nelli, Manuel Pacheco, Lia Brodnax and Paul Chisholm have been patient teachers and helpful colleagues. Shoichi Kaganoi, Joseph Devinentis, Nicole Pauly and Mike Dutchuk have been tremendously helpful, a pleasure to be around and people that I will always remember. It's been a joy to see students who have come in after me develop into good scientists. I thank Norman Yeh, Sharmi Roy, Eric Chen, Amy Nowlin, Susan Chi and Hongyi Dang for their camaraderie. I especially appreciate the help of Hongyi Dang with the equilibrium models used in Chapter 7 of this work and George Goff for his detailed edits and help. Along with group members, I thank all of the friends, roommates and colleagues who have made the last 4 years such a memorable time.

It's been great to have the expertise of the members of my committee readily available and I thank them for their efforts. Dr. Jim Critchfield of Huntsman Chemical has always provided valuable feedback on both technical and non-technical issues. As a former student at UT Austin and a former member of Professor Rochelle's group, he has an interesting perspective on the research being conducted here. Professor Kamy Sephernoori has been a tremendous help with the numerical aspects of my research. His class was one of the best I have attended and, although being exhausted after it was over, I have used much of it in my research. Within the department, Professor Keith Johnston has been a pleasure to interact with. Not only have I enjoyed discussing technical issues with him and attending his class on thermodynamics, It's been a pleasure to work on recruiting new graduate students with him. Professor Bruce Eldridge has also helped me during my 4 years here. His class set up a good basis for my research in separations. It has also been a pleasure to interact with him as Director of the SRP program. Together we initiated a student lecture series that remains well attended for the last 2 years and is also the only student organized, student presented and student attended seminar series in our department.

Financial support from the Separations Research Program at the University of Texas at Austin and other industrial sponsors is greatly appreciated. There are very few programs like SRP that give chemical engineering graduate students the opportunity to interact closely with Industry. Through SRP, I was given the chance to work with the Specialty Alkanolamines and GAS/SPEC Technology group at The Dow Chemical Company in Freeport, Texas during the summer of 1999. The experience and people at Dow were a big part of my education during graduate school. It has been a pleasure to continue interacting with Dr. Steve Bedell, Jenny Seagraves and Karen Kenny. Their opinions about my research and my career have been very valuable to me.

Finally, I would like to thank my family. They have been a tremendous source of encouragement and joy to me. Their accomplishments have not only made me proud, but as the youngest family member, they have served as role models for me. I have had the pleasure of pursuing my Ph.D. in the same branch of engineering that my father teaches in. I have come to appreciate his academic contributions to chemical engineering, his business contributions in starting up Hyprotech Ltd., one of the world's dominant process simulation companies and his ability to balance his professional career and his family. My mother recently retired after a career in health care and academia. I admire her ability to become an associate clinical professor in rehab medicine without missing a beat with her family's upbringing, raising two children who at least give the appearance of being normal. My sister Meena has pursued a career in hospital pharmacy while her husband Bimal has demonstrated exceptional capabilities first as a chemical engineer and now as a strategy consultant, finishing first in the top ranked Canadian M.BA program. All tremendous people who have always asked me to give my best effort to whatever I do and I thank them all for the values they have passed on to me.

December 2000

Austin, Texas

**Carbon Dioxide Absorption and Solution Equilibrium in Piperazine
Activated Methyldiethanolamine**

Publication No. _____

Sanjay Bishnoi, Ph.D.

The University of Texas at Austin, 2000

Supervisor: Gary T. Rochelle

Solubility, rate of absorption and NMR data were taken for carbon dioxide in aqueous piperazine (PZ) and aqueous mixtures of PZ and methyldiethanolamine (MDEA). Solubility and rate data were acquired in a wetted wall contactor. 0.2 to 0.6 M PZ and 4 M MDEA concentrations were studied. The temperature range studied was 298K to 343K. Both nitrogen groups on PZ were found to be reactive. Important PZ reaction products are protonated PZ, PZ carbamate, protonated PZ carbamate and PZ di-carbamate. The di-protonated PZ species was never found since the pH of CO₂ loaded solutions is never low enough for its concentration to be important. The thermodynamic capacity of PZ was found to be very comparable to other amines such as monoethanolamine (MEA) and diethanolamine (DEA). The second order rate constant for PZ ($k^{25C}_2=53000$ L/mol s), however is an order of magnitude greater than MEA ($k^{25C}_2=5000$ L/mol s). Predictions made using a rigorous mass transfer theory that uses eddy diffusivity theory suggests that PZ/MDEA enhancement factors outperform MEA/MDEA and DEA/MDEA blends of the same concentration by a factor of 10. Model prediction at industrially significant conditions suggests that the top of the absorber in ammonia plants or hydrogen plants will be 50% gas film controlled. The success of PZ based solvents for carbon dioxide removal from flue gas was demonstrated. Two systems (PZ/MEA and PZ/K₂CO₃) show potential to reduce the total amount of packing in the absorber by up to a factor of 2.

Table of Contents

List of Tables.....	xii
List of Figures.....	xv
Chapter 1: Introduction to gas treating and scope of work.....	1
1.1 Effect of the chemical solvent.....	3
1.2 Blended Amine Solvents – Piperazine Activated MDEA.....	7
1.3 Scope of Work.....	8
Chapter 2: Mass Transfer with chemical reaction and amine/CO ₂ kinetics.....	13
2.1 Physical mass transfer and comparison of theories on mass transfer.....	13
2.1.1 Film theory.....	14
2.1.2 Higbie penetration theory.....	16
2.1.3 Surface renewal theory.....	17
2.1.4 Eddy diffusivity theory.....	18
2.2 Approximate solutions for mass transfer with chemical reaction.....	20
2.2.1 Pseudo first order.....	21
2.2.1.1 Irreversible reactions.....	21
2.2.1.2 Reversible reactions.....	23
2.2.2 Deviations from pseudo first order.....	24
2.2.3 Modification of pseudo first order for depletion at the interface.....	26
2.2.4 Mass Transfer with equilibrium reactions.....	27
2.3 Rate data and mechanisms for CO ₂ reaction with amines and bases.....	29
2.3.1 Reaction with hydroxide.....	29
2.3.2 Reaction with tertiary amines.....	29
2.3.2.1 Mechanisms.....	29
2.3.2.2 CO ₂ rate data for methyldiethanolamine...	31
2.3.3 Reaction with primary and secondary amines.....	35
2.3.3.1 Rate data for monoethanolamine.....	36
2.3.3.2 Rate data for diethanolamine.....	38
2.3.3.3 Rate data for amines realated to PZ.....	41
2.3.4 Reaction of CO ₂ with hindered amines.....	43
2.3.4.1 2-Amino-2-methylpropanol.....	45
2.4 Blended Amines.....	47

Chapter 3: Background thermodynamics, conditions for equilibrium and system non-idealities.....	53
3.1 The acid gas thermodynamics problem.....	53
3.2 The condition for phase equilibrium.....	55
3.3 The condition for chemical equilibrium.....	56
3.4 Reference states used in this work.....	57
3.5 System non-idealities.....	58
3.5.1 Gas phase non-idealities.....	58
3.5.2 Liquid side non-idealities.....	59
3.5.3 The electrolyte NRTL model.....	60
3.5.3.1 Long range ionic forces.....	60
3.5.3.2 Short range molecular forces.....	61
3.5.3.3 Combination of long range and short Range forces.....	62
3.6 Solution techniques for chemical equilibrium problems.....	65
3.6.1 Stoichiometric method.....	65
3.6.2 Non-stoichiometric method.....	66
Chapter 4: Absorption of carbon dioxide into aqueous piperazine: Kinetics, mass transfer and solubility.....	68
4.1 Experimental apparatus and methods.....	69
4.2 Data analysis.....	78
4.3 Solubility and speciation of carbon dioxide in aqueous piperazine.....	79
4.4 Solubility measurement and modeling.....	80
4.5 Supporting data.....	85
4.6 Rate of reaction measurement and interpretation of data.....	95
4.7 Conclusions.....	102
Chapter 5: Thermodynamics of piperazine/methyldiethanolamine/ Water/carbon dioxide.....	103
5.1 Experimental methods.....	104
5.2 Activity of piperazine in aqueous solutions.....	105
5.3 Solubility of piperazine in water.....	108
5.4 Model description.....	109
5.5 Parameter regression results.....	112
5.6 Solubility of carbon dioxide in aqueous solutions of PZ/MDEA.....	116
5.7 NMR data.....	118
5.8 Model predictions.....	122
5.9 Conclusions.....	130
Chapter 6: Absorption of CO ₂ in aqueous PZ/MDEA blends.....	132

6.1 Model description.....	134
6.2 Physical properties.....	141
6.3 Experimental data.....	143
6.3.1 Interpretation of data at low loading.....	144
6.3.2 Data and interpretation in loaded solutions.....	146
6.3.2.1 Data taken in this work.....	146
6.3.2.2 Data of Kaganoi (1997).....	148
6.3.2.3 Data of Xu et al. (1992).....	151
6.3.3 Model predictions for the single amine systems...	153
6.4 Model predictions.....	154
6.4.1 Comparison with other promoters.	155
6.4.2 Sensitivity to model parameters.....	157
6.4.3 Reaction zones and deviations From approximate solutions.....	158
6.5 Ammonia plants/Hydrogen plants.....	164
6.6 Removal of CO ₂ from coal fired flue gas.....	168
6.7 Removal of CO ₂ from natural gas.....	172
6.8 Conclusions and recommendations.....	173
Chapter 7: Alternative solvents for CO ₂ removal from coal fired flue gas	175
7.2 Model description.....	176
7.3 Evaluation procedure.....	177
7.4 Model inputs.....	179
7.5 Results.....	183
7.6 Conclusions and recommendations.....	187
Chapter 8: Conclusions and recommendations.....	189
8.1 Summary.....	189
8.2 Conclusions.....	189
8.2.1 Thermodynamic interactions of PZ/CO ₂	190
8.2.2 Kinetics of CO ₂ /PZ.....	190
8.2.3 New solvents for flue gas treating.....	191
8.3 Recommendations.....	191
8.3.1 Data acquisition.....	191
8.3.2 Model performance.....	193
8.3.3 Overall Absorber modeling.....	193
Appendix A.....	195
Appendix B.....	202
Appendix C.....	204

Appendix D.....	217
Appendix E.....	221
Appendix F.....	224
Appendix G.....	242
Glossary.....	254
Bibliography.....	258
Vita.....	271

List of Tables

Table 1.1	Acid gas removal using absorber / stripper technology.....	1
Table 1.2	Previous data on PZ/MDEA blends.....	9
Table 2.1	Summary of Methyldiethanolamine (MDEA) Kinetic Data.....	34
Table 2.2	Literature data on the reaction between CO ₂ and aqueous MEA (mostly from Blauwhoff et al., 1984).....	36
Table 2.3.	Literature data on the reaction between CO ₂ and aqueous DEA (mostly from Blauwhoff et al., 1984).....	39
Table 2.4	Rate Data for the Piperazine Family of Amines.....	42
Table 2.5	Literature data on the reaction between CO ₂ and aqueous AMP	47
Table 2.6	Summary of data acquired in blended amine systems.....	51
Table 3.1	Example problem unknowns and equations.....	54
Table 4.1	Absorption of SO ₂ into 0.1M NaOH at Ambient Temperature...	76
Table 4.2	Solubility of Carbon Dioxide in 0.6M Piperazine Solutions.....	83
Table 4.3	Equilibrium Constants for the Solubility Model, mole fraction based.....	84
Table 4.4	Proton and ¹³ C NMR summary for 0.6M PZ solutions in D ₂ O..	91
Table 4.5	Rate of Absorption Data into Aqueous Piperazine. Overall gas flowrates from 5.2 to 5.5 SLPM. Total pressures from 45-60 psig.....	97
Table 4.6	Rate constant values calculated from pseudo first order treatment of low loading data.....	98
Table 4.7	Bronsted Correlation of Piperazine Kinetics at 25°C.....	100

Table 4.8 High loading flux measurements and predictions.....	101
Table 5.1 Activity Coefficients at Infinite Dilution in water at 25°C.....	106
Table 5.2 Excess heat of mixing at infinite dilution and 25°C.....	108
Table 5.3 Solubility limit of piperazine in H ₂ O.....	108
Table 5.4 Miscellaneous Constants for VLE program.....	112
Table 5.5 Temperature dependence of equilibrium constants, mole fraction based.....	113
Table 5.6 Non-Default parameters for the NRTL model.....	114
Table 5.7 CO ₂ Solubility in Piperazine Activated MDEA.....	116
Table 5.8 NMR data for 0.6M PZ/4M MDEA, 298K and CO ₂ loading of 0.52.....	120
Table 5.9 Ratio of species using NMR data at 298K, 1M PZ, 4 M MDEA, loading=0.52.....	122
Table 5.10 Comparison of carbamate stability constants (313K, Mole Fraction).....	125
Table 6.1 Model Equations and Boundary Conditions.....	140
Table 6.2 Absorption of CO ₂ into 0.6M PZ, 4M MDEA at low loading...	144
Table 6.3 Absorption of CO ₂ into partially loaded 0.6M PZ, 4M MDEA solutions at low driving force.....	147
Table 6.4 Absorption of CO ₂ into partially loaded 0.6M PZ, 4M MDEA solutions at high driving force and 313K. Data of Kaganoi (1997).....	149
Table 6.5 Model predictions of CO ₂ into 0.6 M aqueous PZ solutions at 313 K (Data of Bishnoi and Rochelle, 2000)...	154

Table 6.6 Model predictions of CO ₂ absorption into aqueous MDEA solutions.....	155
Table 6.7 Enhancement factors for 0.6M PZ, 4M MDEA at 313K and various driving force.....	159
Table 6.8 Conditions for Ammonia Plant Example.....	165
Table 6.9 Conditions for Coal Fired Flue Gas Example.....	169
Table 7.1 Physical properties for MEA based solvents at 60°C.....	179
Table 7.2 Physical properties for other solvents at 60°C.....	179
Table 7.3 Diffusion coefficients (m/s) of reactants and products in solvents at 60°C	180
Table 7.4 Rate constants at 60°C used in this work along with their sources.....	182
Table 7.5 Summary of equilibrium constants used in this work. Values are mole fraction based at 60°C.....	183

List of Figures

Figure 1.1	Process Flow Diagram of a Typical Absorber / Stripper.....	2
Figure 1.2	Mass transfer accompanied by simultaneous chemical reaction in the liquid phase boundary layer.....	6
Figure 2.1	Physical Absorption using film theory.....	15
Figure 2.2	Description of unsteady state mass transfer theories.....	17
Figure 2.3	Eddy Diffusivity Theory.....	19
Figure 2.4	Glasscock's Comparison of enhancement factors for different mass transfer theories. Figure reproduced from Glasscock (1990). Second order reversible reaction ($A+B=C+D$). $K_{eq}=350$, $D_B=D_C=D_D=0.5D_A$, $C_{B,bulk} / C_{A,int} = 200$, $C_{A,bulk}=C_{B,bulk}=C_{C,bulk}=0$	20
Figure 2.5	Deviations from Pseudo First Order Behavior. $k_l^0 = 1.0e-5$ m/s, $D_{CO_2} = 1.0e-9$ m ² /s, $D_l = 0.5 D_{CO_2}$ for all other species i. $k_2 = 5000$, $K_{eq} = 350$, $[CO_2]_l = 0.01$ mol/l, $[Am]_B=1.0$, $[i]_B \sim 0$ for all species i other than Am...	26
Figure 4.1	Detailed column diagram.....	71
Figure 4.2	Overall flowsheet of equipment.....	72
Figure 4.3	Gas film mass transfer coefficients at ambient temperature and high Reynolds number. SO_2 absorption into NaOH, $P=3.8E5$ to $4.5E5$ Pa.....	76
Figure 4.4	Flux interpolation to determine equilibrium solubility. Data points for absorption into 0.6 M piperazine at CO_2 loading of 0.32 kmol/kmol piperazine and 40°C.....	80
Figure 4.5	Molecular structures of piperazine species.....	82
Figure 4.6	Partial pressure predictions compared to experimental results in 0.6 M PZ.....	86

Figure 4.7	Predicted speciation of 0.6 M piperazine at 25°C.....	87
Figure 4.8	pH of 0.6 M piperazine loaded with carbon dioxide at 25°C.....	88
Figure 4.9	Ionic conductivity of 0.6 M piperazine at ambient conditions (approx. 25°C).....	89
Figure 4.10	¹³ C and proton NMR spectra for 0.6 M piperazine at CO ₂ loading of 0.57 and 25°C	93
Figure 4.11	Functional groups found in NMR spectra of 0.6 M piperazine loaded with carbon dioxide.....	94
Figure 4.12	Straight line fit for rate of CO ₂ absorption into aqueous piperazine solutions at low solution loading.....	98
Figure 4.13	Second order rate constant of piperazine and carbon dioxide.....	99
Figure 4.14	Comparison of predicted and experimental fluxes for absorption of carbon dioxide into partially loaded 0.6 M PZ.....	101
Figure 5.1	Data of Wilson and Wilding (1994) reinterpreted as activity coefficients for the water / PZ system at elevated temperature.....	107
Figure 5.2	Solubility of anhydrous PZ solid in H ₂ O	109
Figure 5.3	Measured and predicted solubility of CO ₂ in 0.6M PZ / 4M MDEA solutions.....	117
Figure 5.4	Model predictions for all CO ₂ solubility data	119
Figure 5.5	Proton, ¹³ C and short range C-H correlation NMR spectra for 1M PZ, 3M MDEA solution at 298K and a CO ₂ loading of 0.52 moles/mol amine.	121
Figure 5.6	Equilibrium partial pressure prediction for CO ₂ in 4M MDEA and various PZ concentrations.....	123

Figure 5.7	Comparison of PZ to other promoters in 0.5M Promoter, 4M MDEA solutions at 313K.....	124
Figure 5.8	Speciation of 0.5M PZ, 4M MDEA solution at 313K. Results are shown as a fraction of total piperazine.....	126
Figure 5.9	Speciation of 0.5M PZ, 4M MDEA solution at 343K. Results are shown as a fraction of total piperazine.....	127
Figure 5.10	Speciation of 0.5M DEA, 4M MDEA solution at 313K. Results are shown as a fraction of total Amine. Predictions made by Chakravorty (1992) using the model of Austgen (1989).....	128
Figure 5.11	Activity coefficients for 0.6M PZ, 4M MDEA blend at 313K.....	129
Figure 5.12	Prediction of PZ volatility in 4M MDEA solution and various PZ concentrations. All calculations are performed at a lean loading of 0.01 mols CO ₂ / mol amine.....	130
Figure 6.1	Parity plot. Rigorous model fit of all PZ/MDEA absorption data.....	143
Figure 6.2	Comparison of absorption into aqueous PZ and PZ/MDEA blends with MEA.....	145
Figure 6.3	Enhancement factors for 0.6 M PZ/4 M MDEA at 313K and $k_1^0=3.3E-5$ m/s.....	151
Figure 6.4	Enhancement factors for 0.1 M PZ/4.21 M MDEA at 313K and $k_1^0=2E-5$ m/s.....	152
Figure 6.5	Comparison of PZ/MDEA blends to conventional blends. Predictions at 313K, $k_1^0=1.0E-4$ m/s. $P^i/P^* = 1.05$ unless specified.....	156
Figure 6.6	Model sensitivity to rate and mass transfer parameters. Predictions in 5/45 wt % PZ/MDEA at 313K and $k_1^0=1.0E-4$	157

Figure 6.7	Concentration gradients for absorption of carbon dioxide into 5/45 wt % PZ/MDEA blend. Loading=0.07, $k_1^0=1.0\text{E-}4$ m/s, $P^i/P^*=10$, $T=313\text{K}$	161
Figure 6.8	Absorption of carbon dioxide into 5/45 wt % PZ/MDEA blend. Loading=0.20, $k_1^0=1.0\text{E-}4$ m/s, $P^i/P^*=10$, $T=313\text{K}$	162
Figure 6.9	Absorption of CO_2 into 5/45 wt % PZ/MDEA blend. Loading = 0.6, $k_1^0=1.0\text{E-}4$ m/s, $P^i/P^*=10$, $T=313\text{K}$	163
Figure 6.10	McCabe Thiele diagram and enhancement factor prediction for ammonia plant case using rigorous model. 313K, $P=300$ psig, $k_1^0=3.0\text{E-}3$ cm/s.....	166
Figure 6.11	Change in liquid and gas phase compositions along column length for ammonia plant example using the rigorous model. 313K, $P=300$ psig, $k_1^0=3.0\text{E-}3$ cm/s.....	167
Figure 6.12	Mass transfer performance parameters for ammonia plant example using rigorous model. 313K, $P=300$ psig, $k_1^0=3.0\text{E-}3$ cm/s.....	168
Figure 6.13	McCabe Thiele diagram and enhancement factor prediction for ammonia plant case using rigorous model. 333K, $P=0$ psig, $k_1^0=6.1\text{E-}3$ cm/s.....	170
Figure 6.14	Change in liquid and gas phase compositions along column length for coal fired flue gas example using the rigorous model. 333K, $P=0$ psig, $k_1^0=6.1\text{E-}3$ cm/s.....	171
Figure 6.15	Mass transfer performance parameters for ammonia plant example using rigorous model. 313K, $P=300$ psig, $k_1^0=3.0\text{E-}3$ cm/s. 333K, $P=0$ psig, $k_1^0=6.1\text{E-}3$ cm/s....	172
Figure 7.1	Effect of gas phase resistance for case studies examined in this work. All calculations at 60°C , $P^{\text{TOT}} = 1$ atm, 10% CO_2 in, 1% CO_2 out, 33% approach to equilibrium in both rich and lean solvent.....	185

Figure 7.2	Volume of packing per transfer unit for case studies examined in this work. All calculations at 60°C, $P^{\text{TOT}} = 1$ atm, 10% CO ₂ in, 1% CO ₂ out, 33% approach to equilibrium in both rich and lean solvent.....	186
------------	--	-----

Chapter 1

Introduction to Gas Treating and Scope of Work

Chemical absorption of acid gases by alkanolamines has found application in a wide variety of industries including the processing of natural gas and the removal of CO₂ from synthesis gas in the production of hydrogen or ammonia. With the recognition of CO₂ as a greenhouse gas, another important application of this technology is CO₂ removal from combustion gases at power plants or manufacturing facilities. The technology of treating process gas with alkanolamines in absorption/stripping systems became popular in the 1930's and has been used successfully since then.

Current research focuses on the use of new solvents and also on increasing our ability to model the complex processes involved in the absorption of a solute which reacts with the solvent. These complexities can be appreciated by considering a typical process flow diagram of an absorption/stripping system shown in figure 1.1.

Sour gas may contain CO₂, H₂S, COS, and other acid gases. The composition of the inlet gas varies widely and depends on the application. Table 1.1 gives typical uses of absorber/stripper systems and the conditions under which they operate.

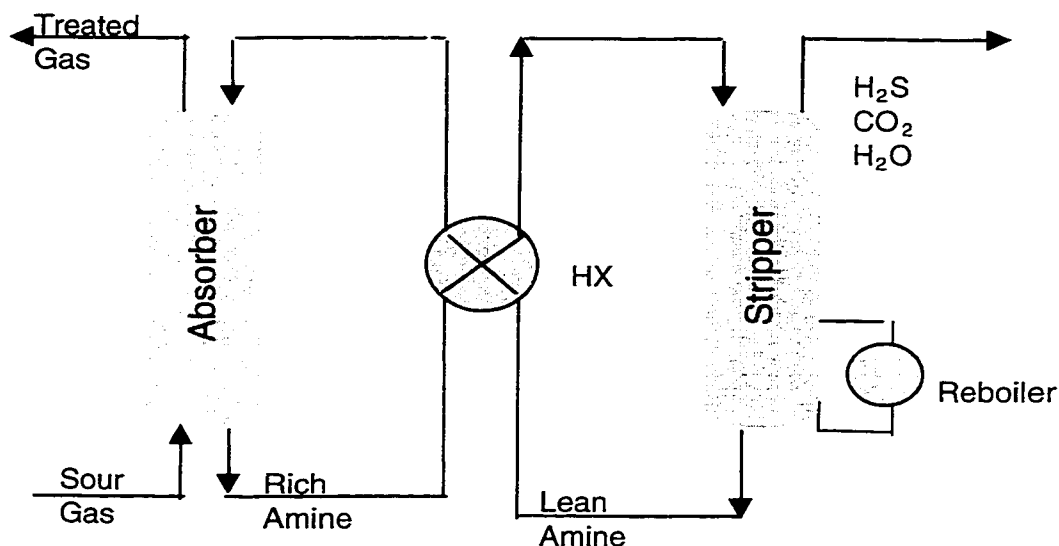


Figure 1.1 Process Flow Diagram of a Typical Absorber / Stripper

Table 1.1 Acid gas removal using absorber / stripper technology

Application	Total Press. (psig)	Inlet Molefrac CO ₂	Outlet Molefrac CO ₂	Inlet Total Sulfur	Outlet Total Sulfur
Ammonia / H ₂ /CO	350	0.18	<2000 ppm	N/A	N/A
Natural Gas	100-1000	0 - 0.50	0.02	0-0.50 vol frac	< 4 ppm
Flue Gas	Coal	0	0.10	2000 ppm	200 ppm
	Nat Gas.	0	0.03	0	0

The sour gas enters the bottom of the absorber column where it is counter currently contacted with lean amine solution that enters the column at the top. The absorber may be a trayed column or a packed column. As the amine solution travels down the column, it becomes loaded with acid gases and leaves the bottom of the absorber as rich amine. The sweetened gas leaves the top of the column where it is further processed. The rich amine is heated by use of a heat exchanger and is then fed to a stripper where the absorbed acid gases are driven out of

solution and the amine is regenerated. The energy required to strip acid gases from solution is provided by a reboiler at the bottom of the stripper. The stripped acid gases are sent for further processing such as a Claus sulfur plant for applications with significant H_2S content.

For ammonia and flue gas applications, the concentration of CO_2 is fairly consistent between different plants. Ammonia plants require a much more stringent removal of CO_2 since it acts as a catalyst poison during the reaction of H_2 and N_2 to form NH_3 . The removal of CO_2 from flue gas is much more lenient since the goal is to minimize the amount of greenhouse gas emitted to the atmosphere.

For natural gas, typical inlet concentrations of CO_2 and / or H_2S can vary over a wide range between 0 and 50% (molar basis) because of naturally occurring variations in the gas found in the reservoir. Usually, CO_2 must be removed down to about 2% while H_2S has more stringent guidelines and must be removed down to about 4 ppm.

The ability to cool the lean amine stream using cooling water usually sets the absorber temperature. Typical operation is at 40°C for all applications except for flue gas which operates at $55\text{--}60^\circ\text{C}$ which is set by the adiabatic saturation temperature of the inlet gas. The absorber operates at a wide range of pressures depending on the process being studied. For flue gas, the absorber could be near atmospheric pressure while at some high pressure natural gas fields or ammonia applications, the absorber could operate at pressures of 1000 psi or higher.

The stripper removes acid gases by increasing the temperature of the amine. Typical operating temperatures of the stripper are around 120°C . The stripper pressure is usually determined by the back pressure required for the acid gas stream to be further processed.

1.1 Effects of the Chemical Solvent

The process flow diagram serves to show us the physical and chemical phenomena involved in acid gas treating. Low stage efficiencies are characteristic of industrial absorption of CO₂ into alkanolamines (Pacheco, 1998). These low efficiencies are due to finite chemical kinetics that occur in the liquid phase during absorption and therefore an understanding of mass transfer with chemical reaction is implicit in the understanding of CO₂ removal by amines.

The approach in quantifying the effect of the solvent is to study enhancement factors. Consider the physical absorption of CO₂ at a finite slice of the absorber into a non-reactive solvent. Across this slice, we can consider the gas and liquid phase concentrations of CO₂ to be relatively unchanged. Therefore, the rate of removal of CO₂ from the gas phase may be expressed as:

$$R_{CO_2}(\text{moles} / s) = k_l^o a ([CO_2]_i - [CO_2]_B) \quad (1.1)$$

Where a is the contact area between the gas and liquid phases, k_l^o is the physical mass transfer coefficient and the driving force is the difference between the CO₂ concentration at the interface and the bulk solution. The subscripts i and B refer to the interface and bulk respectively.

We lump all performance parameters of the solvent into the enhancement factor, E , which we will define as:

$$E = \frac{\text{Flux with reaction}}{\text{Flux without reaction}} \quad (1.2)$$

The rate of removal into a reactive solvent then becomes:

$$R_{CO_2}(\text{moles} / s) = k_l^o a E ([CO_2]_i - [CO_2]_B) \quad (1.3)$$

In order to understand the removal of carbon dioxide we need to understand each of the terms in equation 1.3, which we can categorize as hydraulic parameters, equilibrium conditions and rate considerations.

Hydraulic parameters such as the interfacial area and the mass transfer coefficient are a function of the column internals as well as gas and liquid flowrates. Physical properties such as solvent density, viscosity and surface tension will affect these parameters, but the variations between one solvent and the next should not be severe.

Thermodynamic considerations enter the analysis in two different locations. The first involves the driving force for mass transfer and the bulk phase concentration of CO_2 . At a given partial pressure of CO_2 the solvent will dissolve a certain amount of CO_2 until it reaches saturation. This saturated equilibrium value is the bulk phase equilibrium concentration of CO_2 used in equation 1.3. The more capacity a solvent has to absorb CO_2 , the lower its equilibrium CO_2 concentration and the higher its predicted rate of CO_2 removal by equation 1.3. The second effect of thermodynamics is in calculating the free amine concentration. Chemical equilibrium relationships for all species in the liquid phase will define the amount of free amine for a given overall CO_2 concentration. The more free amine that is present, the faster the rate of reaction of CO_2 . This problem of thermodynamic speciation will be discussed further in Chapter 3.

Most of the effect of a chemical solvent for CO_2 removal is in its rate behavior as described by the enhancement factor. To appreciate the phenomena involved in quantifying the enhancement factor, consider the absorption of CO_2 into a reactive liquid as shown in figure 1.2. The process may be described as convective mass transfer of CO_2 from the bulk gas phase to the vapor liquid interface. Physical absorption at the interface and phase equilibrium exists for all molecular species between the gas and liquid. The chemical reactions that define the interaction of the amine with CO_2 , however, are not necessarily at equilibrium.

Convective mass transfer accompanied with simultaneous chemical reaction occurs from the interface into the bulk liquid.

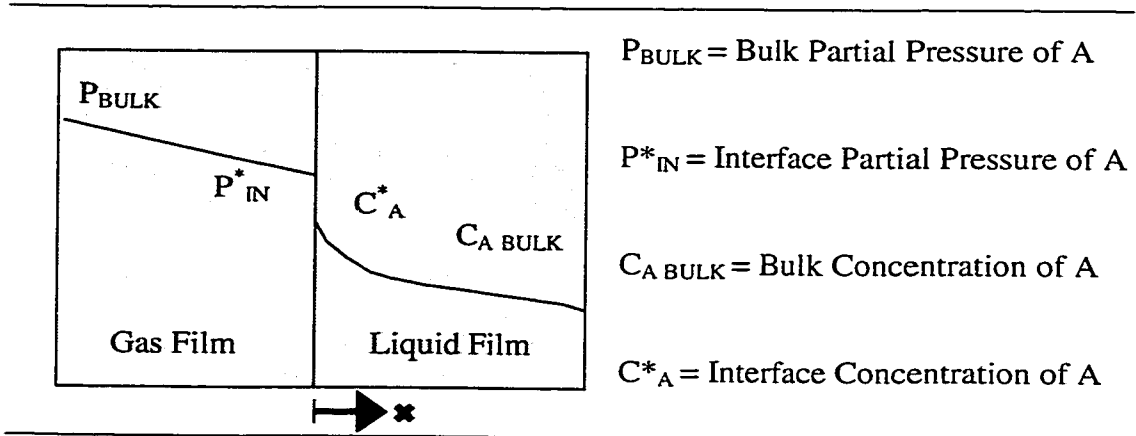


Figure 1.2 Mass transfer accompanied by simultaneous chemical reaction in the liquid phase boundary layer.

The concentration of CO_2 in the liquid film is represented as a function of time (t) and position (x) by:

$$D_{CO_2} \frac{\partial^2 [CO_2]}{\partial X^2} - \frac{\partial [CO_2]}{\partial t} + R_{CO_2} = 0 \quad (1.4)$$

where R_{CO_2} is the rate of reaction. The two boundary conditions and an initial condition for the concentration of CO_2 are:

$$\begin{aligned} [CO_2] &= [CO_2]_i @ X = 0 \\ [CO_2] &= [CO_2]_0 @ X = \infty \\ [CO_2] &= [CO_2]_0 @ t = 0 \end{aligned} \quad (1.5)$$

Given an expression for the reaction of CO₂ with the liquid, this partial differential equation can be solved to give a concentration gradient for CO₂ in the liquid film. Using Fick's law we can now evaluate the enhancement factor as a function of the concentration gradient and equation 1.3.

$$E = -D_{CO_2} \frac{\frac{\partial [CO_2]}{\partial x}}{k_1^o ([CO_2]_i - [CO_2]_B)} \quad (1.6)$$

The determination of the enhancement factor, therefore, shows what phenomena need to be quantified for each solvent studied. The concentration gradient will be a strong function of the reactive expression described in equation 1.4. It is not only necessary to understand by what mechanism CO₂ will react with the amine solvent, but also to quantify how fast this reaction will occur and at what ultimate value it will reach equilibrium. The reaction of CO₂ with most amines will be second order overall.

$$R_{CO_2} = k_2 [CO_2] [Amine] \quad (1.7)$$

1.2 Blended Amine Solvents – Piperazine Activated MDEA

The addition of a primary or secondary amine to a tertiary amine has found widespread application in the absorption and removal of carbon dioxide from process gases. The success of these solvents is due to the high rate of reaction of the primary or secondary amine with carbon dioxide combined with the low heat of reaction and higher capacity of the tertiary amine. By adding small amounts of the primary or secondary amine, a high rate of absorption is seen in the absorber while a low energy of regeneration is required in the stripper.

One such blend of amines is piperazine (PZ) activated methyldiethanolamine (MDEA). These solvents have been used successfully for high capacity carbon dioxide removal in ammonia plants and are patented by BASF (Appl et al., 1982). They have been effective at much lower activator

concentration than conventional blends [Diglycolamine (DGA[®])/MDEA, Diethanolamine (DEA)/MDEA]. The structures of the PZ, DEA, and MDEA are shown in figure 1.3. PZ is seen to differ from other promoters in several ways. Firstly, it is a diamine which raises questions about what the important reactions are with carbon dioxide and what ionic products will be present. It is also a cyclic amine, which will be seen to react differently than other amines in Chapter 4. Lastly, the lack of an alcohol group will make PZ less soluble in water than members of the alkanolamine family that will have implications on its thermodynamic behavior in amine treating applications (Chapter 5).

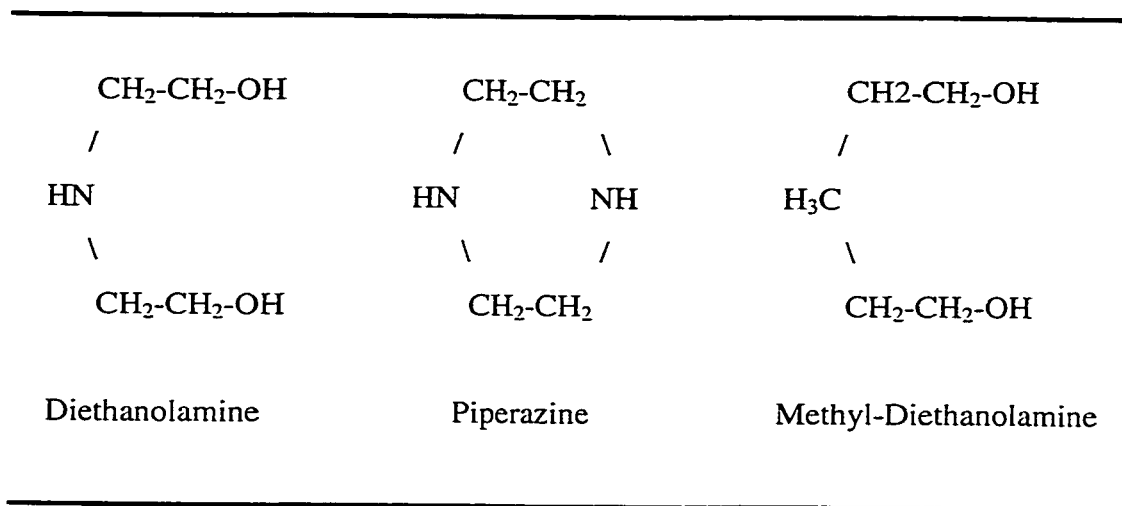


Figure 1-3 Structures of common amines used in gas treating.

1.3 Scope and Outline of Work

To summarize section 1.2, the ability to differentiate one solvent from another comes down to understanding their different kinetic and thermodynamic phenomena. Despite the use of PZ/MDEA solvents, there is not a fundamental

understanding of how they work previous to this study. Table 1.2 shows the data on PZ/MDEA previous to this work.

Table 1.2 Previous data on PZ/MDEA blends

	Investigator	Conditions		Notes
		T (°C)	[CO ₂]/[PZ]	
PZ / MDEA VLE	Xu et al. (1998)	70	>>1	No significant effect of PZ since it is depleted
	Liu et al. (1999)	30-90	>>1	
PZ / MDEA RATES	Xu et al. (1992)	30-60	>>1	
	Kaganoi (1997)	40	>1	Moderate effect of PZ

The success of PZ activated MDEA blends and the lack of data and understanding available in open literature has initiated this project. The primary goal of this work is to quantify the thermodynamics and kinetics of PZ and to quantify the performance of PZ/MDEA blends relative to other solvents used in gas treating. New data presented in this work is as follows:

1. Proton, ¹³C and C-H correlation NMR is run in D₂O at 25°C in the presence and absence of MDEA. Important reaction products are identified.
2. CO₂ solubility data is acquired in 0.6 M PZ and 0.6 M PZ / 4 M MDEA at temperatures of 40 and 70°C. Special attention is paid to loadings where the CO₂ concentration is much less than the PZ concentration.
3. CO₂ absorption is studied at the same temperature and concentration as solubility data. Partial pressures studied are also much lower than previous investigators.

An understanding of the success of PZ activated MDEA solvents will allow us to choose the successful attributes, improve on the less desirable ones and

design more effective solvents for gas treating. We rigorously modeled the absorption phenomenon with the following goals:

1. Determine important phenomenon occurring during absorption
2. Evaluation of analytical solutions in order to understand where they break down.
3. Develop a useful design tool for design engineers using PZ/MDEA solvents
4. Evaluate new solvents for CO₂ removal from flue gas.

A particular example of importance is CO₂ removal from flue gas streams. Although CO₂ removal has been achieved for many years using amine technology, applying this technology to flue gas applications yields many process differences. The overall pressure of the absorber is much lower than in natural gas or ammonia plant applications while the mole fraction of CO₂ in the gas stream can be significantly higher. The level of treating is much less stringent, allowing us think differently about how to design the solvent. Temperatures are much higher than typical gas treating applications since the temperature of the flue gas exiting the boiler is very high. Finally, the amount of gas to be treated is significantly more, placing more importance on conducting the separation with as little energy and contact area as possible.

This work begins by outlining the background needed in electrolyte thermodynamics and mass transfer with chemical reaction. These chapters are written with the intent of supplying a new graduate student with the necessary background in mass transfer with chemical reaction. Chapter 2 discusses the evaluation of the enhancement factor for simple conditions and discusses when these simplifications may be useful. A comprehensive review of amine kinetics that looks at how different amine solvents react with CO₂ as well as summarizing

the previous work in this area is presented as well. It is impossible to understand the mass transfer with chemical reaction without understanding thermodynamics. Chapter 3 provides background in chemical aqueous phase thermodynamics as well as providing information in electrolyte thermodynamics used to interpret the thermodynamic results of this work.

In Chapter 4, the aqueous PZ system is studied. The kinetics of PZ are studied in a wetted wall column and found to be significantly faster than other primary and secondary amines. The difference is attributed to PZ's cyclic nature. PZ also exhibits many mechanisms that are not seen in other amines and these have been studied by measuring CO₂ solubility and NMR spectra for partially loaded PZ solutions. Supporting data, such as pH and ionic conductivity are also presented in this chapter.

Chapter 5 addresses the issues of PZ activated MDEA blend thermodynamics. Solubility data from the wetted wall column are combined with NMR data and the electrolyte NRTL model to predict the speciation of these solutions. Predictions are also made for the CO₂ partial pressure above these solutions at different loadings. An important operating issue with PZ activated MDEA solvents is the loss of PZ. As mentioned in section 1.2, PZ is less soluble in water leading to higher volatility. The solubility limits of PZ are measured in Chapter 5, which leads to the conclusion that several hydrate phases are formed by PZ. Volatility measurements using an FT/IR analyzer are also presented. Although these measurements were not shown to be successful, recommendations are made on how to pursue this project further. The Dortmund modified UNIFAC model is used to predict the activity coefficient of PZ in water and to demonstrate that PZ losses can be as high as MDEA losses in PZ activated MDEA blends.

Chapter 6 shows the behavior of enhancement factors for PZ activated MDEA blends. A rigorous mass transfer model based on the eddy diffusivity theory for mass transfer and a finite difference numerical approach is shown to

match absorption data from the wetted wall column. The rigorous model is used to predict mass transfer rates at industrially relevant conditions. The model is also used to show what the important phenomena are at different operating conditions.

Chapter 7 attempts to summarize the concepts presented throughout this dissertation and apply them towards selecting a solvent for removal of CO₂ from flue gas. Five model systems are analyzed: aqueous MEA (the industry standard for CO₂ removal from flue gas), PZ activated MDEA, PZ/MEA blends, a sterically hindered amine (AMP) and a promoted potassium carbonate system (PZ/K₂CO₃). The ability of these solvents to absorb CO₂ at flue gas conditions is summarized.

Conclusions and recommendations are presented in Chapter 8.

Chapter 2

Mass Transfer with Chemical Reaction & Amine / CO₂ Kinetics

*** Portions of this chapter are taken from G.T. Rochelle et al. (2000) with permission of the authors.**

Theories of mass transfer and kinetics are presented in order to provide background for the results presented in later chapters. Physical absorption is studied first in order to introduce and compare the different theories on mass transfer. A comparison of theories on mass transfer is presented and it is shown that steady state theories such as the eddy diffusivity theory are as effective as most of the unsteady state theories such as surface renewal.

Limiting cases for mass transfer with chemical reaction are presented. The use of these approximations is discussed along with the conditions when they break down. The deviations from the simplified behavior of pseudo-first order are discussed and the rigorous solution applied to PZ activated MDEA blends used in this work is introduced.

Finally, a review of the kinetics of CO₂ with amines is presented. This includes a comprehensive review of work performed on primary, secondary and tertiary amines along with understanding on the most probable mechanisms.

2.1 Physical Mass Transfer and Comparison of Theories on Mass Transfer

Theories on mass transfer serve to provide a conceptual picture of the processes taking place in the liquid mass transfer boundary layer. They also serve

to provide an important link between the theoretical approach of predicting fluxes from shell balances and concentration gradients and the empirical approach of mass transfer coefficients and driving force. The choice of mass transfer theory will rarely make a difference in the predicted flux or in the conclusion about the dominant physical phenomena occurring when CO_2 is absorbed into a reactive liquid. A discussion of the different theories is necessary, however, since it defines the choice of mass transfer theory used in this work and also compares this choice to that of other investigators.

2.1.1 Film Theory

Lewis and Whitman (1924) proposed film theory, the first insight into mass transfer at a vapor liquid interface. Film theory is considered a steady state theory in that no changes occur as a function of time, which differs from surface renewal and penetration theories to be presented later. Film theory suggests that all the mass transfer occurred in two films of finite thickness on each side of the interface. A physical description of film theory is shown in figure 2.1. For absorption with no chemical reaction, film theory predicts a straight concentration gradient in both gas and liquid films for the species being transferred. This may be seen by performing the mathematics for physical absorption of CO_2 using film theory. Our approach is to use film theory to set up the problem and boundary conditions, derive an expression for the concentration gradient of CO_2 , and to use Fick's law at the interface to calculate the flux of CO_2 occurring between the gas and liquid film. This will then be compared to the empirical expression for flux using the mass transfer coefficient.

Performing a material balance for CO_2 in the liquid film leads to equation 1.4. We delete the derivative with respect to time for film theory since it is a steady state theory. Also, we are considering physical absorption with no reaction so equation 1.4 with associated boundary conditions becomes:

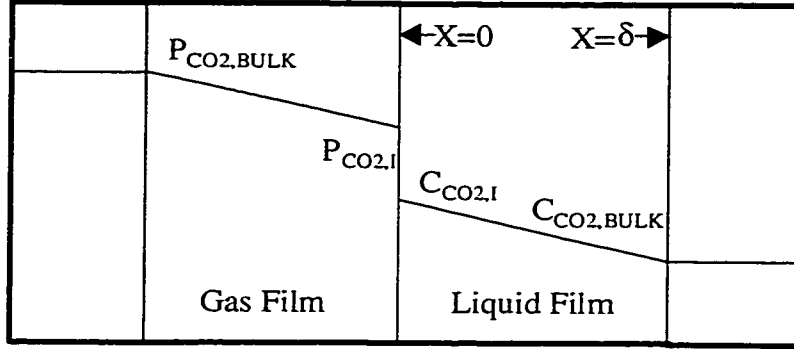


Figure 2.1 Physical Absorption using film theory

$$\frac{\partial^2[CO_2]}{\partial X^2} = 0 \quad (2.1)$$

$$[CO_2] = [CO_2]_i \quad \text{at } x=0$$

$$[CO_2] = [CO_2]_B \quad \text{at } x=\delta$$

Here, δ is the film thickness to be discussed below. Integration of this equation and evaluation of the boundary conditions leads to the following expressions for the concentration gradient of CO₂ throughout the liquid boundary layer.

$$[CO_2] = \frac{[CO_2]_B - [CO_2]_i}{\delta} x + [CO_2]_i \quad (2.2)$$

Use of Fick's law at the interface leads to the expression for the flux of CO₂ shown in equation 2.3. Comparing this to the empirical expression for mass transfer

which states that the flux should be proportional to the driving force for mass transfer and a liquid film mass transfer coefficient. Equation 2.4 shows the definition of the liquid film mass transfer coefficient as derived from film theory.

$$N_{CO_2} = -D_{CO_2} \frac{\partial [CO_2]}{\partial x} = \frac{D_{CO_2}}{\delta} ([CO_2]_i - [CO_2]_B) \quad (2.3)$$

$$k_l^o = \frac{D_{CO_2}}{\delta} \quad (2.4)$$

2.1.2 Higbie Penetration Theory

Although film theory is useful to introduce concepts such as the mass transfer coefficient and driving force, it is hard to believe that a discontinuity such as the concentration gradient shown in figure 2.1 exists at some film thickness. Higbie (1935) proposed an unsteady state theory which considers transient absorption of a solute into an element of the fluid which is in contact with the gas for a contact time τ . After this time, it is transported into the bulk liquid and a new element of fluid comes into contact with the gas. This process is demonstrated in figure 2.2.

Analysis of Higbie penetration theory for physical absorption results in elimination of the reactive term in equation 1.4. Since the transient term is valid the equation is now a partial differential equation. Upon solution of this PDE and an analysis consistent with film theory, we end up with the following expression for the mass transfer coefficient for Higbie penetration theory.

$$k_l^o = \sqrt{\frac{4D_{CO_2}}{\pi\tau}} \quad (2.5)$$

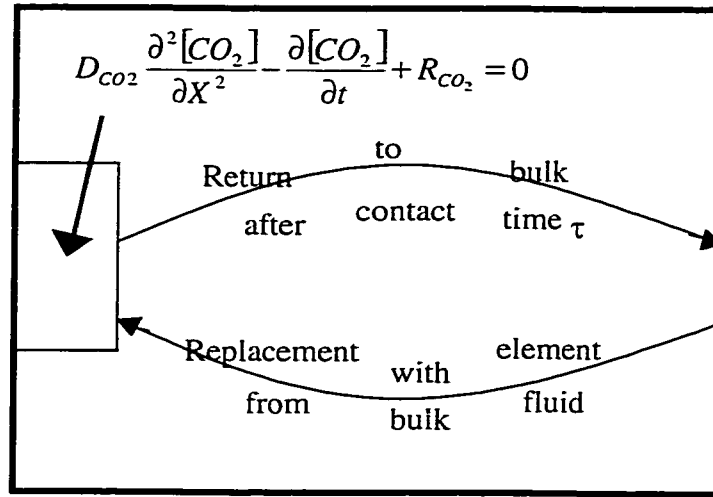


Figure 2.2 Description of unsteady state mass transfer theories.

Penetration theory leads to a square root dependence of the mass transfer coefficient on the diffusion coefficient. This is consistent with experimental data, which observes an order of between 0.5 to 1 on the diffusion coefficient.

2.1.3 Surface Renewal Theory

Danckwerts (1951) presented a modification to Higbie's penetration theory which suggested a normal distribution of contact times instead of the one used by Higbie. The resulting surface renewal theory is very convenient mathematically if Laplace transforms are used. The resulting expression for the mass transfer coefficient is given the following expression where s is the average contact time:

$$k_l^o = \sqrt{D_{CO_2}s} \quad (2.6)$$

2.1.4 Eddy Diffusivity Theory

The major advantage of unsteady state theories is that they seem to predict the correct dependence of the diffusion coefficient on the mass transfer coefficient. However, they introduce another variable (time) which complicates their use. King (1966) proposed a steady state theory that yields a square root dependence of the diffusion coefficient on the mass transfer coefficient. The physical concept is that there are convective eddies in the liquid phase which contribute to the effective diffusion coefficient. At the interface, the effect of these eddies disappears and the dominant phenomena is diffusion. As the liquid depth increases, the effect of the eddies increases until they are the dominant phenomena at infinite liquid depth. This process is illustrated in figure 2.3. Mathematically a material balance for eddy diffusivity theory is as follows:

$$\frac{\partial}{\partial x} \left[(D_{CO_2} + \epsilon x^2) \frac{\partial [CO_2]}{\partial x} \right] = 0 \quad (2.7)$$

Solving equation 2.7 for the concentration gradient and applying Fick's law, we obtain the following expressions for the concentration profile and mass transfer coefficient using the eddy diffusivity Theory.

$$[CO_2] = \frac{2}{\pi} ([CO_2]_b - [CO_2]_i) \cdot \arctan \left(\sqrt{\frac{\epsilon}{D_{CO_2}}} \cdot x \right) + [CO_2]_i \quad (2.8)$$

$$k_l^o = \frac{2}{\pi} \sqrt{D_{CO_2} \epsilon} \quad (2.9)$$

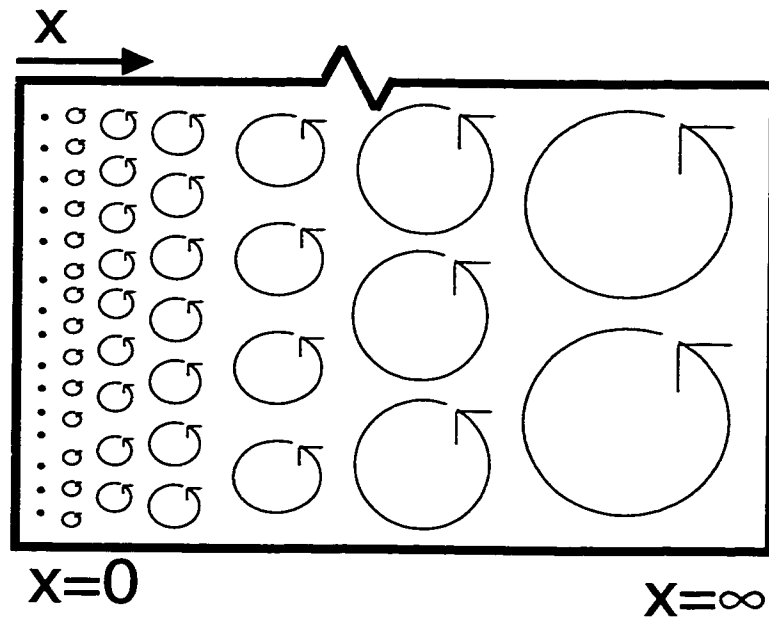


Figure 2.3 Eddy Diffusivity Theory

Eddy diffusivity theory has the advantage of predicting the correct dependence of the diffusion coefficient on the mass transfer coefficient without introducing the added computation complexity of an unsteady state theory. Glasscock (1990) has shown that the absorption with chemical reaction predictions from eddy diffusivity theory are comparable to surface renewal and penetration theory within 5% (figure 2.4). For this reason, eddy diffusivity theory will be used for all the rigorous modeling presented in this work.

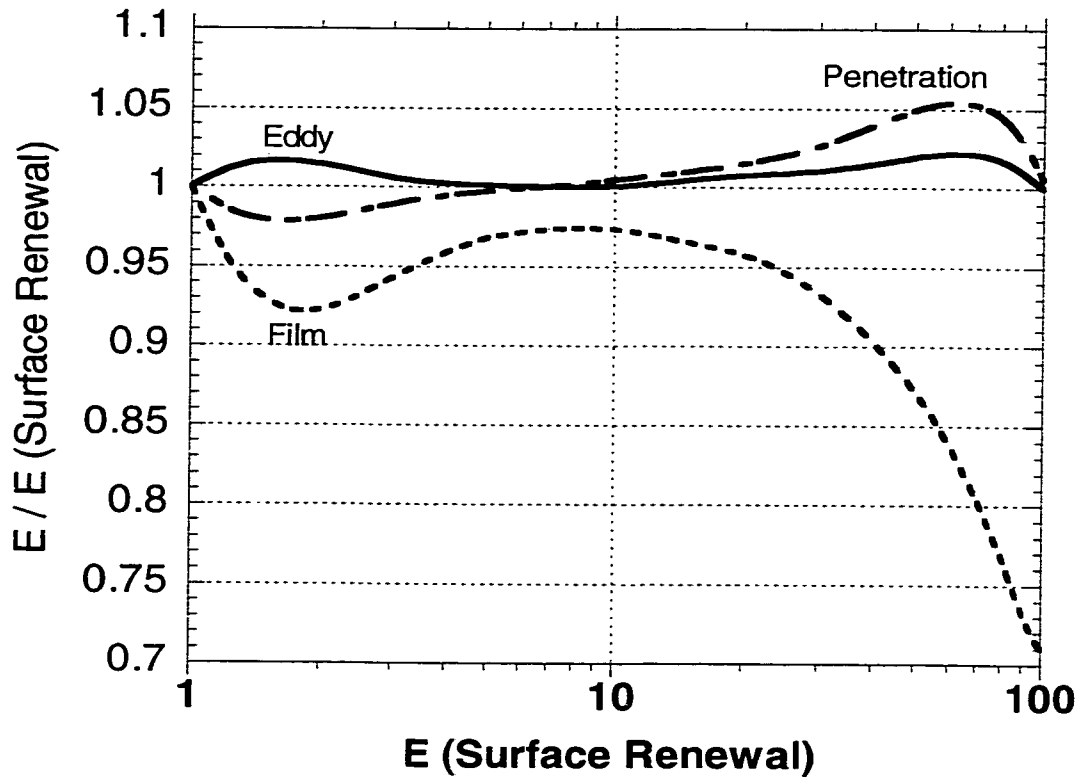


Figure 2.4 – Glasscock's Comparison of enhancement factors for different mass transfer theories. Figure reproduced from Glasscock (1990). Second order reversible reaction ($A+B=C+D$). $K_{eq}=350$, $D_B=D_C=D_D=0.5D_A$, $C_{B,bulk} / C_{A,int} = 200$, $C_{A,bulk}=C_{B,bulk}=C_{C,bulk}=0$.

2.2 Approximate Solutions for Mass Transfer with Chemical Reaction

Several simplifying assumptions lead to asymptotic behavior of the enhancement factor. These assumptions are very valuable when estimating the enhancement factor and, in some cases, are extremely accurate. We discuss the cases of pseudo first order kinetics, a correction of pseudo first order kinetics that

corrects for depletion of amine at the interface, and instantaneous reactions.

2.2.1 Pseudo First Order Case

2.2.1.1 Irreversible Reactions

Pseudo first order behavior assumes the overall reaction kinetics to be first order. Since most amine reactions with CO₂ are first order in CO₂ concentration and first order in amine concentration (second order overall), the pseudo first order assumption is equivalent to assuming a constant amine concentration across the liquid boundary layer. The use of surface renewal theory, penetration theory and film theory yields the same result. We therefore confine our discussion to the solution with film theory and extend results to surface renewal theory.

Making the assumption that the concentration of amine is constant over the length of the liquid boundary layer, we can combine the amine concentration with the rate constant to obtain a pseudo first order rate expression.

$$\frac{\partial^2 [CO_2]}{\partial X^2} - k_1 [CO_2] = 0 \quad (2.10)$$

Where k_1 is the pseudo first order rate constant. With appropriate boundary conditions, this expression can be integrated to obtain the following expression for the concentration of CO₂ in the boundary layer. This case is discussed in Danckwerts (1970). Details of this integration are presented in Appendix A.

$$[CO_2] = \frac{1}{\sinh \sqrt{M}} \left[[CO_2]_b \sinh \left(x \sqrt{\frac{k_1}{D_{CO_2}}} \right) + [CO_2]_i \sinh \left(\frac{D_{CO_2}}{k_1^o} - x \right) \sqrt{\frac{k_1}{D_{CO_2}}} \right] \quad (2.11)$$

Where:

$$\text{Hatta Number} = M = \frac{D_{CO_2} k_1}{k_l^2}$$

k_l^o = Liquid film mass transfer coefficient = D_{CO_2} / δ

Applying Fick's law at the gas liquid interface, the following expression is obtained for the flux under pseudo first order conditions:

$$N_{CO_2} = k_l^o \left([CO_2]_i - \frac{[CO_2]_B}{\cosh \sqrt{M}} \right) \frac{\sqrt{M}}{\tanh \sqrt{M}} \quad (2.12)$$

As the rate of reaction and the Hatta number increase, most of the reaction occurs in the liquid film and $[CO_2]_B$ approaches 0. The tanh contribution approaches one and we obtain the following expression,

$$N_{CO_2} = k_l^o \sqrt{M} [CO_2]_i \quad (2.13)$$

We see that the enhancement factor is equal to the square root of the Hatta number (by using equations 1.2 and 2.3).

Using surface renewal theory, we obtain the following result for the flux of CO_2 .

$$N_{CO_2} = k_l^o [CO_2]_i \sqrt{1 + M} \quad (2.14)$$

Under the same condition of large Hatta number (>5), we obtain the same result as film theory. A derivation of equation 2.14 is also shown in Appendix A. Numerically, equations 2.14 and 2.12 are practically equivalent. They lead to several insights regarding pseudo first order absorption of a gas into a reactive liquid. Firstly, we see that when the Hatta number becomes large (around 5), we can ignore the 1 under the square root of equation 2.14 with only minimum error ($<10\%$). This yields an enhancement factor which is, again, equal to the square

root of the Hatta number. Furthermore, substituting the Hatta number into this expression (equation 2.14 without the 1, and equation 2.13), the mass transfer coefficient inside and outside the square root term cancel. We obtain the result that the flux is independent of the liquid film mass transfer coefficient and directly related to the square root of the amine concentration and the rate constant.

$$N_{CO_2} = \sqrt{k_2[Am]D_{CO_2}}[CO_2]_i \quad (2.15)$$

The criteria of Hatta numbers being greater than 5 is often satisfied with CO₂ reaction with amines. Expression 2.15 will, therefore, be extremely useful in analyzing experimental results in Chapter 4. In order for the solvent to be regenerable, the reaction of CO₂ with amines must be reversible.

2.2.1.2 Reversible Reactions

Consider the reversible reaction of CO₂ with an amine to form an arbitrary CO₂ product denoted as CO_{2,PROD} and an amine product denoted as Am_{PROD}. Again, consider the amine concentration along the length of the boundary layer to be constant. By material balance then, the concentration of the amine product will also be constant. We can write the reaction as a first order reversible reaction with an associated equilibrium relationship:



$$r_{CO_2} = k_1[CO_2] - \frac{k_1}{Keq}[CO_{2,PROD}] \quad (2.17)$$

$$Keq = \frac{[CO_{2,PROD}]}{[CO_2]^*} \quad (2.18)$$

Substituting the definition of Keq into the rate of reaction expression for CO₂, we can express the rate of reaction as:

$$r_{CO_2} = k_1([CO_2] - [CO_2]^*) \quad (2.19)$$

Where: $[CO_2]^*$ is the concentration of CO_2 in equilibrium with $[CO_{2,PROD}]$

Danckwerts (1970) has shown the solution for a reversible first order reaction using surface renewal theory. The expression for the flux is a simple extension of equation 2.14 and its derivation is also shown in Appendix A.

$$N_{CO_2} = k_l^o([CO_2]_i - [CO_2]_e)\sqrt{1 + M} \quad (2.20)$$

Where $[CO_2]_e$ is the concentration of CO_2 in equilibrium with the bulk phase concentration of $CO_{2,PROD}$.

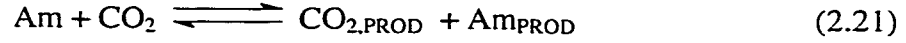
2.2.2 Deviations from Pseudo first order behavior.

The assumption of pseudo first order breaks down when the concentration of the amine is depleted at the interface. We see an increase in depletion at the interface due to:

- An increase in the partial pressure of CO_2 at the interface.
- An increase in the reactivity of the amine leading to a faster reaction at the interface.
- A decrease in the liquid film mass transfer coefficients which limits the amine's ability to be replenished at the interface and also limits the removal of the reaction products from the interface.

The depletion of amine at the vapor liquid interface introduces significant complexity to the problem. A change in amine concentration not only makes equation 2.12 nonlinear, it also introduces several coupled differential equations

that must be solved simultaneously. Consider again the reaction of CO₂ with an amine to form an amine product and a CO₂ product.



A rigorous solution of this system of equations using film theory would consider a material balance of each species.

$$\frac{\partial^2 [\text{CO}_2]}{\partial X^2} - k_2 \left\{ [\text{Am}][\text{CO}_2] - \frac{1}{K_{eq}} [\text{Am}_{\text{PROD}}][\text{CO}_{2,\text{PROD}}] \right\} = 0 \quad (2.22)$$

$$\frac{\partial^2 [\text{Am}]}{\partial X^2} - k_2 \left\{ [\text{Am}][\text{CO}_2] - \frac{1}{K_{eq}} [\text{Am}_{\text{PROD}}][\text{CO}_{2,\text{PROD}}] \right\} = 0 \quad (2.23)$$

$$\frac{\partial^2 [\text{CO}_{2,\text{PROD}}]}{\partial X^2} + k_2 \left\{ [\text{Am}][\text{CO}_2] - \frac{1}{K_{eq}} [\text{Am}_{\text{PROD}}][\text{CO}_{2,\text{PROD}}] \right\} = 0 \quad (2.24)$$

$$\frac{\partial^2 [\text{Am}_{\text{PROD}}]}{\partial X^2} + k_2 \left\{ [\text{Am}][\text{CO}_2] - \frac{1}{K_{eq}} [\text{Am}_{\text{PROD}}][\text{CO}_{2,\text{PROD}}] \right\} = 0 \quad (2.25)$$

with boundary conditions:

$$[i] = [i]_{\text{BULK}} \text{ @ } x = \infty \text{ for all species } i$$

$$[\text{CO}_2] = [\text{CO}_2]_i \text{ @ } x = 0$$

$$d[i]/d[x] = 0 \text{ @ } x = 0 \text{ for all species } i \text{ other than } \text{CO}_2$$

A solution to this set of equations is shown in figure 2.5. Here it is seen that the amine concentration is about 70% depleted from its bulk solution value of 1 mol/l. The concentration of amine and CO₂ reaction product is also seen to be much higher at the interface than in the bulk solution. The majority of the reaction occurs very close to the interface (within the first 10 microns). This is demonstrated by evaluating the ratio of product to reactant concentrations.

This number approaches the equilibrium constant value of 350 at a liquid depth of around 5 microns.

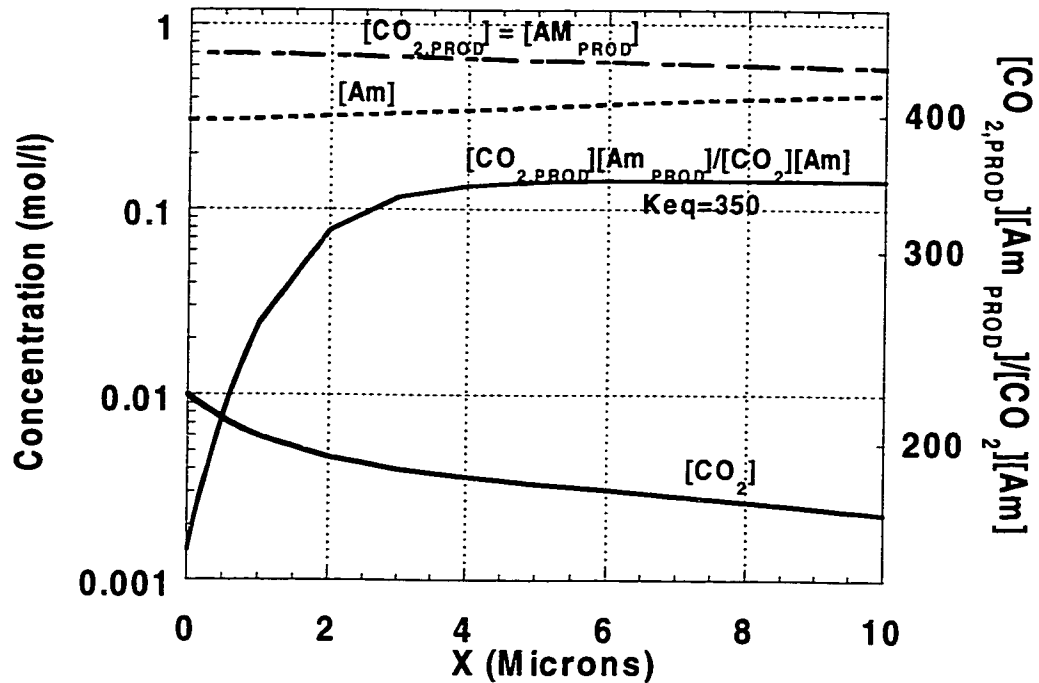


Figure 2.5 Deviations from Pseudo First Order Behavior. $k_1^0 = 1.0\text{e-}5$ m/s, $D_{\text{CO}_2} = 1.0\text{e-}9$ m²/s, $D_l = 0.5 D_{\text{CO}_2}$ for all other species i. $k_2 = 5000$, $\text{Keq} = 350$, $[\text{CO}_2]_l = 0.01$ mol/l, $[\text{Am}]_B = 1.0$, $[i]_B \sim 0$ for all species i other than Am.

2.2.3 Modification of Pseudo First Order for Depletion at the Interface

Figure 2.5 suggests approximations that can be made for estimating the depletion of amine at the interface. The majority of the reaction occurs very close to the vapor liquid interface. Throughout this region, the concentration of CO_2 is

reduced significantly while the concentration of other species is relatively constant. Incorporating these observations into equation 2.20, we simply replace the amine concentration and the equilibrium concentration of CO₂ with their corresponding values at the interface to obtain:

$$N_{CO_2} = k_l^o ([CO_2]_i - [CO_2]_e) \sqrt{1 + \frac{k_2 [Am]_i D_{CO_2}}{(k_l^o)^2}} \quad (2.26)$$

In order to use equation 2.26, the free amine at the interface must be calculated by:

$$[Am]_B = \frac{N_{CO_2}}{k_l^o} \sqrt{\frac{D_{CO_2}}{D_{Am}}} \quad (2.27)$$

2.2.4 Mass Transfer with Equilibrium Reactions

The limiting case of equilibrium reactions may apply to absorption/desorption of CO₂ in highly reactive alkanolamine solvents such as PZ at high temperatures.

With instantaneous, reversible (equilibrium) reactions, absorption can be represented to a first approximation as physical absorption by considering all of the dissolved forms of a gas in representing its solubility. Therefore the rate of absorption would be given by:

$$r \text{ (moles/cm}^3\text{)} = k_l^o [a ([CO_2]_{i,T}^* - [CO_2]_T)] \quad (2.28)$$

$[CO_2]_{i,T}^*$ is the total concentration of dissolved gas species that would be in equilibrium with the gas partial pressure at the gas liquid interface. This approximation requires that we have all of the equilibrium constants and activity coefficients needed to define the total solubility of the gas at the gas liquid interface.

For example, the total dissolved CO₂ in aqueous MEA is given by:

$$[CO_2]_T = [CO_2] + [HCO_3^-] + [CO_3^{2-}] + [MEACOO^-] \quad (2.29)$$

$[CO_2]_i^*$ would be determined by a bubble point calculation with a specified gas concentration and a specified total amine concentration. This first order approximation assumes that all solution species have the same diffusion coefficients. In most cases, the absorption rate is best represented using a value of k_l^o derived from the diffusion coefficient of the free amine salt product, e.g. amine bicarbonate.

A limiting case is when instantaneous reactions are combined with a very small driving force. In this case, the total free amine concentration at the interface and in the bulk solution can be related to the slope of the equilibrium curve. In this case, the flux may be determined using the following expression:

$$r(\text{moles/cm}^3) = a \cdot k_l^{o, PROD} \frac{[Am]_T}{\partial P_{CO_2}^* / \partial \alpha} [P_{CO_2, i} - P_{CO_2, B}^*] \quad (2.30)$$

Here, $P_{CO_2, i}$ and $P_{CO_2, B}^*$ represent the free CO_2 concentration at the interface and bulk respectively. The solution loading in mol CO_2 / mol amine is represented by α .

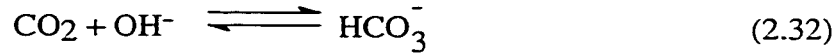
In the case when reactions approach instantaneous behavior, the pseudo first order enhancement can be combined with the instantaneous enhancement like resistance in series to obtain the following expression:

$$r(\text{moles / cm}^3) = a \cdot k_l^o \left(\frac{1}{\frac{1}{E^{Inst}} + \frac{1}{E^{1st}}} \right) ([CO_2]_i - [CO_2]^*_B) \quad (2.31)$$

2.3 Rate data and mechanisms for CO₂ reaction with amines and bases

2.3.1 Reaction with hydroxide

In aqueous solution CO₂ reacts with hydroxide to form bicarbonate:



The second-order rate constant for the reaction of CO₂ with hydroxide has been correlated by Sherwood et al. (1975) and corrected for ionic strength by Astarita et al. (1983):

$$\ln k_{\text{OH}^-} = 31.396 - \frac{6658}{T} + 0.184 I_c \quad (2.33)$$

where k is in units of m³/kmole/s, and I_c is the concentration-based ionic strength:

$$I_c = \frac{1}{2} \sum_{i=1}^N C_i z_i^2 \quad (2.34)$$

The reaction of hydroxide with carbon dioxide is the major rate phenomena in the absorption of CO₂ into hot potassium carbonate solutions.

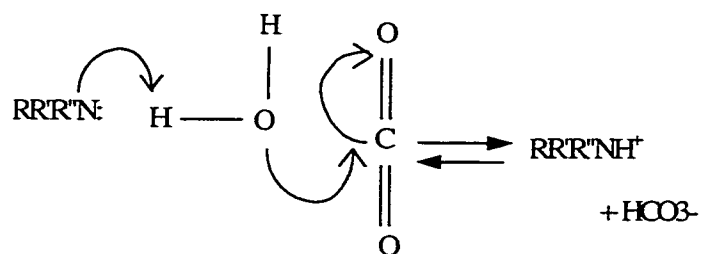
2.3.2 Reaction of CO₂ with Tertiary Amines

2.3.2.1. Mechanisms

The generally accepted rate expression for the reaction of tertiary amines with CO₂ is given by:

$$r = k_2 [\text{MDEA}] [\text{CO}_2] \quad (2.35)$$

This rate expression is consistent with a mechanism in which the amine enhances the reaction rate of CO₂ by a homogeneous catalytic effect.

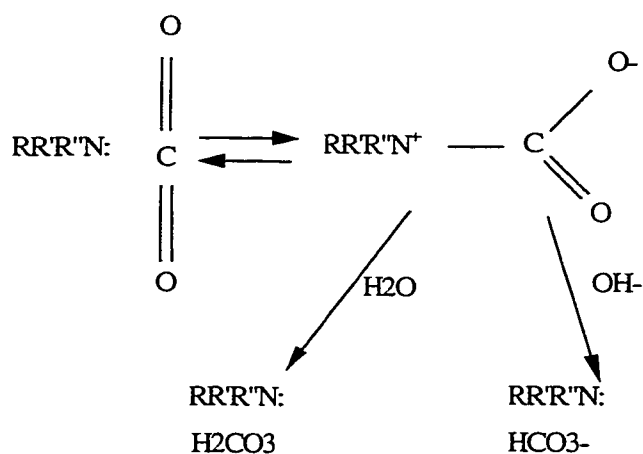


(2.36)

Water must be present for the reaction to occur by the above mechanism. Direct reaction of the amine with CO_2 is not possible.

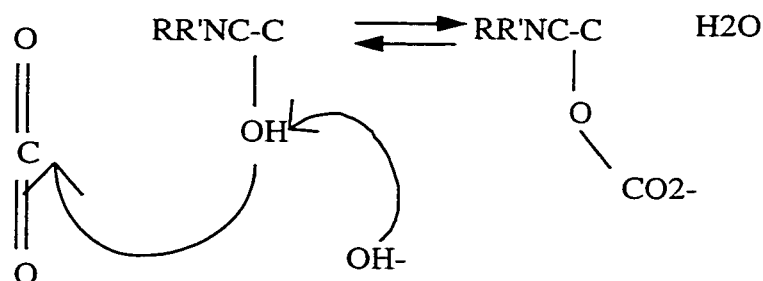
The early research on the kinetics of tertiary amines was concerned with whether or not the enhanced CO_2 absorption rate could be explained by the hydroxide reaction (Barth et al., 1981; Jorgensen and Faurholt, 1954; Jorgensen, 1956). It has been demonstrated by numerous authors that this reaction alone does not account for the enhanced absorption rates.

In addition to the simple second order mechanism, Barth et al. (1981) provide an enlightening discussion of two other possible mechanisms for the reaction of CO_2 with alkanolamines. The first is the possibility of forming an intermediary such as in the zwitterion mechanism.



(2.37)

The other possibility is the formation of alkylcarbonates, which is generally considered unlikely except in solutions of very high pH (Blauwhoff et al., 1984):



(2.38)

2.3.2.2 CO₂ Rate Data for Methyldiethanolamine

The rate data for MDEA, the most significant commercial tertiary amine, are summarized in Table 2.1. The apparent second order rate constants vary by a factor of 2 depending on the authors. This range of discrepancy does not seem large, and is to some extent a function of experimental conditions.

MDEA first appeared in the public literature in 1981 with the study of Barth et al. who also studied TEA. Reaction rates were measured by a stopped-flow technique in which the color change of a pH indicator was used to follow the reaction. In this work, it was reported that MDEA did not significantly enhance the reactivity beyond its effect to create more hydroxide in the system via buffer equilibria.

Blauwhoff et al. (1984) studied a variety of amines, including MDEA using a stirred tank. Both gas and liquid phases were batch, and the absorption rate was measured by the drop in CO₂ pressure with time. Typically, they would allow the pressure to drop for awhile until the change in partial pressure become constant with time – leading to what they assumed to be pseudo first-order conditions. It should be noted that this technique does not allow a study of kinetics at very low

loadings. They report a second-order rate constant in amine and CO₂ of 4.8 m³/kmole/sec at 298K, assuming only the simplified mechanism. They contend that under all practical conditions, monoalkylcarbonate formation is negligible. However, they also report that it was difficult to obtain a constant absorption rate with MDEA. It should be noted that in this work, they assumed first-order conditions with respect to both the amine and hydroxide – in the case of hydroxide this is probably not true. Even at relatively low partial pressures, the hydroxide can become significantly depleted at the gas-liquid interface. Finally, in this work, one cannot determine the partial pressure or loading at which experimental datapoints were taken, so a detailed analysis of the data is not possible.

In 1984, Barth et al. published a paper that essentially retracted their original conclusions about MDEA. In this case, they state that a second-order rate constant of 3.2 m³/kmole/s would fit the MDEA data from their previous paper.

Critchfield and Rochelle (1987) report results for CO₂ absorption into MDEA over a range of temperatures (282-350K). The CO₂ nominal pressure was 1 atm and the loadings were varied. From the dissertation of Critchfield (1988) it is possible to determine all data necessary to reinterpret the results, if necessary. In addition, in 1988, Critchfield and Rochelle presented results for MDEA desorption, showing that the desorption of CO₂ could be reasonably well predicted using the absorption results and an equilibrium model.

Haimour et al. (1987), Tomcej and Otto (1989), Versteeg and van Swaaij (1988b) and Yu et al. (1985) all studied CO₂ absorption into MDEA using various apparatus (see Table 3.1).

Littel et al. (1990a) revised the interpretation of the results of Versteeg and van Swaaij. Based on the work of Glasscock and Rochelle (1989), Littel et al. accounted for the depletion of hydroxide at the interface. With this correction the rate constant is increased by a factor of 1.18. We believe that completely

neglecting the hydroxide ion at the interface is not correct, neither is the assumption of pseudo first-order conditions.

Toman and Rochelle(1989) have studied the rates of absorption of pure CO₂ into an aqueous 50% MDEA solution as well as in another solution of equal strength in which 50% of the MDEA had been neutralized with sulfuric acid. The rate constant in the modified solution was found to be slightly higher indicating a weak catalytic effect. A decrease in free MDEA and the physical solubility of CO₂ causes a decrease in absorption rate in the low to moderate loading region.

The generally accepted second-order rate expression for the reaction of CO₂ with MDEA could not explain the observation that the rate constant would decrease with increasing driving force. Hence Glasscock (1990) proposed a rate expression that showed this decrease to be a direct consequence of the depletion of hydroxide ion at the interface for high driving forces.

$$r = [\text{CO}_2][\text{MDEA}]\{k_{\text{H}_2\text{O}}(\text{H}_2\text{O}) + k_{\text{OH}^-}(\text{OH}^-)\} + k'_{\text{OH}^-}[\text{CO}_2][\text{OH}^-] \quad (2.39)$$

The new rate expression was found to be in agreement with the data. Glasscock (1990) regressed the available rate data using activities rather than concentrations as the driving force for the reaction. As the partial pressure of CO₂ increases the hydroxide ion concentration at the interface gets depleted so that at low loadings the rate constant becomes a strong function of pressure. The apparent rate constant obtained using the model of Glasscock(1990) can easily span the range of data found in literature. This model predicts that the rate constant increases as the mass transfer coefficient is increased or the partial pressure of CO₂ is decreased because less depletion of hydroxide occurs at the interface. This is indeed the trend in the data found in literature.

Rangwala et al. (1992), Rinker et al. (1995) and Pani et al. (1997) have all

obtained results consistent with the conclusions of other investigators discussed in this work. A summary of their work is presented in table 3.1.

At typical absorber conditions (40°C , $D_{\text{CO}_2}=5 \times 10^{-10} \text{ m}^2/\text{s}$, $k_1^{\circ}=1.5 \times 10^{-4} \text{ m/s}$, $[\text{MDEA}]=4000 \text{ gmol/m}^3$), the expected second-order rate constant for MDEA ($0.01 \text{ m}^3/\text{gmol-s}$) gives a Hatta number squared (Ha^2) of about 0.7. Therefore, the rate of CO_2 absorption will be at least partially determined by mass transfer with a finite rate of chemical reaction.

Pacheco et al. (2000) have extended the temperature range by studying kinetics up to 100°C in a wetted wall column. The high temperature data not only quantify the kinetics at stripper conditions, they place confidence in the activation energy by looking at a wider temperature range. The data of Pacheco et al. (2000) give a Hatta number squared of about 5 at typical stripper conditions, so CO_2 desorption in the stripper is certainly controlled by mass transfer with fast reaction. In general, Carey (1990) also showed that the rate of CO_2 was not fast enough to approximate the CO_2 desorption process by mass transfer with equilibrium reaction. The rate data presented in the Pacheco, Critchfield, and Toman work is also unique in that it is regressed from data taken at a variety of loading instead of at zero loading like much of the other data presented in table 3.1

Table 2.1. Summary of Methyldiethanolamine (MDEA) Kinetic Data

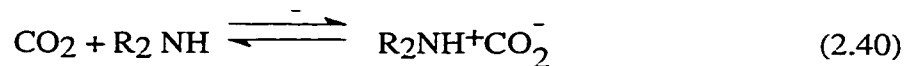
Reference	T (°K)	[MDEA] (gmol/l)	P_{CO_2} (atm)	$k_{298\text{K}}$ ($\text{m}^3/\text{kmol-s}$)	Ea (kJ/gmol)	Method
Barth et al.(1981)	293-313	0.02-0.2	0.0028-0.030	0	-	Stopped-flow
Barth et al.(1984)	298	0.02-0.2	0.0028-0.030	3.2	-	Stopped-flow
Blauwhoff et al. (1984)	298	0.5-1.6	< 1	4.8	-	Stirred tank
Yu et al.(1985)	313-333	0.2-2.5	1	5.7	39	Stirred tank
Critchfield & Rochelle (1987)	282-350	1.7	1	2.5	56	Stirred tank

Haimour et al.(1987)	288-308	0.9-1.7	1	2.4	72	Stirred tank
Versteeg & van Swaaij (1988b)	293-333	0.2-2.4	< 1	4.4 5.1#	42	Stirred tank
Tomcej & Otto (1989)	298-348	1.7-3.5	1	5.4	42	Sphere
Toman & Rochelle(1989)	298-308	4.3	0.02-0.12	5.5	-	Stirred tank
Littel et al.(1990a)	298	0.2-2.7	< 1	5.2	48	Stirred tank
Glasscock(1990)	298	1.7	0.1-1	3-10	27-42	stirred tank and data regression
Rangwala et al. (1992)	298-333	0.8-2.5	0.15-0.3	4.4	48	Stirred Cell
Rinker et al. (1995)	293-342	0.8-2.5	1	6.2	38	Wetted Sphere
Pani et al. (1997)	296-343	0.8-4.4	1-3	5.2	44	Stirred tank
Pacheco et al. (2000)	298-373	2.9-4.3	0.5-8	2.5	49	Wetted wall column

The second order reaction rate constant as reinterpreted by Littel et al.(1990a).

2.3.3 Reactions of CO₂ with Primary and Secondary Alkanolamines

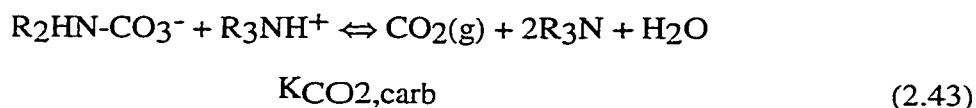
Caplow (1968) presented a hypothesized mechanism for carbamate formation involving the formation of an intermediate zwitterion (a locally ionic, net neutral, molecule). His proposed mechanism showed a hydrated amine group (with a hydrogen on the amine weakly bonded to the oxygen in water) forming the zwitterion. The deprotonation step then referred to the separation of a hydronium ion and the carbamate. Danckwerts (1979) introduced this mechanism into the chemical engineering literature, and Blauwhoff et al. (1984) showed that this mechanism reconciled much of the data in the literature, especially for DEA and other secondary amines. Although Danckwerts and other investigators after him consider the zwitterion species to be attacked by a base which extracts a proton in their work, they ignore the suggestion that the amine group may be hydrated before forming the zwitterion. Mathematically, however, these expressions result in the same expression.



This mechanism leads to the following rate expression for CO_2 :

$$r = \frac{k_2 [\text{R}_2\text{NH}][\text{CO}_2] - [\text{CO}_2]_e}{1 + \frac{k_{-1}}{\sum k_b[\text{B}]}} \quad (2.42)$$

Critchfield and Rochelle (1987) showed that reversibility was correctly accounted for if $[\text{CO}_2]_e$ is defined using the overall equilibrium constant for carbamate:



This gives:

$$[\text{CO}_2]_e = \frac{K_{\text{CO}_2, \text{carb}} [\text{R}_2\text{HN-CO}_3^-][\text{R}_3\text{NH}^+]}{[\text{R}_3\text{N}]^2} \quad (2.44)$$

2.3.3.1 Rate Data for Monoethanolamine (MEA)

Blauwhoff et al. (1984) reviewed the data available for the reaction of CO_2 with MEA (Table 3.4) and concluded that they were in good agreement. All authors found a first order dependence for the reaction rate of CO_2 with MEA, leading to the rate equation:

$$r_{\text{CO}_2} = k_2 [\text{CO}_2][\text{MEA}] \quad (2.35)$$

Table 2.2. Literature data on the reaction between CO_2 and aqueous MEA (mostly from Blauwhoff et al., 1984).

Reference	Temp K	[MEA] mole/l	$k_{298\text{ K}}$ $\text{m}^3/(\text{kmole.s})$	E_{act} $\frac{\text{kJ}}{\text{mole}}$	Experimental technique
-----------	-----------	-----------------	---	---	------------------------

Jensen et al. (1954)	291	0.1, 0.2	6103	(41)	Competition method with 0.1 and 0.2 M NaOH
Astarita (1961)	295	0.25 – 2.0	6443	(41)	Laminar jet
Clarke (1964)	298	1.6 - 4.8	7500	(41)	Laminar jet
Danckwerts and Sharma (1966)	291-308	1.0	7600, 6970	41.8	Laminar jet
Groothius (1966)	298	2.0	6500, 5720	–	Stirred cell
Leder (1971)	353		7194	39.7	Stirred cell
Sada et al. (1976)	298	0.25 - 1.9	8400	–	Laminar jet
Sada et al. (1976)	298	0.2 – 1.9	7140	–	Laminar jet
Hikita et al. (1977a)	278 – 315	0.015 – 0.18	5868	41.2	Rapid mixing method
Alvarez-Fuster et al. (1980)	293	0.2 - 2.0	5750	(41)	Wetted wall column
Donaldson and Nguyen (1980)	298	0.027 – 0.083	6000	–	Facilitated transport in aqueous amine membranes
Laddha & Danckwerts (1982)	298	0.5 - 1.7	5720	–	Stirred cell
Penny & Ritter (1983)	278-303	0.009-0.06	4990	42.2	Stopped Flow
Alper et al. (1990)	278-298	0.013-1.5	5545	46.7	Stopped Flow
Littel et al. (1992)	318 - 333		3703	(41)	Stirred Cell

Blauwhoff et al. (1984) concluded that the rate expression of Hikita et al. (1977a) fits the data extremely well over the range of 5 - 80°C:

$$\log_{10} k_2 = 10.99 - \frac{2152}{T} \quad (2-45)$$

k_2 is in units of $\text{m}^3/\text{kmole}/\text{s}$. Barth et al. (1986) studied the reaction rate at a later date, and found that the results compared very well with the previous literature data.

Although there is general agreement regarding the activation energy, order, and absolute value of the kinetics of CO_2/MEA kinetics, there are a few points of

concern regarding the type of data and the temperature / amine concentration ranges studied. None of the investigators have studied a wide temperature range including the temperature range usually seen in an absorber (35-60°C). Furthermore, most studies are at very low amine concentration and at very low loading. No work has been done at flue gas conditions with 5M amine and in partially loaded solution.

2.3.3.3 Rate Data for Diethanolamine (DEA)

Because of its prevalence, the literature data covering DEA is extensive. The review of Blauwhoff et al. (1984) has been extended to include more recent data (Table 2.3). However, there is general disagreement as to the order and rate of reaction with respect to DEA. The zwitterion mechanism, with its ability to allow the order of reaction to vary with changing conditions, does help to reconcile the existing data.

Recently, Crooks and Donnellan (1989) have questioned the validity of the zwitterion mechanism. Their criticisms come from calculating the equilibrium constant for the deprotonation step and showing that the pK_a of this deprotonation is stronger than expected. Instead, they propose a single, termolecular reaction step. Several researchers (Littel et al, 1992; Rinker et al., 1996) point out that the Crooks and Donnellan expression does not explain data taken for absorption of CO₂ into DEA in anhydrous solvents (Versteeg and Van Swaaij, 1988; Davis and Sandall, 1993) and, therefore cannot be completely valid. Their expression mathematically represents an extreme of the zwitterion mechanism. It is still not completely understood why a proton transfer step such as the base proton extraction in the zwitterion mechanism should be rate limiting, however no other mechanism adequately represents the data and, therefore the zwitterion mechanism is used quite universally to explain CO₂ / DEA kinetics (Rinker et al., 1996; Littel et al., 1992).

As with MDEA the rate constants at stripper temperature are not well known. However, it is possible that desorption at 120°C is usually controlled by mass transfer with equilibrium reaction.

Table 2.3. Literature data on the reaction between CO₂ and aqueous DEA (mostly from Blauwhoff et al., 1984).

Reference	Temp K	DEA mole/l	k_{app} @ 2.5M (m ³ /gmol s)	Mechanism with respect to DEA	Experimental technique
Van Krevelen & Hoftijzer (1948)	292 – 329	0.05 ~3	650	Second Order	Packed column
Jensen et al. (1954)	291	0.1 - 0.2	8240*	First Order	Competitive reaction with 0.1, 0.2 M NaOH
Jorgensen (1956)	291	0.1 - 0.3	6500*	First Order – Hydroxide catalyzed	Competitive reaction with 0.2, 0.3 M NaOH
Jorgensen (1956)	273	0.1 - 0.3	3332	Second Order – Hydroxide Catalyzed	Competitive reaction with 0.1, 0.2, 0.3 M NaOH
Sharma (1964)	291	1.0	1624*	First Order	Laminar jet
Sharma (1964) Danckwerts & Sharma (1966)	298	1.0	1500	First Order	Laminar jet
Sharma (1964) Danckwerts & Sharma (1966)	308	1.0	1298	First Order	Laminar jet
Groothuis (1966)	298	2.0	1300	First Order	Stirred cell
Leder (1971)	353	–	7757*	First Order	Stirred cell
Sada et al. (1976)	298	0.25 - 1.9	1340	First Order	Laminar jet
Coldrey & Harris (1976)	292	0.1 - 1.0	1612*	First Order	Rapid mixing method with 0.002 - 0.005 M NaOH
Hikita et al. (1977a)	278 – 313	0.17 - 0.72	3132	Second Order	Rapid mixing method
Alvarez-Fuster et al. (1980)	293	0.25 - 0.82	2963*	Second Order	Wetted wall column
Donaldson & Nguyen (1980)	298	0.031 - 0.088	1400	First Order	Facilitated transport of aqueous amine membranes

Blanc & Demarais (1981)	293 – 333	0.05 - 4.0	660	First Order	Wetted wall column
Laddha & Danckwerts (1982)	298	0.46 - 2.9	960	Zwitterion	Stirred cell
Laddha & Danckwerts (1982)	284	0.5 - 2.0	1471*	Zwitterion	Stirred cell
Blauwhoff et al. (1984)	298	0.51 - 2.3	515	Zwitterion	Stirred cell
Barth et al. (1986)	298	0.019 - 0.021	275	First Order	Stopped flow
Versteeg & Van Swaaij (1988a)	298	–	1162	Zwitterion	Stirred cell
Versteeg & Oyevaar (1989)	298	0.086 - 4.4	1143	Zwitterion	Stirred cell
Crooks & Donellan (1989)	298	0.1-1.0	2250	First Order - H ₂ O Catalyzed Second Order – DEA Catalyzed	Stopped Flow
Glasscock & Rochelle (1991)	298 – 313	0.5 - 3.0	475	Zwitterion	Regression
Littel et al. (1992)	303 – 333	0.2-4.0	1433*	Zwitterion	Stirred Cell
Davis & Sandall (1993)	293 – 313	0.25-2	351 note: nonaqueous	Zwitterion	Wetted Sphere
Rinker et al. (1996)	293-343	0.25-2.8	1500	Zwitterion	Laminar Jet

* Second order rate constant extrapolated to 298K using activation energy of 50 kJ/mol

The expression of Rinker et al. (1996) is seen to best fit the data and is recommended for calculating DEA rate constants at absorber conditions:

$$r(\text{moles/s}) = \frac{[\text{DEA}]}{\frac{1}{1.24\text{E}6\exp\left(-\frac{1701}{T}\right)} + \frac{1}{3.18\text{E}7\exp\left(-\frac{3040}{T}\right)}[\text{DEA}]} \quad (2.46)$$

2.3.3.4 Rate Data for Amines Related to Piperazine

The rate constant of several cyclic amines have been studied (Sharma, 1965; Littel et al., 1992; Alper, 1990; Crooks and Donnellan, 1989; Bishnoi and Rochelle, 2000). In most cases, it has been observed that the second order rate constant of the cyclic amines lies above the Bronsted plot for amines with similar pKa. Bishnoi and Rochelle (2000) have attributed this to a reduction in steric hindrance around the amine group and a consequent increase in the zwitterion formation rate.

PZ activated MDEA blends have found widespread use as a solvent for high capacity CO₂ removal. They have been patented by Appl et al. (1980) of the BASF corporation and have found their major application in ammonia or synthesis gas production. The success of these solvents is probably due to the very high rate constant of PZ and its ability to be effective at very low activator concentration.

Table 2.4 summarizes the rate data obtained for cyclic amines. Note that the rate expressions presented are first order rate expressions, unlike the other tables in this report. Results for ethylene diamine and dimethyl ethylene diamine are also presented in table 2.4 since they are related to the PZ molecule. The overall reaction of morpholine is a second order function of amine strength and seems to follow the zwitterion mechanism, however PZ demonstrates second order overall kinetics. This may be due to self proton extraction by the second nitrogen in the PZ ring. Two investigations of PZ have been performed in blends (Xu et al., 1992; Seo et al., 2000). Although rate constants for the PZ reaction are extracted in these two works, they will be discussed in section 2.3.5. The extremely low value of the rate constant extracted in these two investigations is due to severe depletion of the PZ at the interface.

Table 2.4 Rate Data for the Piperazine Family of Amines

Reference	Amine	Temp (K)	[Amine] mol/l	$k_1 = \frac{r}{[CO_2]} s^{-1}$	Experimental technique
Sharma (1965)	Piperidine	298	-	60255[PDN]	Stirred cell
	Morpholine	298	-	19952[MOR]	
	Ethylene Diamine	298	-	15135[EDA]	
Weiland and Trass (1971)	Ethylene Diamine	298	0.394	100400[EDA]	Laminar Jet
Hikita et al. (1977)	Ethylene Diamine	288-308	0.00744-0.0284	$[EDA] * 10^4 \left(13.49 - \frac{2799}{T} \right)$	Stopped Flow
Sada et al. (1985)	Ethylene Diamine	298	-	17500[EDA]	Laminar Jet
Crooks and Donnella n (1989)	Morpholine	298	0.1-1.0	$14200*[MOR]^2 + 48*[MOR][H_2O]$	Stopped Flow
Alper (1990)	Morpholine	298	0.025-0.50	$3855*[MOR] + 16665*[MOR]^2$	Stopped Flow
Xu et al. (1992)	Piperazine	303-333	<4 M Total	$2.98*10^{11} \exp\{-6424/T\}[PZ]$	Wetted Disk
Littel et al. (1992)	Morpholine	303	0.15-4	$\frac{[MOR]}{\frac{1}{12400} + \frac{1}{12.1 \cdot [MOR]}}$	Stirred Cell
Bishnoi et al. (1999)	Piperazine	303	0.2	68000[PZ]	Stirred Cell
	Hydroxy Ethyl Piperazine	303	0.2	14500[HEP]	
	Amino Ethyl Piperazine	303	0.2	37000[AEP]	

	Dimethyl Ethylene Diamine	303	0-2	100000[DMEDA]	
Bishnoi and Rochelle (2000)	Piperazine	298-333	0-2,0.6	$5.37E4 \cdot \exp \left[-\frac{3.36E4}{8.314} \left(\frac{1}{T} - \frac{1}{298.15} \right) \right]$	Wetted Wall
Seo et al. (2000)	Piperazine	303, 313	0.057 – 0.23	4096[PZ], 7075[PZ]	Wetted Sphere

2.3.4 Reaction of CO₂ with Hindered Amines

Exxon and others have performed a great deal of work in the field of acid gas absorption with hindered amines. This includes a number of bench scale experiments and pilot plant tests from which there have been a number of publications, patents as well as papers in various journals. FLEXSORB SE and FLEXSORB PS are two proprietary gas treating agents that Exxon has developed for selective removal of H₂S and bulk removal of acid gases respectively.

Sterically hindered amines are generally primary or secondary amines that do not form a stable carbamate. A sterically hindered amine typically has a bulky alkyl group attached to the amino group. It can be a primary amine in which the amino group is attached to a tertiary carbon atom or a secondary amine in which the amino group is attached to a secondary or a tertiary carbon atom (Sartori and Savage, 1983).

More generally, the hindered amines can be classified as either moderately hindered or severely hindered amines. The moderately hindered amines are used for bulk non-selective removal of H₂S and CO₂ while the severely hindered amines are employed in the selective removal of H₂S. Because of its interest in bulk removal of CO₂ this work will focus on moderately hindered amines and not discuss severely hindered amines.

Primary and secondary amines are limited in their capacity to absorb CO₂

because of the formation of a stable carbamate:

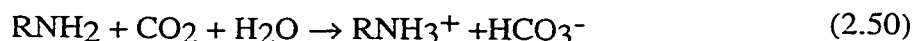


Thus the stoichiometry of the reaction limits the amount of CO_2 that can be absorbed. The maximum possible is 0.5 mole CO_2 per mole of amine.

Tertiary amines, on the other hand exhibit greater capacity to absorb CO_2 but have lower rates of absorption as compared to the primary and secondary amines. Because tertiary amines absorb CO_2 as bicarbonate rather than carbamate, the maximum stoichiometry is one mole of CO_2 per mole of amine:



Moderately hindered amines are characterized by forming carbamates of low to intermediate stability. The reaction with carbon dioxide proceeds mainly through the production of bicarbonate. Carbamate reversion to bicarbonate is also a significant reaction. Hence these moderately hindered amines have a high thermodynamic capacity that approaches 1.0 mole of CO_2 per mole of amine:



The CO_2 amine reaction rate could be given by the following expression:

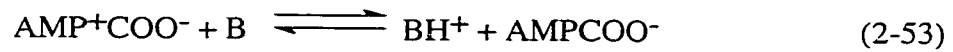
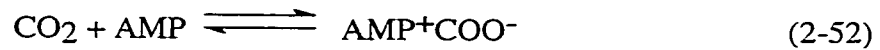
$$\text{Rate} = k_{\text{AM-CO}_2} [\text{AMINE}][\text{CO}_2] \quad (2.51)$$

The reaction suggests that less amine is tied down with 1 mole of CO_2 as compared to the primary and secondary amines. Hence the fraction of free amine is greater. This higher free amine concentration can compensate for a decrease in rate constant owing to hindrance thus making the rate of absorption comparable to that attained for primary and secondary amino alcohols (Sartori et al., 1987).

2.3.4.1 2-Amino-2-Methylpropanol

AMP(2-amino-2-methylpropanol) is a moderately hindered amine that can achieve a greater solution loading at any given partial pressure of CO₂ than MEA (Sartori and Savage, 1983). This behavior is also predicted by the equilibrium data and model of Erga and Lidal (1990) for CO₂ absorption. Solubility measurements of CO₂ and H₂S in AMP have been performed by Roberts and Mather (1988) and Teng and Mather (1989) over a wide range of partial pressures. Teng and Mather (1989) also proposed a mathematical model to correlate the equilibrium data.

Table 2.5 shows the rate of absorption data for AMP. Unlike other primary amines, there seems to be a fair amount of disagreement between investigators on both the speed and mechanism of reaction. Although most investigators seem to agree on the zwitterion mechanism, there are conflicting results on which step is rate limiting. . The overall rate expression is derived by applying the pseudo-steady state approximation to the zwitterion species (Blauwhoff et al.,1984):



$$r = \frac{[\text{CO}_2][\text{AMP}]}{\frac{1}{k_2} + \frac{k_{-1}}{\sum_B k_B [\text{B}]}} \quad (2-54)$$

Chakraborty et al. (1986) studied the rate of absorption of CO₂ into aqueous AMP and suggest that the reaction rate is due to the amine catalyzed formation of bicarbonate. They report a second order rate constant of 100 l /gmols.

Yih et al. (1988) were the first to suggest that the reaction rate may

correspond to the formation of a carbamate, even though it is thermodynamically limited. They report a second order rate constant significantly higher than that of Chakraborty et al. at 1270 l/gmol s at 40°C.

Bosch et al. (1990) have measured absorption rates of CO₂ into aqueous solutions of AMP under reaction-controlled conditions. Unlike other investigators, the deprotonating reaction is found to be the rate limiting step. The investigators do, however, point out a large degree of uncertainty in their values of the zwitterion formation rate constant and, therefore, their conclusion about the deprotonation kinetics being rate limiting is questionable. Another important conclusion of the work of Bosch et al. (1990) is that reversibility and mass transfer considerations should be taken into account when analyzing AMP kinetic data.

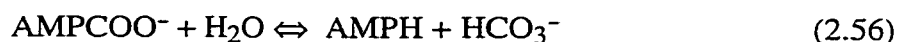
Since Bosch et al. (1990) showed that mass transfer limitations could be significant with AMP, Alper (1990) studied the kinetics of AMP/ CO₂ using a stopped flow technique. Alper compared his results with MEA and found the order of the reaction to be around 1.15 versus 1.0 for MEA suggesting that the overall rate may be slightly affected by the deprotonation step but was largely controlled by the zwitterion formation. Alper (1990) reports a second order rate constant of 520 l/gmol s at 25°C.

Xu et al. (1996) used a stirred cell reactor to measure CO₂ / AMP kinetics. They found the reaction order to be between 1.15 at 25°C to 1.32 at 45°C for AMP, consistent with the zwitterion mechanism and the results of Alper. Furthermore, the overall rate of reaction seems to be consistent with Bosch et al. It is our belief that the mechanism and rate constants reported by Xu et al. (1996) represents all the data most sufficiently.

In a solution of AMP, CO₂ also reacts directly with the hydroxyl ion. The contribution of the hydration reaction,



as well as the carbamate reversion to bicarbonate are significant:



$$K_c = \frac{[\text{AMPCOO}^-]}{[\text{AMPH}][\text{HCO}_3^-]} \quad (2.57)$$

The rate constant parameters of Xu et al are tabulated in table 2.5.

Table 2.5 Literature data on the reaction between CO₂ and aqueous AMP

Reference	Temp (K)	AMP mole/l	k _{app} @ 2.5M	Mechanism with respect to AMP	Experimental technique
Chakraborty et al. (1986)	315	—	42*	First Order	Stirred Cell
Yih and Shen (1988)	313	0.26-3.0	585*	First Order	Wetted Wall
Bosch et al. (1990)	298	0.2-2.4	612	Zwitterion	Stirred Cell
Alper (1990)	278-298	0.52-5.6	520	First Order	Stopped Flow
Saha et al. (1995)	294-318	0.5-2.0	555	First Order	Wetted Wall
Xu et al. (1996)	288-318	0.25-3.5	681	Zwitterion	Stirred Cell

* An activation energy of 40 kJ/kmol is used to compare rate constants at 298K.

2.4 Kinetic Data for Blended Amines

Blending a primary or secondary amine with a tertiary amine has been discussed for many years as a way to increase the enhancement factors of a tertiary amine while keeping its high capacity and low heat of regeneration (Chakravarty et al, 1985). Although this concept has been recognized for many years, very little fundamental data has been acquired for the rate of absorption of CO₂ into blends of amines.

Several additional considerations arise when blending a carbamate forming amine with a slower tertiary amine. Thermodynamics becomes very important for predicting the correct enhancement as a function of loading. Since the initial concentration of the carbamate forming amine is low, it is significantly depleted even at fairly low overall loading. However, even though its concentration is low, enhancement of CO₂ absorption is dictated by the carbamate former since its rate of reaction is usually orders of magnitude higher than the tertiary amine. Accurate prediction of the free promoter concentration in partially carbonated solutions of amine blends becomes vital in tertiary amines promoted by primary or secondary amines.

The low promoter concentration also makes depletion of the amine at the vapor liquid interface more likely. Therefore, it becomes more important to model the mass transfer with accompanying chemical reaction in the liquid boundary layer and the interactions of the promoter with the tertiary amine.

De-protonation of the zwitterion by the tertiary amine becomes important in blended amine solutions as well. The apparent rate of reaction of the carbamate former, therefore, seems to increase in the presence of another amine in high concentration. The contribution of the tertiary amine to the zwitterion mechanism must be quantified in order to predict rate of absorption measurements in blended amine solutions.

Table 2.6 summarizes the data for CO₂ absorption into blended amine systems. We believe that four important effects must be dealt with in order to predict rate of absorption of CO₂ into blended amine systems at conditions relevant to gas treating.

1. Data should be obtained at industrially significant amine concentration in order to correctly quantify the effect of the tertiary amine on zwitterion de-protonation.

2. Rigorous speciation must be performed in the thermodynamic model in order to accurately quantify the amount of free promoter in partially carbonated solutions.
3. The liquid boundary layer should be rigorously modeled in order to properly account for the mass transfer of amines and amine reaction products to and from the vapor liquid interface to the bulk solution.
4. Data should be obtained in partially carbonated blends in order to validate the model extrapolation to the practical conditions of absorption into blends at a finite loading.

Versteeg and Van Swaaij (1988) have studied blends of MMEA/MDEA, MEA/MDEA, DIPA/MDEA and DIPA/TEA with a rigorous boundary layer model based on film theory, penetration theory and a finite difference approach. Their model does an excellent job of predicting their data and demonstrating the zwitterion mechanism. Extrapolation of their model to loaded solutions, however may not be accurate due to the approximate equilibrium model used. Furthermore, no rate of absorption data has been taken into solutions with a significant CO₂ loading.

The work of Bosch et al. (1989) follows a similar trend to the work of Versteeg and Van Swaaij. A subset of DEA/MDEA data taken by Critchfield (1988) is used (Critchfield and Rochelle, 1987). All this data is at low loading and an approximate equilibrium model is used.

Glasscock et al. (1991) was the first to consider the rigorous treatment of all four conditions described above. The data considered in this work is from the work of Glasscock (1990) and Critchfield (1988) and includes data taken in partially loaded solutions of MEA/MDEA and DEA/MDEA. The overall concentration of the amine studied is only up to 3 M which is on the lower end of amine solutions used in industry.

Littel et al. (1992 a & b) present the most thorough investigation of the zwitterion mechanism to date. Along with monoamine data over a wide concentration range, they have taken data in solutions of DEA and DIPA in tertiary amines (TEA, MDEA, DMMEA, DEMEA). Their results show that the tertiary amine contributes significantly to the de-protonation of the carbamate zwitterion. Deprotonation by the tertiary amine increases with the pK_a of the tertiary amine. Their experimental work includes amines up to a total concentration of 1 to 3.5 M. This approaches the concentrations of industrial significance. No data are taken in solutions with significant CO_2 loading.

Mshewa (1995) has obtained experimental data for absorption of CO_2 into loaded blends of DEA/MDEA. He analyzed his data using an approximate VLE model. Film theory with a correction for surface renewal theory was used to calculate the depletion of the amines at the vapor liquid interface. Enhancement factors were calculated by using these concentrations at the interface. Although the methods for thermodynamics and mass transfer with chemical reaction were approximate, Mshewa's data was taken at industrially significant concentrations and significant CO_2 loading. There has been no attempt to re-analyze Mshewa's data using rigorous models.

Pacheco et al. (2000) have presented comprehensive data on DGA[®]/MDEA blends. They have studied a variety of concentrations and a wide range of loading. Rigorous thermodynamics based on the work of Austgen (1989) is used to speciate the solution. An approximation based on the work of Decoursey (1992) is used to model the boundary layer. The combined model matches the rate of absorption data well.

Xu et al. (1992) have obtained rate of absorption data of CO_2 into PZ/MDEA blends. Although their data was taken at industrially significant amine concentrations, it is all taken at very high CO_2 partial pressure and a region where

the PZ is completely depleted at the interface. As a result, the kinetics that they extract from their rate of absorption data is erroneous. The same applies for the work of Seo and Hong (2000) who have studied the absorption of CO₂ into blends of PZ and AMP.

Kaganoi (1997) has presented data for PZ/MDEA blends in a wetted wall contactor. The concentration of the amine is high (4.6M overall) and data are taken at significant CO₂ loading. No formal interpretation of VLE or rates is presented.

This work extends the data for PZ/MDEA at low solution loading and also at significant solution loading. Rigorous VLE based on the electrolyte NRTL model and rate modeling based on eddy diffusivity theory and a finite difference approach are applied to the data. The data of Kaganoi (1997) and Xu et al. (1992) can be predicted using the model presented in this work.

Table 2.6 Summary of data acquired in blended amine systems

Investigator	Amines	Overall Amine Conc. (M)	Rigorous Rates (Y/N)	Rigorous Thermo (Y/N)	Data in Loaded Solns (Y/N)
Versteeg and Van Swaaij (1988)	MMEA/MDEA MEA/MDEA DIPA/TEA DIPA/MDEA	0 – 4	Y	N	N
Bosch et al. (1989)	DEA / MDEA	0 – 2 *	Y	N	N
Glasscock et al. (1991)	DEA / MDEA MEA / MDEA	0 – 3	Y	Y	Y
Littel et al. (1992)	DEA and DIPA In TEA, MDEA, DMMEA, DEMEA	0 – 3.5	Y	N	N
Rangwala et al. (1992)	MEA / MDEA	2	N	N	N
Xu et al. (1992)	PZ/MDEA	4	N	N	Y
Rinker et al. (1997)	DEA / MDEA	0 – 4.5	Y	N	N
Mshewa (1995)	DEA / MDEA	4 – 5	N	N	Y

Weiland (1996)	DEA/MDEA MEA/MDEA	2-4	N	N	Y
Kaganoi (1997)	PZ / MDEA	4.6	N	N	Y
Pacheco et al. (2000)	DGA [®] / MDEA	4 – 5	N	Y	Y
Bishnoi and Rochelle (2000)	PZ / MDEA	4.6	Y	Y	Y
Seo and Hong (2000)	PZ / AMP	0-3.5	N	N	N

* Reinterpretation of the data of Critchfield and Rochelle (1987)

VLE data for CO₂ are generally not statistically adequate to predict accurately the speciation of blended amine systems. Such speciation is necessary to model adequately the CO₂ rate behavior of such systems. We must know the concentration of free secondary amine to predict the enhancement factor for CO₂ absorption. Such speciation data could also be used to predict amine volatility. This prediction would be especially important with more hydrophobic amines such as MDEA or hindered amines. Clever experiments such as liquid/liquid equilibration or calorimetry might be used to facilitate the collection of this data. Proton and ¹³C NMR have also shown to be useful in quantifying speciation of loaded amine solutions.

Chapter 3

Background Thermodynamics, Conditions for Equilibrium and System Non-Idealities

Chapter 1 shows the importance of thermodynamics in acid gas treating. Not only does thermodynamics quantify the speciation of amine solutions it also describes boundary conditions for the material balances discussed at the beginning of Chapter 2. A consistent thermodynamic model also quantifies the volatility and enthalpic behavior of the amine solvent.

Acid gas thermodynamics is often used to solve for the speciation and partial pressure of each component when the liquid phase is specified (temperature, pressure and total amine and CO₂ concentrations are known). This special case is introduced. Models to account for system non-idealities for the gas and liquid phase are presented.

3.1 The Acid Gas Thermodynamic Problem

The typical acid gas thermodynamics problem is as follows. The temperature and pressure of the system is known. The loading and amine concentration in the liquid phase are also known. Calculate the mole fraction of all species present in the liquid phase along with the partial pressure of each molecular species in the gas phase.

Consider the following example involving CO₂ in aqueous MDEA. For simplicity, we summarize the reaction of CO₂ with MDEA as follows:



We define the following symbols:

x_i = molefraction of i in the liquid phase

y_i = molefraction of i in the vapor phase

α_{CO_2} = solution loading = moles of total CO₂ (reacted + free) / moles of amine

P = Total Pressure

T = Temperature

Keq = Equilibrium Constant for reaction 2.1

The solution of this problem is analogous to a bubble point calculation. In this case, the macroscopic qualities of the liquid phase are specified (T,P, total CO₂, total amine, total H₂O) and we wish to speciate the solution and calculate the composition of the gas phase. A list of the unknowns and equations are listed in Table 3.1.

Table 3.1 Example problem unknowns and equations

Unknowns	Equations
x_{CO_2}	Raoult's Law
x_{MDEA}	
x_{MDEAH^+}	$y_{H_2O} = x_{H_2O} P^{SAT}_{H_2O}/P$ $y_{MDEA} = x_{MDEA} P^{SAT}_{MDEA}/P$
x_{H_2O}	
$x_{HCO_3^-}$	Henry's Law
y_{CO_2}	$y_{CO_2} = x_{CO_2} H_{CO_2}$
y_{MDEA}	Chemical Eqm in Liquid Phase
y_{MDEAH^+}	$Keq = \frac{x_{HCO_3^-} x_{MDEAH^+}}{x_{CO_2} x_{MDEA} x_{H_2O}}$
y_{H_2O}	Material Balance
$y_{HCO_3^-}$	
	Charge Balance

The eight equations listed above completely define the system and can be solved to obtain the desired solution. Many simplifications and solution techniques are possible. Since the example problem was introduced for illustrative purposes only, we will not discuss these solution procedures or simplifications any further here.

The example problem also assumes ideal solutions and ideal gas. In reality, these assumptions are not valid. Mixtures of amine and water are not ideal solutions as can be observed by the large amount of heat released when they are mixed. When the solution is loaded with CO₂ the ionic products lead to Coulombic forces making the solution even less ideal. At high CO₂ concentration in the gas phase or at high pressure, gas phase non-idealities also become important (leading to Raoult's law and Henry's law breaking down). In order to treat these problems we discuss the thermodynamic models used in this work to account for gas and liquid phase non-idealities.

3.2 The Condition for Phase Equilibrium

A thorough derivation of the conditions of phase equilibrium is given in Smith and Van Ness (1975). The fugacity in each phase (α and β) is equal for each component.

$$f_i^\alpha = f_i^\beta \quad (3.2)$$

Equation 3.2 can also be expressed as:

$$\phi_i y_i P = x_i \gamma_i P_i^* \exp \left(\frac{v_i (P - P_i^*)}{RT} \right) \quad (3.3)$$

for solvents and:

$$\phi_i y_i P = x_i \gamma_i^* H_i \exp \left(\frac{v_i^\infty (P - P_{solv}^*)}{RT} \right) \quad (3.4)$$

for solutes.

Where:

P_i^* = Vapor pressure of component i

ϕ_i = Fugacity coefficient of i

γ_i = Symmetric activity coefficient of i

γ_i^* = Assymetric activity coefficient of i

3.3 The Conditions for Chemical Equilibrium

Chemical equilibrium is commonly expressed in two ways. The Gibbs free energy is minimized at equilibrium yielding:

$$\partial G = \sum_i \mu_i \partial n_i = 0 \quad (3.5)$$

Where μ is the chemical potential defined as:

$$\mu_i = G_i^o + RT \ln(\gamma_i x_i) \quad (3.6)$$

A more common definition is the definition of the equilibrium constant

$$\prod (\gamma_i x_i)^{\nu_i} = K = \exp\left(\frac{\Delta G^o}{RT}\right) \quad (3.7)$$

3.4 Reference States Used in This Work

A combination of reference states is used in this work which differs from the reference states of previous investigators (Austgen, 1989, Posey, 1996). This section summarizes the reference states used in this work compared with the reference states used in previous works.

The system being studied consists of water, MDEA, PZ and CO₂. Water and MDEA are both liquids at room temperature while PZ is an anhydrous solid in its pure form. Carbon dioxide is a gas at room temperature and is the solute being transferred from the gas phase to the liquid phase.

The reference state of all solvents has followed the symmetric convention in all previous works and is unchanged in this work. The reference state for water in the liquid phase is, therefore, pure water at the system temperature and pressure. The reference state for MDEA and PZ also follows the symmetric convention.

The reference state for solute molecules has been changed from previous models that were created within the Aspen PlusTM framework. The structure of the electrolyte-NRTL model within Aspen PlusTM defines this reference state as infinite dilution in the mixed solvent. For example, the activity coefficient approaches one as the concentration of carbon dioxide in the mixed solvent approaches zero. This reference state does not allow us to account for changes in the activity of carbon dioxide as a function of amine strength. For example, when the MDEA concentration on an acid gas free basis is 0 wt % (water), the activity coefficient of carbon dioxide approaches one as its concentration approaches zero

in water. If another calculation is performed in 50 wt % MDEA on an acid gas free basis, the activity coefficient of carbon dioxide will approach one as the concentration of carbon dioxide approaches zero. This would suggest that the activity of carbon dioxide is the same in a 50 wt % MDEA solution as it is in a 0 wt % MDEA mixture which is not useful.

To correct for this, the reference state for carbon dioxide is now defined as infinite dilution in water. This allows us to model the change in activity of carbon dioxide as a function of amine strength.

3.5 System Non-Idealities

This work uses the Soave-Redlich-Kwong equation of state to predict gas phase non-idealities. The liquid phase non-idealities are expressed by using the electrolyte-NRTL model. These models are now discussed individually.

3.5.1 Gas Phase Non-Idealities

The Soave-Redlich-Kwong equation of state (Soave, 1972) is used in this work. The following is its pressure explicit form.

$$P = \frac{RT}{V - b} - \frac{a \alpha}{V(V + b)} \quad (3.8)$$

where:

$$a = 0.42747R^2T_c^2/P_c$$

$$b = 0.08664RT_c/P_c$$

$$\alpha = [1 + (0.48508 + 1.55171\omega - 0.15613\omega^2)(1 - T_r^{0.5})]^2$$

T_c = Critical Temperature

P_c = Critical Pressure

ω = Accentricity Factor

$T_r = T/T_c$

And for Mixtures

$$a\alpha = \sum \sum y_i y_j (a\alpha)_{ij}$$

$$b = \sum y_i b_i$$

$$(a\alpha)_{ij} = (1-k_{ij})\sqrt{[(a\alpha)_i(a\alpha)_j]}$$

k_{ij} = interaction parameter between molecule i and j

The following expression is obtained for the fugacity coefficient when using the SRK equation of state.

$$\ln(\phi_i) = \frac{b_i}{b}(z-1) - \ln\left[z\left(1 - \frac{b}{V}\right)\right] + \frac{a\alpha}{bRT}\left[\frac{b_i}{b} - \frac{2}{a\alpha}\sum_j y_j(a\alpha)_{ij}\right]\ln\left(1 + \frac{b}{V}\right) \quad (3.9)$$

where:

$$z = PV/RT$$

For practical purposes, equation 3.8 must be solved iteratively to obtain the specific volume at a given temperature and pressure. Once this has been accomplished, equation 3.9 can be used to solve for the fugacity coefficient of a component.

In carbon dioxide VLE data, the pressures are usually not above 100 atmospheres. At these conditions, the gas phase is usually completely carbon dioxide and the vapor side non-idealities are well represented by the SRK equation of state and are not a major area of study in this work. In industrial acid gas treating, column pressures can be quite high and the vapor phase can be a complex mixture of hydrocarbons at which condition, the vapor side non-idealities are appreciable but still dealt with satisfactorily by the SRK equation of state.

3.5.2 Liquid Side Non-Idealities

Liquid phase non-idealities are usually represented by an excess Gibbs free energy model that accounts for unequal intermolecular forces in a mixture. An

understanding of reference states should also be kept in mind when throughout this discussion. A solution is arbitrarily called ideal at its reference state that must be carefully defined in order for the excess Gibbs free energy model to match the reference state. The electrolyte-NRTL model used to describe non-idealities in the liquid phase in this work.

3.5.3 The Electrolyte-NRTL Model: Historical Development and Structure

The representation of solution phase non-idealities in electrolyte systems has been a challenge that dates back almost one hundred years. Solutions are difficult to model because of the strong non-idealities present and the nature of the intermolecular forces. In gas treating, it is common to find electrolyte solutions with ionic strengths and solvent concentrations as high as 4 or 5 molar. These solutions are strong enough in solvent concentration and ionic strength that there are important molecule/molecule interactions as well as important ion-ion interactions.

According to Coulomb's law, the forces between ions vary as the inverse of the square of the distance of separation. For this reason, these forces are exhibited over a longer range of separation than dispersion or other forces characteristic of molecular interactions which vary as the inverse of the sixth power of the distance of separation. The characterization of acid gas treating systems, therefore, depends on being able to predict the close range molecule / molecule and ion / molecule forces as well as the long range ion/ion forces.

3.5.3.1 Long Range Ionic Forces

The excess Gibbs free energy term predicted by the Pitzer-Debye-Huckel model as documented by Chen (1979) is described below:

$$\frac{G^{EX.PDH}}{RT} = -\sum_k x_k \left(\frac{1000}{M_s} \right)^{\frac{1}{2}} \left(\frac{4A_\phi I_x}{\rho} \right) \ln \left(1 + \rho I_x^{\frac{1}{2}} \right) \quad (3.10)$$

$$A_\phi = \frac{1}{3} \left(\frac{2\pi N_o d}{1000} \right)^{\frac{1}{2}} \left(\frac{e^2}{DkT} \right)^{\frac{3}{2}}$$

$$I_x = \frac{1}{2} \sum_i Z_i^2 x_i$$

where:

A_ϕ = The Debye Huckel Parameter

I_x = Ionic Strength on a Mole Fraction Basis

ρ = Closest Approach Parameter

M_s = Molecular Weight of the Solvent

N_o = Avagadro's Number

d = Solvent Density

D = Solvent Dielectric Constant

k = Boltzmann's Constant

This expression accounts for the long range coulombic forces between ion / ion pairs and molecules / ions.

3.5.3.2 Short Range Molecular Forces

In addition to long range coulombic forces, molecules also exert forces on each other due to dispersion and induction forces or specific chemical forces such as hydrogen bonding. These forces influence molecules over a shorter distance than the coulombic forces discussed in the previous section. Several empirical theories exist regarding the excess Gibbs free energy of molecules in solutions. One such theory is the Non-Random Two Liquid (NRTL) theory proposed by Renon and Prausnitz (1968).

The NRTL theory considers the liquid to be composed of different types of cells that have one molecule at the center of the cell and the other molecules of the solution surrounding the central molecule.

Renon and Prausnitz developed expressions for the excess Gibbs free energy due to short range interactions.

$$G^{EX,NRTL} = \sum_{i=1}^N x_i \frac{\sum_{j=1}^N \tau_{ji} G_{ji} x_j}{\sum_{k=1}^N G_{ki} x_k} \quad (3.11)$$

where:

$$\tau_{ji} = (g_{ji} - g_{ii}) / RT$$

$$G_{ji} = \rho_{ji} \exp(-\alpha_{ji} \tau_{ji})$$

The τ_{ji} parameters are the difference between the interaction energy of molecule i with itself and the energy of molecule i with j . They are treated as adjustable parameters and may be positive or negative values. The parameter α_{ij} is the non-randomness parameter. It is an adjustable parameter as well that usually takes on values between 0.1 and 0.4.

3.5.3.3 Combination of Long Range and Short Range Forces

Solutions of electrolytes exhibit long range forces due to coulombic charge separation and close range forces due to two and three body interactions. The 'Electrolyte NRTL' model of Chen et al. (1982) uses the NRTL equation and is the model that has been used by previous investigators studying the thermodynamics of acid gas systems (Posey, 1996, Austgen, 1989). The original model considers different sorts of molecular cells analogous to the cells in the NRTL model. There are three cells considered: cells with cations at the center, anions at the center, and

molecular species at the center. There are important assumptions involved in the derivation of the close range NRTL terms associated with each of these terms. The first is the assumption of local electroneutrality in each cell. This assumption states that the net charge around each cell should be zero. The second assumption is the assumption of like ion repulsion. This assumption states that no two ions of similar sign will be in the same cell. A paper by Chen and Evans (1986) extended the original model to represent multicomponent electrolyte systems in a thermodynamically consistent manner. Mock et al. (1986) showed that the effect of salts on multi-solvent systems could be predicted using the NRTL model. Mock was primarily interested in the activities of multiple solvents as a function of ionic strength.

An important attribute of the Debye-Huckel formulation is that it considers the work and hence the excess Gibbs free energy of charging an ion in a given solvent. Therefore, the associated reference state of the Debye-Huckel formulation is the infinite dilute state in the solvent being studied. In order to have the reference state changed to infinite dilution in water, Scaufaire et al.(1989) added a Born Correction. Using the latest version of the electrolyte NRTL model, the expression for the excess Gibbs free energy becomes:

$$G^{EX} = G^{EX,PDH} + G^{EX,BORN} + G^{EX,NRTL} \quad (3.12)$$

The Pitzer-Debye-Huckel term is the same as described in section 2.7.1. The Born correction accounts for the difference between the dielectric constant of the solvent and of water.

$$\frac{G^{EX,BORN}}{RT} = \frac{e^2}{2kT} \left(\frac{1}{D_m} - \frac{1}{D_w} \right) \sum_i \frac{x_i z_i^2}{r_i} 10^{-2} \quad (3.13)$$

where

r_i = Born Radius

D_m = Dielectric Constant of the Mixed Solvent

D_w = Dielectric Constant of Water

The short range NRTL contributions to equation 2.41 follow the same format as equation 2.40. The three type of cells discussed above are considered. The resulting expression is shown below where the subscripts m,c, and a refer to molecules, cations, and anions respectively.

$$\begin{aligned} \frac{G^{EX,NRTL}}{RT} = & \sum_m x_m \frac{\sum_j x_j G_{jm} \tau_{jm}}{\sum_k x_k G_{km}} + \sum_c x_c \sum_{a'} \frac{x_{a'}}{\sum_{a''} x_{a''}} \frac{\sum_j x_j G_{jc,a'c} \tau_{jc,a'c}}{\sum_k x_k G_{kc,a'c}} \\ & + \sum_a x_a \sum_{c'} \frac{x_{c'}}{\sum_{c''} x_{c''}} \frac{\sum_j x_j G_{ja,c'a} \tau_{ja,c'a}}{\sum_k x_k G_{ka,c'a}} \end{aligned} \quad (3.14)$$

where

$$G_{cm} = \frac{\sum_a x_a G_{ca,m}}{\sum_{a'} x_{a'}} \quad G_{cm} = \frac{\sum_c x_c G_{ca,m}}{\sum_{c'} x_{c'}}$$

$$\alpha_{cm} = \frac{\sum_a x_a \alpha_{ca,m}}{\sum_{a'} x_{a'}} \quad \alpha_{cm} = \frac{\sum_a x_a \alpha_{ca,m}}{\sum_{a'} x_{a'}}$$

$$G_{jc,a'c} = \exp(-\alpha_{jc,a'c} \tau_{jc,a'c}) \quad G_{ja,c'a} = \exp(-\alpha_{ja,c'a} \tau_{ja,c'a})$$

$$G_{im} = \exp(-\alpha_{im} \tau_{im}) \quad G_{im} = \exp(-\alpha_{im} \tau_{im})$$

$$\tau_{ma,ca} = \tau_{am} - \tau_{ca,m} + \tau_{m,ca} \quad \tau_{mc,ac} = \tau_{cm} - \tau_{ca,m} + \tau_{m,ca}$$

x_j = molefraction of j multiplied by charge of j (unity for molecules)

The first term in equation 2.42 is equivalent to the molecular NRTL term discussed in section 2.7.1. The next two terms are summations for cells with cations and anions at the center. The $\tau_{ca,m}$ and $\tau_{m,ca}$ parameters are treated as adjustable parameters just like molecule / molecule τ in the molecular NRTL. The molecule/cation and molecule/anion parameters are solved for using the other parameters. All salt pair / molecule and molecule / salt pair τ parameters in this work are assumed to have the following temperature dependent form.

$$\tau = A + B \left(\frac{1}{T} - \frac{1}{T_{ave}} \right) \quad (3.15)$$

Molecule / molecule parameters still have the old temperature dependent form.

$$\tau = A + \frac{B}{T} \quad (3.16)$$

3.6 Solution Techniques for Chemical Equilibrium Problems

There are two distinct methods used in this work for solving the equilibrium relationships in the liquid. The stoichiometric method is used in chapter 4 and 7. The non-stoichiometric method is used for the stand alone electrolyte NRTL model developed by Austgen (1989) and used in Chapter 5 for PZ / MDEA / CO₂ / H₂O systems

3.6.1 Stoichiometric Method

The stoichiometric method is the procedure of considering the equilibrium constant relationships as direct equations to be solved. The stoichiometric method

for an ideal solution has already been illustrated in the example problem of section 3.2. Rigorously, however we would consider the activity of each species instead of the mole fraction. The stoichiometric method has the advantage of being easily visualized and straightforward to set up if the reaction chemistry is known.

3.6.2 Non-Stoichiometric Method

The advantage of the non-stoichiometric method is that no knowledge of the reaction chemistry is needed. It is only necessary to know which species are present in the solution at equilibrium (Smith and Missen, 1988). This is a trivial advantage if only a few species are being considered. As a general rule, the non-stoichiometric method is only advantageous if a large amount of species are present (>30).

Mathematically the non-stoichiometric method considers the problem as a minimization of free energy subject to constraints imposed by material balances for each element in the system. The method of Lagrangian multipliers is often used to solve the constrained minimization.

To describe the non-stoichiometric method in more detail, we consider our example problem once again. In our problem, we have five species (CO_2 , H_2O , MDEA, MDEAH^+ and HCO_3^-) and four elements (C, H, O and MDEA). Although MDEA is not an element, mathematically we can consider it one and we can express each species using these four elements. Mathematically,

$$\min \left(\sum_{i=1}^N n_i \mu_i \right) \quad (3.17)$$

Subject To:

$$n_{\text{CO}_2} + n_{\text{HCO}_3^-} = n_{\text{C},T} \quad (3.18)$$

$$n_{\text{MDEA}} + n_{\text{MDEAH}^+} = n_{\text{MDEA},T} \quad (3.19)$$

$$2n_{\text{H}_2\text{O}} + n_{\text{MDEAH}^+} + n_{\text{HCO}_3^-} = n_{\text{H},\text{T}} \quad (3.20)$$

$$n_{\text{H}_2\text{O}} + 3n_{\text{HCO}_3^-} + 2n_{\text{CO}_2} = n_{\text{O},\text{T}} \quad (3.21)$$

Where equations 3.18 to 3.21 represent material balances for each of the four elements (C, MDEA, H and O respectively). In these equations, $n_{i,\text{T}}$ represents the total moles of element i present in the system.

Using the method of Lagrangian multipliers, we obtain the following set of algebraic equations that need to be solved in conjunction with equations 3.18 to 3.21:

$$\mu_{\text{H}_2\text{O}} - 2\lambda_{\text{H}} - \lambda_{\text{O}} = 0 \quad (3.22)$$

$$\mu_{\text{CO}_2} - 2\lambda_{\text{O}} - \lambda_{\text{C}} = 0 \quad (3.23)$$

$$\mu_{\text{MDEA}} - \lambda_{\text{MDEA}} = 0 \quad (3.24)$$

$$\mu_{\text{MDEAH}^+} - \lambda_{\text{MDEA}} - \lambda_{\text{H}} = 0 \quad (3.25)$$

$$\mu_{\text{HCO}_3^-} - \lambda_{\text{H}} - \lambda_{\text{C}} - 3\lambda_{\text{O}} = 0 \quad (3.26)$$

Here, λ are the Lagrangian multipliers.

The combination gives 9 equations in 9 unknowns which include the chemical potential of each five species and the 4 Lagrangian multipliers. It is clear that the non-stoichiometric method increases the number of equations needed to be solved. Several previous investigators have developed algorithms using the nonstoichiometric method (Austgen, 1989, Glasscock, 1990). For this reason, the non-stoichiometric method is used in chapter 5 of this work to describe the PZ / MDEA / H_2O / CO_2 system.

Chapter 4

Absorption of Carbon Dioxide into Aqueous Piperazine: Reaction Kinetics, Mass Transfer and Solubility

The addition of a primary or secondary amine to a tertiary amine has found widespread application in the absorption and removal of carbon dioxide from process gas. The success of these solvents is due to the high rate of reaction of the primary or secondary amine with carbon dioxide combined with the low heat of reaction of the tertiary amine. By adding small amounts of the primary or secondary amine, a high rate of absorption is seen in the absorber while a low energy of regeneration is required in the stripper.

One such blend of amines is piperazine (PZ) activated methyldiethanolamine (MDEA). These solvents have been used successfully for high capacity carbon dioxide removal in ammonia plants and are patented by BASF (Appl et al., 1982). They have been effective at much lower activator concentration than conventional blends (DGA[®]/MDEA, DEA/MDEA).

The equilibrium solubility of carbon dioxide in aqueous MDEA solutions has been experimentally studied by several investigators (Jou et al., 1982,1984; Jou et al., 1993; Bhairi, 1984; Ho and Eguren, 1988, Austgen et al., 1991). Knowledge about the chemical reactions of carbon dioxide with MDEA has been combined with theories of electrolyte solutions in order to model the vapor liquid equilibrium as well (Bishnoi and Rochelle, 2000; Posey and Rochelle, 1997;

Austgen et al., 1989). Similarly, the reaction kinetics of carbon dioxide with MDEA has been well documented by several investigators (Pacheco, 1998; Rinker et al., 1995; Versteeg, 1987; Critchfield, 1988).

The equilibrium solubility of carbon dioxide in blends of piperazine / MDEA as well as the rate of absorption into these blends has been studied by Xu and coworkers (Xu, et al., 1992; Xu et al., 1998). Kaganoi (1997) extended the database of experimental work by studying piperazine in the absence of MDEA as well as piperazine / MDEA blends. This chapter further studies aqueous piperazine.

CO₂ absorption rates were measured in a region where the rate constant of carbon dioxide with piperazine could be quantified. An Arrhenius rate expression is presented for the carbon dioxide / piperazine reaction. Solubility data at moderately low to high carbon dioxide loading were obtained in order to extract information about the speciation of the carbon dioxide / piperazine / water system. A carbamate stability constant and a pK_a for piperazine carbamate were regressed from the data and the resulting speciation model was compared to pH data and ionic conductivity data. A dicarbamate equilibrium constant was estimated from proton, ¹³C NMR and C-H correlation NMR.

4.1 Experimental Apparatus and Methods

Figure 4.1 shows the wetted wall column used in this work. The wetted wall column was constructed from a stainless steel tube with a well defined surface area (38.52cm²) and a characteristic liquid film mass transfer coefficient similar to that of a packed tower. The stainless steel tube is 9.1 cm long and has an outside diameter of 1.26 cm. Figure 4.2 shows the overall flow diagram of the apparatus used in this study to obtain rate of absorption and solubility data. The apparatus was originally built by Mshewa (1995) and modifications were made by

Pacheco (Pacheco, 1998; Pacheco et al., 1999).

Flow from two gas cylinders was regulated using Brooks mass flow controllers. A 20 SLPM flow controller was usually set at 25% for the nitrogen flow. A 1 SLPM flow controller was usually used for a blend mixture of 0.5 vol% CO₂ in nitrogen. For experiments at higher loading and CO₂ partial pressure, pure CO₂ was used instead of the mixture gas. The gas was sent to a water saturator that is kept at the same temperature as the wetted wall column. The saturator consisted of a 400 mL calorimeter bomb filled with water. The gas was sparged using an open stainless steel tube at the bottom of the bomb. After the water saturator, the gas was sent to the wetted wall column where it was contacted with the amine solution. Total pressures used in this work varied from 1 to 8 atm. In the wetted wall, a portion of the carbon dioxide was transferred from the gas phase to the liquid phase.

The gas was sent from the top of the column through a needle valve where the pressure was reduced to atmospheric. From the downstream side of the needle valve, the gas was sent to a condenser that consisted of an Erlenmeyer flask submerged in ice water. The gas was then passed on to a series of Horiba PIR 2000 carbon dioxide analyzers where the outlet carbon dioxide concentration was measured by infrared spectroscopy. Three analyzers were used, each having a different concentration range (0-25%, 0-1%, and 0-0.25%). This series of analyzers allows the accurate measurement of carbon dioxide down to 100-200 ppm. Calibration of these analyzers was performed by bypassing the reactor, varying the concentration of CO₂ in the gas to the analyzer and observing the analyzer reading at each CO₂ concentration.

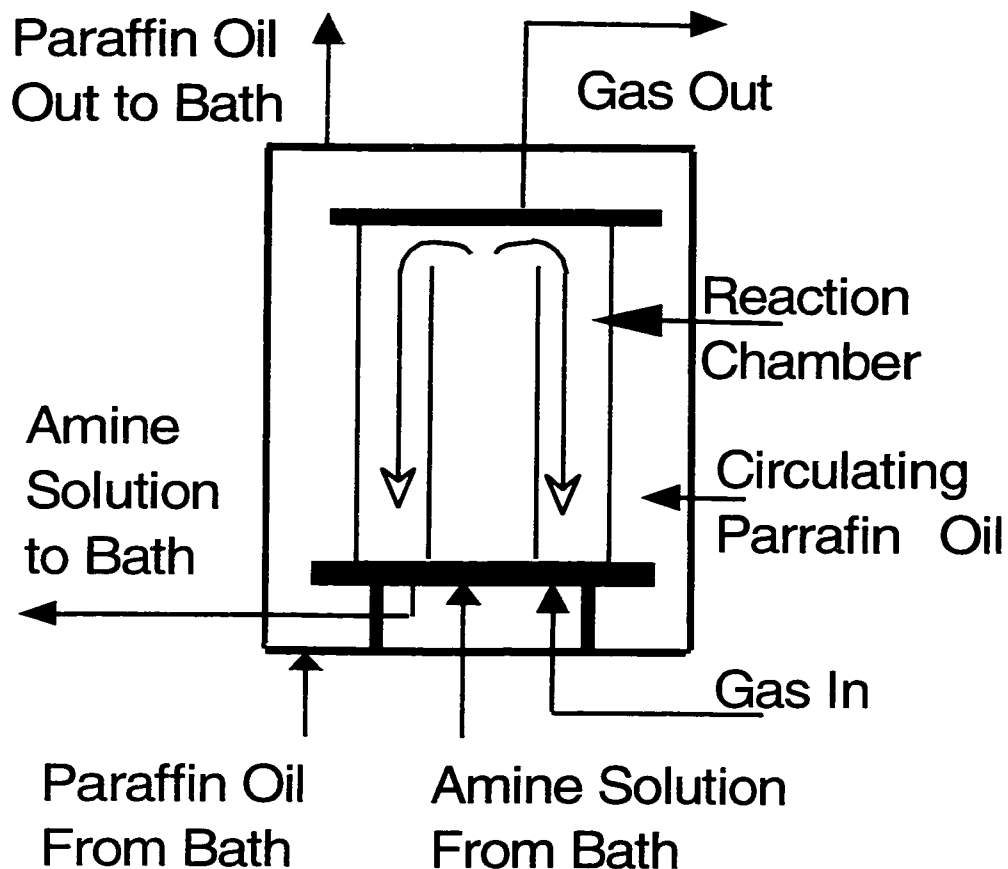


Figure 4.1: Detailed column diagram

The amine solution was kept in a reservoir and passed through a coil submerged in a paraffin oil bath to heat it to the reactor temperature. Anhydrous piperazine flakes (CAS No. 110-85-0, 99.9% purity) were obtained from Aldrich Chemical (Lot No. 09525AU) and mixed with de-ionized water to make up the amine solution. Two reservoir configurations were used in this work: one with a total liquid holdup of 400 cm^3 and the other with a 2400 cm^3 holdup.

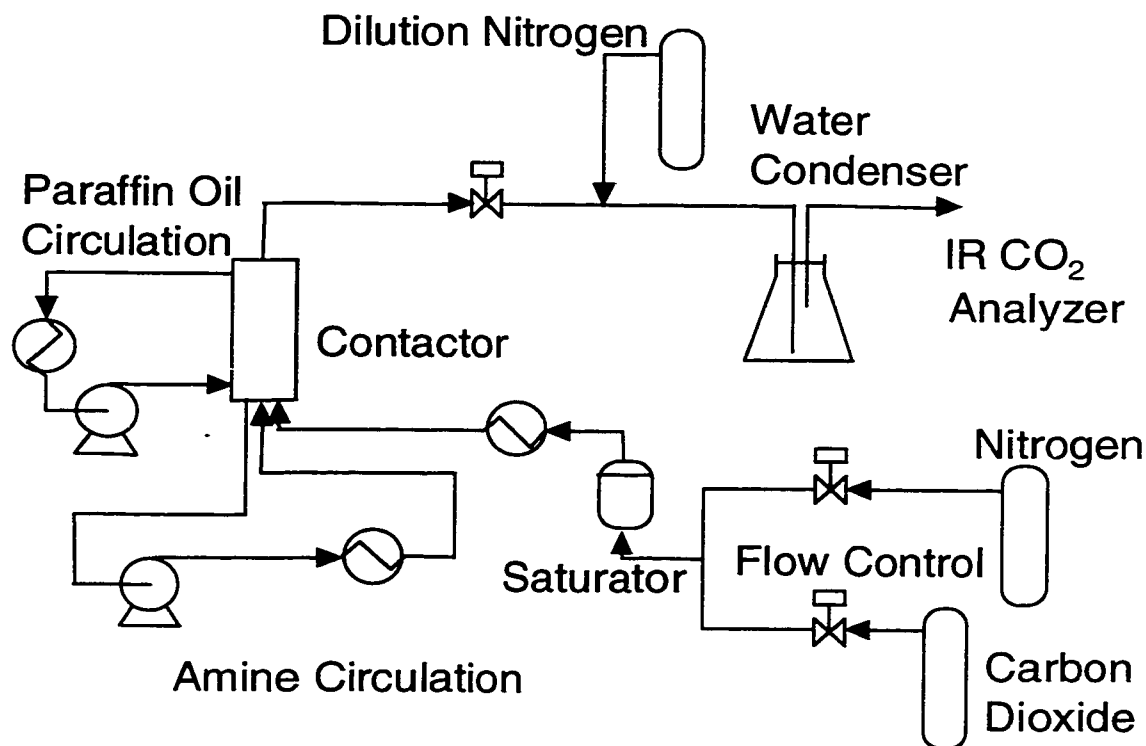


Figure 4.2: Overall flowsheet of equipment

The removal of the reservoir from the paraffin oil bath and the introduction of the coiled heat exchanger allowed us to keep the reservoir beside the oil bath. This allowed us to readily change the reservoir volume without having to fit it in the oil bath. A series of stainless steel bombs (1L) were added in series to another 400 mL calorimeter bomb to adjust the size of the reservoir. The flow of amine solution was provided by a Cole-Parmer micropump and was measured by a liquid rotameter. The liquid flow rate used in this work was around $2 \text{ cm}^3/\text{s}$. The flowrate was assumed to be a function of solution viscosity and rotameter reading. The rotameter was calibrated by flowing solutions of MDEA through the rotameter and making tables of flowrate vs. rotameter reading. The results have

been correlated using the following relationship.

$$Q_L = Ax^2 + Bx + C \quad (4.1)$$

where

$$\begin{aligned} A &= -1.5361 \cdot 10^{-4} \mu^2 + 1.9243 \cdot 10^{-2} \\ B &= 6.6596 \cdot 10^{-3} \mu^2 - 9.3319 \cdot 10^{-2} \mu + 0.35810 \\ C &= 2.0916 \cdot 10^{-3} \mu^2 - 2.5337 \cdot 10^{-2} \mu + 5.9803 \cdot 10^{-2} \end{aligned}$$

The paraffin oil in the bath is also circulated to the wetted wall column, keeping the entire apparatus at a uniform temperature.

Rate of absorption was determined from the gas phase material balance using the measured inlet and outlet gas concentration. Periodically, liquid samples were withdrawn from a sample port close to the reactor outlet and analyzed for total carbon dioxide loading using the same method as previous investigators (Pacheco et al., 1999; Pacheco, 1998; Kaganoi, 1997; Mshewa, 1995). This is done by introducing the sample into a solution of phosphoric acid which reverses the amine / carbon dioxide reaction and liberates all the carbon dioxide as gas. This gas was swept with nitrogen carrier gas to an IR analyzer where the total carbon dioxide was determined by measuring peak height. The sensitivity of the technique can be adjusted by modifying the volumes used. For data points at low loading, 300 μ L of solution from the reactor was combined with 3 mL of DI H₂O to form a sample vial. For higher loading samples, 150 μ L of solution from the reactor was combined with 10 mL of DI H₂O. Usually samples of 50 μ L from the sample vial were input into the analyzer. Calibration of the analyzer was achieved by introducing known amounts (between 10 μ L and 200 μ L) of 7mM Na₂CO₃ into the analyzer. The method was found to be reproducible within 2%.

Solubility was measured by bracketing equilibrium with both absorption and desorption measurements. The partial pressure in the contactor was adjusted

while keeping the solution loading approximately constant. A solubility data point at a given solution loading is then obtained by finding the partial pressure that corresponds to an interpolated flux of zero.

The liquid film mass transfer coefficient of the wetted wall column was measured by Mshewa (1995) and Pacheco (1998) by carbon dioxide desorption from water and ethylene glycol mixtures. Pacheco found that the theoretical model of Pigford (1941) predicted the experimental data within 15%. This model relies on solving the momentum balance (Bird et al., 1960) for a falling film to determine the film thickness (δ) and surface velocity (u_{surf}) where W is the wetted perimeter length.

$$\delta = \sqrt[3]{\frac{3\mu Q}{\rho g W}} \quad (4.2)$$

$$u_{surf} = \frac{\rho g \delta^2}{2\mu} \quad (4.3)$$

$$\tau = \frac{l}{u_{surf}} \quad (4.4)$$

The mass transfer coefficient is then given as a function of the parameter $\eta = D\tau/\delta^2$, where τ is the surface contact time calculated from the surface velocity and the length of the contactor ($l=9.1\text{cm}$). The contact area between liquid and gas phases is a (38 cm^2).

$$\Theta = \frac{[A]_b^L - [A]_b^{L,out}}{[A]_b^L - [A]_b^{L,in}} = 0.7857 \exp(-5.12 \ln \eta) + 0.1001 \exp(-39.2 \ln \eta) + 0.036 \exp(-105.6 \ln \eta) + 0.0181 \exp(-204.7 \ln \eta) \quad ; \quad \text{for } \eta > 0.01 \quad (4.5)$$

$$\Theta = \frac{[A]_b^L - [A]_b^{L,out}}{[A]_b^L - [A]_b^{L,in}} = 1 - 3 \sqrt{\frac{\eta}{\pi}} \quad ; \quad \text{for } \eta < 0.01 \quad (4.6)$$

$$k_{L,A}^o = \frac{Q_L}{a}(1 - \Theta) \quad (4.7)$$

Pacheco (1998) determined the gas phase mass transfer coefficient of the apparatus by absorption of carbon dioxide into aqueous MEA. The Pacheco correlation was confirmed in this work by the absorption of sulfur dioxide into sodium hydroxide solutions at greater gas rates (5-6 SLPM). Instead of using the IR analyzers for CO₂, a Perkin-Elmer system 2000 FT/IR analyzer was used. The SO₂ peak between 2370-2340 cm⁻¹ was analyzed while a baseline was taken at 2425-2424 cm⁻¹. Details of the Perkin Elmer system 2000 analyzer and basic procedures are given in Chisholm (1999). A baseline for the analyzer was taken by first sending approximately 3-5 SLPM N₂ through the wetted wall column. The liquid solution used was 0.1 M NaOH. After 30-40 minutes, approximately 0.1 SLPM of 5000 ppm SO₂ in N₂ was introduced after the reactor in order to calibrate the analyzer. After 30-40 minutes, the SO₂ mixture gas was moved to a port before the reactor and the removal of SO₂ was measured at the analyzer. Figure 4.3 and table 4.1 show the results of these experiments. The gas film mass transfer coefficient is given by:

$$Sh = 1.075 \left(Re \cdot Sc \cdot \frac{d}{h} \right)^{0.85} \quad (4.8)$$

where d is the hydraulic diameter of the annulus (0.44 cm) and h is the length of the column (9.1 cm).

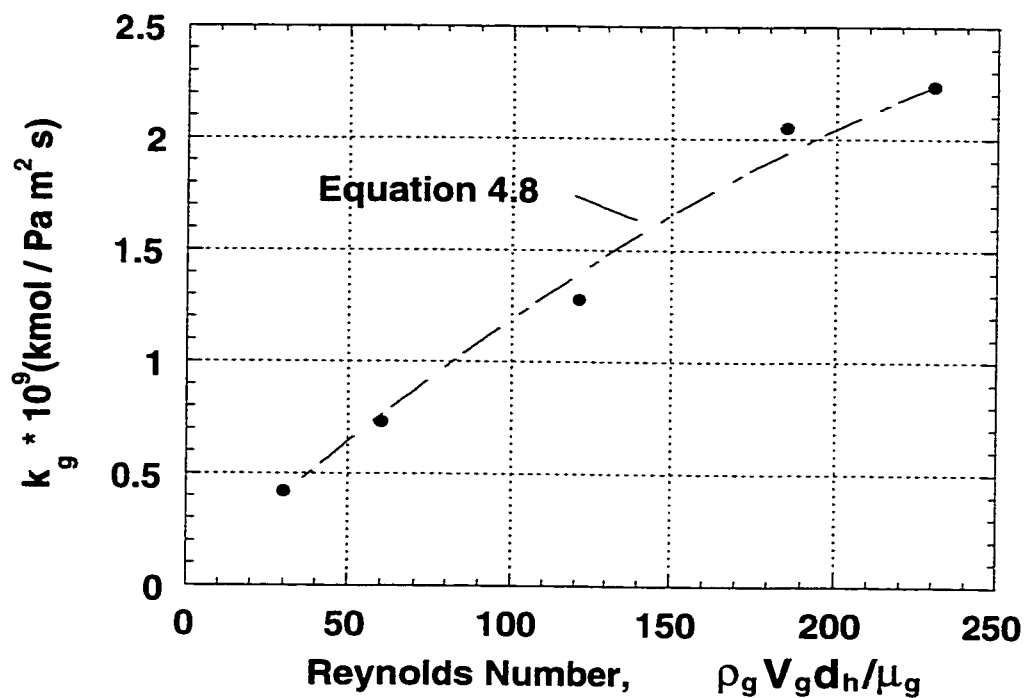


Figure 4.3: Gas film mass transfer coefficients at ambient temperature and high Reynolds number. SO₂ absorption into NaOH, P=3.8E5 to 4.5E5 Pa. d_h is the hydraulic diameter of the annulus (0.44 cm).

Table 4.1 Absorption of SO₂ into 0.1M NaOH at Ambient Temperature

Molefraction of SO ₂ *10 ⁵		Flux *10 ⁹ mol/cm ² s	Log Mean P _{SO2} (atm) *10 ⁴	kg (mols/atm cm ² s)*10 ⁵	N _{Re}
Inlet	Outlet				
8.85	2.96	5.35	2.4	2.26	229
11.0	3.76	5.32	2.6	2.08	185
16.8	5.1	5.61	4.3	1.30	121
24.6	6.2	4.23	5.7	0.74	60
46.1	10.1	4.39	10.0	0.42	30

Equation 4.8 matches measurements of the gas film mass transfer coefficient taken in this work within 10%. Note that there are two expressions used by Pacheco, one in his dissertation (1998) and one in his paper (Pacheco et al., 2000). Although very similar in their prediction, equation 4.8 was found to match the data taken in this work.

The reaction of carbon dioxide with piperazine is a much faster reaction than with conventional carbamate forming amines such as MEA, DGA[®], or DEA. For this reason, experiments had to be conducted at different conditions than the work of Pacheco (1998) and Mshewa (1995). Analysis of the data was simplified significantly by running experiments at three conditions: high gas rates, very low partial pressure and very low solution loading.

To minimize gas film resistance the flow rate used in this work was approximately 5 to 6 SLPM compared to the work of Pacheco (1998) where the overall flow rates were no greater than 2 SLPM. The overall gas phase resistance was 30 to 55% for data collected in this work. To avoid depletion of reactants at the interface, experiments in this work were run at very low partial pressure. This lowered the fluxes and mass transfer in the liquid film was limited almost purely by reaction kinetics and not by the ability of piperazine to diffuse to the vapor liquid interface. Since very little equilibrium data is available, most of the rate experiments in this work were conducted at very low loading (fresh solution) so that the equilibrium partial pressure was essentially zero. In order to accommodate the larger gas rates, tubing from the wetted wall column to the condenser and analyzer was increased from 1/8" to 1/4". The piperazine solution was usually titrated with 2N HCl at the beginning and end of each experiment in order to determine the solution concentration. Although no large differences in concentration were observed, a small decrease in PZ concentration usually occurred over the course of long experiments, probably due to the volatility of the

amine and loss to the gas phase. As a general rule, fresh amine solution was used each experiments.

The rate of absorption has been determined from a gas phase material balance and this has been combined with the gas/liquid contact area to determine flux. Equations 2.15 and 2.20 have been used to extract information on the kinetics of piperazine with carbon dioxide.

All NMR data was obtained at UT's Department of Chemistry and Biochemistry NMR laboratories. Samples of 25mL were prepared by using D₂O solvent and the PZ flakes described above. For loaded samples, CO₂ was sparged through the solution for approximately 1 hour. At this point, the solution loading was quite high and could be mixed with unloaded solution to obtain samples at intermediate loading. Usually 1.5 mL of sample was introduced into the NMR tube. Proton, ¹³C and H-C close range correlation was requested for all samples. Samples were also analyzed for loading before and after the NMR experiments. Loading was usually found to remain constant, however a decrease of approximately 5% was observed for some samples at very high loading probably due to CO₂ escaping from the plastic top of the NMR tubes.

4.2 Data analysis

The data presented in this work have been obtained at conditions that greatly simplify the mathematical treatment of the mass transfer problem. The most significant simplification arises from the pseudo first order assumption for kinetics discussed in Chapter 2.

$$\begin{aligned} R_{\text{CO}_2} &= k_2 [\text{PZ}] \{ [\text{CO}_2] - [\text{CO}_2]^* \} = k_1 \{ [\text{CO}_2] - [\text{CO}_2]^* \} \\ k_1 &= k_2 [\text{PZ}]_{\text{BULK}} \end{aligned} \quad (4.9)$$

where [CO₂]* is the equilibrium concentration of carbon dioxide.

In most experiments conducted, the equilibrium partial pressure will approach zero since the solution loading is low. The enhancement factor will also be much greater than 1. With these simplifications, equation 2.15 becomes:

$$N_{\text{CO}_2} = \frac{\sqrt{k_2[\text{PZ}]D_{\text{CO}_2}}}{H_{\text{CO}_2}} P_{\text{CO}_2}^i \quad (4.10)$$

Values of the diffusion coefficient and Henry's law constant for carbon dioxide in water were used when analyzing the data. The diffusion coefficient of carbon dioxide in water was calculated with the correlation of Versteeg and van Swaaij. (1988):

$$D_{\text{CO}_2}^0 \text{ (cm}^2\text{/s)} = 0.0240 \exp \{-2122 / T \text{ (K)}\} \quad (4.11)$$

Pacheco (1998) correlated the Henry's Law constant for carbon dioxide in pure water measured by Versteeg and van Swaaij. (1988) and reported by Al-Ghawas et al. (1989):

$$H_{\text{CO}_2}^0 \text{ (atm cm}^3\text{ / mol)} = 1.7107\text{E}+07 \exp \{-1886.1 / T \text{ (K)}\} \quad (4.12)$$

4.3 Solubility and Speciation of Carbon Dioxide in Aqueous Piperazine

The distribution of ionic and molecular species in solution dictates the partial pressure of carbon dioxide in equilibrium with an aqueous piperazine solution loaded with carbon dioxide. This work presents equilibrium solubility data, ionic conductivity data, pH data (Kaganoi 1997) and proton and ^{13}C NMR data to gain insight into the speciation of aqueous piperazine systems.

4.4 Solubility Measurement and Modeling

Figure 4.4 shows three experimental points at 40°C that switch from desorption to absorption. All the data points in this series are at a loading of approximately 0.32. Interpolating the data to a flux of zero, an estimate of the equilibrium solubility can be made as 42 Pa for this temperature and solution loading. Note that the partial pressure of CO₂ used in figure 4.4 is the interfacial partial pressure estimated from the experimental flux and k_g .

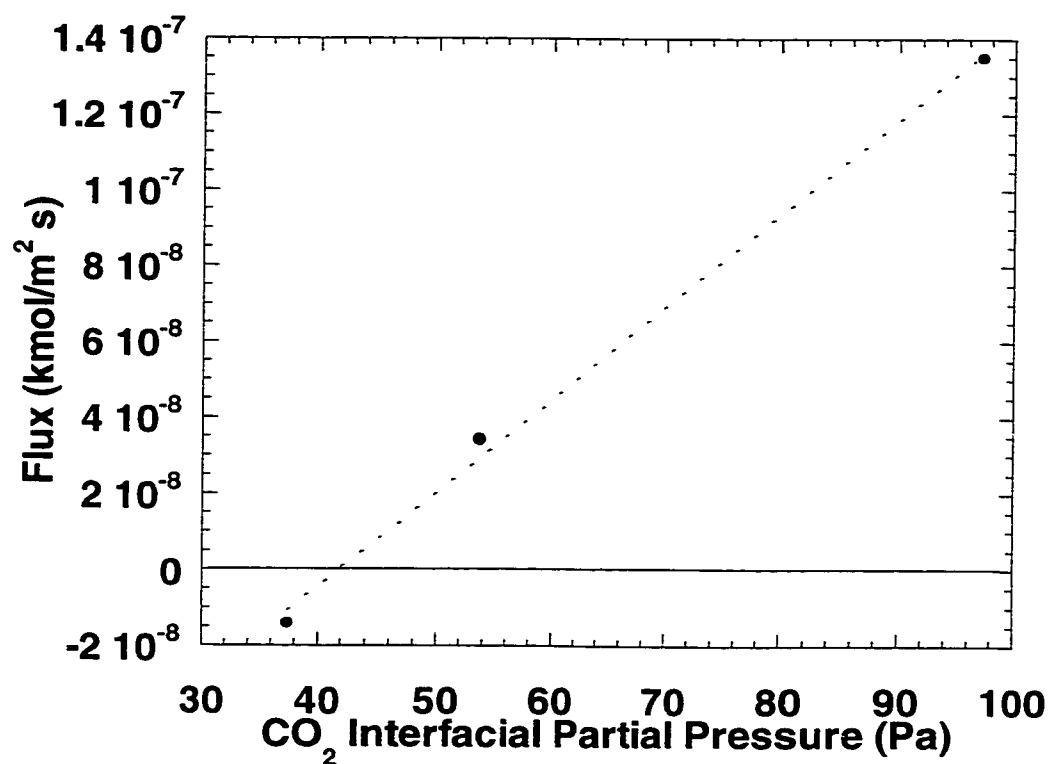


Figure 4.4: Flux interpolation to determine equilibrium solubility. Data points for absorption into 0.6 M piperazine at CO₂ loading of 0.32 kmol/kmol piperazine and 40°C

Table 4.2 presents the results of solubility measurements in 0.6 M piperazine solutions. The data was analyzed by solving a series of chemical reaction equilibria. The following reactions were considered:

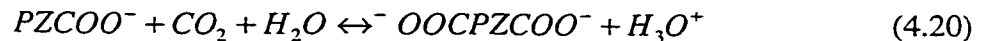
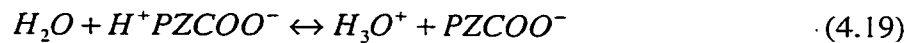
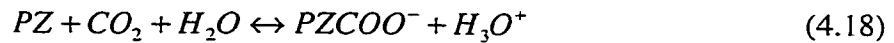
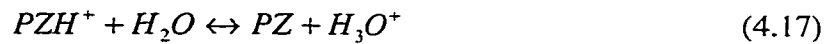
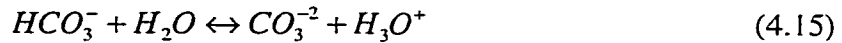
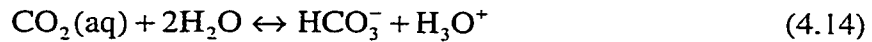
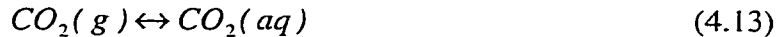


Figure 4.5 shows the molecular structure of the piperazine compounds in reactions 4.17 to 4.20. The second pK_a of piperazine to form diprotonated piperazine is 5.3 and is low enough that it can be neglected in this model. The model solves the chemical equilibria associated with these reactions along with the material and charge balance equations shown below using a Newton Raphson technique. A copy of the simple solubility and speciation code is included in Appendix C.

$$X_{CO_2T} = X_{CO_2} + X_{HCO_3^-} + X_{CO_3^{2-}} + X_{PZCOO^-} + X_{^+HPZCOO^-} + 2X_{^-OOC PZCOO^-} \quad (4.21)$$

$$X_{PZT} = X_{PZ} + X_{PZH^+} + X_{PZCOO^-} + X_{^+HPZCOO^-} + X_{^-OOC PZCOO^-} \quad (4.22)$$

$$\sum_i X_i = 1.0 \quad (4.23)$$

$$2X_{CO_3^{2-}} + 2X_{^-OOC PZCOO^-} + X_{HCO_3^-} + X_{OH^-} + X_{PZCOO^-} = X_{H_3O^+} + X_{PZH^+} \quad (4.24)$$

Equilibrium constants for equations 4.13 to 4.17 are available from literature (Posey, 1996). Equation 4.17 is the pK_a of piperazine and was found to be 9.48 at 40°C by Pagano et al. (1961). Equilibrium constants for equations 4.18 and 4.19 are estimated from the partial pressure data in table 4.2. Both these

equilibrium constants are adjusted by GREG (Generalized REGression package, Caracotsios (1987)) until the following objective function is minimized.

$$\sum_n \left(\log \left(\frac{P_{CO_2}^{PREDICTED}}{P_{CO_2}^{MEASURED}} \right) \right)^2 = \min \quad (4.25)$$

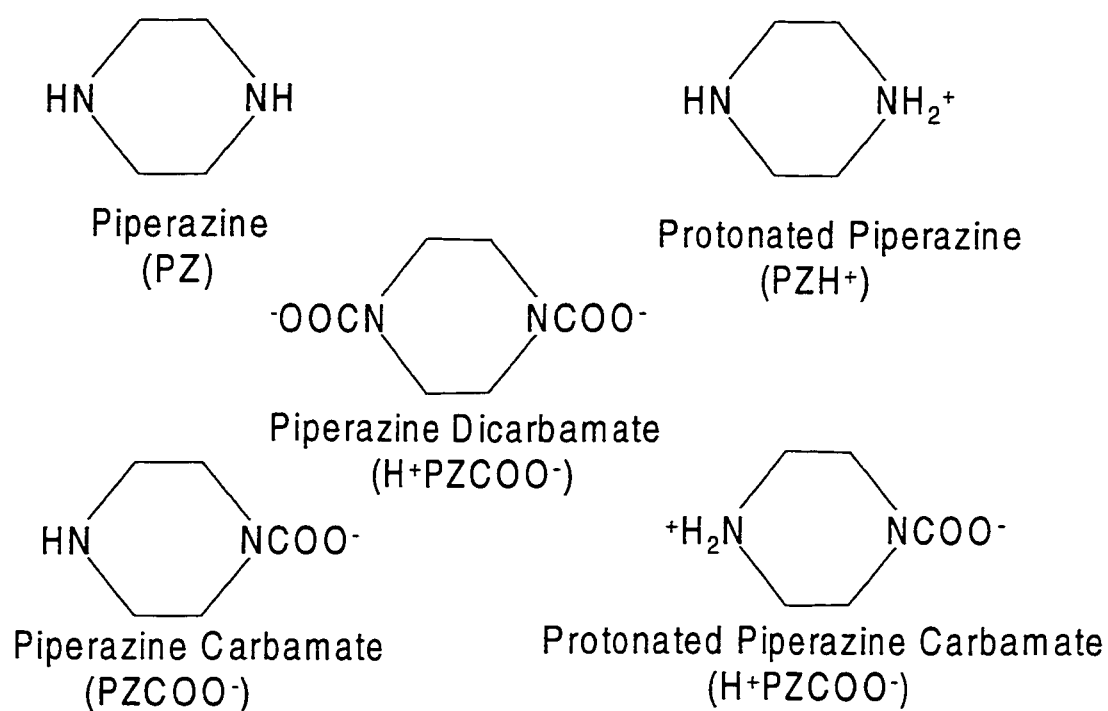


Figure 4.5: Molecular structures of piperazine species

Table 4.2: Solubility of Carbon Dioxide in 0.6M Piperazine Solutions.

Solution Loading ² (mol CO ₂ /mol PZ)	313K		Solution Loading (mol CO ₂ / mol PZ)	343K	
	CO ₂ Partial Pressure ¹ (Pa)			CO ₂ Partial Pressure (Pa)	
	Measured	Predicted		Measured	Predicted
0.32	32	31	0.16	63	57
0.32	42	31	0.22	132	127
0.47	80	118	0.35	448	468
0.48	110	129	0.42	648	842
0.55	250	234	0.47	1440	1249
0.61	450	395	0.59	3430	3097
0.72	850	1086	0.72	7875	8330
0.72	950	1086			
0.82	3000	3124			
0.96	40000	259124			

1. Estimated error in partial pressure is $\pm 30\%$ by propagation of error
2. Estimated error in loading is $\pm 5\%$ by propagation of error

The equilibrium constant for equation 4.20 was estimated by measuring ratios for dicarbamate to piperazine carbamate and protonated piperazine carbamate in proton NMR at 25°C as discussed in the following section. The dicarbamate equilibrium is given the same temperature dependence as piperazine carbamate equilibrium. The resulting equilibrium constants are presented in table 4.3 along with the equilibrium constants used for equations 4.14 to 4.17 and their literature sources. Table 4.3 also compares the carbamate formation constant to that of another secondary amine (DEA). The two constants are within a factor of 2 from each other which demonstrates that the thermodynamics of piperazine carbamate formation are comparable to other secondary amines.

Table 4.3: Equilibrium Constants for the Solubility Model, mole fraction based.

Equilibrium Constant	Eq. No.	Value at 40°C	ln K _x = A + B/T + C ln T			Source
			A	B	C	
$K_{14} = \frac{x_{HCO3-} x_{H3O+}}{x_{CO2} x_{H2O}^2}$	14	9.032E-09	231.4	-12092	-36.78	Posey (1996)
$K_{15} = \frac{x_{H3O+} x_{CO3=}}{x_{HCO3-} x_{H2O}}$	15	1.079E-12	216.0	-12432	-35.48	Posey (1996)
$K_{16} = \frac{x_{H3O+} x_{OH-}}{x_{H2O}^2}$	16	9.284E-18	132.9	-13446	-22.48	Posey (1996)
$K_{17} = \frac{x_{PZ} x_{H3O+}}{x_{H2O} x_{PZH+}}$	17	6.900E-12	-11.91	-4351	-	Pagano et al. (1961)
$K_{18} = \frac{x_{H3O+} x_{PZCOO-}}{x_{PZ} x_{CO2} x_{H2O}}$	18	1.144E-05	-29.31	5615	-	This Work Regressed
$K_{19} = \frac{x_{PZCOO-} x_{H3O+}}{x_{H+PZCOO-} x_{H2O}}$	19	1.267E-11	-8.21	-5286	-	This Work Regressed
$K_{20} = \frac{x_{H3O+} x_{-OOC PZCOO-}}{x_{PZCOO-} x_{CO2} x_{H2O}}$	20	2.62E-6	-30.78	5615	-	This Work NMR
$K_{DEA} = \frac{x_{DEACOO-} x_{H3O+}}{x_{DEA} x_{CO2} x_{H2O}}$	-	2.68E-5		N/A		Posey (1996)

The equilibrium constant for equation 4.19 is essentially a pK_a for piperazine carbamate. Hendrickson et al. (1970) suggest that the carboxylate group will participate in several resonance structures which will delocalize the

negative charge. This behavior makes the carbamate an electron withdrawing group that will, in turn, shift the electron density towards the carbamate making it harder to protonate the first nitrogen and slightly lowering its pK_a . Changing the units of equilibrium constant for equation 4.19 to be concentration based, we see that it represents a pK_a of 9.15 at 25°C which is slightly lower than the 9.48 of piperazine and in accordance to the theory presented. The estimation of equilibrium constants 15 and 16 represent an approach similar to that of Kent and Eisenberg (1976) to match VLE data for acid gas solubility.

This speciation and solubility model has been used to predict the partial pressure of carbon dioxide and the mole fractions of species in solution as a function of amine loading. Figure 4.6 shows the predicted partial pressure of carbon dioxide. It can be seen that the data points obtained in this work match the model predictions quite well.

Figure 4.7 shows the distribution of species as a function of loading. As carbon dioxide is added to a fresh solution, the dominant product is piperazine carbamate. At a loading of approximately 0.6 the carbamate is progressively replaced by protonated carbamate. It is around this loading that the pH of the solution becomes low enough to protonate the carbamate. Figure 4.7 also shows the two dicarbamate concentrations predicted by NMR.

4.5 Supporting Data

The resulting model has also been compared to other data on the pH, ionic conductivity and NMR response. It is seen that the model is able to rationalize these data without any further modifications. Since the model provides us with a prediction of the speciation, it can be used to compare pH predictions to measurements. Figure 4.8 shows the pH data of Kaganoi (1997) in 0.6M piperazine at 25°C along with model predictions.

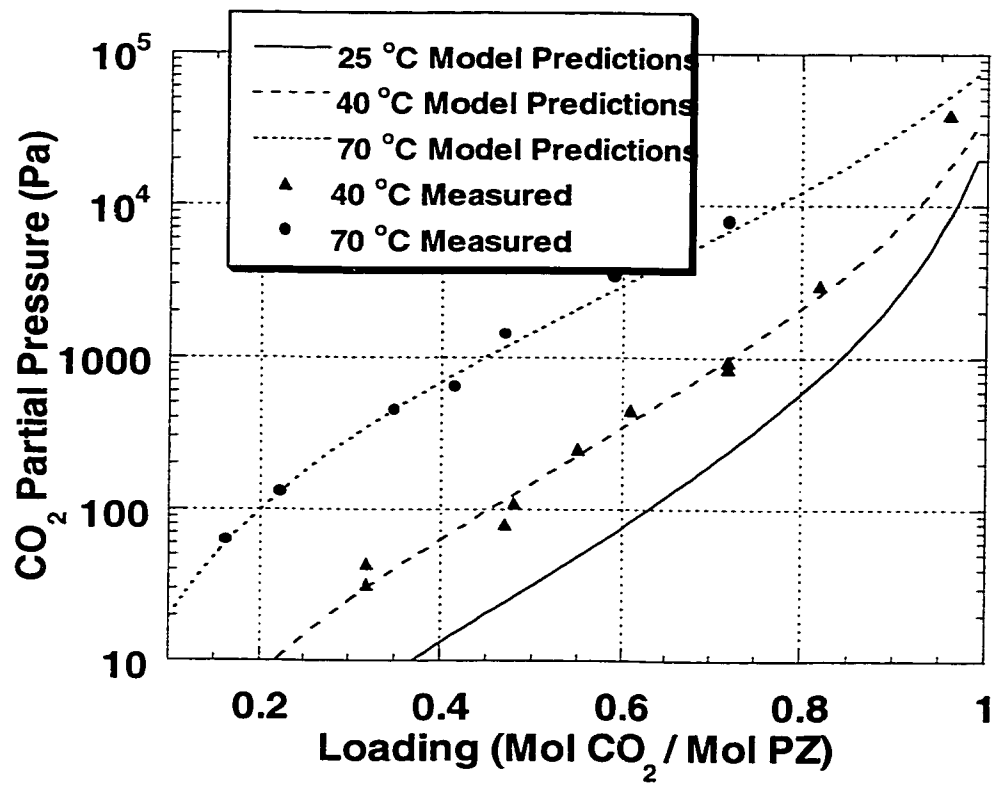


Figure 4.6: Partial pressure predictions compared to experimental results in 0.6M piperazine

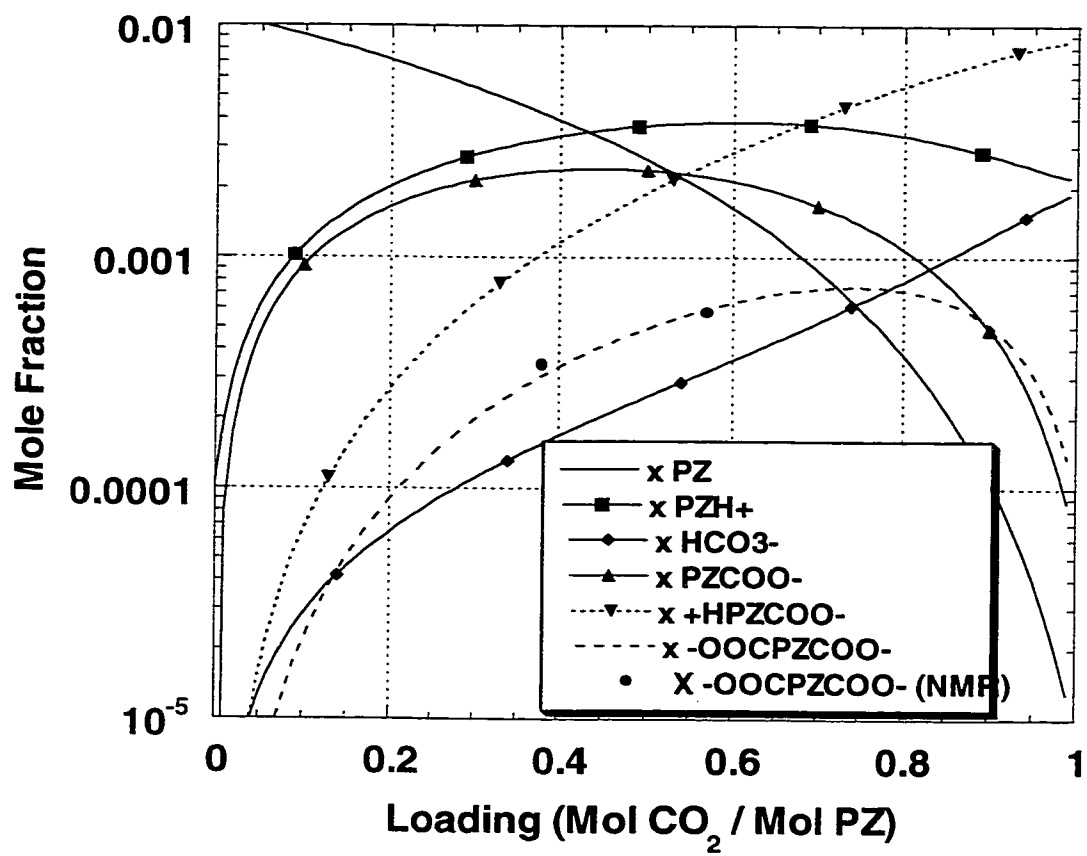


Figure 4.7: Predicted speciation of 0.6 M piperazine at 25°C

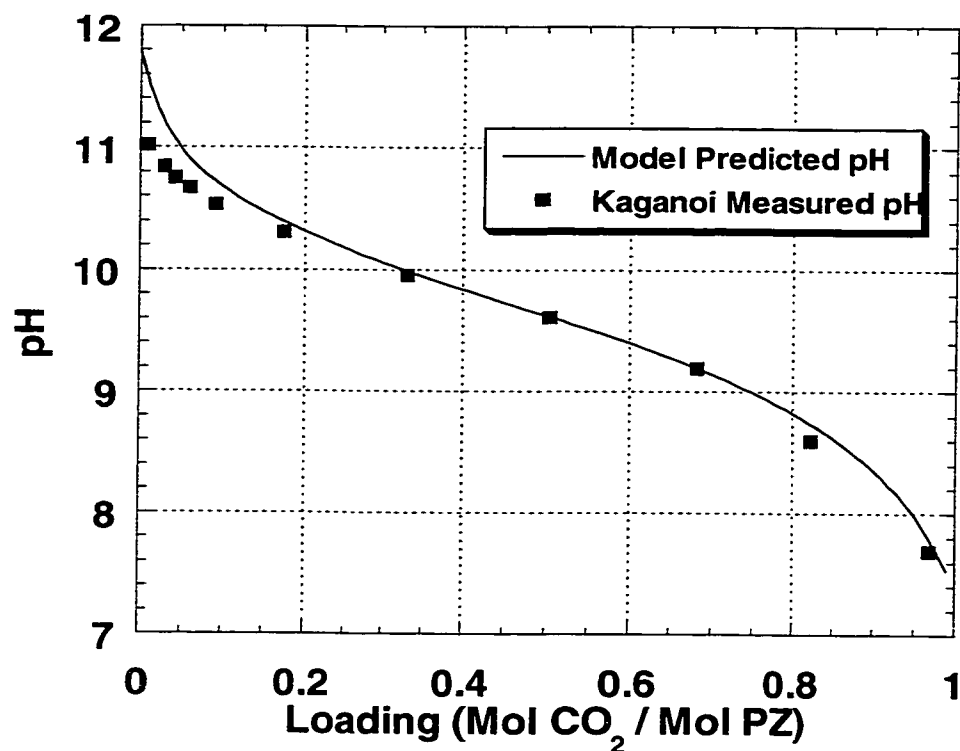


Figure 4.8: pH of 0.6 M piperazine loaded with carbon dioxide at 25°C

Measurement of the ionic conductivity in solution is shown in figure 4.9. This data was acquired by loading a 0.6M PZ solution to high loading (>0.7) and diluting it with fresh PZ solution. Ionic conductivity was measured using a conductivity probe at each point. Samples were also analyzed for loading at each point. The data shows a decrease in ionic strength of the solution at high loading. This is consistent with the speciation model that shows the conversion of piperazine carbamate to protonated carbamate at high loading. The protonated carbamate has a net charge of zero and will therefore not be affected by the imposition of an electric field.

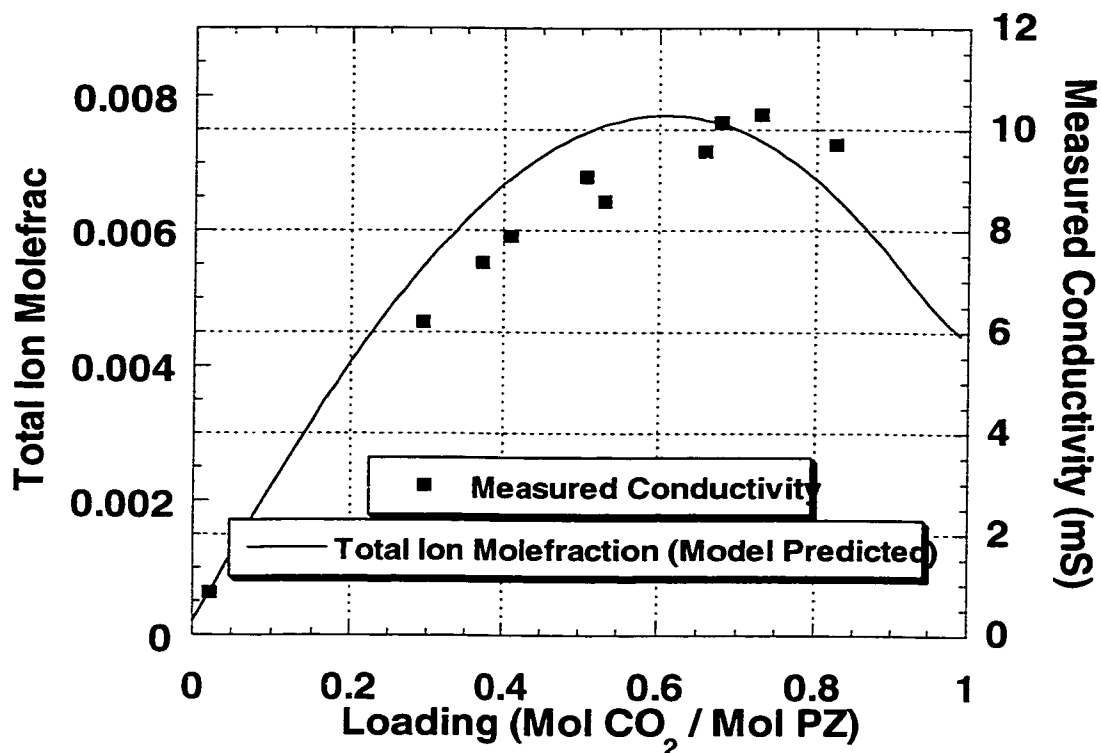


Figure 4.9: Ionic conductivity of 0.6 M piperazine at ambient conditions (approx. 25°C)

¹³C, Proton and C-H correlation NMR has been conducted on piperazine solutions in D₂O at different loading. NMR has been performed on alkanolamine solutions by previous investigators to qualitatively and quantitatively describe speciation. Sartori and Savage (1983) describe how ¹³C NMR was used to quantify carbamate formation in hindered amines. Fleyfel et al. (1993) describe the NMR spectra of aqueous MDEA / CO₂ solutions.

Figure 4.10 shows the Proton NMR spectra on the Y axis, the ¹³C NMR spectra on the X axis and the C-H correlation for a 0.6M PZ solution at a loading of 0.57. The triplet peak on the proton spectra at 2.84 ppm denotes the average

response of protons on carbons adjacent to an unreacted amine group and a protonated amine group in a piperazine carbamate since the two are in equilibrium and the reactions are too fast to see separately with NMR. These protons are shown in bold on figure 4.11-A. The singlet at 2.9 ppm represents the average peak of protons on carbons adjacent to an unreacted amine group and a protonated amine group in piperazine and protonated piperazine (figure 4.11-B). The singlet at 3.15 ppm denotes the protons of piperazine dicarbamate (figure 4.11-C). The triplet centered at 3.35 ppm denotes an average of the protons adjacent to the carbamate group on protonated piperazine carbamate and piperazine carbamate (figure 4.11-D).

Moving downfield on the ^{13}C spectra, the first peak at 42.1 ppm represents carbons adjacent to the carbamate group (bold face carbons in figure 4.11-D). The second peak at 42.6 ppm represent all the carbons in piperazine/piperazine carbamate (figure 4.11-B). The third peak at 43.6 ppm represents carbons adjacent to the unreacted or protonated nitrogen group in the carbamate molecules (figure 4.11-A). The fourth peak at 44.1 ppm represents the ring carbons in piperazine dicarbamate (figure 4.11-C). There are other peaks present downfield on the ^{13}C spectra for the carbons in the carbamate groups as well as carbons in bicarbonate which are not shown in figure 4.10. Other NMR experiments were performed and the peak locations and intensities are reported in table 4.4.

The NMR data verifies the presence of the species represented by equations 4.17 to 4.20 including the piperazine dicarbamate. Proton NMR also quantifies the amount of dicarbamate present at a given loading. Since the area under the peak in proton NMR is directly proportional to the amount of protons in the species and the amount of the species present, the ratio of dicarbamate to protonated carbamate and carbamate can be determined. The equilibrium constant for piperazine dicarbamate has been estimated in order to be consistent with the proton NMR data.

Table 4.4: Proton and ^{13}C NMR summary for 0.6M PZ solutions in D_2O

Loading $\cong 0$

^1H Peak

δ (ppm)	Intensity	Species
2.61	13.12	Piperazine / Protonated Piperazine Ring Protons

Loading = 0.38

^1H Peak

δ (ppm)	Intensity	Species
3.28	1.02	Carbamate / Protonated
3.27	1.31	carbamate – Protons on
3.26	1.08	carbons next to carbamate nitrogen
3.17	0.74	Dicarbamate ring protons
2.82	12.84	Piperazine / Protonated Piperazine Ring Protons
2.70	1.14	Carbamate / Protonated
2.69	1.30	Carbamate – Protons on
2.68	1.02	carbons next to amine / amineH+

Loading = 0.57

^1H Peak

^{13}C Peak

δ (ppm)	Intensity	Species	δ (ppm)	Intensity	Species
3.37	1.02	Carbamate / Protonated carbamate – Protons on carbons next to	42.12	4.08	Carbamate /Protonated Carbamate - Ring C's next to carbamate
3.36	1.31	carbamate nitrogen	42.63	14.90	Piperazine/Protonated Piperazine Ring C's
3.34	1.08		43.59	4.41	Carbamate / Protonated carbamate – Ring C's next to amine/amineH+

3.15	0.74	Dicarbamate ring protons	44.10	0.92	Dicarbamate Ring C's
2.90	12.84	Piperazine / Protonated Piperazine Ring Protons	161.63	0.15	Bicarbonate
2.85	1.14	Carbamate / Protonated	162.37	0.84	Carbamate C
2.84	1.30	Carbamate – Protons on			
2.83	1.02	carbons next to amine / amineH+			
			163.01	0.16	Di Carbamate C's

Loading = 0.91

¹ H Peak			¹³ C Peak		
δ (ppm)	Intensity	Species	δ (ppm)	Intensity	Species
2.96	124.73	Piperazine / Protonated Piperazine Ring Protons	40.78	10.90	Carbamate / Protonated carbamate – Protons on carbons next to carbamate nitrogen
3.01	26.98	Carbamate / Protonated Carbamate – Protons on	42.24	14.91	Piperazine / Protonated Piperazine Ring Protons
3.02	36.67	carbons next to amine / amineH+	43.12	11.24	Carbamate / Protonated Carbamate – Protons on carbons next to amine / amineH+
3.03	27.50		160.03	1.08	Carbamate C's
3.46	26.43	Carbamate / Protonated carbamate – Protons on	161.99	1.90	Bicarbonate C's
3.47	34.82	carbons next to			
3.48	24.31	carbamate nitrogen			

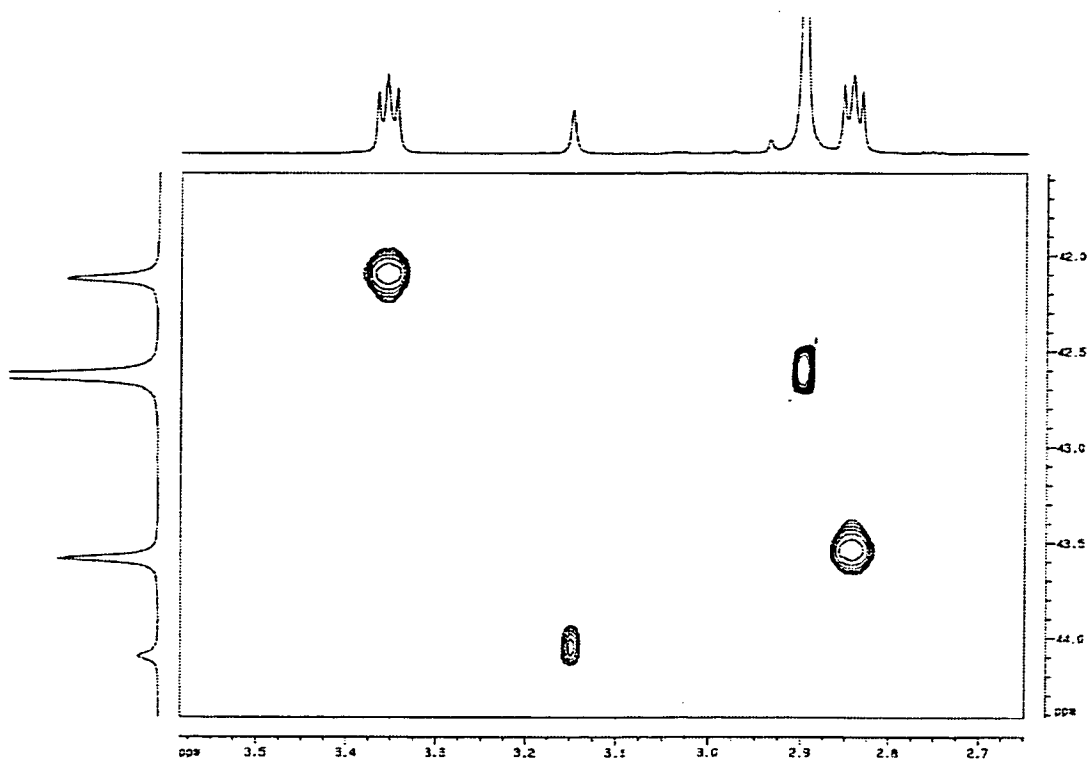


Figure 4.10: ¹³C and proton NMR spectra for 0.6 M piperazine at CO₂ loading of 0.57 and 25°C

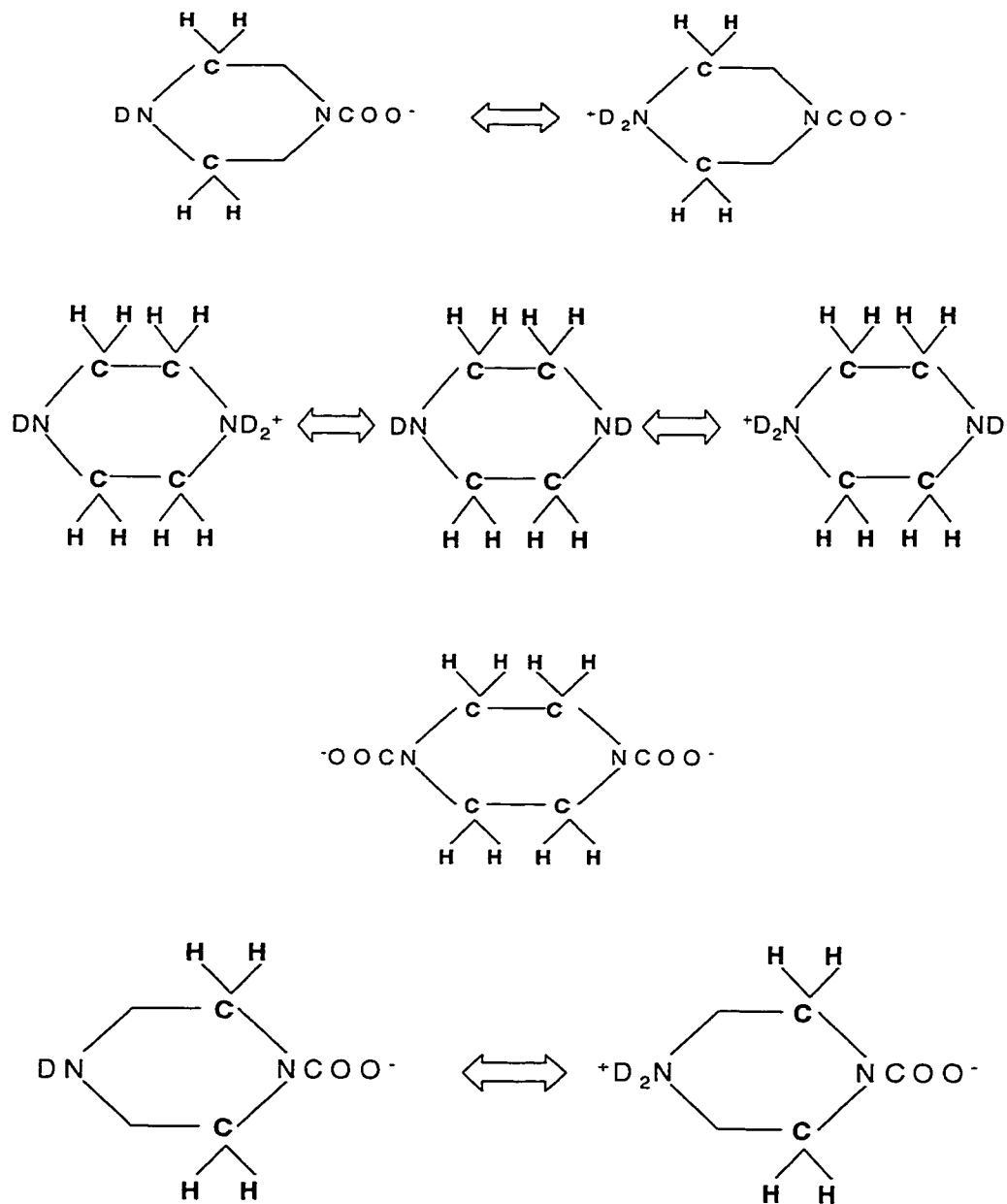


Figure 4.11: Functional groups found in NMR spectra of 0.6 M piperazine loaded with carbon dioxide

4.6 Rate of Reaction Measurement and Interpretation of Data

From equation 4.10 we can see that a plot of the flux versus interfacial partial pressure will yield a straight line. Figure 4.12 shows the results of several temperatures, partial pressures and two amine concentrations (0.6M and 0.2M). The data fits a straight line with a y-intercept of approximately zero as predicted by equation 4.10. Table 4.5 also presents the absorption data obtained in this work at low solution loading. The second order rate constant was extracted by taking the best fit straight line of each series represented in figure 4.12 and correcting the slope for the diffusion coefficient and Henry's law constant for carbon dioxide. Temperature dependence of the rate constant is shown in figure 4.13 as an Arrhenius plot.

Values of the rate constant obtained in this work are shown in table 4.6. An Arrhenius expression obtained from these data can be expressed as:

$$k_2 = k_{25^\circ C} \cdot \exp \left[-\frac{\Delta H_a}{R} \left(\frac{1}{T} - \frac{1}{298.15} \right) \right] \quad (4.26)$$

where $k_{25^\circ C} = 5.37\text{E}4 \text{ m}^3/\text{kmol s}$

$\Delta H_a = 3.36\text{E}4 \text{ kJ/kmol}$

$R = 8.314 \text{ kJ/kmol K}$

The second order rate constant obtained in this work is an order of magnitude higher than that of MEA as measured by Hikita et al. (1979) and a factor of 50 higher than DEA as measured by Sada et al. (1976) in the same amine concentration range. The pseudo first order rate constant obtained by Xu et al. (1992) is much lower than the rate constant obtained in this work. Their data was taken at very high carbon dioxide partial pressure compared to this work; a region

where the piperazine concentration is depleted at the interface and the pseudo first order assumption breaks down. Using their experimental data, one can extract the rate contribution of MDEA and, using our estimation of the rate constant for piperazine, a free piperazine concentration can be calculated at the interface. This number is very small showing that the piperazine concentration is depleted at the interface. Similar calculations show that the pseudo first order assumption is valid for data presented in this work and that there is very little depletion of piperazine at the interface.

The activation energy obtained in this work for PZ compares favorably with the activation energy of other amines. Hikita et al. (1979) measured activation energy for MEA ($1.79\text{E}4$ kJ/kmol). Danckwerts and Sharma (1966) present an activation energy for DEA ($4.18\text{E}4$ kJ/kmol). Xu et al. (1992) obtained a much higher value for the activation energy for piperazine / carbon dioxide ($5.34\text{E}4$ kJ/kmol) which may be due to the reasons discussed above.

It is hypothesized in this work that the high reactivity of piperazine compared to other amines with similar pK_a values is due to two characteristics: it's cyclic and diamine nature. Several other amines are compared to piperazine in table 4.7. Ethylenediamine has a pK_a very close to that of piperazine at 25°C . Its rate constant is quite high compared to monoethanolamine even though pK_a values for the two molecules are approximately equal. Interestingly enough, the rate constant for MEA is approximately half that of ethylenediamine and the local concentration of primary nitrogens on MEA is also half that of ethylenediamine. A portion of the difference between the rate constant of piperazine and other amines can be rationalized by the fact that piperazine is a diamine.

Table 4.5 – Rate of Absorption Data into Aqueous Piperazine. Overall gas flowrates from 5.2 to 5.5 SLPM. Total pressures from 45-60 psig.

$\frac{[PZ]_T}{m^3}$	T °C	$P_{CO_2}^{OUT}$ Pa	Flux *10 ⁷ $\frac{kmol}{m^2s}$	$k_g^o*10^9$ $\frac{kmol}{m^2Pa \cdot s}$	$k_l^o*10^5$ m/s	$P_{CO_2}^I$ Pa	CO ₂ Loading $\frac{mol}{mol}$
0.2	23.4	152	1.69	2.78	9.1	120	0.044
0.2	24.2	243	2.67	2.94	9.2	195	0.043
0.2	24.3	176	1.93	2.82	9.3	140	0.043
0.2	24.3	223	2.39	2.90	9.3	179	0.046
0.2	24.7	200	2.16	2.86	9.4	160	0.046
0.2	24.5	14	0.14	2.57	9.4	11	0.046
0.6	23.3	251	3.95	2.34	9.2	159	0.022
0.6	23.2	111	1.80	2.39	9.2	70	0.026
0.6	23.2	26	0.37	2.41	9.2	18	0.031
0.6	40.7	123	2.44	2.82	11.5	77	0.023
0.6	40.7	144	2.80	2.85	11.5	92	0.023
0.6	40.6	162	3.18	2.90	11.5	103	0.025
0.6	40.7	181	3.53	2.94	11.5	117	0.030
0.6	40.7	197	3.95	2.98	11.5	126	0.033
0.6	40.9	24	0.38	2.62	11.5	17	0.033
0.6	40.8	14	0.15	2.60	11.5	11	0.033
0.6	40.7	122	2.47	2.82	11.5	76	0.020
0.6	40.2	197	3.96	2.98	11.4	126	0.022
0.6	61.5	111	2.69	2.89	14.4	63	0.027
0.6	60.6	182	4.22	3.04	14.3	111	0.030
0.6	60.3	138	3.12	2.93	14.3	83	0.031
0.6	60.7	160	3.73	2.99	14.3	96	0.032
0.6	60.7	11	0.20	2.66	14.3	7	0.032

Table 4.6 – Rate constant values calculated from pseudo first order treatment of low loading data

T °C	[PZ] kmol/m ³	k ₂ * 10 ⁻⁵ (m ³ /kmol s)
23.2	0.2	4.59
24.2	0.6	5.35
40.6	0.6	11.48
60.7	0.6	21.98

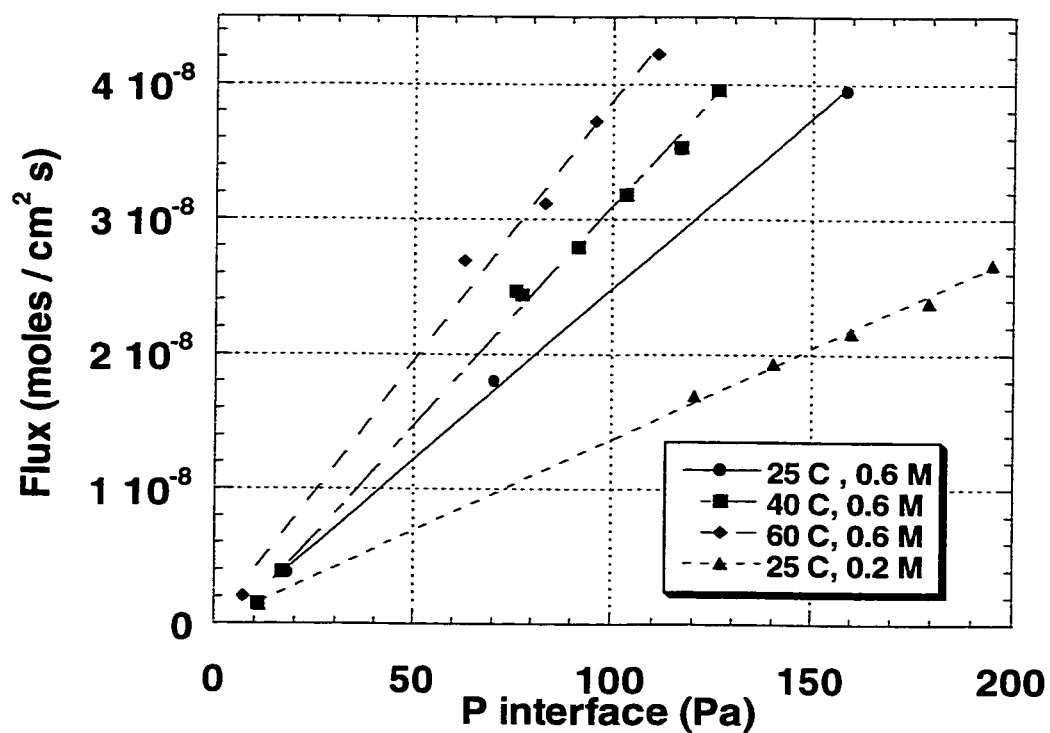


Figure 4.12: Straight line fit for rate of CO₂ absorption into aqueous piperazine solutions at low solution loading

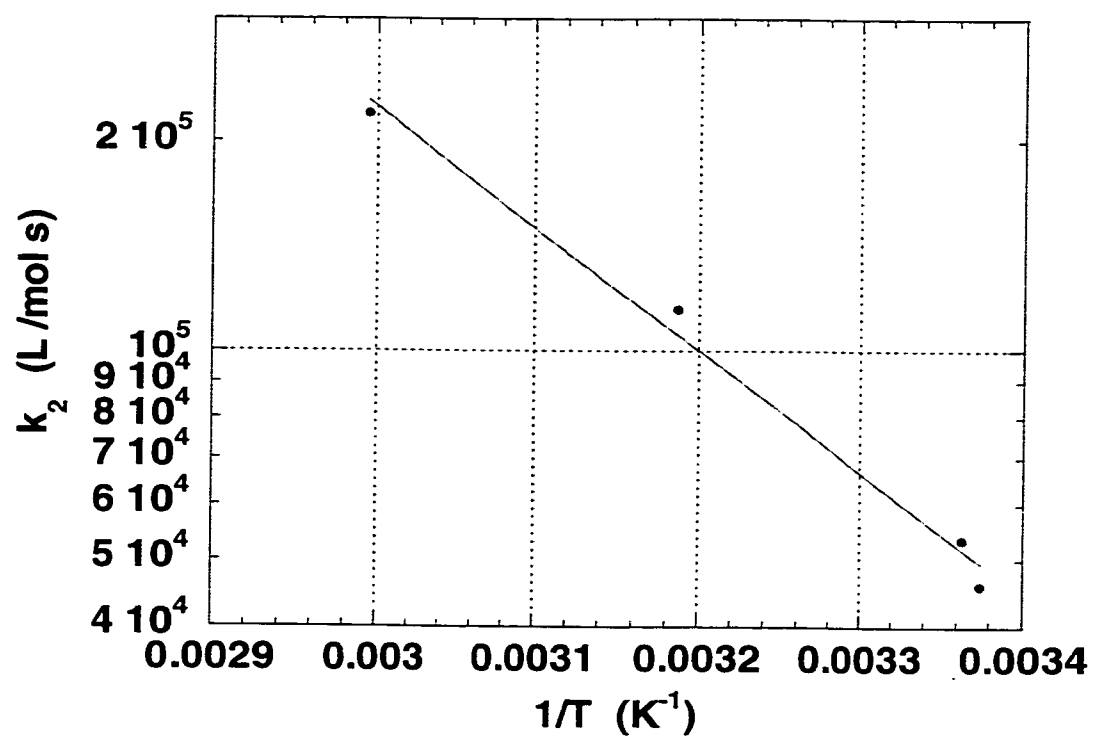


Figure 4.13: Second order rate constant of piperazine and carbon dioxide

Table 4.7 Bronsted Correlation of Piperazine Kinetics at 25°C

Amine	Rate Constant at 25°C (m ³ /kmol s)	pK _a at 25°C	Source
Piperazine	53700	9.83	This Work
Ethylenediamine	15000	9.90	Sharma (1966)
Monoethanolamine	7000	9.50	Hikita et al. (1979)
Morpholine	20000	8.70	Sharma (1966)
Diethanolamine	1200	8.88	Sada et al. (1976)
Piperidine	60000	11.12	Sharma (1964)

Comparison of morpholine and piperidine to piperazine leads to the hypothesis that the cyclic nature of piperazine also contributes to its increased reactivity. The pK_a value for morpholine is comparable to other secondary amines such as DEA, however its rate constant is much higher than that of DEA. Piperidine also has a very high rate constant, however its pK_a is also much higher.

A second data set for the absorption of carbon dioxide into partially loaded aqueous solutions of piperazine is presented in table 4.8. The free amine concentration and the equilibrium partial pressure were estimated using the speciation and solubility model presented in this work. The rate constant used in table 4.8 is the rate constant estimated by the data in table 4.5 and presented in equation 4.26. Using these constants, the flux for each experimental point is estimated using equation 2.16 and compared to the measured flux. Figure 4.14 compares the predicted flux to the measured flux for this series of data. It can be seen that equation 2.16 consistently underestimates the flux of carbon dioxide and that the error seems to increase with loading. This is probably attributed to the fact that carbon dioxide can also react with the carbamate and with protonated piperazine and these kinetics are ignored by equation 2.16. Recommendations on quantifying the kinetics of these reactions are presented in the following section.

Table 4.8 – High loading flux measurements and predictions

Loading mol/mol	[PZ] kmol/m ³	P ^I _{CO₂} Pa	Interface Loading mol/mol	P* _{BULK} Pa	P* _{INT} Pa	[PZ] _{INT} kmol/m ³	Flux * 10 ⁶ kmol/ m ² s	
							Pred.	Meas.
0.29	0.298	1061	0.34	23	37	0.257	2.19	2.39
0.47	0.163	1211	0.52	118	181	0.134	1.60	2.14
0.56	0.112	1530	0.60	255	361	0.092	1.52	1.88
0.67	0.063	1862	0.70	676	895	0.053	1.02	1.47

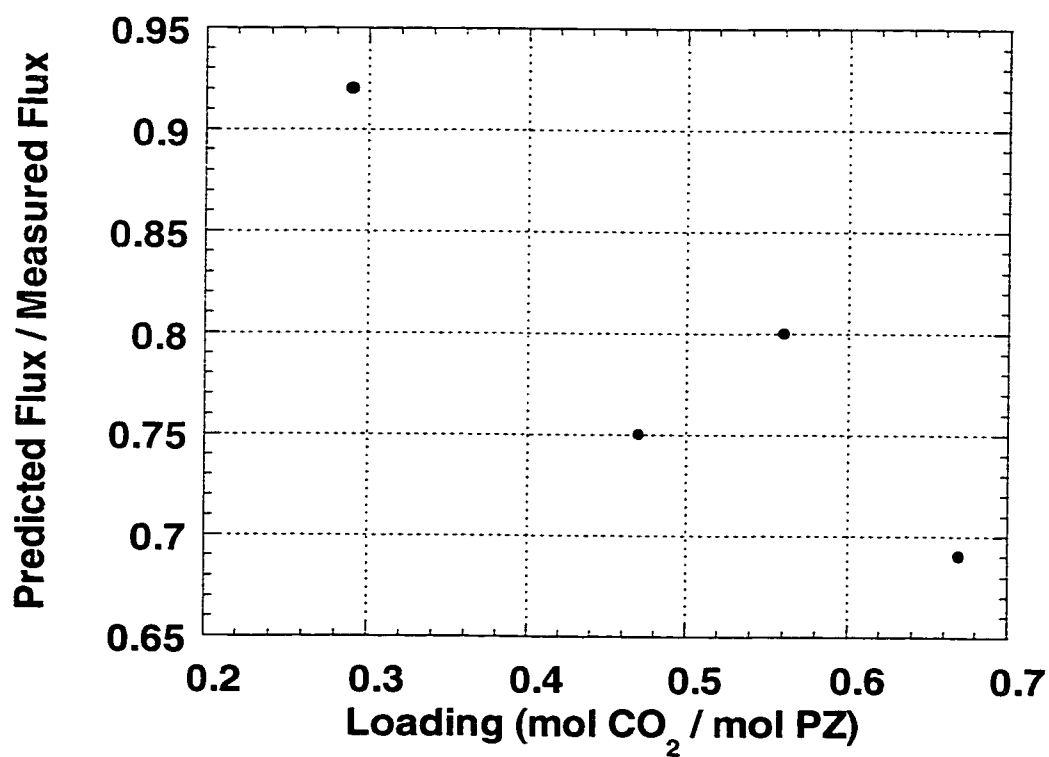


Figure 4.14: Comparison of predicted and experimental fluxes for absorption of carbon dioxide into partially loaded 0.6 M piperazine

4.7 Conclusions

Carbon dioxide solubility, NMR, ionic conductivity, and pH data obtained on the $\text{CO}_2/\text{PZ}/\text{H}_2\text{O}$ system in this work support the conclusion that aqueous piperazine has two reaction zones. At low solution loading, the dominant reaction products are piperazine carbamate and protonated piperazine. At high loading, the dominant reaction product is protonated piperazine carbamate. Although piperazine dicarbamate is present, it is never the dominant reaction product.

The kinetics of PZ demonstrate why it is an effective promoter for carbon dioxide removal from gas streams. The rate constant is an order of magnitude higher than primary amines such as MEA or DGA[®] while the first carbamate stability constant is comparable.

Measurements of the rate constant in this work are much higher than previously reported values. Values reported in this work represent true second order intrinsic kinetics. Previously measured values by Xu et al. (1992) were analyzed using the pseudo first order assumption while their data were obtained at conditions where piperazine was severely depleted at the interface.

Absorption data into partially loaded piperazine solutions and low partial pressure are also presented. The measured flux compared to well with the flux predicted by pseudo first order treatment. The predicted values are lower than expected perhaps due to an additional reaction of piperazine carbamate or protonated piperazine to form protonated piperazine carbamate.

Chapter 5

Thermodynamics of piperazine / methyldiethanolamine / water / carbon dioxide

Thermodynamics of aqueous amine systems are crucial to understanding their industrial use to remove acid gas from process gas streams. The equilibrium partial pressure of acid gas above a solution of the amine defines pinch conditions for the absorber and stripper. Speciation of the amine and reaction products define the driving force for the forward and reverse reactions with CO₂. An understanding of this is important since the reactions are usually rate controlling. Furthermore, a consistent thermodynamic model can quantify the energy required for regenerating the solvent and solvent losses due to amine volatility.

This work studies piperazine (PZ) / methyldiethanolamine (MDEA) / H₂O solvents that have been applied to synthesis gas and natural gas (Wammes et al., 1994). This chapter explains how thermodynamics affects the performance of these solvents for engineers currently running absorption units using PZ solvents and for scientists designing new solvents for gas treating.

Blended amine solvents have been studied by several researchers. Austgen (1989) studied the thermodynamics of MDEA blends with MEA, DEA and DGA[®] using the electrolyte NRTL model. Posey (1996) improved the models by studying the activity coefficient of the amines at infinite dilution.

Pacheco et al. (2000) studied the absorption of CO₂ into aqueous DGA[®]/MDEA blends. Glasscock et al. (1991) and Critchfield (1988) have studied

blends of DEA and MEA/MDEA. Littel et al. (1992a&b) as well as many others (see Chapter 2) have studied a variety of tertiary amines promoted by primary or secondary amines.

Specifically, this work will use the thermodynamic frameworks presented by Bishnoi and Rochelle (2000), Austgen et al. (1989) and Posey and Rochelle (1997). Data acquired by Xu et al. (1998) and Liu et al. (1999) for the PZ/MDEA system at high loading will also be discussed. Insight into the interaction of PZ with CO₂ discussed in Chapter 4 of this work will also be useful in setting up the chemistry framework of the model.

The simple system of PZ/H₂O is represented in section 5.2 by estimating the infinite dilution activity coefficient of PZ using the Dortmund modification of the UNIFAC model (Gmehling et al., 1993). The solubility limit of PZ was also measured and results are presented in section 5.3. A wetted wall column was used to measure CO₂ solubility at conditions where the ratio of total carbon dioxide to PZ is less than one. Parameters of the electrolyte NRTL model were adjusted in order to match the CO₂ solubility data at low loading and the NMR data at high loading. Results of the regression are presented in section 5.5 while model predictions are presented in section 5.6 through 5.8.

5.1 Experimental Methods

Solubility of carbon dioxide was determined using the wetted wall apparatus and techniques discussed in Chapter 4. The use of this apparatus to extract data on the solubility of CO₂ in amine solutions has been described in Chapter 4.

A round bottom flask was used to mix solid PZ and water and measure the solubility of PZ in H₂O. The flask was agitated from above and temperature was controlled using a Lauda heater and water bath. Anhydrous PZ solid (CAS No. 110-85-0, 99% purity; Aldrich Chemical, Lot No. 09525AU) was added until the solubility limit was achieved. The agitator was shut off and the solution was

allowed to settle before liquid samples were withdrawn off the top of the flask and titrated with 2N HCl to an endpoint pH of 2 to determine the total PZ content. The sampling technique was tested by performing the experiment at ambient temperature and filtering the solid/liquid mixture. The sampling technique gave the same result as the filtered experiment.

NMR experiments were performed at UT's Department of Chemistry and Biochemistry NMR laboratory. ^{13}C , Proton, and C-H short range correlation experiments were performed using D_2O solvent. All experiments were run at 25°C on a Varian EM-390 machine.

5.2 Activity of piperazine in aqueous mixtures

Table 5.1 presents the activity coefficients at infinite dilution predicted by the Dortmund modification of the UNIFAC theory (Gmehling et al., 1993). All parameters necessary for calculation of the activity coefficients are given in the paper by Gmehling et al. The value obtained for the PZ activity coefficient matches that of similar molecules measured at 25°C . Table 5.1 shows a comparison of measured activity coefficients at infinite dilution and 25°C . The comparison of pentane with 1-amino-pentane, demonstrates that the addition of a nitrogen to a hydrocarbon significantly reduces its activity coefficient. The comparison of piperidine to 1-amino-pentane demonstrates that a cyclic secondary amine has a lower activity coefficient than a comparable non-cyclic primary amine. Piperidine is also very similar to PZ in that it is a six membered ring. To convert piperidine to PZ, we would remove one hydrophobic methylene group and add a hydrophilic amine group. This would decrease the activity coefficient to a value less than that of piperidine (<5.6). The calculated value of 0.24 using the Dortmund modified UNIFAC model reported in this work is consistent with this trend. Furthermore, amino-ethane has the same ratio of methylene groups to amine groups. Amino-ethane is, in fact, half a PZ molecule. The experimental

value of 0.53 for amino-ethane compares qualitatively well with the estimated PZ value.

Table 5.1 also shows the behavior of the PZ activity coefficient in the presence of MDEA. The model predictions of UNIFAC suggest that the activity of PZ decreases as MDEA is added to the system.

Table 5.1 – Activity Coefficients at Infinite Dilution in water at 25°C

Species	Infinite Dilution Activity Coefficient	Source
PZ	0.24	Dortmund Modified UNIFAC
Piperidine	5.6**	Dortmund Database
Amino-Ethane	0.53*	Dortmund Database
Hexylamine	29	Dortmund Database
Hexane	871*	Dortmund Database
PZ (in 4.28 M MDEA)	0.11	Dortmund Modified UNIFAC

* interpolated from data at 20 and 30°C

** extrapolated from data at 70-100°C

Wilson and Wilding (1994) have measured vapor liquid equilibrium for the PZ/H₂O system at elevated temperatures (112.9 and 198.8 °C). Figure 5.1 shows manipulation of their data to obtain activity coefficients for the system. Analysis of activity coefficients at the two temperatures they studied and equation 5.1 yields an excess heat of mixing at infinite dilution of -37.7 kJ/mol for liquid PZ.

$$\ln \left(\frac{\gamma^{(2)}_{PZ}}{\gamma^{(1)}_{PZ}} \right)_{P,x} = \frac{h_2^{Ex}}{R} \left[\frac{1}{T^{(2)}} - \frac{1}{T^{(1)}} \right] \quad (5.1)$$

The absolute value of the activity coefficients should not be compared with those at temperatures of 25°C since the data of Wilson and Wilding (1994) is taken above the triple point and with respect to liquid PZ instead of the reference of solid PZ used in this work. A comparison of the excess heat of mixing at infinite dilution is provided in table 5.2. The value for amines is consistently negative and seems to be related to the amino group. The value of -37.7 seems reasonable

compared to other amines such as piperidine, butylamine and morpholine. Since piperazine has two amine functions, it could have a value 2 times greater than piperidine (-59). The calculated value of the excess heat of mixing from the Dortmund modification of the UNIFAC is also presented in table 5.2. It should be noted that most components in the Dortmund database are liquid at standard conditions and, therefore the heat of mixing refers to a deviation from the pure liquid instead of the anhydrous reference state used for piperazine in this work.

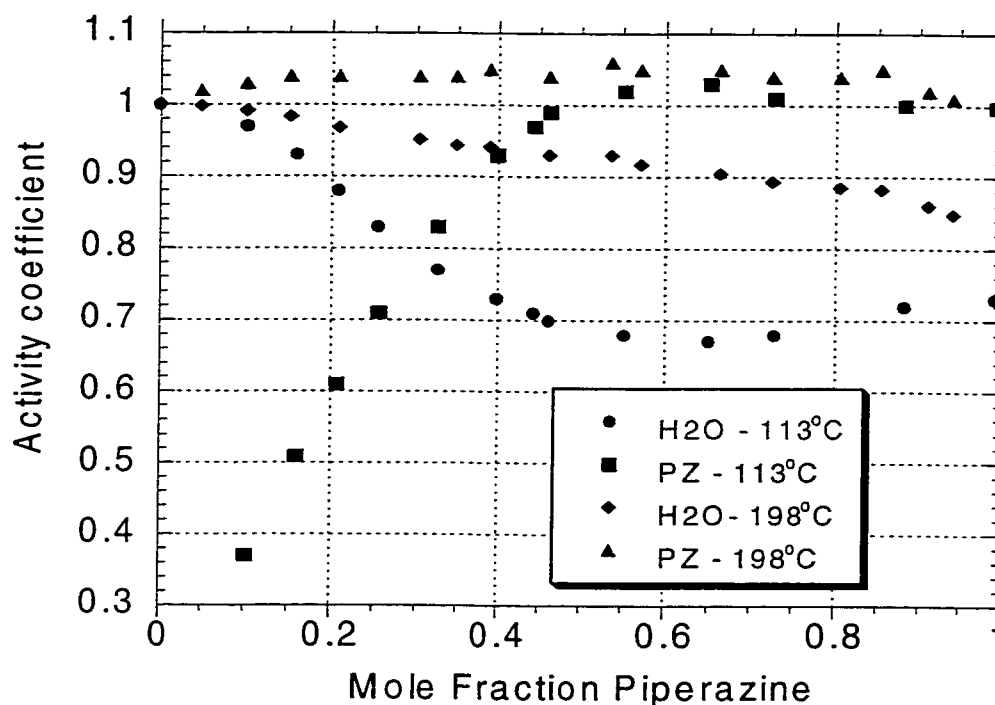


Figure 5.1 Data of Wilson and Wilding (1994) reinterpreted as activity coefficients for the water / PZ system at elevated temperature.

The values compare well with the value from the data of Wilson and Wilding (1994). In this work, NRTL parameters for PZ/H₂O and H₂O/PZ are fit to the infinite dilution activity coefficient values calculated by the Dortmund modified UNIFAC model. These parameters are reported later in table 5.6. Accurate prediction of the PZ activity coefficient is useful in two ways. It helps

predict the volatility and losses of the amine as well as correcting the equilibria that involve PZ for the effect of MDEA. The correction of equilibria will be discussed in section 5.4-5.6.

Table 5.2 – Excess heat of mixing at infinite dilution and 25°C

Species	$h_{AM}^{EX,\infty}$ (KJ/mol)	Source
Piperazine	-59	Dortmund Modified UNIFAC
Piperazine	-38	Wilson and Wilding (1994)
Piperidine	-26	Dohnal et al. (1994)
Morpholine	-25	Dohnal et al. (1994)
Cyclohexylamine	-23	Dohnal et al. (1994)

*All species listed are liquids in their pure state at ambient conditions except PZ

**Reference state of most components in Dortmund UNIFAC database is liquid

5.3 Solubility of piperazine in water

The initial concentration of PZ in the solvent is limited on the higher end by its solubility in water and MDEA solutions. This solubility limit was measured using the apparatus discussed above and the results are presented in table 5.3 and figure 5.2. Below 40°C (313K) the solubility is limited by formation of the PZ hexahydrate which melts at 316K (Schwarzenbach, 1968). The melting point of the hydrate explains the discontinuity at around 40°C (313K) in table 5.3 and figure 5.2. Densities of the solutions were not found to deviate more than 5% from water.

Table 5.3 – Solubility limit of piperazine in H₂O

Temperature (K)	Solubility Limit (M)	Solubility Limit (mole fraction PZ)
273	0.52	9.7E-3
294	1.64	3.3E-2
298	1.88	3.4E-2
313	7.42	0.270
323	7.83	0.323
333	8.17	0.376
343	8.40	0.414

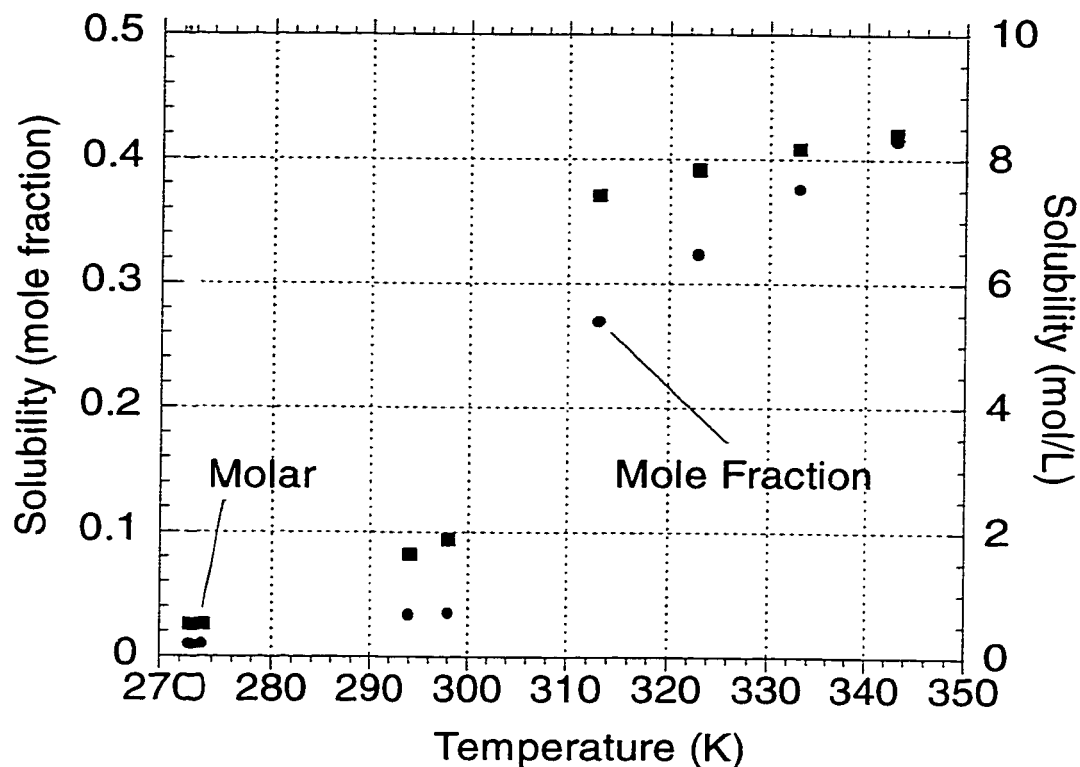
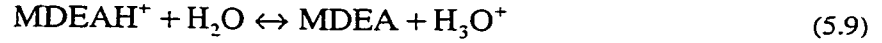
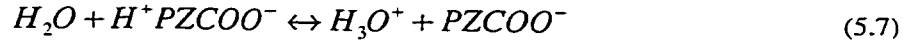
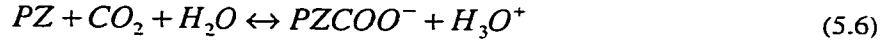
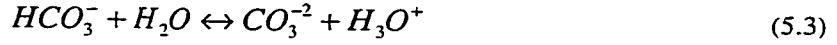
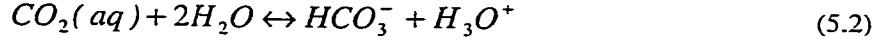


Figure 5.2 Solubility of anhydrous PZ solid in H₂O

5.4 Model Description

A flexible Fortran code for the solution and phase equilibrium of acid gas systems was developed by Austgen (1989). This code was modified slightly to model PZ activated MDEA blends. The model uses the Smith and Missen (1988) non-stoichiometric algorithm to speciate the liquid solution (see chapter 2). Equilibrium constants were used to calculate the standard state chemical potentials using the method described by Austgen (1989). The following reactions and

species are considered. All PZ species shown have been shown to exist in aqueous PZ solutions loaded with CO₂ in Chapter 4.



The total amount of water, carbon dioxide, PZ and MDEA present in the liquid phase are specified. Equilibrium is first calculated in the liquid phase and then vapor/liquid equilibrium is calculated for all molecular species (PZ, MDEA, H₂O, CO₂).

Gas phase non-idealities are calculated using the SRK equation of state (Soave, 1972). Liquid phase non-idealities are calculated using the electrolyte NRTL model (Chen and Evans, 1982; Chen et al., 1986, Mock et al., 1986). The use of the electrolyte NRTL model in amine / acid gas systems has been described previously by Austgen (1989), Posey (1996) and Bishnoi and Rochelle (2000). This work most closely resembles that of Bishnoi and Rochelle (2000) with CO₂ referenced to infinite dilution in water. All ions are also referenced to infinite dilution in water. PZ, MDEA and H₂O are all referenced to the respective pure components at the system temperature (ie. pure anhydrous PZ solid). The reader is referred to Chapter 3 for a more detailed description of the gas and liquid phase models used to account for non-ideality.

Protonated PZ carbamate (H⁺PZCOO⁻) is defined as an anion with no net charge. As a result, its activity coefficient does not deviate significantly from

unity. Identifying this species as an anion, even though it does not have net charge, allows us to get away from dealing with its volatility. It is assumed that this species is non-volatile.

Tau parameters are defined in order to be consistent with the work of Bishnoi and Rochelle (2000). Tau parameters for molecule / molecule interactions are defined as:

$$\tau = A + \frac{B}{T} \quad (5.10)$$

Tau parameters for salt pair / molecule and molecule / salt pair are defined as:

$$\tau = A + B \left(\frac{1}{T} - \frac{1}{T_{ave}} \right) \quad (5.11)$$

Here, T is temperature in Kelvin and T_{ave} is 353.15K.

Default parameters consistent with Aspen Plus™ version 8.5 were used in this work. This is consistent with the work of Austgen (1989), Posey (1996) and Bishnoi and Rochelle (2000). A description of these defaults follows. All B parameters are 0. For A parameters, all molecule / molecule are 0, all water / salt pair are 8.0, all salt pair / water are -4, all molecule (other than water) / salt pair are 15, all salt pair / molecule (other than water) are -8. All molecule / molecule, water / salt pair, and salt pair / water non-randomness parameters are 0.2. All other non-randomness parameters are 0.1.

Critical constants used by the SRK equation of state and the accentric factor were taken from the DIPPR database (Rowley et al., 1994). The Henry's law constant for CO₂ was fit by Chen et al.(1979). Brevli-O'Connell parameters used in this work were obtained from the original work of Brelvi and O'Connell (1972). Critical compressibilities used in the Rackett model were obtained from the DIPPR database. The dielectric constant of PZ was assumed to be the same as MEA. Although this is purely an assumption, the mole fraction of PZ is so small

that it will have a negligible effect on the calculated results. The Antoine equation for PZ was obtained from Stephenson and Malanowski (1987). It is important to note that the vapor pressure of PZ below 106°C refers to the sublimation pressure of anhydrous PZ. The Antoine equation in the DIPPR database is only valid above the triple point and would, therefore, incorrectly describe the sublimation of solid PZ below 106°C. Values of all these constants are documented in table 5.4.

Table 5.4a – Miscellaneous Constants for VLE program

Constant	Carbon Dioxide	Water	MDEA	Piperazine
Critical T (K)	304.2	647.3	677.79	638.0
Critical P (kPa)	7376	22090	3876	6870
Critical V (m ³ /mol)	9.4E-2	5.7E-2	0.39	0.23
Accentric Factor	0.23	0.34	1.24	0.80
Rackett Z _{RA}	0.27	0.24	0.19	0.20
Brelvi-O'Connell	9.6E-2	-	-	-

Table 5.4b – Temperature dependent constants

Henry's Law Constant (Pa / Mole Fraction) : $\ln H_x = A + B/T + C \ln(T) + DT$					
Carbon Dioxide	A=170.7126	B=-8477.711	C=-21.95743	D=0.005781	
Dielectric Constant : $D = A + B[1/T - 1/273.15]$					
H2O	A=88.36	B=33030			
MDEA	24.76	8989			
PZ	36.76	14836			
Antoine Equation (Pa) : $\ln P^{SAT}=A + B/T + C \ln T + D T^E$					
H2O	A=72.55	B=-7206.7	C=-7.1385	D=4.04E-6	E=2.0
MDEA	26.137	-7588.5	0.0	0.0	0
PZ	172.78	-13492	-21.91	1.378E-5	2.0

5.5 Parameter regression results

Equilibrium constants for reactions 5.2 through 5.9 are documented in table 5.5 along with their sources. The first and second dissociation constants of CO₂, the MDEA protonation and water dissociation constants are unchanged from the work of Austgen (1989). Constants for reactions 5.6 through 5.9 are based on the

experimental work of Bishnoi and Rochelle (2000b) presented here in Chapter 4. These constants were re-regressed here with GREG (Caracotsios, 1987) to match the new reference states defined in this chapter.

Table 5.5 – Temperature dependence of equilibrium constants, mole fraction based
*Ln (Kx) = A + B/T + Cln T + DT

Eq No.	Equilibrium Constant	A	B	C	D	Value at 313 K	Source
11	$\frac{a_{\text{HCO}_3^-} a_{\text{H}_3\text{O}^+}}{a_{\text{CO}_2} a_{\text{H}_2\text{O}}^2}$	231.4	-12092	-36.78	0.0	8.55E-9	Posey (1996)
12	$\frac{a_{\text{H}_3\text{O}^+} a_{\text{CO}_3^{2-}}}{a_{\text{HCO}_3^-} a_{\text{H}_2\text{O}}}$	216.0	-12432	-35.48	0.0	1.04E-12	Posey (1996)
13	$\frac{a_{\text{H}_3\text{O}^+} a_{\text{OH}^-}}{a_{\text{H}_2\text{O}}^2}$	132.9	-13446	-22.48	0.0	9.15E-18	Posey (1996)
14	$\frac{a_{\text{PZ}} a_{\text{H}_3\text{O}^+}}{a_{\text{H}_2\text{O}} a_{\text{PZH}^+}}$	4.964	-9714.2	0.0	0.0	4.76E-12	Pagano et al. (1961)
15	$\frac{a_{\text{H}_3\text{O}^+} a_{\text{PZCOO}^-}}{a_{\text{PZ}} a_{\text{CO}_2} a_{\text{H}_2\text{O}}}$	-41.583	9288.2	0.0	0.0	6.73E-6	This Work
16	$\frac{a_{\text{PZCOO}^-} a_{\text{H}_3\text{O}^+}}{a_{\text{H}^+} a_{\text{PZCOO}^-} a_{\text{H}_2\text{O}}}$	-13.041	-3961.6	0.0	0.0	6.91E-12	This Work
17	$\frac{a_{\text{H}_3\text{O}^+} a_{\text{-OOC PZCOO}^-}}{a_{\text{PZCOO}^-} a_{\text{CO}_2} a_{\text{H}_2\text{O}}}$	-44.7	9288.2	0.0	0.0	2.98E-7	This Work
18	$\frac{a_{\text{MDEA}} a_{\text{H}_3\text{O}^+}}{a_{\text{MDEAH}^+} a_{\text{H}_2\text{O}}}$	-9.4165	-4234.98	0.0	0.0	1.09E-10	Austgen (1989)

CO₂ Solubility and NMR data were re-regressed to obtain equilibrium constants consistent with the aqueous PZ data and the reference state of this work. It should be noted here that all parameters involving PZ salts / water were kept at their default values in this work. All parameters involving MDEA salt pairs and water are the parameters regressed by Bishnoi and Rochelle (2000). The resulting

model, therefore, matches data in aqueous PZ solutions as well as data in MDEA and MDEA/PZ solutions.

Values of all non-default parameters are listed in table 5.6 along with their default values and sources. The $\text{CO}_3^{2-} \text{MDEAH}^+ / \text{MDEA}$ A parameter was changed to 15 from its regressed value of 24.5 since the model would not converge with a value of 24.5. This parameter was seen to have a very large standard deviation (Bishnoi and Rochelle, 2000; Posey, 1996) and, therefore, changing it has had a very small effect on calculated partial pressure. More importantly, the model still matches data in aqueous MDEA.

$\tau_{\text{PZ/MDEA}}$ was also adjusted instead of using the value calculated by the UNIFAC model. It was found that only a very approximate fit of the CO_2 solubility data could be achieved unless this parameter was adjusted. The resulting activity coefficient for PZ predicted by the model at very low loading, 313K and 4M MDEA, 0.6M PZ is 0.09 compared to 0.35 predicted by the UNIFAC model.

Table 5.6 – Non-Default parameters for the NRTL model. C5+ is protonated MDEA.

Parameter	A	B	τ_{40}	Default τ
H2O (C5+ HCO3-)	9.645	0	9.65	8
(C5+ HCO3-) H2O	-4.483	652.4	-4.25	-4
(C5+ HCO3-) MDEA	-6.211	-3056.8	-7.32	-8
(C5+ CO3=) MDEA	15	0	15	-8
(C5+ OH-) H2O	-5.16	0	-5.16	-4
(C5+ HCO3-) CO2	-8.08	2840.8	-7.05	-8
CO2 MDEA	1.637	0	1.64	0
H2O CO2	0	0	0	0
CO2 H2O	0	0	0	0
H2O MDEA*	9.473	-1902.4	3.40	0
MDEA H2O*	-2.173	-147.4	-2.64	0
(PZH+ PZCOO-) MDEA	-7.305	-2625.5	-8.25	-8
PZ/MDEA	-12.182	2801.1	-3.23	0
(PZ(COO-)2 C5+) H2O	-4.2	0	-4.2	-4

*Obtained by Posey

$$\tau = A + B \left(\frac{1}{T} - \frac{1}{T_{\infty}} \right) \text{ for salt pair / molecule and molecule / salt pair}$$

$$\tau = A + \frac{B}{T} \text{ for molecule / molecule}$$

The shift in the activity coefficient from water to a concentrated MDEA solution, therefore, matches the UNIFAC model in direction, but not quantitatively. The inability to match data without adjusting this parameter stresses its importance. Measurement of the activity coefficient of PZ, however, will prove difficult using the methods previously applied for amine systems. Chang et al. (1992) used a freezing point depression method to measure the activity coefficient of DEA and MDEA in aqueous solution. He had to use solutions with concentrations up to 5 M, however, in order to get a reasonable estimate of the activity coefficient of the amine. Since the solubility limit of PZ is about 0.5 M at 0°C, it is not reasonable to expect freezing point depression experiments to quantify the activity coefficient of PZ. Posey (1996) used calorimetry and measurements of the heat of mixing to get good estimates of the temperature dependence of the activity coefficient of DEA and MDEA. Again, the solubility of PZ in aqueous solutions will limit the use of this technique to very dilute solutions. It is doubtful that any useful information can be gathered by calorimetry. Any method based on equating the fugacity of aqueous PZ to solid PZ at its solubility limit will be complicated by the formation of the hydrate phase. Methods with the highest probability of success will be based directly on measuring the volatility of the amine in aqueous solutions and solutions containing MDEA. Predictions of speciation and partial pressure in PZ activated MDEA solutions can be greatly improved by developing a method to measure the volatility of PZ above these solutions.

The regressed τ value for $\text{PZH}^+ \text{PZCOO}^- / \text{MDEA}$ obtained in this work does not deviate far from the default value. This places some confidence in their absolute value. The value for $\text{PZ(COO)}_2 \text{MDEAH}^+ / \text{H}_2\text{O}$ has been adjusted to match NMR data taken in 1M PZ, 3M MDEA solutions loaded with carbon dioxide. Once this parameter was adjusted, the regression of τ values for PZH^+

PZCOO⁻ / MDEA and PZ/MDEA to match equilibrium partial pressure data for CO₂ was re-run. This was done several times until none of the parameters observed any significant changes from the previous iteration. The NMR data will be discussed further in section 5.8.

5.6 Solubility of carbon dioxide in aqueous solution of PZ/MDEA

Data for CO₂ solubility in PZ/MDEA/H₂O blends were obtained in this work. Data in 0.6M PZ, 4M MDEA at 313 and 343 K and 4.28M MDEA at 313 K are given in Table 5.7 and figure 5.3. Throughout this work, loading is represented as moles CO₂/mole Amine where the total concentration of amine is equal to the concentration of MDEA + the concentration of PZ.

Table 5.7 – CO₂ Solubility in Piperazine Activated MDEA

313 K 4.28M MDEA		0.6M PZ, 4 M MDEA		343 K 0.6M PZ, 4M MDEA	
Loading ²	P* _{CO2} (Pa) ¹	Loading	P* _{CO2} (Pa)	Loading	P* _{CO2} (Pa)
0.013	108	0.027	33	0.006	34
0.024	505	0.061	115	0.014	241
0.032	730	0.073	236	0.020	491
		0.089	367	0.046	780
		0.140	1140	0.093	3600
		0.140	1335		
		0.188	2550		
		0.285	7480		

1. Estimated error in partial pressure is $\pm 30\%$ by propagation of error
2. Estimated error in loading is $\pm 5\%$ by propagation of error

The addition of roughly 5 wt% PZ to a 45 wt% aqueous MDEA solution reduces the equilibrium partial pressure of CO₂ by a factor of 10 at low loading. The data converges with the equilibrium partial pressure of MDEA at CO₂ loading greater than 0.2. The model presented in this work matches data in aqueous PZ, MDEA and PZ/MDEA blends.

Xu et al. (1998) obtained solubility data for CO₂ in solutions of 4.28M MDEA and 0-0.5M PZ solutions at 343K. Their data is all taken at conditions where the ratio of total carbon dioxide to PZ is close to or greater than 1. The equilibrium partial pressure of CO₂ was not found to be significantly different than MDEA at those conditions. Their data, however, are very helpful in studying the high loading region since our experimental data was not acquired in this region.

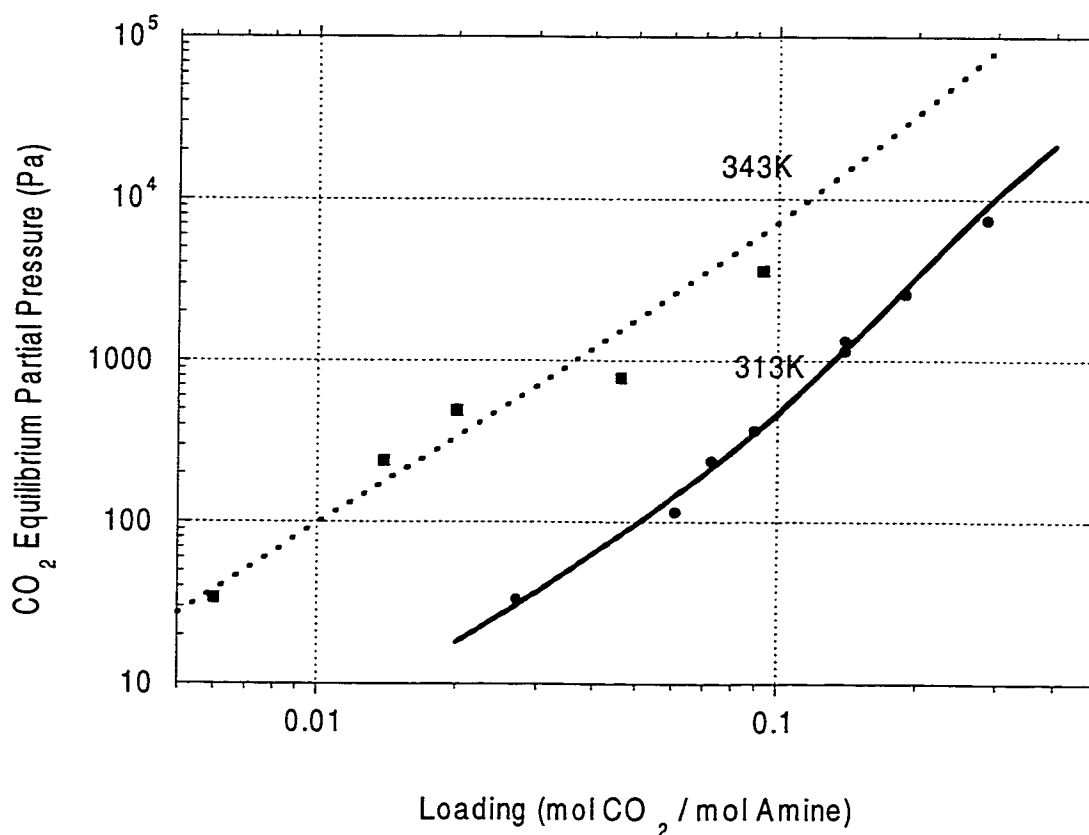


Figure 5.3 Measured and predicted solubility of CO₂ in 0.6M PZ / 4M MDEA solutions

In a further piece of work by the same research laboratory, Liu et al. (1999) obtained a large amount of data in solutions of variable MDEA and PZ

concentration. Again, most data taken complements the data taken in this work since it is at high loading with respect to PZ concentration. Our model is found to predict their data well as shown by the parity plot in figure 5.4. The data of Xu et al. (1998) and Liu et al. (1999) taken within the temperature range studied in this work has approximately the same standard deviation as our data presented here. Although represented well by the model, the data taken outside the temperature range studied in this work (303 and 363 K) has a larger standard deviation. This may be due to an erroneous temperature extrapolation of equilibrium constants or activity coefficient parameters beyond the range of our data. A detailed list of all other data for CO₂ solubility in PZ/MDEA blends is shown in Appendix E along with the predictions of the model presented in this work.

Analysis of Xu et al. (1998) data in aqueous MDEA shows that their data is increasingly lower in partial pressure than the data of other investigators (Jou et al., 1982) as loading is increased. This trend is consistent with the downward trend in data shown in figure 5.4 for the PZ/MDEA data taken in the same equipment leading us to believe that there may be some systematic error in the data.

No formal analysis or modeling of the PZ reactions was presented in the work of Xu et al. (1998). The work of Liu et al. (1999) considers only the protonation of PZ. They ignore the formation of the carbamate, dicarbamate and protonated carbamate in their work. Since their data was taken at conditions where the equilibrium partial pressure of CO₂ is mainly dictated by MDEA, they were able to explain their data. No attempt was made to replicate their model and to run it at the conditions of our data.

5.7 NMR data

Proton, ¹³C, and C-H correlation NMR experiments were performed on several solutions. These were 1M PZ/3 M MDEA, CO₂ loaded solutions of 1 M PZ/3 M

MDEA, CO₂ loaded solution of 3 M MDEA alone. We were able to distinguish between PZ/protonated PZ, carbamate/protonated carbamate, dicarbamate and MDEA/protonated MDEA with the NMR spectra. Figure 5.5 shows the ¹³C-Proton NMR correlation spectra. Comparing this spectrum with that presented in Chapter 4, we can see that the carbon peaks have not shifted significantly in the presence of MDEA solvent. The hydrogen peaks have shifted quite a bit. We are unable to see the triplets associated with the carbamate species.

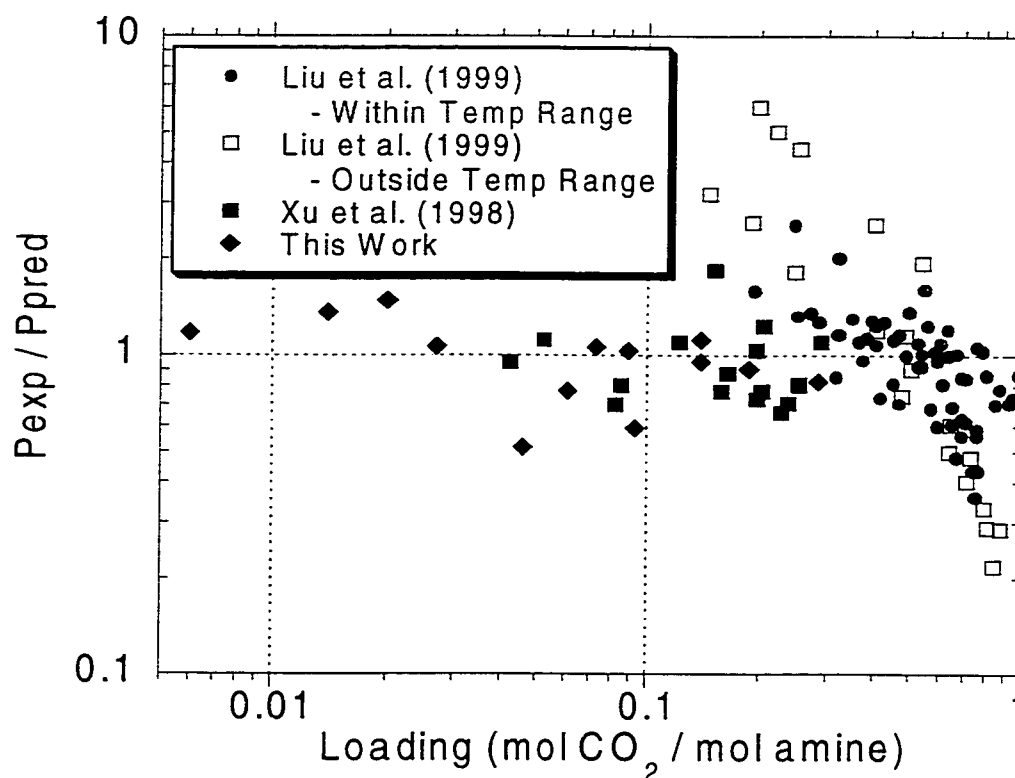


Figure 5.4 Model predictions for all CO₂ solubility data in PZ/MDEA blends

This is most probably due to a faster transfer of the deuterium. The C-H correlation, however, confirms that the relative position of the species have not shifted. Numerical placement of the peaks is shown in table 5.8.

Table 5.8 NMR data for 0.6M PZ/4M MDEA, 298K and CO₂ loading of 0.52

¹ H Peak			¹³ C Peak	
δ	Area	Species	δ	Species
(ppm)			(ppm)	
3.323	2.67	Methylene H's adjacent to alcohol in	41.08	Methyl C in MDEA
3.311		MDEA	41.60	Carbamate ring C's adjacent to carbamate side
3.300			42.55	
3.067	0.49	Protonated Carbamate / carbamate methylene H's on carbamate side	43.41	Carbamate ring C's adjacent to non carbamate side
2.812	0.62	Methylene H's in piperazine dicarbamate	44.2	Dicarbamate ring C's
2.571	0.73	Protonated carbamate / carbamate methylene H's on noncarbamate side	58.69	Methylene C's adjacent to alcohol in MDEA
2.517	2.67	PZ / Protonated PZ methylene H's & Methylene H's adjacent to amine in	57.78	Methylene C's adjacent to amine in MDEA
2.505		MDEA		
2.494				
2.136	2.00	MDEA Methyl H's		

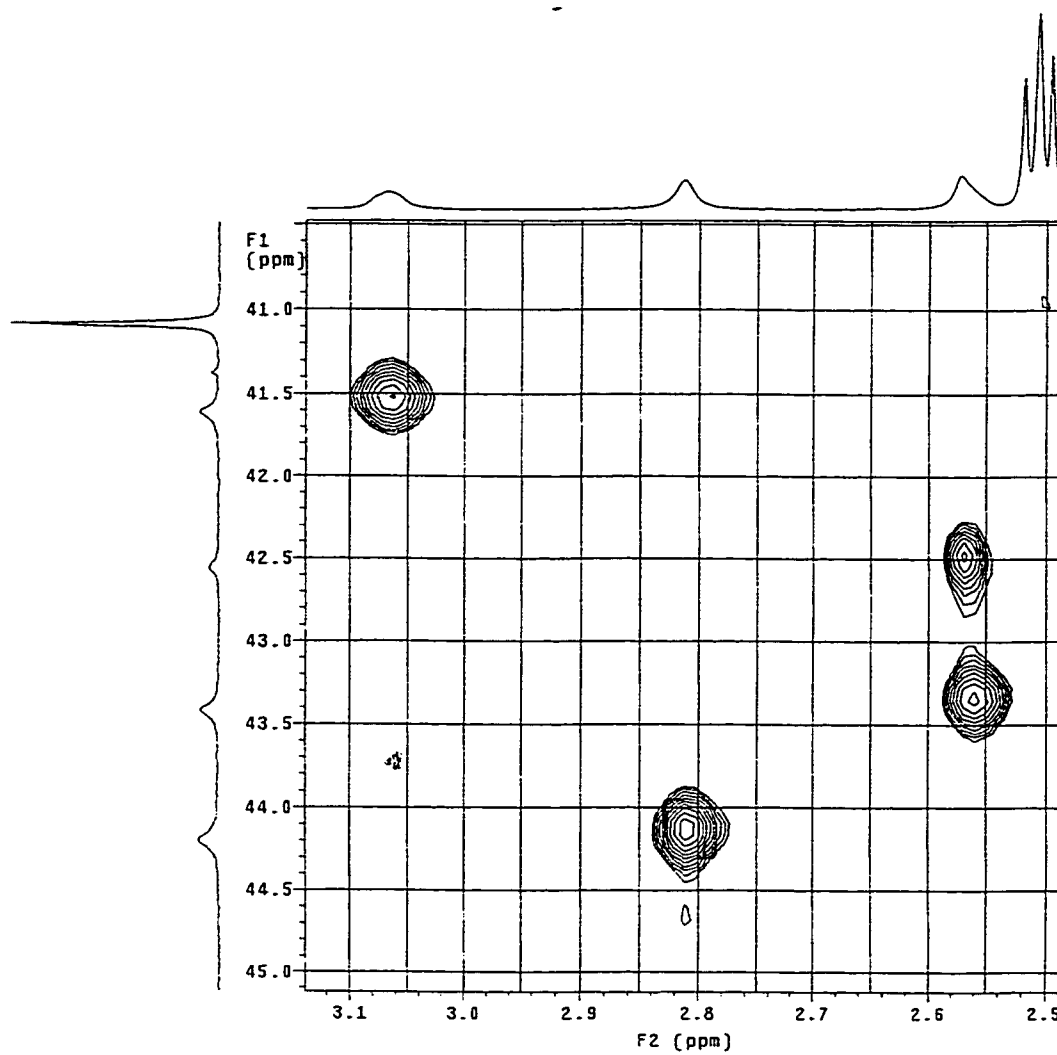


Figure 5.5 Proton, ^{13}C and short range C-H correlation NMR spectra for 1M PZ, 3M MDEA solution at 298K and a CO_2 loading of 0.52 moles/mol amine.

We can calculate the ratios of species present using the areas of the proton spectra. Table 5.9 shows the ratios of several PZ and MDEA species as measured by Proton NMR data along with the model predicted values at the same conditions. The ratio of dicarbamate to mono and protonated carbamate was matched by adjusting the $\text{PZ}(\text{COO}^-)_2 \text{MDEAH}^+ / \text{H}_2\text{O}$ A parameter. Other predicted ratios match the experimentally observed values well.

Table 5.9 – Ratio of species using NMR data at 298K, 1M PZ, 3 M MDEA, loading=0.52

Ratio	NMR Result	Model Predicted
$x_{\text{PZ}(\text{COO}^-)_2} / (x_{\text{PZCOO}^-} + x_{\text{H}+\text{PZCOO}^-})$	0.63	0.63
$(x_{\text{PZCOO}^-} + x_{\text{H}+\text{PZCOO}^-}) / (x_{\text{PZ}} + x_{\text{PZH}^+})$	4.1	3.1
$x_{\text{PZ}(\text{COO}^-)_2} / (x_{\text{MDEAH}^+} + x_{\text{MDEA}})$	0.12	0.11

5.8 Model predictions

Figure 5.6 shows the calculated value for the equilibrium partial pressure of CO_2 above PZ/MDEA solutions at 313 and 343 K. It can be seen that the effect of PZ is prevalent mainly at low loading. This is seen more clearly in figure 5.7 which compares the ratio of equilibrium partial pressure in several promoted MDEA systems (0.5M promoter, 4M MDEA) to that of 4M MDEA. The curves for MEA and DEA are those calculated by Austgen (1989). The effect of the promoter is most prevalent at low loading. The ratio of partial pressures at a loading approaching 0 is determined exclusively by the carbamate stability constant. Table 5.10 includes values of the carbamate stability constants for PZ and DEA at several different reference states. Since the carbamate stability of DEA and PZ are almost identical, it is not apparent at first that there is any

correlation between the ratio of partial pressures at very low loading and the carbamate stability constant.

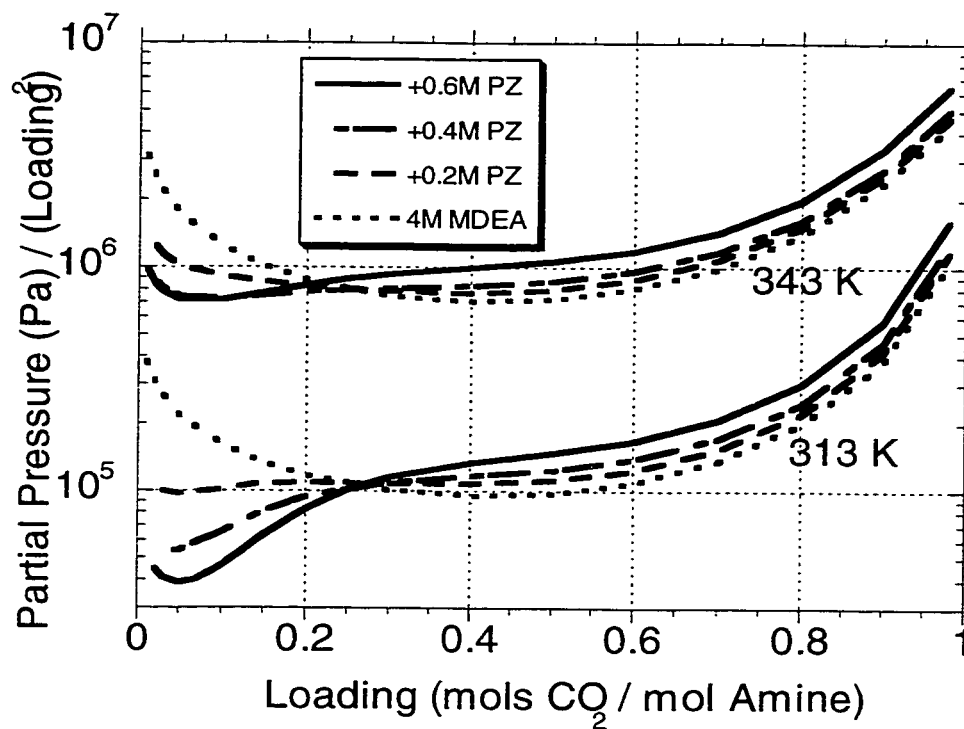


Figure 5.6 Equilibrium partial pressure prediction for CO₂ in 4M MDEA and various PZ concentrations.

When the carbamate stability is re-normalized to the solution concentration (in the presence of 4M MDEA) the correlation becomes more apparent. It is seen that the carbamate stability constant of DEA and PZ differ substantially in 4M MDEA even though they are comparable when all species are at their reference states.

The partial pressure in promoted MDEA systems is often higher than that of MDEA systems at higher loading. This is seen to be the case for MEA, DEA and PZ in figure 5.7.

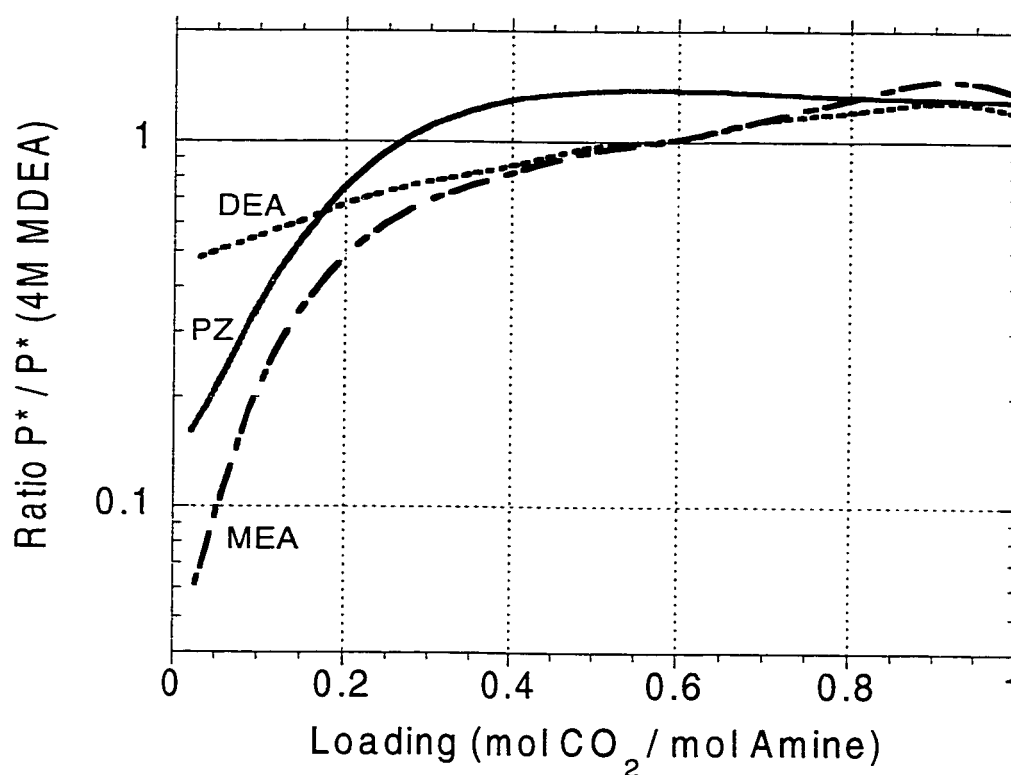


Figure 5.7 Comparison of PZ to other promoters in 0.5M Promoter, 4M MDEA solutions at 313K.

Table 5.10 Comparison of carbamate stability constants (313K, Mole Fraction based)

Amine	All Species at their Reference States	1 M Amine in Water	In 4M MDEA (0 Loading)
DEA	4.8E-6	2.6E-6	2.5E-7
PZ	6.7E-6	1.1E-5	8.7E-6
PZCOO ⁻	3.0E-7	2.6E-6	5.3E-6

$$* K_{CARB} = \frac{x_{RR'NCOO^-} x_{H3O^+}}{x_{H2O} x_{CO2} x_{RR'NH}}$$

Austgen (1989) presents a discussion on this phenomenon where he shows this to be related to the two to one stoichiometry of carbamate formation. In DEA and MEA blends, this crossover point occurs around a loading of 0.6. In the PZ system, however, we see the crossover at a much lower loading. This appears to be due to the fact that many different carbamate species are formed, resulting in greater than a two to one stoichiometry for overall carbamate formation. Explained a different way, the presence of the protonated PZ carbamate and the PZ dicarbamate result in less free PZ for every mole of CO₂ absorbed.

This can be observed by comparing the speciation of the PZ system to the DEA system. Figure 5.8 and 5.10 compare the speciation of the PZ and DEA blends at 313K. The PZ concentration disappears almost completely by a loading of 0.2 and the concentration of PZ carbamate and protonated PZ seem to track each other, rising at low loading and reaching a maximum at a loading of 0.2. Conceptually these trends exist in DEA as well with the concentration of free DEA staying higher than PZ until a loading of 0.5 while the carbamate and protonated DEA species reach their maximum around a loading of 0.6 or 0.7.

We also show a curve for PZ + PZCOO⁻ on figure 5.10. This compares the reactive amine in PZ/MDEA to DEA/MDEA. We see that the total reactive amine

in the PZ blend is comparable to the DEA blend. From a kinetics point of view, the advantage of the PZ system is that its rate constant is much higher than DEA or MEA. Comparing the effect of temperature on carbamate stability in figure 5.9, we see that the dicarbamate concentration is much lower at 343K than at 313K.

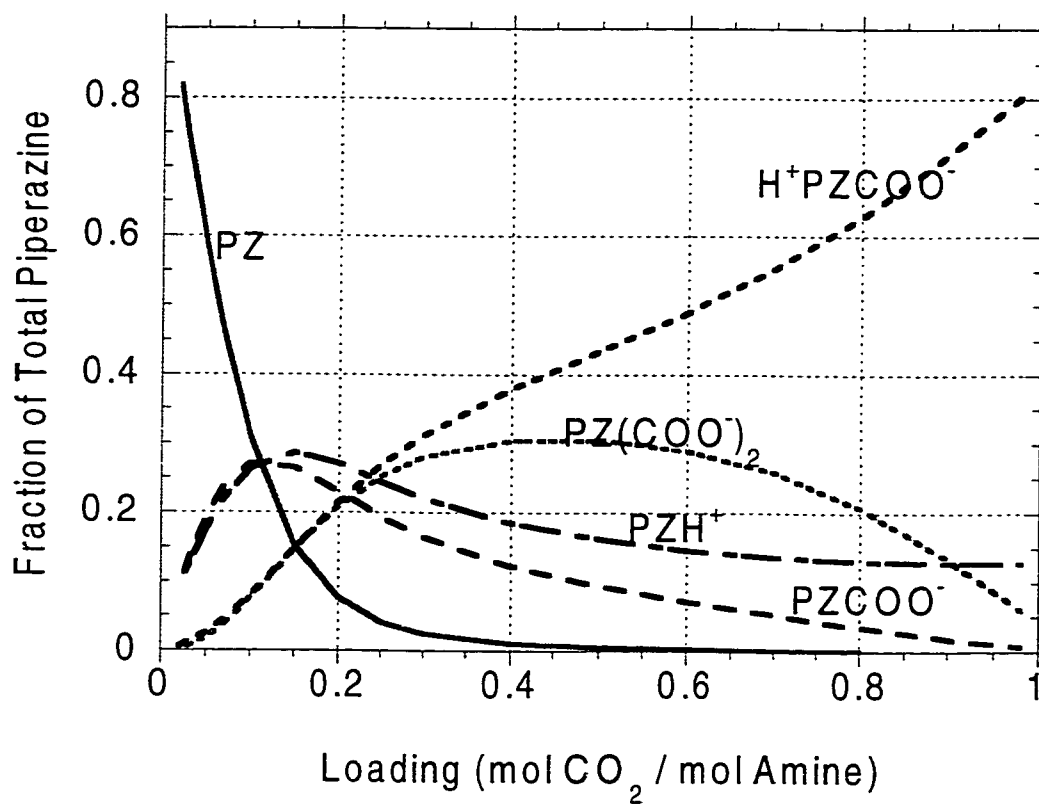


Figure 5.8 Speciation of 0.5M PZ, 4M MDEA solution at 313K. Results are shown as a fraction of total piperazine.

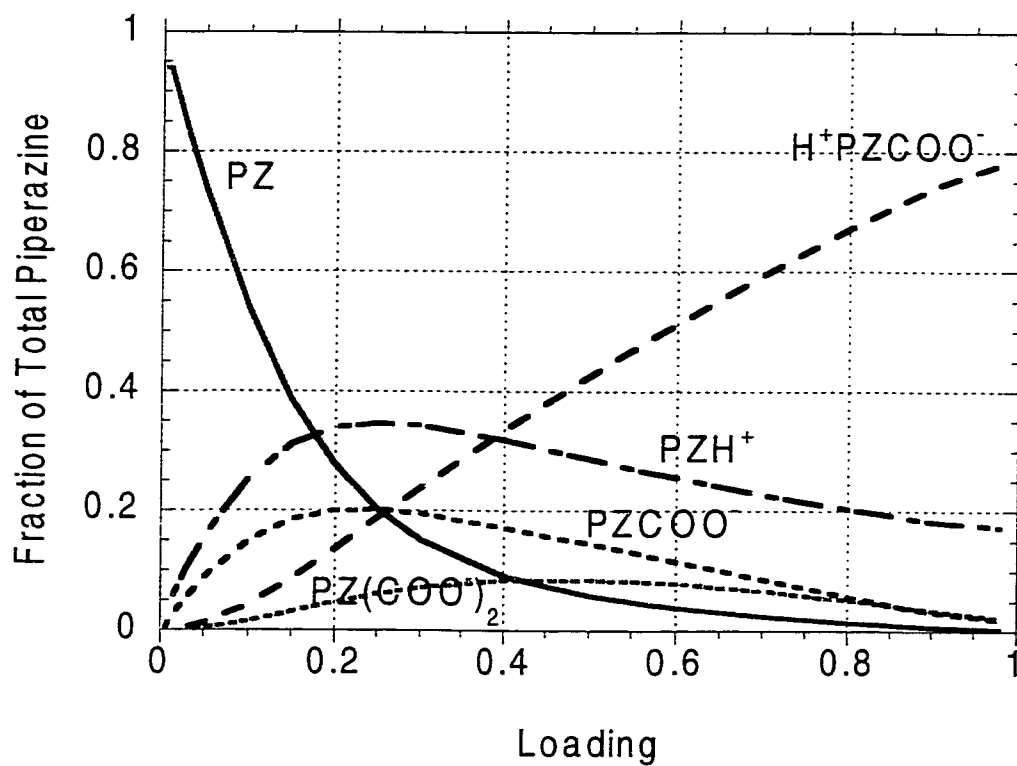


Figure 5.9 Speciation of 0.5M PZ, 4M MDEA solution at 343K. Results are shown as a fraction of total piperazine.

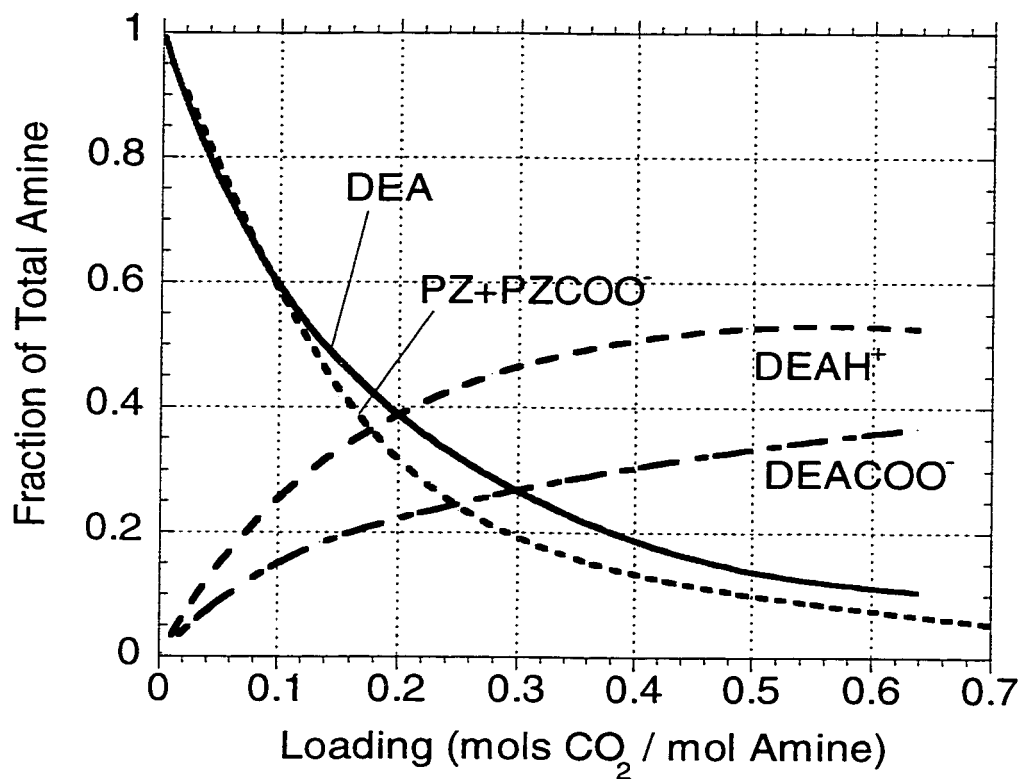


Figure 5.10 Speciation of 0.5M DEA, 4M MDEA solution at 313K. Results are shown as a fraction of total Amine. Predictions made by Chakravorty (1992) using the model of Austgen (1989).

Figure 5.11 shows activity coefficients of species at 313K, 0.6M PZ and 4M MDEA. Volatility estimates of PZ in PZ activated MDEA solutions are presented in figure 5.12. Since total pressures and gas phase compositions vary widely in industrial absorbers, results are presented as the vapor side fugacity of

PZ. Since the gas leaving the absorber will last be in contact with the lean amine solution entering the top of the column, all calculations are done at a lean loading of 0.01. PZ is seen to be very volatile compared to MDEA and other promoters. Although the vapor pressure of PZ is comparable to MEA, the activity coefficient at infinite dilution in water is a little bit higher. At 40°C, 0.6M PZ, 4M MDEA (5wt% PZ, 45wt% MDEA), PZ losses are seen to be as large as MDEA losses even though the MDEA concentration is higher by a factor of 7.

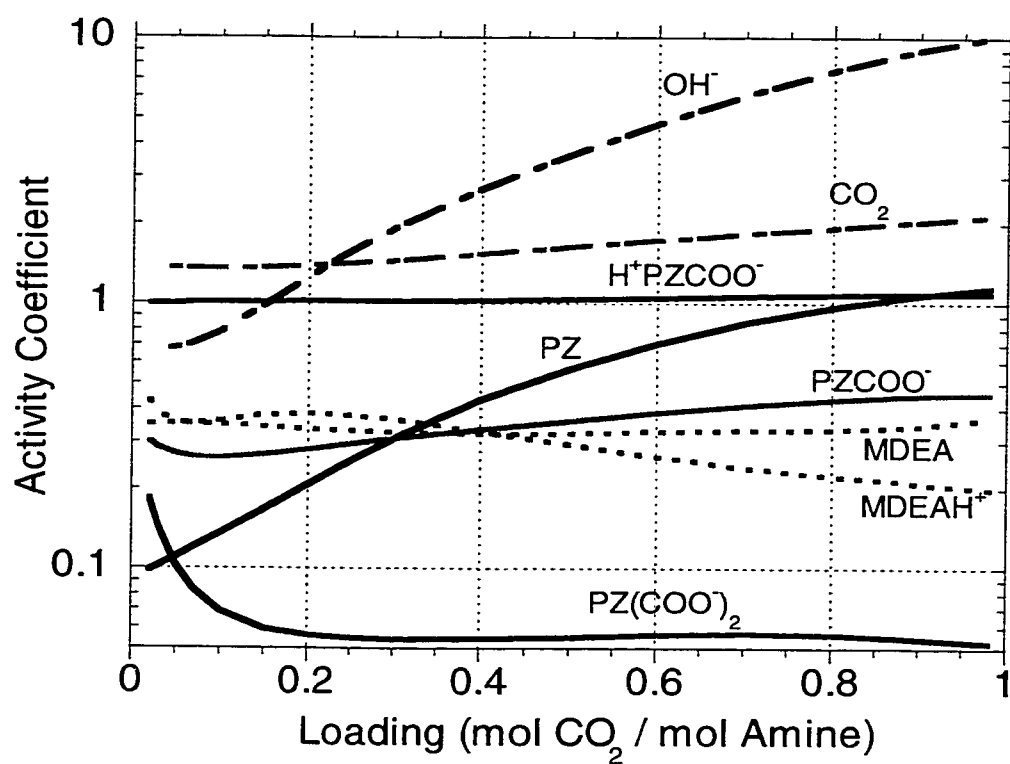


Figure 5.11 Activity coefficients for 0.6M PZ, 4M MDEA blend at 313K

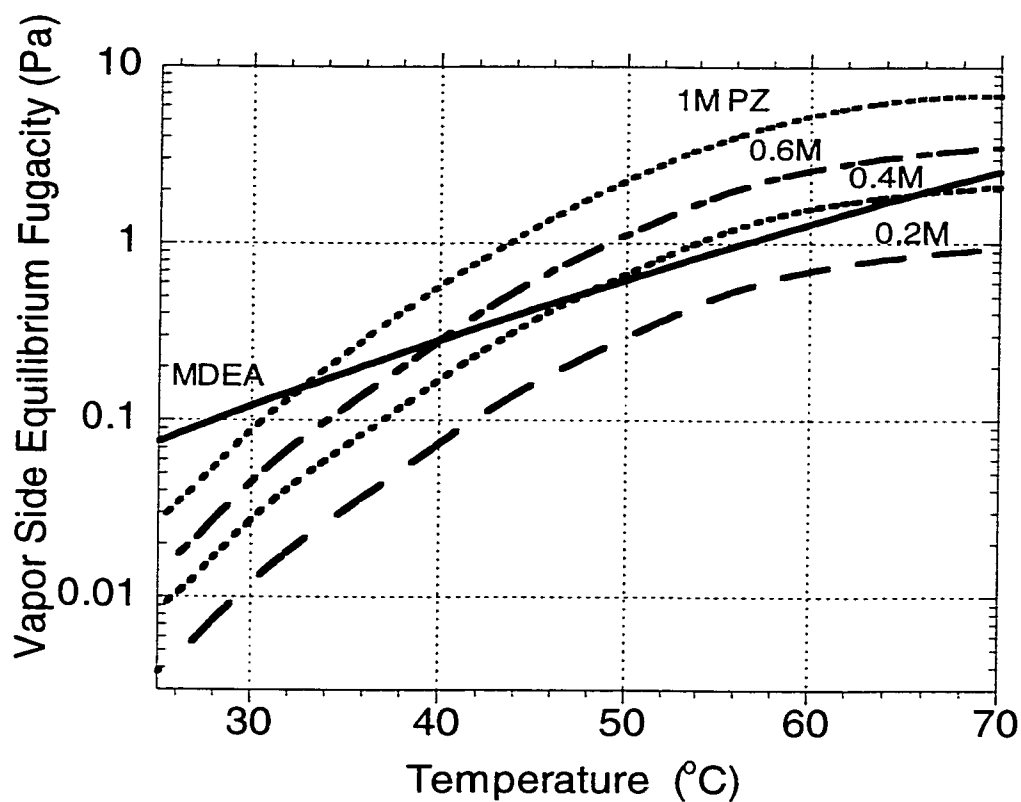


Figure 5.12 Prediction of PZ volatility in 4M MDEA solution and various PZ concentrations. All calculations are performed at a lean loading of 0.01 mols CO_2 / mol amine.

5.9 Conclusions

1. Equilibrium partial pressure compared to other amines: The experimental solubility of CO_2 and model predictions presented in this work suggest that PZ activated MDEA blends offer a lower equilibrium partial pressure of CO_2 at

low loading than DEA / MDEA blends. Partial pressures at low loading are, however, seen to be higher than those in MEA promoted MDEA. This is due to the carbamate stability of each of these promoters.

2. Reactivity: The fraction of reactive amine in PZ/MDEA blends is the same as other promoted MDEA systems (DEA/MDEA) as loading is increased.
3. Reaction products at different conditions: The most prevalent reaction product at low loading (<0.2 at low loading) is PZ carbamate. At higher loading, however, most of the PZ is seen to be in the form of protonated PZ carbamate.
4. Effect of additional carbamate species: The existence of the protonated carbamate and the dicarbamate have the adverse effect of stabilizing the overall carbamate formation. This leads to a higher partial pressure than that observed in MDEA at loadings above 0.3 at 313K.
5. PZ losses due to volatility: The volatility of PZ is higher than other promoters and losses of PZ may be as high as those of MDEA in industrially significant concentrations. Measurements of PZ volatility in H₂O and MDEA solutions will enhance the prediction of equilibrium CO₂ partial pressure and speciation in PZ activated MDEA blends.
6. NMR has proven to be a useful technique in stabilizing carbamate species and quantifying their equilibrium constants.
7. Previous data on CO₂ solubility: Our model and data show that PZ only has a large effect on the solubility when the ratio of total carbon dioxide to PZ is less than one. The model presented in this work predicts the data of other investigators at high loading as well.
8. Modeling conclusions of previous investigators: PZ carbamate, dicarbamate and protonated carbamate were erroneously neglected by Liu et al. (1999). These species have been detected using Proton and ¹³C NMR.

Chapter 6

Absorption of CO₂ in aqueous PZ/MDEA blends

Blends of DEA and DGA[®] with MDEA have been used for removing CO₂ from natural gas (Chakravarty, 1985). In the early 80's, the BASF corporation patented activated MDEA solvents (aMDEA[®]; Appl et al., 1982). Activated MDEA uses blends of PZ (up to 0.8M) in MDEA (1.5 to 4.5M, Appl et al., 1982). These solvents have found widespread application in the removal of carbon dioxide from synthesis gas in ammonia plants and hydrogen/carbon monoxide plants (Wammes et al., 1994).

The popularity of these solvents appears to be due to very fast kinetics (Bishnoi and Rochelle, 2000b) which enables PZ to be added in very low concentrations (<0.8M, Appl et al., 1982). Fundamental data on the PZ/MDEA/H₂O/CO₂ system is very limited.

The VLE measurements of Xu et al. (1998) and Liu et al. (1999) have been discussed in Chapter 5. Unfortunately, these data have not been acquired in a region where there is any significant deviation from the behavior of MDEA. Xu et al. (1992) have also studied the absorption of CO₂ from gas at ambient pressures into aqueous blends of PZ / MDEA. The work of Xu et al. was performed at conditions where PZ was almost completely depleted at the gas/liquid interface and, therefore, no information can be gained about the kinetics of CO₂ with PZ. This is discussed in detail in Chapter 4.

Kaganoi (1997) has used the same wetted wall apparatus as this work to study CO₂ absorption into 0.6M PZ, 4M MDEA at 313K. His data was acquired at high driving force and moderate to high loading.

Bishnoi and Rochelle (2000) (chapter 4 in this work) study the aqueous PZ system and show that the rate constant of PZ with CO₂ is an order of magnitude higher than that of conventional carbamate formers such as MEA. Their studies on equilibrium partial pressure and NMR have shown that the second nitrogen on PZ is reactive to form protonated PZ carbamate and PZ dicarbamate. The pH of these systems is never low enough to observe di-protonated PZ.

Chapter 5 in this work discusses the equilibrium of MDEA/PZ blends. Data has been obtained at CO₂ loading from 0.005 to 0.2 in solutions of 0.6M PZ, 4M MDEA and 313 to 343K. In this loading region, PZ species make a significant difference on the partial pressure and information can be obtained about the speciation of these systems at low loading. The electrolyte NRTL model has been used to model partial pressure data in the blended amine system at low loading and NMR data at high loading.

We now combine knowledge of the single amine systems (PZ/H₂O/CO₂) and (MDEA/H₂O/CO₂) with knowledge of the thermodynamics of the blended amine system to study the rate of absorption of CO₂ into PZ/MDEA blends. We specifically target experiments at loading where the total CO₂ concentration is less than the total PZ concentration and driving forces where PZ is not depleted at the interface. The apparent second order rate constant of PZ / CO₂ is seen to double in the presence of 4M MDEA, leading us to believe that MDEA participates in the reaction of PZ with CO₂. This is consistent with the zwitterion mechanism proposed for DEA and other secondary amines (Caplow, 1968). Measurements are also made at loading, partial pressure and temperature representative of industrial absorption.

A new rigorous model for calculating the concentration gradients of all species throughout the boundary layer and the enhancement factor for CO₂ absorption is presented. The new model is based largely on the findings of Glasscock (1990) who showed the eddy diffusivity theory to give answers as accurate as penetration theory or surface renewal theory. The resulting rate-based model is combined with the thermodynamics model of Chapter 5 to predict rate of absorption, enhancement factor, and height and volume of transfer unit predictions at industrially significant conditions of absorption. These results are presented and compared to other promoted MDEA systems in sections 6.5 through 6.7.

6.1 Model Description

Glasscock and Rochelle (1989) have studied theories on mass transfer applied to the removal of acid gas using amines. For a second order reaction, Glasscock's work showed film theory (Lewis and Whitman; 1924) to deviate 30% at enhancement factors of about 100. This requires us to use a better mass transfer theory than film theory. For the test problem they studied, results show that the eddy diffusivity theory never deviates more than 3% from surface renewal theory. Eddy diffusivity theory will be used in this work.

For absorption of CO₂ into a non-reactive solvent, Glasscock and Rochelle used the following expression to represent the material balance of CO₂ across the boundary liquid layer.

$$\frac{d}{dx} \left[\left(D_{CO_2} + \epsilon x^m \right) \frac{d}{dx} [CO_2] \right] = 0 \quad (6.1)$$

Equation 6.1 displays eddy diffusivity theory conceptually. It shows that with x close to 0, mass transfer is dominated by the diffusion coefficient of CO₂. As x

increases, the effect of eddies becomes more important.

We assume all ion diffusion coefficients to be equal. This is analogous to ignoring the effect of electrical potential on ion diffusion. Glasscock and Rochelle show the effect of electrical potential to be insignificant for promoted amine systems.

We use a value of 2 for m . This value is suggested by Prasher and Fricke (1974) and is consistent with the work of Glasscock. The mass transfer coefficient then becomes.

$$k_{l,i}^o = \frac{2}{\pi} \sqrt{\epsilon D_i} \quad (6.2)$$

This work uses the space variable transformation used in the work of Glasscock, originally proposed by Versteeg (1987).

$$r = \frac{2}{\pi} \tan^{-1} \left(x \sqrt{\frac{\epsilon}{D}} \right) \quad (6.3)$$

This dimensionless transformation variable is convenient in two ways:

1. It bounds the space variable: as x goes from 0 to ∞ , r goes from 0 to 1.
2. It results in a straight line concentration gradient for physical mass transfer.

This work divides r space from 0 to 1 into 38 nodes (starting at the gas liquid interface and moving into the liquid phase: 1 node at $r=0$, 10 nodes with grid spacing of $1.0E-4$, 9 nodes with grid spacing of $1.0E-3$, 9 nodes with grid spacing of $1.0E-2$, 9 nodes with grid spacing of 0.1). Three point forward differencing was used at the interface to describe all derivatives:

$$\left(\frac{df}{dr} \right)_i = \frac{1}{2\Delta r} (-3f_i + 4f_{i+1} - f_{i+2}) \quad (6.4)$$

Three point central difference formulas were used where there were equal gridsizes on each side of the node of interest.

$$\left(\frac{df}{dr} \right)_i = \frac{1}{2\Delta r} (-f_{i-1} + f_{i+1}) \quad (6.5)$$

$$\left(\frac{d^2 f}{dr^2} \right)_i = \frac{1}{(\Delta r)^2} (f_{i-1} - 2f_i + f_{i+1}) \quad (6.6)$$

The finite difference scheme for non-uniform gridsize of Liu et al. (1994) was used at nodes where the gridsize changed.

The material balance equations using the transformed variable are lengthy. Material balance equations in the transformed variables are derived in Glasscock (1990). Although the ultimate use of these equations appears to be correct, unfortunately one of the terms was omitted during documentation. These equations are derived and presented in Appendix E.

In x space we can express the material balance in the following form:

$$\nabla \left(\left(Di + \epsilon x^2 \right) \nabla [i] \right) = -\mathfrak{R}_i \quad (6.7)$$

where i is a component to be included in the model
 ϵ is the mass transfer coefficient parameter
 \mathfrak{R}_i is the overall rate of reaction of species i
 ∇ is the derivative operator with respect to the space variable x

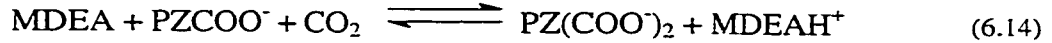
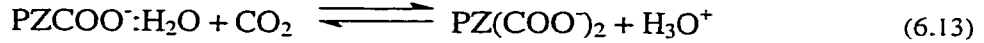
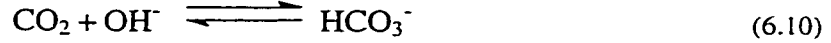
we simplify this further as:

$$\nabla^2 [i] = -\mathfrak{R}_i \quad (6.8)$$

where ∇^2 can be considered the Eddy Diffusivity operator.

A proper understanding of the model used in this work begins with a

discussion of all species and reactions used. The following six equations are assumed to be kinetically controlled.



For each kinetically controlled reaction, we consider the overall reversible rate of reaction. Thus, for the MDEA reaction with CO_2 (reaction 6.9), we express the overall rate of reaction as:

$$R_9 = k_{\text{MDEA}} \left([\text{MDEA}][\text{CO}_2] - \frac{[\text{MDEAH}^+][\text{HCO}_3^-]}{K_9} \right) \quad (6.15)$$

where the equilibrium constant $K_9 = \frac{[\text{MDEAH}^+][\text{HCO}_3^-]}{[\text{MDEA}][\text{CO}_2]}$ and is calculated by

the ratio of the species in the bulk solution.

Note that water is left out of the kinetic and equilibrium expressions since it is considered to be constant across the boundary layer and, therefore, can be lumped with the apparent rate and equilibrium constants.

In order to avoid having H_3O^+ as a species in the model, rates of reaction for carbamate formation are described as:

$$R_{11} = k_{\text{PZ}} \left([\text{PZ}][\text{CO}_2] - [\text{PZCOO}^-] \frac{K_w}{K_6[\text{OH}^-]} \right) \quad (6.16)$$

where : $K_w = [H_3O^+][OH^-]$ and $K_6 = \frac{[H_3O^+][PZCOO^-]}{[PZ][CO_2]}$

Other rate expressions for equations 6.9 through 6.14 follow. Values for the rate constants for reactions 6.9 through 6.14 are documented below. The rate constant for MDEA used in this work is the expression of Littel et al. (1991). Although never found to be an important contribution to the overall reaction, the reaction of hydroxide with CO₂ is considered in this work. The rate constant for reaction 6.10 is the expression presented by Pinsent et al. (1956). The determination of k_{PZ} is described in chapter 4. The expression for k_{PZ/MDEA} from rate of absorption data at low loading is presented below but discussed later in the context of the zwitterion mechanism in section 6.3.1. The rate constants for reactions 6.13 and 6.14 are fit to match absorption data into loaded solutions and are discussed in section 6.3.2.

$$k_2 = k_{25^\circ C} \cdot \exp \left[-\frac{\Delta H_a}{R} \left(\frac{1}{T} - \frac{1}{298.15} \right) \right] \quad (6.17)$$

where

For reaction 6.12 (carbamate formation by PZ/MDEA)

$$k_{25C} = 1.46E4 \text{ m}^6/\text{kmol}^2 \text{ s}$$

$$\Delta H_a = 8.43E4 \text{ kJ/kmol}$$

For reaction 6.13 (di-carbamate formation)

$$k_{25C} = 4.70E4 \text{ m}^3/\text{kmol s}$$

$$\Delta H_a = 3.36E4 \text{ kJ/kmol}$$

For reaction 6.14 (di-carbamate formation by PZCOO⁻/MDEA)

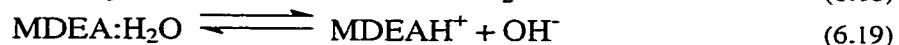
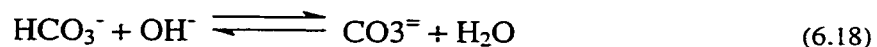
$$k_{25C} = 1.27E4 \text{ m}^6/\text{kmol}^2 \text{ s}$$

$$\Delta H_a = 8.43E4 \text{ kJ/kmol}$$

and

$$R = 8.314 \text{ kJ/kmol K}$$

Reactions involving only a proton transfer are considered to always be in equilibrium. These reactions are:



There are eleven species that need to be considered. At each node, therefore, there are 11 unknowns that need to be determined. The equations to be solved at each node are presented in table 6.1. Along with these 11 equations at each node, we define boundary conditions at the interface and in the bulk solution. We use the condition that all concentrations are equal to the equilibrium concentrations as liquid depth approaches infinity. We also assume phase equilibrium of CO_2 at the interface leading to a known concentration of CO_2 at the interface for a given interfacial partial pressure of CO_2 . The concentration of species which undergo proton exchange are defined by the combined buffer system flux being zero at the interface and chemical equilibrium between the two species involved in the proton exchange. Since dicarbamate does not go through a rapid proton exchange, its flux is considered to be zero at the interface. Electroneutrality is also assumed at the interface. Table 6.1 also documents the boundary conditions used in this work.

Table 6.1 – Model Equations and Boundary Conditions

Conservation Equations at Each Node

Overall Species Material Balance

$$\nabla^2[\text{PZ}] + \nabla^2[\text{PZCOO}^-] + \nabla^2[\text{H}^+\text{PZCOO}^-] + \nabla^2[\text{PZH}^+] + \nabla^2[\text{PZ}(\text{COO}^-)_2] = 0$$

$$\nabla^2[\text{MDEA}] + \nabla^2[\text{MDEAH}^+] = 0$$

$$\nabla^2[\text{CO}_2] + \nabla^2[\text{HCO}_3^-] + \nabla^2[\text{CO}_3^{2-}] + \nabla^2[\text{PZCOO}^-] + \nabla^2[\text{H}^+\text{PZCOO}^-] + 2\nabla^2[\text{PZ}(\text{COO}^-)_2] = 0$$

Equilibrium Relationships

$$K_{18} = \frac{[\text{MDEAH}^+][\text{OH}^-]}{[\text{MDEA}]}$$

$$K_{19} = \frac{[\text{PZH}^+][\text{OH}^-]}{[\text{PZ}]}$$

$$K_{20} = \frac{[\text{H}^+\text{PZCOO}^-][\text{OH}^-]}{[\text{PZCOO}^-]}$$

$$K_{17} = \frac{[\text{CO}_3^{2-}]}{[\text{HCO}_3^-][\text{OH}^-]}$$

Material Balance for Molecular CO₂

$$\nabla^2[\text{CO}_2] - (\text{R}_9 + \text{R}_{10} + \text{R}_{11} + \text{R}_{12} + \text{R}_{13} + \text{R}_{14}) = 0$$

Carbamate Buffer System Balance

$$\nabla^2[\text{PZCOO}^-] + \nabla^2[\text{H}^+\text{PZCOO}^-] + \text{R}_{11} + \text{R}_{12} - (\text{R}_{13} + \text{R}_{14}) = 0$$

Dicarbamate Material Balance

$$\nabla^2[\text{PZ}(\text{COO}^-)_2] + \text{R}_{13} + \text{R}_{14} = 0$$

Electroneutrality

$$[\text{MDEAH}^+] + [\text{PZH}^+] = [\text{HCO}_3^-] + 2[\text{CO}_3^{2-}] + [\text{OH}^-] + [\text{PZCOO}^-] + 2[\text{PZ}(\text{COO}^-)_2]$$

Boundary Conditions

At x=0

$$[\text{CO}_2] = [\text{CO}_2]_i$$

$$D_{\text{PZ}} \nabla[\text{PZ}] + D_{\text{PZH}^+} \nabla[\text{PZH}^+] = 0$$

$$K_{19}[\text{PZ}] - [\text{PZH}^+][\text{OH}^-] = 0$$

$$D_{\text{MDEA}} \nabla[\text{MDEA}] + D_{\text{MDEAH}^+} \nabla[\text{MDEAH}^+] = 0$$

$$K_{18}[\text{MDEA}] - [\text{MDEAH}^+][\text{OH}^-] = 0$$

$$D_{\text{PZCOO}^-} \nabla[\text{PZCOO}^-] + D_{\text{H}^+\text{PZCOO}^-} \nabla[\text{H}^+\text{PZCOO}^-] = 0$$

$$K_{20}[\text{PZCOO}^-] - [\text{H}^+\text{PZCOO}^-][\text{OH}^-] = 0$$

$$D_{\text{HCO}_3^-} \nabla[\text{HCO}_3^-] + D_{\text{CO}_3^{2-}} \nabla[\text{CO}_3^{2-}] = 0$$

$$K_{17}[\text{HCO}_3^-][\text{OH}^-] - [\text{CO}_3^{2-}] = 0$$

$$\nabla[\text{PZ}(\text{COO}^-)_2] = 0$$

$$[\text{MDEAH}^+] + [\text{PZH}^+] = [\text{HCO}_3^-] + 2[\text{CO}_3^{2-}] + [\text{OH}^-] + [\text{PZCOO}^-] + 2[\text{PZ}(\text{COO}^-)_2]$$

At x = ∞

$$[i] = [i]_o \quad \text{For all species } i \text{ in solution}$$

6.2 Physical Properties

The Henry's law constant for CO₂ (H_{CO_2}) is obtained using the N₂O analogy that states that the solubility of CO₂ is proportional to the solubility of N₂O.

$$H_{CO_2} = \frac{H_{CO_2.H_2O}}{H_{N_2O.H_2O}} \quad (6.22)$$

Data for N₂O solubility in MDEA solutions has been correlated by Al-Ghawas et al. (1989) to represent the solubility of CO₂ (eq. 6.22)

$$H_{CO_2} (atmL/mol) = \exp(k_{10} + \frac{k_{11}}{T(K)} + \frac{k_{12}}{T^2}) \quad (6.23)$$

Where:

$$K_{10} = 2.01874 - 23.7638 x_{am} + 290.09 x_{am}^2 - 480.196 x_{am}^3$$

$$K_{11} = 3135.49 + 15493.1 x_{am} - 183987 x_{am}^2 + 300562 x_{am}^3$$

$$K_{12} = -813702 - 2480810 x_{am} + 29201000 x_{am}^2 - 47085200 x_{am}^3$$

x_{am} = Weight fraction of amine

The diffusion coefficient of MDEA in aqueous solutions has been studied experimentally by Rowley (1999). He studied solutions from 0-50 wt% MDEA and temperatures from 298 to 373K. His data has been fit in this work to the following correlation.

$$D_{MDEA} = d_0 + d_1 x_{am} + d_2 x_{am}^2 \quad (6.24)$$

Where:

$$d_0 = 4.272E - 4T^2 - 2.8582E - 2T - 22.036$$

$$d_1 = 4.88E - 3T^2 - 3.4444T + 576.98$$

$$d_2 = -7.92E - 3T^2 + 5.1699T - 822.13$$

Diffusion coefficients for PZ are calculated using the diffusion coefficient

of MDEA corrected for molecular weight by multiplying by a factor of 1.2. Diffusion coefficients of all ions are arbitrarily set at the same value as PZ.

The diffusion coefficient of CO₂ in concentrated MDEA solutions is calculated using the N₂O analogy.

$$D_{CO_2} = \frac{D_{CO_2.H_2O}}{D_{N_2O.H_2O}} \quad (6.25)$$

The diffusion coefficient of CO₂ and N₂O in water have been determined by Versteeg et al. (1988) to be:

$$D_{N_2O.H_2O} (cm^2 / s) = 0.04041 \exp\left(-\frac{2288.4}{T}\right) \quad (6.26)$$

$$D_{CO_2.H_2O} (cm^2 / s) = 0.02397 \exp\left(-\frac{2122.2}{T}\right) \quad (6.27)$$

Pacheco (1998) presents a correlation for the diffusion coefficient of N₂O in amine solution that takes the form of the Stokes-Einstein equation.

$$D_{N_2O} (cm^2 / s) = 5.33E - 8 \frac{T}{\mu^{0.545}} \quad (6.28)$$

Here, the solution viscosity is calculated using the correlation of Glasscock (1990) given in equation

$$\ln \mu = A + \frac{B}{T} + CT \quad (6.29)$$

$$A = -19.52 - 23.40x_{am} - 31.24x_{am}^2 + 36.17x_{am}^3$$

$$B = 3912 + 4894x_{am} + 8477x_{am}^2 - 8358x_{am}^3$$

$$C = 0.02112 + 0.03339x_{am} + 0.02780x_{am}^2 - 0.04202x_{am}^3$$

We assume constant physical properties with solution loading.

6.3 Experimental Data

Experimental data obtained in this work are presented in tables 6.2 and 6.3 along with model predictions. Model predictions from this work and raw data of Kaganoi (1997) are presented in table 6.4. The data of Xu et al. (1992) are presented in Appendix E along with model predictions. The model does a good job of fitting data over a wide range of measured fluxes as shown by the parity plot in figure 6.1. The data of Xu et al. (1992) are divided into two subsets: accepted and rejected. The details of this will be discussed in section 6.3.2.3.

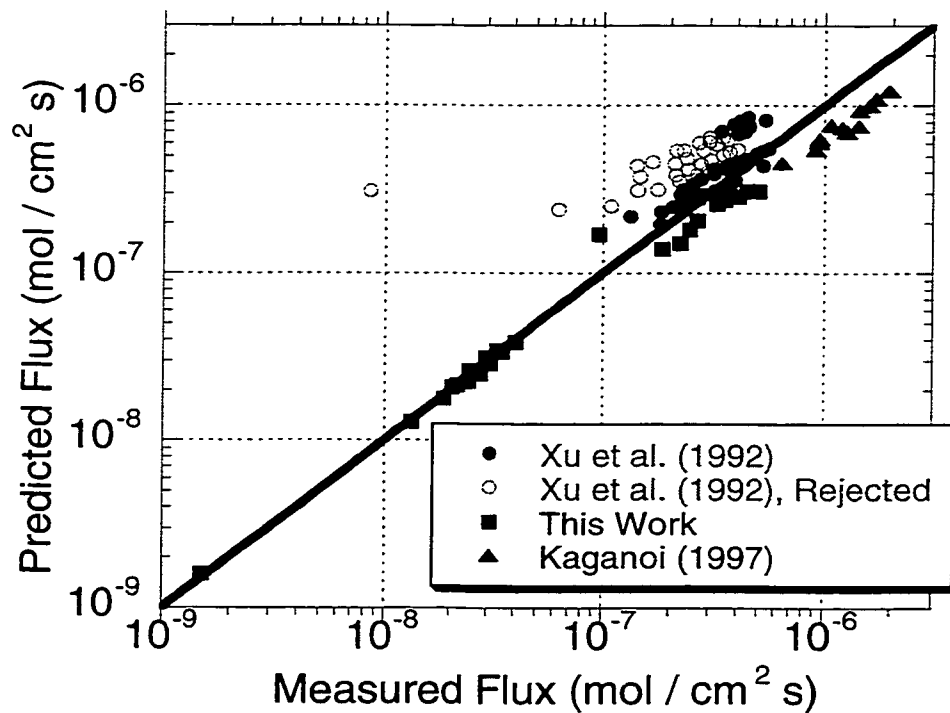


Figure 6.1 Parity plot. Rigorous model fit of all PZ/MDEA absorption data

6.3.1 Interpretation of data at low loading.

Table 6.2 shows data for the absorption of CO₂ into 0.6 M PZ, 4 M MDEA at low loading. The bulk phase partial pressure of CO₂ in this table is the log mean average of inlet and outlet pressures, like Chapter 4. At these conditions, the concentration of all ionic species is very low making all reactions except 6.9 through 6.12 unimportant. Furthermore, the rate constant for equation 6.9 is so much slower than the rest of the reactions presented in this work that it does not need to be considered at these conditions. The concentration of hydroxide ion is also low enough that reaction 6.10 can be neglected as well. Since the concentration of all reaction products is low, we only need to consider the forward reactions at these conditions.

Table 6.2 – Absorption of CO₂ into 0.6M PZ, 4M MDEA at low loading. Model predictions are from the rigorous model.

T (K)	P _{CO2} (Pa)		k _g *10 ⁵ (mol/atm cm ² s)	k ₁ *10 ⁵ (m/s)	Loading (mol CO ₂ / mol amine)	Flux*10 ⁸ mol/cm ² s		CO ₂ Removal (%)
	Gas Bulk	Eqm				Meas.	Pred.	
295	151	0.2	2.84	1.83	0.0015	1.32	1.30	27
295	207	0.4	2.87	1.82	0.0021	1.87	1.78	27
295	261	0.3	2.90	1.82	0.0018	2.44	2.27	28
295	290	0.2	2.89	1.83	0.0013	2.77	2.51	28
313	15	1.7	2.86	2.36	0.0056	0.15	0.16	30
313	169	0.9	2.89	2.06	0.0039	2.05	2.10	35
313	212	1.4	2.90	2.47	0.0050	2.47	2.64	34
313	252	1.1	2.91	2.06	0.0044	2.95	3.15	34
313	276	1.1	2.95	2.07	0.0044	3.31	3.45	34
343	127	.9	3.02	5.38	0.0011	2.15	2.17	44
343	188	2.6	3.06	5.30	0.0020	3.10	2.89	42
343	224	3.7	3.14	5.42	0.0024	3.49	3.39	40
343	243	1.8	3.17	5.32	0.0016	4.02	3.88	41

Figure 6.2 shows the apparent second order reaction of PZ with CO_2 for PZ alone and in the presence of 4 M MDEA. Each point represents several experimental partial pressures and the procedure of extracting the apparent second order rate constant from the data shown in table 6.2 has been described in chapter 4. The rate constant for reaction 6.11 was documented in chapter 4 as well. The presence of 4M MDEA appears to catalyze the reaction of CO_2 and PZ to form carbamate. This effect is consistent with the zwitterion mechanism observed for other secondary amines (Caplow, 1968; Danckwerts, 1979; Littell, 1991).

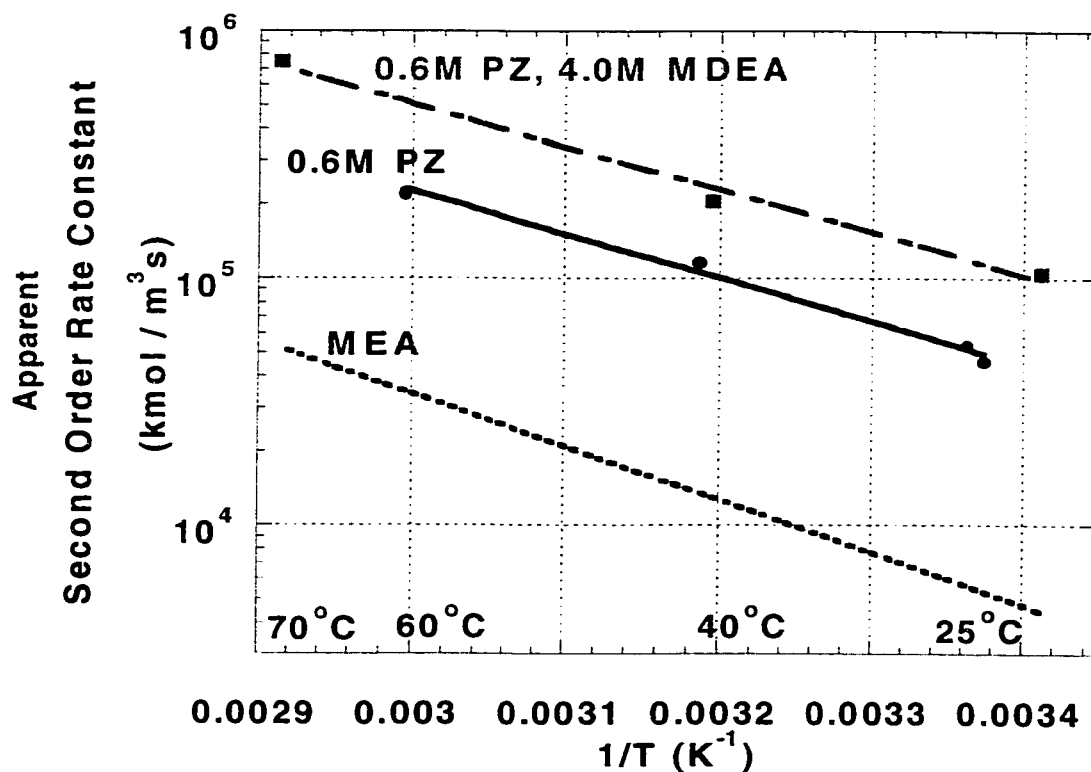


Figure 6.2 Comparison of absorption into aqueous PZ and PZ/MDEA blends with MEA (Hikita, 1977).

Glasscock et al. (1991) showed that this effect can be modeled by including the MDEA catalyzed carbamate formation (reaction 6.12). The third order rate constant for this reaction was regressed to fit the absorption data at low loading and found to follow the Arrhenius expression presented in section 6.1. It should be noted that modeling the zwitterion mechanism as two parallel reactions (one with water deprotonation and one with MDEA deprotonation) assumes that the deprotonation by PZ is negligible. This appears to be true based on the data presented in Chapter 4 where there was no effective change in the second order rate constant of PZ in 0.2M solutions and 0.6M solutions. We would expect the deprotonation by PZ to be as fast as the deprotonation by MDEA. The reason we can ignore the PZ reaction is because it is never dominant. In the aqueous system, the water seems to dominate. In the presence of MDEA, there is significantly more MDEA and, therefore, the MDEA deprotonation will dominate.

As shown by table 6.2, the model does a good job of matching absorption of CO₂ into unloaded solutions.

6.3.2 Data and Interpretation in Loaded Solutions

6.3.2.1 Data taken in this work

Table 6.3 shows the rate of absorption measurements taken in this work and model predictions in loaded solutions of PZ / MDEA. We have included a finite rate for the reaction of PZ mono-carbamate to form PZ di-carbamate (reaction 6.13 and 6.14). Without the inclusion of reactions 6.13 and 6.14, the data taken in loaded solutions was always underpredicted (40% lower than current model predictions). The sensitivity of the predicted flux to the rate constant for reactions 6.13, however, is low requiring us to manually adjust it to the Arrhenius expression presented in section 6.1. The rate constant for reaction 6.14 is set by assuming the same ratio for the rate constant of 6.14 to 6.13 as 6.12 to 6.11. This assumes that the effect of MDEA on the reaction of PZ with CO₂ is the same as the

effect of MDEA on the reaction of PZCOO^- with CO_2 .

Figure 6.3 compares measured enhancement factor and predictions from several simple models. The solid points represent experimental data while the open points represent the model predictions.

The pseudo first order model for 4M MDEA solutions is a good assumption since the reaction of MDEA is slow enough that no significant depletion of MDEA occurs at the interface. The relative position of the pseudo first order curve matches the data only at low loading. However, it is not a good assumption for PZ / MDEA blends at the practical conditions of the data taken in loaded solutions in this work.

Table 6.3 – Absorption of CO_2 into partially loaded 0.6M PZ, 4M MDEA solutions at low driving force. Predictions made with the rigorous model.

T (K)	P_{CO_2} (kPa)		$k_g \cdot 10^5$ (mol/(at m cm ² s))	$k_l \cdot 10^5$ (m/s)	Loading (mol CO_2 / mol amine)	Flux $\cdot 10^7$ (mol / cm ² s)		CO_2 Removal (%)
	Gas Bulk	Eqm				Meas	Pred	
313	5.25	0.4	1.43	2.87	0.095	3.61	3.09	41
313	3.42	0.5	2.36	3.00	0.111	2.61	2.07	29
313	3.47	0.8	2.36	2.87	0.125	2.43	1.83	27
313	3.53	1.0	2.36	2.89	0.140	2.19	1.52	25
313	4.29	1.3	2.88	2.89	0.151	0.96	1.72	8
313	9.04	2.4	2.85	2.87	0.185	2.60	2.85	10
313	14.4	4.3	2.29	2.84	0.225	3.33	3.09	10
313	20.5	7.9	1.62	2.84	0.281	3.21	2.61	10
313	27.3	10.3	1.19	2.87	0.311	4.02	2.87	13
343	1.08	0.0	3.42	6.31	0.004	1.83	1.41	40
343	2.32	0.1	3.42	6.19	0.013	3.47	2.75	36
343	3.53	0.4	3.42	6.00	0.027	4.43	3.10	32
343	4.44	0.8	3.44	6.14	0.038	5.02	3.10	29

The enhancement factor predicted by the simple model of instantaneous reactions and small driving force ($E^{\text{GLBL,INST}}$, equation 2.30) is also not a good

approximation of the data. A good approximation is obtained at high loading if we only consider the PZ reactions to be instantaneous by increasing all carbamate rate constants to very large numbers ($E^{PZ,INST}$). The dashed line in figure 6.3 is the combined enhancement factor for pseudo first order with instantaneous PZ reactions (equation 2.31 assuming only carbamate and dicarbamate formation are instantaneous).

The open circles show that the rigorous model predicts the data within 20%. The PZ carbamate rate constant was adjusted to match this data. A value of 90,000 L/mol s was obtained for this rate constant at 40°C compared to a value of 102,000 L/mol s for PZ. The Bronsted theory predicts a decrease in the rate constant for a decrease in the amine pK_a . In chapter 4 we showed the pK_a of the mono-carbamate to be lower than that of PZ. This would lead to a rate constant for the mono-carbamate lower than that of PZ (around 60,000 L/mol s). We believe that we have found a much higher value since the mono-carbamate rate constant is the only parameter adjusted to match the high loading data. It, therefore, encompasses many other changes as the solution is loaded with CO₂.

The raw experimental data and model predictions taken in this work are within a factor of 5 to 6 from equilibrium. The presence of 0.6 M PZ enhances the rate of removal above that of 4M MDEA by almost two orders of magnitude at moderate loading (<0.15) and up to an order of magnitude at high loading (<0.3).

6.3.2.2 Data of Kaganoi (1997)

Kaganoi (1997) measured CO₂ absorption rates in 0.6M PZ, 4M MDEA at 40°C in the same wetted wall apparatus used in this work. His experimental data and our model predictions of his work are shown in table 6.4. The main difference between the experimental work of Kaganoi (1997) and the experimental data presented in this work is the driving force. Kaganoi has studied bulk phase partial pressures of CO₂ up to 2 atm while this work only studies partial pressures up to

0.3 atm.

The model presented in this work consistently underpredicts the flux measured by Kaganoi by 30-40%. No further parameters were adjusted, however, to match this data. This is because no parameters were found to make a significant difference in the model fit of the data, within reasonable changes of the parameters. The sensitivity of parameters on model prediction of flux is discussed in section 6.4.2. The rate constant of PZ, PZ mono-carbamate and MDEA were increased by a factor of 4 without being able to match the data. The diffusion coefficient of MDEA, PZ and ions was increased by a factor of 4 without being able to match the data. Since we are confident of the measured value of all these constants except, perhaps the rate constant of PZ mono-carbamate, there are two explanations for the discrepancy of the model predictions and the measured values.

Table 6.4 - Absorption of CO₂ into partially loaded 0.6M PZ, 4M MDEA solutions at high driving force and 313K. Data of Kaganoi (1997)

Bulk Gas P _{CO2} (Pa)*10 ⁻³	k _g *10 ⁶ (moles/(atm cm ² s))	k _l *10 ⁵ (m/s)	Loading (mol CO ₂ / mol amine)	Flux*10 ⁶ (mol/cm ² s)	
				Measured	Predicted (Rigorous)
97	9.35	3.44	0.244	1.93	1.23
100	9.23	3.43	0.278	1.70	1.10
99	9.39	3.46	0.309	1.59	1.00
103	9.13	3.49	0.335	1.43	0.94
95	9.30	3.53	0.391	1.20	0.74
100	9.04	3.46	0.384	1.07	0.77
150	3.08	3.66	0.466	1.42	0.76
156	3.03	3.49	0.493	1.27	0.70
155	3.07	3.62	0.500	1.25	0.70
165	3.04	3.63	0.539	0.95	0.64
166	3.04	3.64	0.558	0.94	0.61
167	3.03	3.67	0.582	0.91	0.55
175	3.01	3.65	0.625	0.64	0.46

1. The data of Kaganoi is taken at significantly higher loading where the enhancement factor has been significantly reduced from the unloaded solution. For this reason, the percent removal of CO_2 across the wetted wall contactor is only about 15-20% (This is also true of some of the data taken in this work). This means that the flux is calculated by taking the difference of two large numbers and can lead to large errors. A combined error of 5% in reading the partial pressure in and out of the contactor can result in a 30% error in the flux. Also, the model is very sensitive to loading at these conditions. All of the data of Kaganoi (1997) was taken in two experiments where it appears that the amine solution and analyzer calibrations were not changed from one run to the next. Therefore, there is a possibility that the discrepancy between the model prediction and the data could be experimental error.
2. The model does not account for the direct reaction of MDEA with carbamate species. In section 6.4.3 we show that carbamate reversion to CO_2 and the subsequent reaction of the freed CO_2 with MDEA occurs, but is never significant. Therefore, it is a possibility that there is a direct reaction of carbamate with MDEA which makes absorption faster than predicted in this work. We recommend experimental investigation of this phenomenon by keeping the loading of the solution constant and varying the driving force. If there is a direct interaction of the carbamate with MDEA, the model prediction of the flux will increasingly under predict the measured flux with increasing driving force.

The data of Kaganoi is also shown in figure 6.3. Even with high driving force, it appears as though 0.6 M PZ results in significant enhancement above the performance of 4M MDEA.

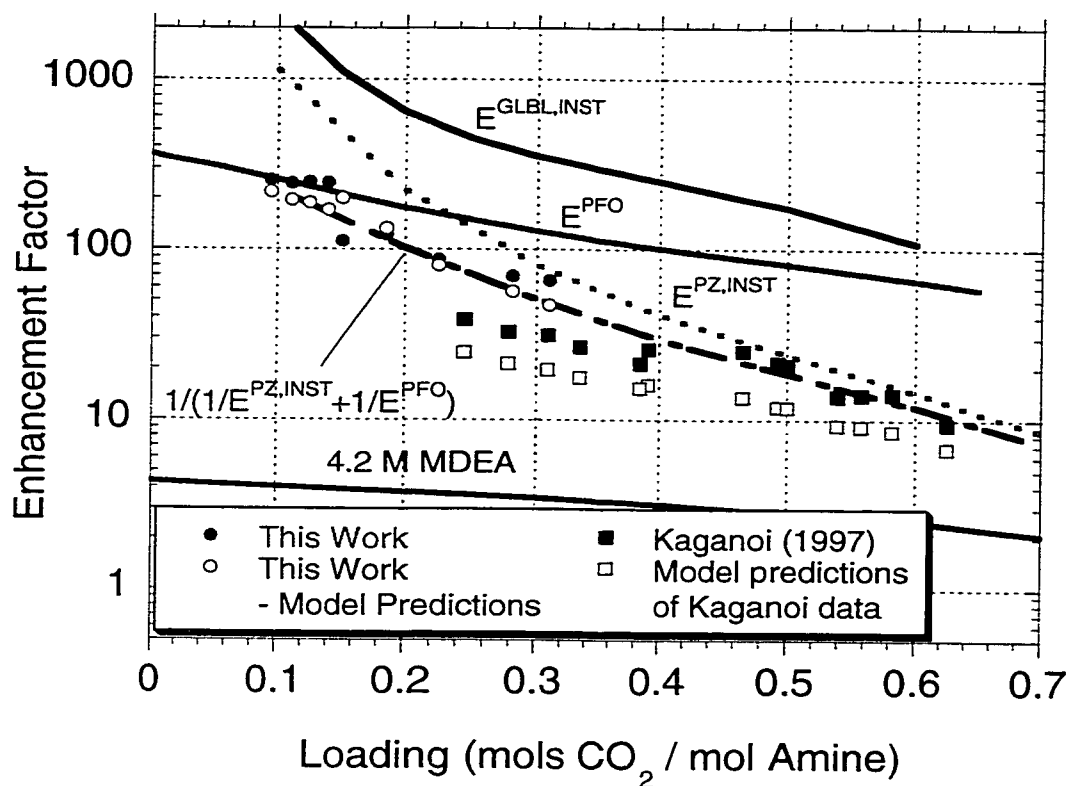


Figure 6.3 Enhancement factors for 0.6 M PZ/4 M MDEA at 313K and $k_1^0=3.3E-5$ m/s

Once again, the assumption of instantaneous reactions with small driving forces or pseudo first order behavior would result in very large error of the predicted enhancement factor. The combination of instantaneous PZ reactions with pseudo first order does an adequate job of modeling the data ($1/E^{PZ,INST} + 1/E^{PFO}$). The rigorous model does an adequate job of predicting the measured flux.

6.3.2.3 Data of Xu et al. (1992)

Xu et al. (1992) measured CO_2 absorption into PZ / MDEA solutions with a

wetted disk column. They used pure CO_2 gas instead of a N_2 / CO_2 mixture. This only allowed them to study high partial pressures and, therefore, their data is all at high driving force. Furthermore, the percent removal of CO_2 in their work will be small (around 10%). Their inlet and outlet flows of gas are measured using a bubble soap gas meter. With the flux determined by taking the difference of two large numbers, their data will be prone to large expected error.

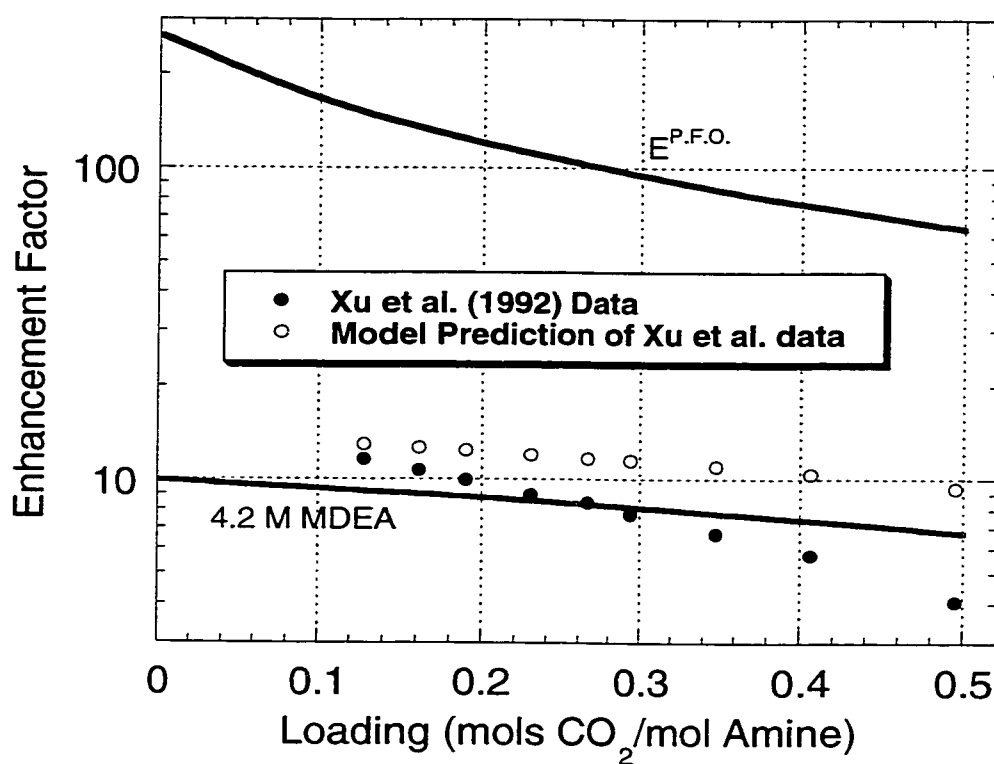


Figure 6.4 Enhancement factors for 0.1 M PZ/4.21 M MDEA at 313K and $k_1^0=2\text{E-}5$ m/s

Unfortunately, their data is of limited use since they do not consider conditions where the performance of the blend is significantly different from MDEA. Their data and our model predictions of their data are shown in appendix

D. They have studied a much lower concentration of PZ than we have in our work. They have also only obtained data at conditions where the total concentration of CO_2 in the liquid is much greater than the concentration of PZ. At these conditions, the solution appears to perform like MDEA. This is shown in figure 6.4, which is directly analogous to figure 6.3 where our data is represented. Figure 6.4 examines a subset of the Xu et al. (1992) data at 40°C and 0.1 M PZ, 4.21 M MDEA. This shows that the data of Xu et al. is best described as pseudo first order absorption into unpromoted MDEA.

Furthermore, there are some experimental concerns with their data. Figure 6.4 shows the pseudo first order predictions for 4.21 M MDEA. There are several experimental points of Xu that are below the 4.21 M MDEA curve. Our predictions of the equilibrium partial pressure of CO_2 were used in calculating the experimental enhancement factor. The partial pressure of CO_2 is certainly expected to be about 20% higher than that of 4.21 M MDEA (See chapter 5), however since the data are well removed from equilibrium, this small difference in equilibrium partial pressure should not make much difference in the calculated experimental enhancement factor. It is unreasonable to expect that PZ has a negative effect on the enhancement factor, yet this is what the data seems to suggest. Furthermore one of the published points predicts a enhancement factor of 0.3 which is unreasonable. The data set of Xu et al., therefore, is divided into two sets: accepted points (those that lie above the MDEA curve) and rejected points (those that lie below). The model predictions presented in this work do an adequate job of matching the data of Xu et al. (1992).

6.3.3 Model predictions for the single amine systems

The data presented in chapter 4 for CO_2 absorption into aqueous PZ have been reinterpreted using the rigorous model presented in this Chapter. The new

model predictions are shown in table 6.5. As can be seen, the inclusion of the PZ carbamate rate constant has improved the model predictions to within 10%, showing that the model can be used in the limit of no MDEA.

Table 6.5 – Model predictions of CO₂ into 0.6 M aqueous PZ solutions at 313 K (Data of Bishnoi and Rochelle, 2000b).

Bulk Gas P _{CO₂} (Pa)	k _g *10 ⁵ (moles/(atm cm ² s)	k _i *10 ⁴ (m/s)	Loading (mol CO ₂ / mol amine)	Flux *10 ⁷ (mol/cm ² s)		
				Measured	Previous Prediction*	Predicted (rigorous)
2208	2.11	1.11	0.29	2.39	2.19	2.18
2207	2.02	1.10	0.47	2.14	1.60	1.81
2470	2.18	1.12	0.56	1.88	1.52	1.79
2600	2.11	1.11	0.67	1.47	1.02	1.29

*Predictions of Chapter 4 which exclude PZCOO⁻ kinetics.

Subsets of the experimental data of Critchfield (1988), Toman (1989) and Pacheco (1998) have been reinterpreted using the model presented in this work. The model does a good job of predicting the MDEA data, even at the concentrated conditions studied by Toman and Xu. Model results for aqueous MDEA are shown in table 6.6 and verify that the model may be used for predictions in the absence of PZ.

6.4 Model Predictions

The model developed in this work has been used to generate insight as to how PZ activated MDEA blends derive their effectiveness. We present a comparison of PZ/MDEA blends to other promoted systems (MEA/MDEA and DEA/MDEA). The relative sensitivity of model parameters is also shown along with predictions that show what the important reactions are at different conditions. The specific cases of ammonia plants, natural gas plants and flue gas cleaning applications are discussed.

Table 6.6 – Model predictions of CO₂ absorption into aqueous MDEA solutions.

T (K)	Loading (mol CO ₂ /mol Amine)	P ⁱ CO ₂ Interface (kPa)	k ₁ ^o m/s *10 ⁵	[MDEA] mol/L	Flux*10 ⁷ (mol/cm ² s)		Investigator
					Measured	Predicted (Rigorous)	
313	0.164	92.0	1.16	1.6	2.28	2.57	Critchfield (1988)
313	0.184	92.0	1.16	1.6	2.22	2.51	Critchfield (1988)
313	0.217	92.0	1.16	1.6	2.13	2.41	Critchfield (1988)
313	0.256	92.0	1.16	1.6	2.00	2.29	Critchfield (1988)
313	0.288	92.0	1.16	1.6	1.89	2.18	Critchfield (1988)
313	0.079	25.0	1.00	4.28	0.93	0.83	Toman (1990)
313	0.220	94.0	8.60	4.28	1.79	2.56	Toman (1990)
313	0.087	96.2	2.07	4.28	3.55	3.35	Xu et al. (1992)
313	0.161	96.2	2.07	4.28	3.14	3.10	Xu et al. (1992)
313	0.225	96.2	2.07	4.28	2.65	2.88	Xu et al. (1992)
313	0.277	96.2	2.07	4.28	2.24	2.68	Xu et al. (1992)
313	0.322	96.2	2.07	4.28	2.05	2.50	Xu et al. (1992)
313	0.366	96.2	2.07	4.28	1.81	2.32	Xu et al. (1992)
343	0.056	74.6	4.26	4.28	5.23	4.42	Xu et al. (1992)
343	0.103	74.6	4.26	4.28	3.91	3.60	Xu et al. (1992)
343	0.139	74.6	4.26	4.28	3.10	2.94	Xu et al. (1992)
343	0.168	74.6	4.26	4.28	2.33	2.40	Xu et al. (1992)
343	0.191	74.6	4.26	4.28	1.80	1.95	Xu et al. (1992)
313	0.127	66.2	4.10	3.00	3.95	2.46	Pacheco (1998)
313	0.077	102.0	4.64	3.00	3.91	4.03	Pacheco (1998)
313	0.243	138.0	4.29	3.00	4.86	4.65	Pacheco (1998)
313	0.344	125.0	4.67	3.00	3.30	3.79	Pacheco (1998)
313	0.192	128.0	2.67	4.28	4.48	4.09	Pacheco (1998)

6.4.1 Comparison with other promoters

Figure 6.5 compares the effectiveness of PZ/MDEA blends with DEA/MDEA and MEA/MDEA blends. Calculations are performed in 5 wt% MEA or PZ with 45 wt% MDEA at 40°C and a k_1 of 1.0×10^{-4} m/s. 10 wt% DEA 40 wt% MDEA blend is also compared. We present results as a function of equilibrium partial pressure. Low driving force ($1.05 \cdot P^*_{\text{CO}_2}$) is considered as well

as high driving force ($10 \cdot P^*_{CO_2}$). Results are compared to pseudo first order predictions for MDEA. The MEA and DEA blend calculations are from the work of Glasscock et al. (1991). We see that the PZ blend enhances the performance of MDEA by a factor of 50 at low loading. Even at high loading (0.5), the PZ blend enhances the absorption above MDEA by a factor of 5 at low driving force and a factor of 2 at high driving force.

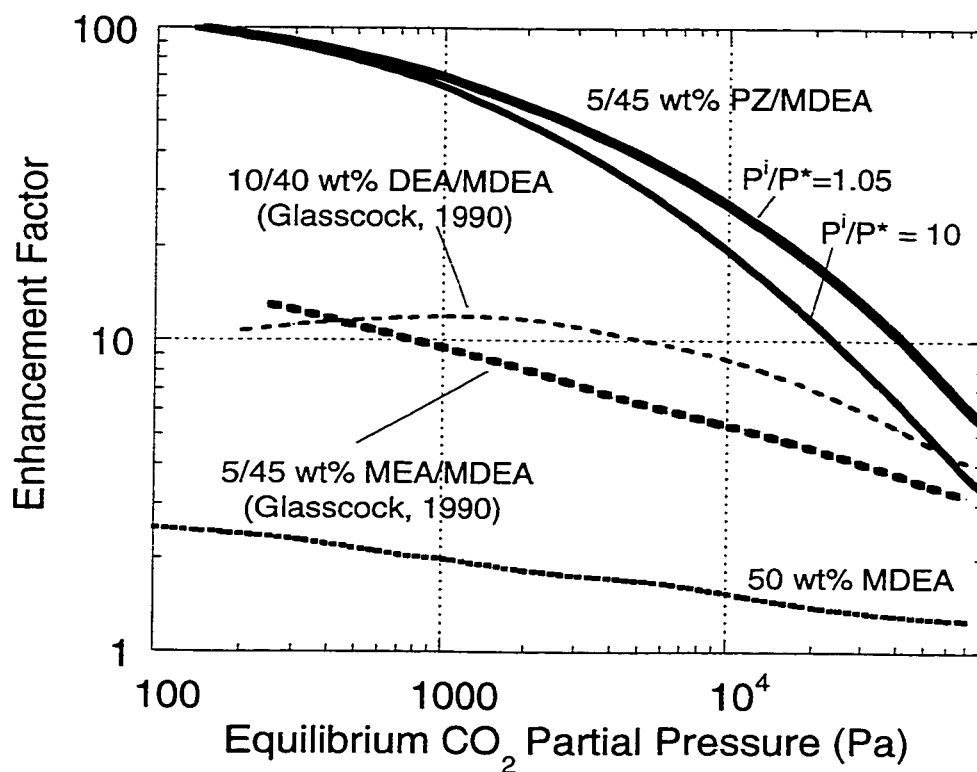


Figure 6.5 Comparison of PZ/MDEA blends to conventional blends. Predictions at 313K, $k_l^0 = 1.0 \times 10^{-4}$ m/s. $P^i/P^* = 1.05$ unless specified

PZ is found to be a more effective promoter than MEA or DEA if we compare the enhancement factors. PZ blends are seen to be a factor of 5 to 6 more effective than MEA at low loading and keep their performance edge over the other promoted MDEA systems at higher loading. The high driving force is not seen to have a major effect on the predicted enhancement factor until a high loading. The decrease in enhancement is due to the depletion of PZ and PZ carbamate at the interface.

6.4.2 Sensitivity to model parameters

Figure 6.6 shows the sensitivity of different parameters to the flux predicted by the rigorous model with 5 wt% PZ/45 wt% MDEA at 313K.

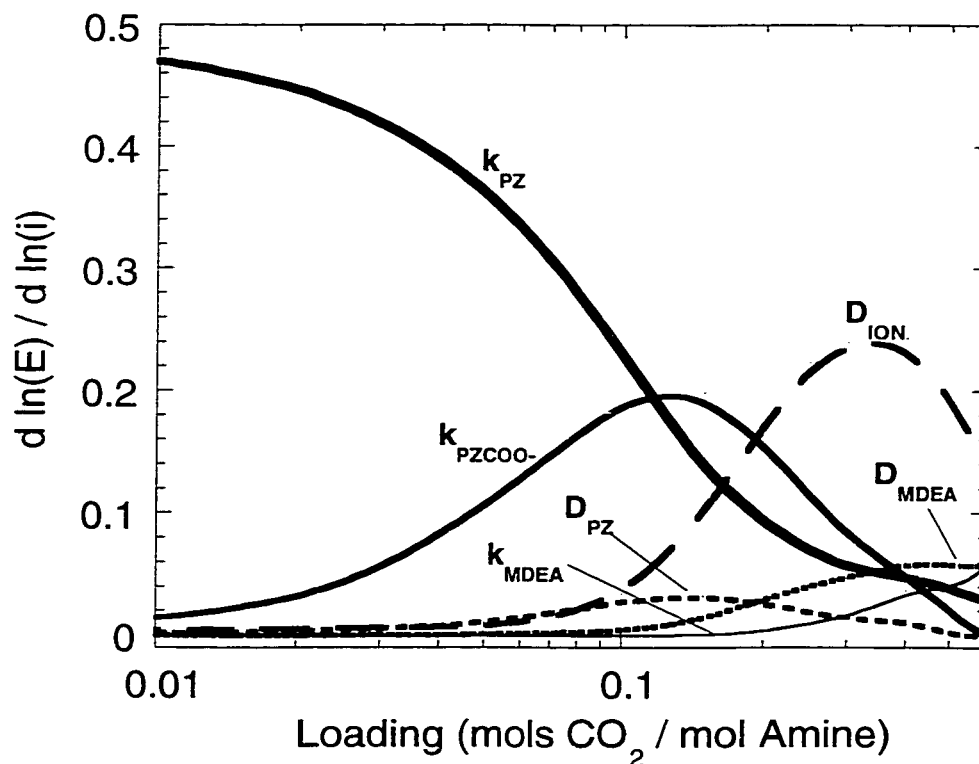


Figure 6.6 Model sensitivity to rate and mass transfer parameters. Predictions in 5/45 wt % PZ/MDEA at 313K and $k_1^0=1.0E-4$.

The value for k_1^0 used during the sensitivity analysis is $1.0\text{E-}4$ m/s. The rate constants for PZ and MDEA catalyzed PZ are lumped into one parameter as are the rate constants for PZCOO^- and PZCOO^- catalyzed with MDEA. The diffusion coefficients of MDEA, PZ and ions are also studied. The results can be divided into three regions. The first region is where the concentration of CO_2 is lower than the total concentration of PZ (loading <0.13). The second where the total concentration of CO_2 is lower than two times the concentration of PZ (loading <0.26) and the third where the total concentration of CO_2 is higher than two times the total concentration of PZ. At low loading (region 1), the rate constant of PZ is by far the most sensitive parameter showing that the dominant phenomenon is still the direct reaction of CO_2 with PZ. As the loading increases and the concentration of PZ drops, the rate constant of PZ carbamate becomes the most sensitive parameter (region 2). This is quickly replaced by the diffusion coefficient of ions (end of region 2 and region 3) showing that the removal of reaction products and the diffusion of PZCOO^- to the interface have become the dominant phenomena. Another interesting result is that the rate constant of MDEA is not more sensitive than the rate constant of PZ or PZ carbamate until a loading of around 0.4.

6.4.3 Reaction zones and deviation from approximate solutions

Table 6.7 shows model predictions of the enhancement factor of CO_2 absorption into 0.6M/4M blend of PZ/MDEA at 313K and a $k_1^0=1.0\text{E-}4$ m/s. A series of driving force conditions varying from low driving force ($1.05 \cdot P^*_{\text{CO}_2}$) to high driving force ($10.0 \cdot P^*_{\text{CO}_2}$) is considered. Also included are predictions of the pseudo first order enhancement factor, the enhancement factor predicted assuming global instantaneous reactions ($E^{\text{GLBL,INST}}$, reaction 2.30), the enhancement factor predicted assuming all carbamate formation approaches

instantaneous behavior ($E^{PZ,INST}$) and the combined pseudo first order / PZ instantaneous enhancement factor ($1/E^{PFO} + 1/E^{PZ,INST}$). $E^{PZ,INST}$ is calculated by increasing all rate constants for carbamate formation until the enhancement factor approaches a steady value and will increase no more with increasing rate constant.

We continue to discuss results in terms of the regions introduced in section 6.4.2. Region 1 is when the overall concentration of CO_2 is less than the total concentration of PZ. Region 2, when it is between the total concentration of PZ and two times the total concentration of PZ. Region 3 is when the overall concentration of CO_2 is greater than 2 times the total concentration of PZ.

Table 6.7 Enhancement factors for 0.6M PZ, 4M MDEA at 313K and various driving force. $k_1^0 = 1.0E-4$ m/s.

Loading	$P^*_{CO_2}$ (Pa)	$E^{P.F.O.}$	$E^{1.05P^*}$	$(1/E^{PFO} + 1/E^{PZ,INST})^{-1}$	E^{2P^*}	E^{5P^*}	E^{10P^*}	$E^{PZ,INST}$	$E^{GLBL,INST}$
0.01	5	123.9	121.9		121.8	121.8	121.7		26600
0.02	17	118.4	115.8		115.7	115.6	115.4		
0.05	82	110.6	106.9	106.9	106.7	106.2	105.4	3214	7840
0.07	167	103.3	98.5		98.2	97.2	95.6		4810
0.10	404	92.4	85.5	85.8	84.8	82.8	79.7	1194	2480
0.15	1272	75.7	64.8	65.2	63.4	59.3	53.5	469	1120
0.20	2991	62.7	48.4	49.5	46.3	40.7	34.0	235	647
0.25	5685	53.1	36.5	37.5	34.0	28.1	22.0	128	451
0.30	9309	46.0	28.0	29.3	25.5	20.0	15.0	81	356
0.40	19099	36.0	17.8	18.9	15.5	11.4	8.2	40	252
0.50	25400	29.0	11.8	12.8	10.0	7.2	5.2	23	176
0.60	32800	23.3	7.8		6.6	4.7	3.5		109
0.70	89700	18.2	5.0		4.2	3.1	2.4		

We first compare pseudo first order to the rigorous model at small driving force. The model predicted enhancement factor essentially follows the pseudo first order enhancement factor in region 1. Here, the major process occurring is the reaction of CO_2 with PZ throughout the boundary layer. In region 2, we start to see

significant deviations from pseudo first order behavior even at the low driving force conditions. This is because the carbamate forming reactions are approaching instantaneous reactions. In region 3, there are major deviations from pseudo first order conditions and the enhancement factor at the higher end of region 3 is mainly dictated by the instantaneous enhancement factor.

Table 6.7 leads to two conclusions. Although the reaction of PZ with CO₂ is fast, it is not fast enough to be considered instantaneous at any of the practical ranges considered in the analysis. The behavior does, however approach instantaneous reaction with respect to the carbamate formation at high loading. Pseudo first order is also not a good assumption at higher loading. A simple addition of the pseudo first order resistance and the PZ instantaneous resistance leads to very accurate prediction of the enhancement factor with low driving force ($1/E^{PFO} + 1/E^{PZ,INST}$).

The enhancement factor decreases with increasing driving force as well. At low loading, there appears to be no affect of an increase in driving force. In regions 2 and 3, however, increasing the driving force from $1.05 \cdot P^*_{CO_2}$ to $10 \cdot P^*_{CO_2}$ can decrease the enhancement factor by a factor of two.

Figures 6.7, 6.8 and 6.9 show concentration profiles of species in 5/45 wt% PZ / MDEA blend at 313K. These calculations are performed using a k_1 of $1.0E-4$ m/s and an interfacial concentration of CO₂ of 10 times the bulk phase concentration of CO₂. Figures 6.7, 6.8 and 6.9 shows concentration profiles for regions 1, 2, and 3 respectively at loadings of 0.07, 0.20 and 0.6, respectively. Within region 1, it is easy to see that pseudo first order is a good approximation. There is not much depletion of PZ at the interface and there is still enough PZ around. The reaction of PZ with CO₂ to form mono-carbamate is dominant in region 1. Examining the concentration of PZ carbamate, it is diffusing away from the interface, which makes it appear as a reaction product. Region 2 demonstrates

that there is beginning to be a significant amount of depletion of PZ at the interface (about 60% depletion). Interestingly, the production of PZ carbamate from PZ under these conditions helps the depletion of carbamate to form dicarbamate. As a result there is almost no depletion of PZ carbamate at the interface. At higher loading in region 3, we finally see some depletion of the MDEA. PZ is severely depleted as well as PZ carbamate which has moved from being a reaction product in region 1 to a reactant in region 3. There is also a steep gradient in dicarbamate at these conditions showing that much of the CO_2 is moving across the boundary layer in the form of dicarbamate.

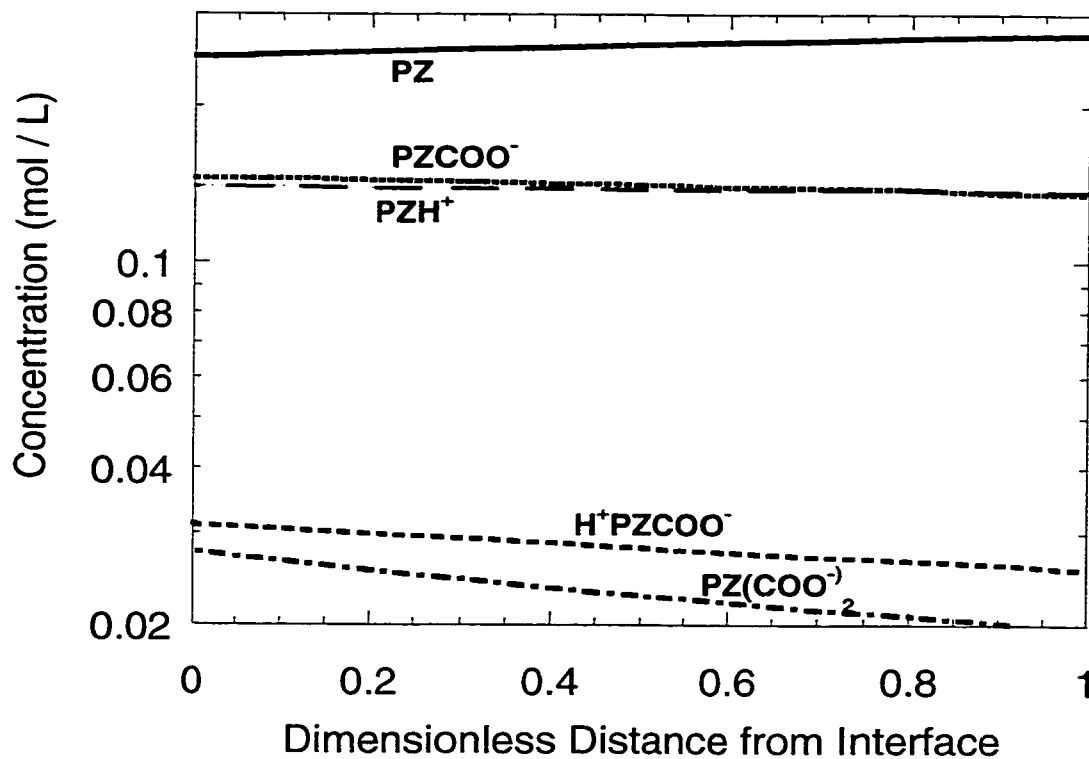


Figure 6.7 Concentration gradients for absorption of carbon dioxide into 5/45 wt % PZ/MDEA blend. Loading=0.07, $k_1^0=1.0\text{E-}4$ m/s, $P^i/P^*=10$, $T=313\text{K}$

The values of the mono and di-carbamate equilibrium constant expressions are evaluated at the interface for each of the cases corresponding to figure 6.7, 6.8 and 6.9. In region 1 (figure 6.7) the ratio of products to reactants for mono-carbamate is seen to be 13% of its equilibrium value whereas the di-carbamate is seen to be 14% of its equilibrium value. The corresponding values are 28 and 40% for region 2 (figure 6.8) and 46 and 86% for region 3 (figure 6.9). This is consistent with our observation that the behavior of the system at high loading approaches instantaneous behavior for all carbamate formation.

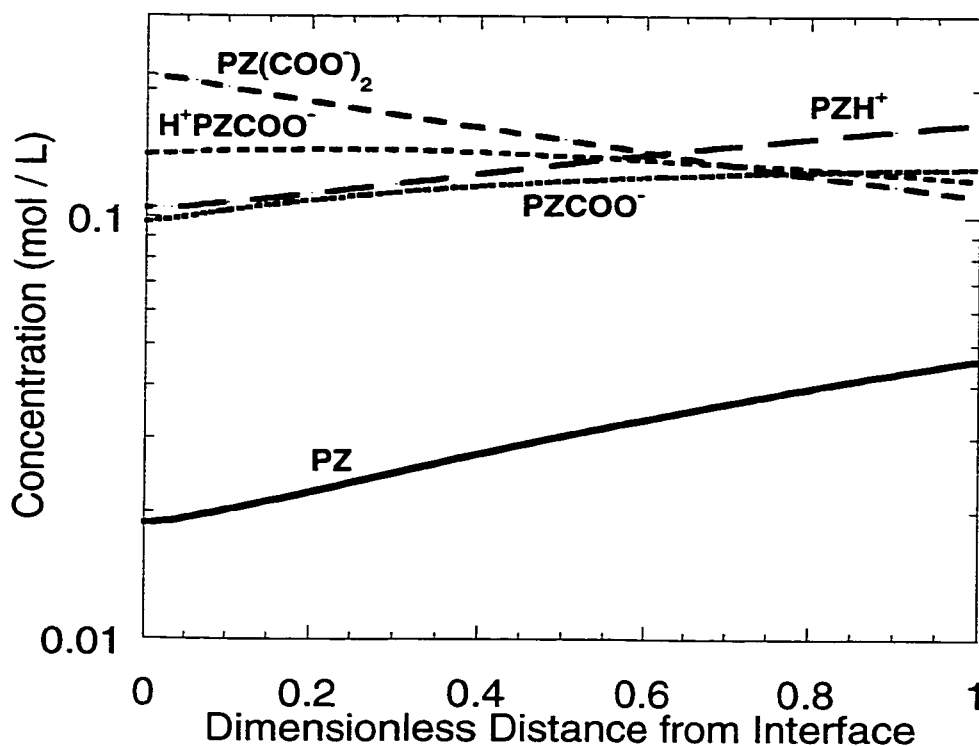


Figure 6.8 Absorption of carbon dioxide into 5/45 wt % PZ/MDEA blend. Loading=0.20, $k_i^o=1.0\text{E-}4$ m/s, $P^i/P^*=10$, $T=313\text{K}$.

It is also useful to analyze the total amount of CO₂ being transferred across the boundary layer by different mechanisms. We define the total amount of carbamate and carbonate species respectively as:

$$[\text{CARBAMATE}] = [\text{PZCOO}^-] + [\text{H}^+\text{PZCOO}^-] + 2[\text{PZ}(\text{COO}^-)_2]$$

$$[\text{CARBONATE}] = [\text{HCO}_3^-] + [\text{CO}_3^{2-}]$$

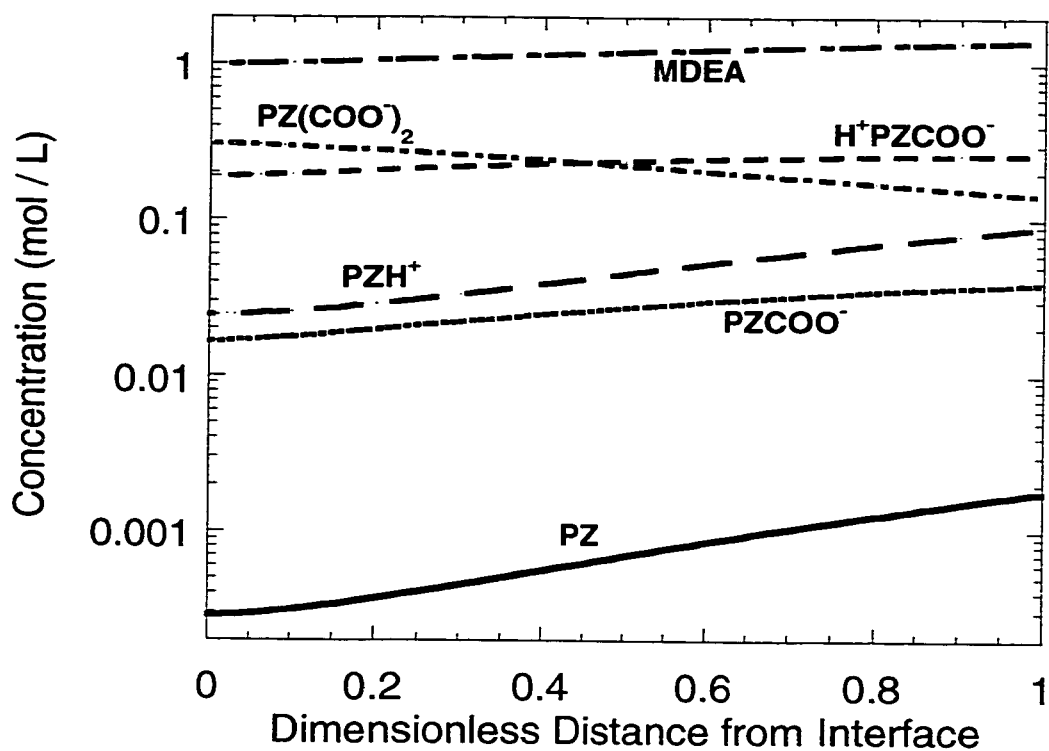


Figure 6.9 Absorption of CO₂ into 5/45 wt % PZ/MDEA blend. Loading = 0.6, $k_1^0 = 1.0\text{E-}4$ m/s, $P^i/P^* = 10$, $T = 313\text{K}$

In region 1, almost all the gradient in total CO₂ species is in the form of carbamate

species (99%). The same can be said about region 2 where 94% of total CO₂ is being transferred as carbamate species. In region 3, however only 66% of the total CO₂ gradient is due to carbamate species while 24% is due to molecular CO₂ and the balance is due to carbonate species.

6.5 Ammonia Plants / Hydrogen Plants

We consider a typical ammonia or hydrogen plant scrubber and make model predictions at industrial conditions. Table 6.8 shows the conditions used in developing the example. Calculated parameters such as lean amine loading, mass transfer coefficients calculated using the model of Onda et al. (1968) and other performance parameters are shown in table 6.8. We have used a factor of three away from equilibrium at the lean and rich ends in order to define the solvent rate. Mathematically,

$$P^*_{CO_2} @ Top, Bottom = \frac{P_{CO_2}}{3} @ Top, Bottom \quad (6.29)$$

Although we do not account for a temperature bulge in order to keep the example simple, the chosen solvent rate would still lie above the equilibrium curve for a bulge of 15°C at the bottom of the column. Figure 6.10 shows the operating line for this example and the corresponding isothermal equilibrium curve. The operating line may be as much as a factor of 30 deviated from the equilibrium curve at a loading of 0.20. Also shown on figure 6.10 are the predicted and approximate enhancement factors according to equation 2.31 assuming instantaneous reactions for all carbamate formation. The approximate enhancement factors are quite accurate at the top and bottom but have significant deviation from the rigorous enhancement factors in the middle. The rigorous enhancement factors themselves and the overall column material balance show that

the mass transfer is in region 1 at the top of the column. The high driving forces occur mainly when the mass transfer is in region 2 followed by low enhancement factors at the bottom of the column in region 3.

Table 6.8 Conditions for Ammonia Plant Example

Parameter	Value	Notes
Temperature	313K	Hefner et al. (1992)
Pressure	300 psi	Hefner et al. (1992)
Treated Gas CO ₂ Concentration	0.05 vol %	Typical Ammonia Plant
Inlet Gas CO ₂ Concentration	18 vol %	Typical Ammonia Plant
Lean Loading (mol CO ₂ /mol Amine)	0.095	Calculated using VLE code Assumes factor of 3 away from pinch
Rich Loading (mol CO ₂ /mol Amine)	0.75	Calculated using VLE code Assumes factor of 3 away from pinch
Average Molecular Weight - Gas	16.11 g/mol	Hefner et al. (1992)
Mass Velocity (Gas)	2.55 Kg/m ² s	Hefner et al. (1992)
Mass Velocity (Liquid)	10.3 Kg/m ² s	Calculated from required solvent rate
Packing Specific Area	170m ⁻¹	From Wagner et al. (1997) for IMTP#40
Calculated Wetted Area	132m ⁻¹	Calculated using Onda et al. (1968)
Packing Particle Diameter	40mm	Nominal Packing Diameter
k _g (moles/(cm ² atm s))	1.19E-5	Calculated from Onda et al. (1968)
k _l (cm/s)	3.04E-3	Calculated from Onda et al. (1968)

Using the height of transfer unit curve generated above, the bed height was estimated for the isothermal case being studied. Although this is a simplification, the top of the column will approach isothermal behavior and, therefore we can gain insight into the dominant physical phenomenon at the top of the column. The total bed depth calculated was 65 ft, which is larger than expected yet reasonable. This is probably due to the fact that most plants would use a higher solvent rate to account for the temperature bulge and to reduce the rich loading. Figure 6.11 shows the loading and partial pressure as a function of bed depth. The mass transfer will be in region 1 for approximately the first 15% of the bed height. Region 2 is passed through quickly (at 30% of bed depth). The bulk of the

column is in region three. Figure 6.12 shows overall gas phase transfer unit height and gas film resistance (%) as a function of bed depth. We define gas film control (%) as:

$$Resistance(\%) = \frac{1/k_g}{1/K_G} \quad (6.30)$$

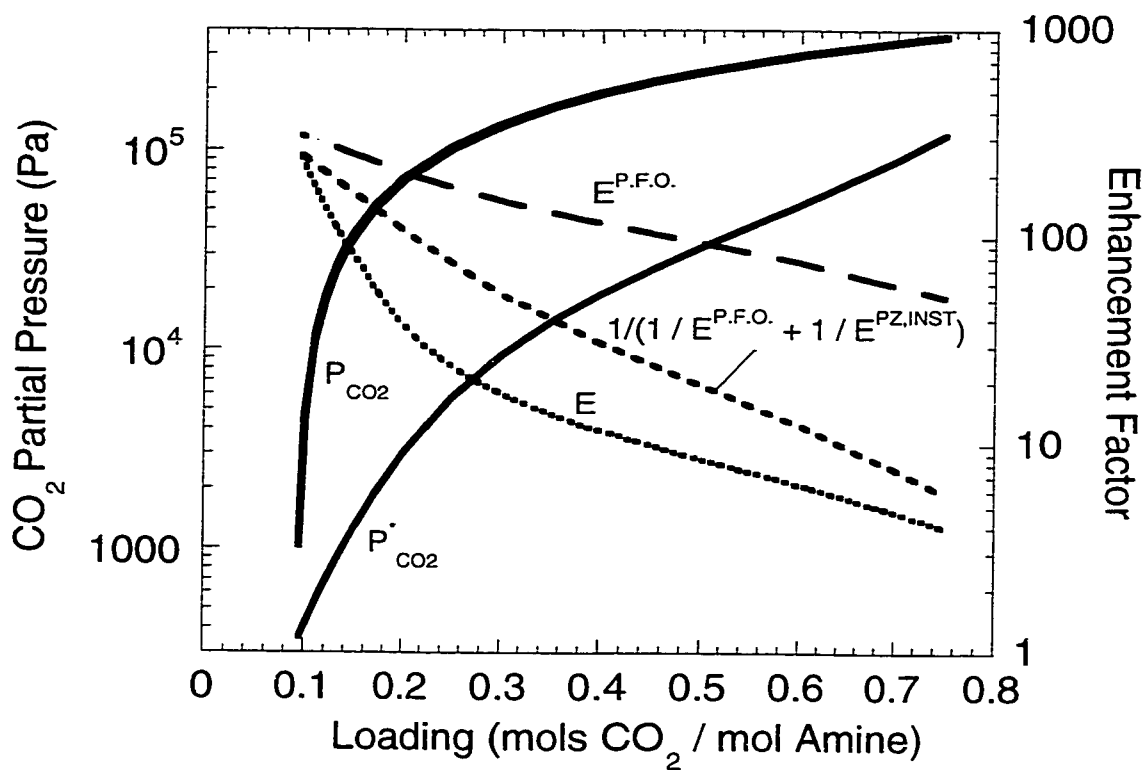


Figure 6.10 McCabe Thiele diagram and enhancement factor prediction for ammonia plant case using rigorous model. 313K, P=300 psig, $k_1^0=3.0E-3$ cm/s.

The top of the column is 50% controlled by gas film resistance. The gas

film resistance has reduced to 20% at a dimensionless bed depth of 0.2.

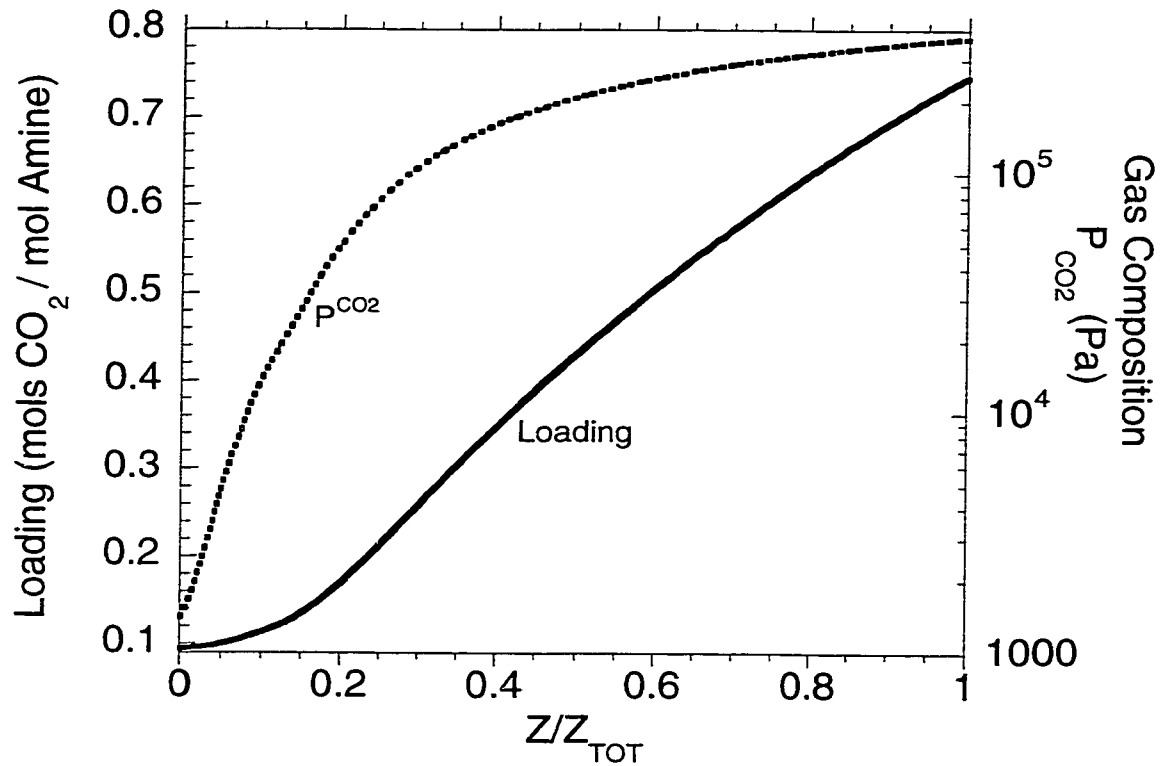


Figure 6.11 Change in liquid and gas phase compositions along column length for ammonia plant example using the rigorous model. 313K, $P=300$ psig, $k_1^0=3.0E-3$ cm/s.

The transfer unit curve distinctly shows the three regions. At dimensionless bed depths of less than 20%, the HTU curve has one slope that corresponds to region 1. At bed depths above a dimensionless depth of 0.35 has a second slope that corresponds to region 3 and is analogous to absorption into MDEA.

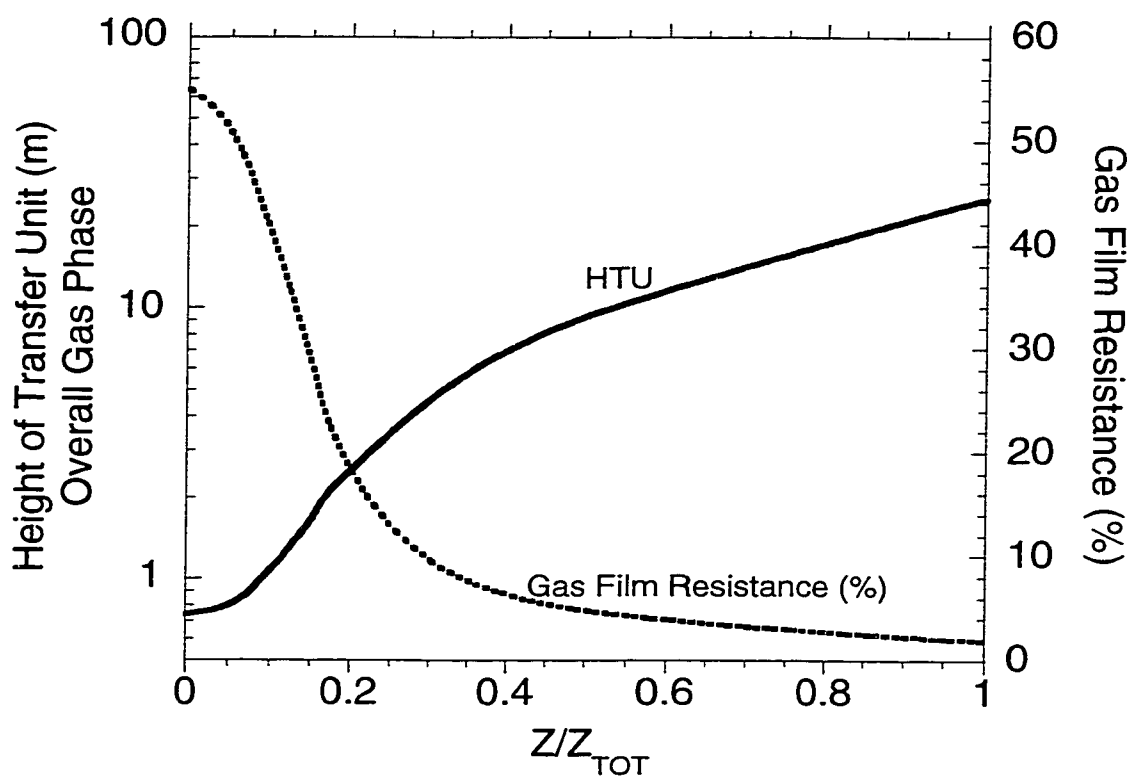


Figure 6.12 Mass transfer performance parameters for ammonia plant example using rigorous model. 313K, $P=300$ psig, $k_1^0=3.0E-3$ cm/s.

6.6 Removal of CO_2 from coal fired flue gas

Table 6.9 describes the coal fired flue gas example considered in this work. The rich end loading is significantly lower than in the ammonia plant due to the lower pressure of operation. Gas film mass transfer coefficients are also higher due to the difference in pressure.

Figure 6.13 shows the operating and equilibrium line for this case while figure 6.14 shows the concentration profiles of the gas and liquid for the isothermal example. The absorption occurs exclusively in region I. The total height of packing calculated for the isothermal case was 20 ft. Enhancement factors are significantly reduced from pseudo first order values, even at low loading where they matched for the ammonia plant case. This is due to the increased temperature of the flue gas application and the approach to instantaneous reactions. As shown, the approximate enhancement factor matches the rigorously calculated enhancement factor well across the contactor.

Table 6.9 Conditions for Coal Fired Flue Gas Example

Parameter	Value	Notes
Temperature	333K	Assumed
Pressure	1 atm	Assuming treated gas is vented
Treated Gas CO ₂ Concentration	1 vol %	Assuming 90% removal
Inlet Gas CO ₂ Concentration	10 vol %	Typical Coal Fired Flue Gas
Lean Loading (mol CO ₂ /mol Amine)	0.045	Calculated using VLE code Assumes factor of 3 away from pinch
Rich Loading (mol CO ₂ /mol Amine)	0.129	Calculated using VLE code Assumes factor of 3 away from pinch
Average Molecular Weight - Gas	28 g/mol	Typical Coal Fired Flue Gas
Mass Velocity (Gas)	1.07 Kg/m ² s	Calculated using Ekerdt method
Mass Velocity (Liquid)	10.8 Kg/m ² s	Calculated from required solvent rate
Packing Specific Area	170 m ⁻¹	Wagner et al. (1997) for IMTP#40
Calculated Wetted Area	139 m ⁻¹	Calculated using Onda et al. (1968)
Packing Particle Diameter	40mm	Nominal Packing Diameter
k _g (moles/(cm ² atm s))	8.27E-5	Calculated from Onda et al. (1968)
k _l (cm/s)	6.10E-3	Calculated from Onda et al. (1968)

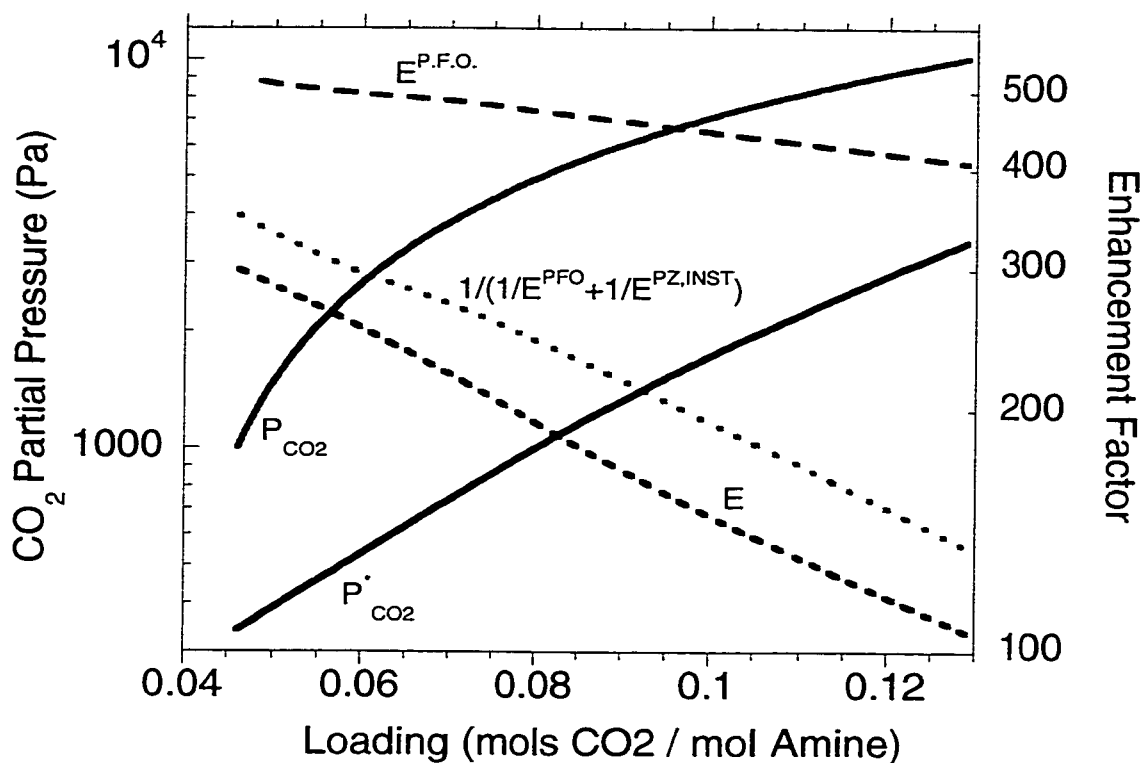


Figure 6.13 McCabe Thiele diagram and enhancement factor prediction for coal fired flue gas example using rigorous model. 333K, $P=0$ psig, $k'_l=6.1E-3$ cm/s.

Figure 6.15 shows the gas phase limitations and the height of overall gas phase transfer unit. Gas phase resistance is not as high as the ammonia plant case due to the higher gas film mass transfer coefficient, but may still reach 25% at the top of the column. The height of transfer unit does not go through the large

changes observed in the ammonia plant. This is because the entire column is in region 1 instead of spanning regions 1, 2 and 3 like the ammonia plant example.

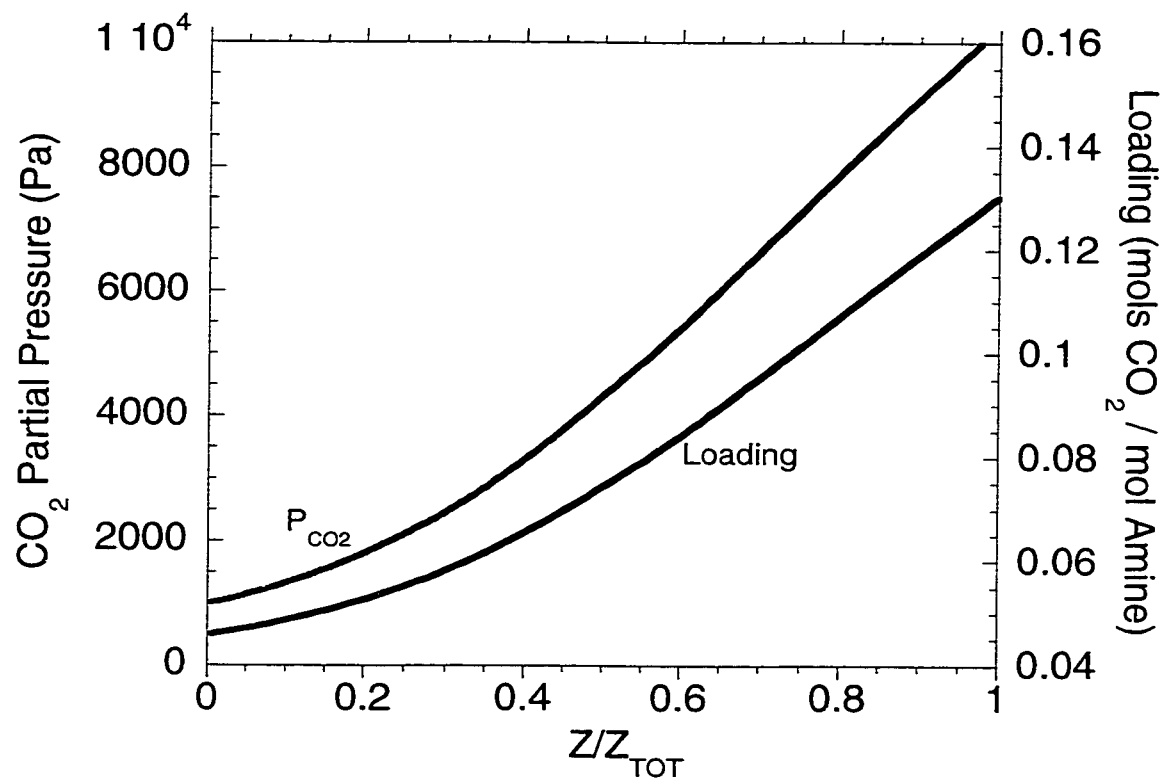


Figure 6.14 Change in liquid and gas phase compositions along column length for coal fired flue gas example using the rigorous model. 333K, $P=0$ psig, $k_l^0=6.1E-3$ cm/s.

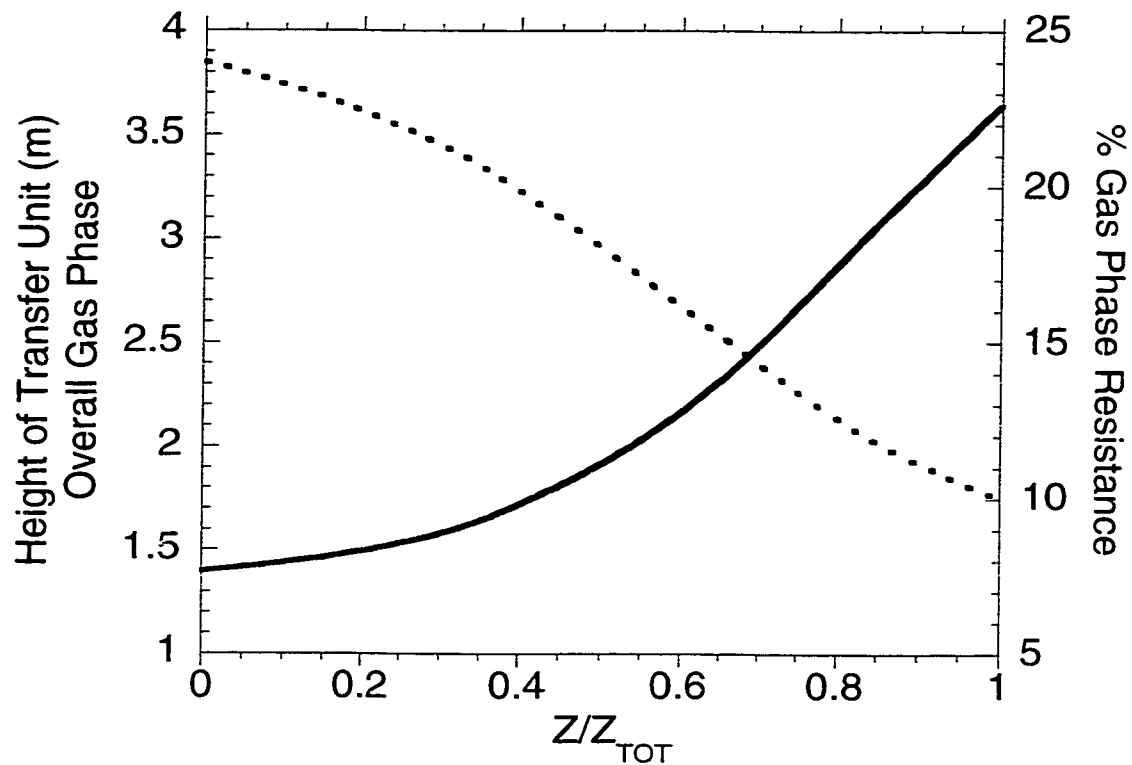


Figure 6.15 Mass transfer performance parameters for coal fired flue gas example using rigorous model. 313K, $P=300$ psig, $k_1^o=3.0E-3$ cm/s. 333K, $P=0$ psig, $k_1^o=6.1E-3$ cm/s.

6.7 Removal of CO_2 from natural gas

Since the variation in total pressure is large in natural gas applications, it is difficult to present a general case. We conceptually discuss the results of the ammonia plant and coal fired flue gas examples as they apply to natural gas applications.

Wammes et al. (1994) presents several applications of PZ activated MDEA

blends in natural gas plants. For most gas plants with absorbers operating from 200 to 1000 psi, the lean end partial pressure of CO₂ will be high (between 3E5 Pa and 1.4E6 Pa) which should not result in region 1. Therefore, natural gas plants will observe the same characteristics as the bottom of the ammonia plant example. We do not expect large gas phase resistance at these conditions.

6.8 Conclusions and Recommendations

PZ/MDEA Blend Performance

5/45 wt % blend of PZ/MDEA provides almost two orders of magnitude enhancement above 50 wt % MDEA at low loading and one order of magnitude enhancement at moderate loading. PZ/MDEA solvents outperform MEA/MDEA and DEA/MDEA blends at the same concentration.

Approximate Solutions

Pseudo first order is a good approximation to absorption into PZ/MDEA blends at low loading. At moderate to high loading, however, it is not seen to be a good approximation. At high loading, instantaneous carbamate formation is approached. A simplified model that combines the resistance of pseudo first order reactions in series with instantaneous carbamate formation matches the experimental data and rigorous model well.

Important Phenomena at Different Conditions

The reaction of PZ to form mono-carbamate is the dominant effect at low loading. At moderate loading the dominant reaction is the reaction of mono-carbamate to form di-carbamate. At high loading, the solution behaves like MDEA with instantaneous carbamate reactions.

Gas phase limitations are important at the top of an absorber in an ammonia plant. At lower pressure such as some natural gas applications and flue

gas applications, gas phase limitations are not seen to be large.

Recommendations

We recommend obtaining absorption data at constant loading, varying the driving force to determine if there are any direct reactions of carbamate species with MDEA.

Chapter 7

Alternative Solvents for CO₂ removal from coal fired flue gas

The recent interest in recovery of CO₂ from flue gas comes from the desire to reduce green house gas emissions. Proposed legislation may require up to 90% removal of CO₂ from flue gas at coal fired and natural gas power plants. A commercial technology for removing CO₂ from flue gas is summarized by Chapel et al. (1999). This technology is scrubbing using 30 wt% aqueous monoethanolamine (MEA) in a packed tower.

The addition of a CO₂ absorption/stripping system to a conventional coal fired power plant introduces significant capital and operating costs. Among the most promising areas discussed by Chapel et al. (1999) for further minimization of the operating costs are:

1. Reduction of steam consumption
2. Reduction of gas side pressure drop in the absorber

They also suggest areas for reduction in the overall capital cost of the absorption/stripping system including reducing the size of the absorber and stripper.

We study the effectiveness of four ideas for new solvents in the removal of CO₂ by aqueous absorption/stripping. We confine our discussion here to four examples that illustrate each of the following concepts

- 1 Moderately hindered amines maintain their capacity above MEA solutions at moderate to high loading since they do not have high carbamate stability. The example we study in this work is 2-Amino-2-Methyl-Propanol (AMP).
- 2 Promoted tertiary amines have a lower heat of reaction than carbamate forming amines such as MEA. This work studies PZ activated MDEA.
- 3 Promoted potassium carbonate solutions (PZ/K₂CO₃) have the advantage of low solvent cost and lower heat of reaction.
- 4 Piperazine activated monoethanolamine (PZ/MEA) improves on the current technology by replacing a portion of the MEA with piperazine, a faster cyclic amine.

A variation of the model presented in chapter 6 of this work is used to study the effectiveness of the solvent and to define the overall K_G . Modifications of this model in order to study the four systems above are discussed in section 7.2.

7.2 Model Description

The rate model presented in chapter 6 was modified by introducing monoethanolamine (MEA), MEA carbamate, protonated MEA and potassium ion (K^+). The introduction of these four species necessitates the introduction of four new equations. These are an overall material balance for MEA, an overall material balance for potassium, a equilibrium relationship for the protonation of MEA and a material balance for MEA carbamate. These equations are listed below:

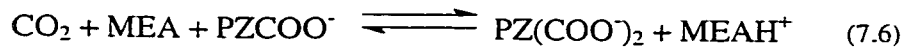
$$\nabla^2[MEA] + \nabla^2[MEACOO^-] + \nabla^2[MEA H^+] = 0 \quad (7.1)$$

$$\nabla^2[K_2^{2+}] = 0 \quad (7.2)$$

$$K_{MEA H^+} = \frac{[MEA H^+][OH^-]}{[MEA]} \quad (7.3)$$

$$\nabla^2[\text{MEACOO}^-] - R_{\text{MEACOO}^-} = 0 \quad (7.4)$$

Several existing relationships had to be updated as well due to the addition of several new reactions. The formation of PZCOO^- and $\text{PZ(COO}^-)_2$ catalyzed by the deprotonation by MEA must be considered. Also, the formation of MEA carbamate was added as a kinetically controlled reaction. The value of these and other rate constants used in this work are summarized in table 7.4.



The overall carbon balance was updated to include MEACOO^- . The material balance for molecular CO_2 was modified to include reactions 7.5 through 7.7. The carbamate buffer system balance was modified to include reactions 7.5 and 7.6 while reaction 7.6 was added to the dicarbamate material balance. The equation for electroneutrality was modified by adding all new ionic species (K_2^{2+} , MEACOO^- , and MEAH^+).

Concentrations in the bulk solution are equal to the equilibrium concentrations. New boundary conditions at the interface are direct extensions of the modifications discussed above.

7.3 Evaluation Procedure

Figure 7.1 shows the procedure for evaluating the different solvents. We design an isothermal absorber at 60°C for the removal of CO_2 from flue gas using each of the solvents. Where operational assumptions are made, they are made in a consistent manner from one solvent to the next. VLE data is obtained where available and equilibrium constants are adjusted to fit the data using a modified

Kent-Eisenberg approach similar to the one presented in Chapter 4. Data on the physical properties of most systems studied here was available from literature. Kinetic data reviewed in chapter 2 of this work was used to determine the appropriate rate constants to be used. The lean and rich end loading were calculated from the respective equilibrium models assuming a equilibrium partial pressure a factor of 3 less than the bulk phase partial pressure of CO₂. The L/V ratio can be calculated from a straightforward material balance over the entire column and the construction of an operating line follows directly from the L/V calculation. The method of Eckert (1970) is used to calculate the gas rate that would result in flooding. The actual gas rate was chosen as ¼ of the flooding value in all cases and the absolute gas and liquid rates per unit area were calculated. The method of Onda et al. (1968) was used to calculate the gas and liquid mass transfer coefficients and the wetted specific contact area. Stainless Steel # 40 IMTP[®] (Norton Chemical Process Products Corporation) random packing was used for all calculations. A packing factor was obtained from the vendor brochure while the specific packing area was listed by Wagner et al. (1997). The nominal diameter of 40mm was used for the packing particle diameter.

Using the model generated in this work, enhancement factors and overall gas film mass transfer coefficients were calculated using equation 7.8. The height of a transfer unit and the volume per transfer unit are directly related to the calculation of K_g.

$$\frac{1}{K_g} = \frac{1}{k_g} + \frac{H}{Ek^o_l} \quad (7.8)$$

$$H_{OG} = \frac{G_M}{K_g aP} = G_M V \quad (7.9)$$

7.4 Model Inputs

Tables 7.1 through 7.5 show summaries of important parameter inputs. The major difference in the physical properties of the solvents is the viscosity. The viscosity of MEA, PZ/K₂CO₃, and PZ/MEA solutions is significantly lower than the viscosity of the MDEA solutions studied in this work. This leads to high diffusion coefficients and, therefore, high liquid film mass transfer coefficients. The viscosity of the AMP solution is between that of MEA and MDEA.

Table 7.1 Physical properties for MEA based solvents at 60°C

Parameter	Units	5M MEA	Source	4.4M MEA/0.6 M PZ	Source	5M AMP	Source
Henry's Constant	L atm/mol	66.8	Dang (2001)	66.8	Assumed same as MEA	109	Xu et al. (1991)
Viscosity	cP	0.90	Snijder et al. (1993)	0.90		1.8	Xu et al. (1991)
Density	kg/m ³	991	Weiland (1996)	991		970	Xu et al. (1991)
Surface Tension	Dyne/cm	51	Vazquez et al. (1997)	51		31.9	Vazquez et al. (1997)

Table 7.2 Physical properties for other solvents at 60°C

Parameter	Units	0.6M PZ / 4M MDEA	Source	2.2M K ₂ CO ₃ /0.6M PZ	Source
Henry's Constant	L atm/mol	69.6	See Chapter 6	83.0	Water (Posey, 1996)
Viscosity	cP	2.65		1.03	Correia et al. (1980)
Density	kg/m ³	1020		1010	Correia et al. (1980)
Surface Tension	Dyne/cm	45.5	Rinker et al. (1997)	51	*Assumed

Diffusion coefficients of CO₂ are generally estimated from the viscosity of the solution, using a Stokes-Einstein type relationship:

$$D_{CO_2,SOLN} = D_{CO_2,H_2O} \left(\frac{\mu_{H_2O}}{\mu_{SOLN}} \right)^{0.5} \quad (7.10)$$

Diffusion coefficients for the amines are estimated by correcting the diffusion coefficient of CO₂ for the molecular weight of the amine. The data of Snijder et al. (1993) is used to estimate the diffusion coefficient of MEA. In general the diffusion coefficient of all ions is set to the value of the smallest amine in the solution.

Table 7.3 Diffusion coefficients (m/s) of reactants and products in solvents at 60°C

Species	5M MEA	0.6M PZ, 4.4M MEA	5M AMP	0.6M PZ, 4 M MDEA	0.6M PZ, 2.2 M K ₂ CO ₃
CO ₂	2.98E-9	2.98E-9	1.9E-9	1.05E-9	2.75E-9
MEA	1.64E-9	1.64E-9	N/A	N/A	N/A
MDEA or AMP	N/A	N/A	1.0E-9	6.7E-10	N/A
PZ	N/A	1.64E-9	N/A	8.04E-10	1.5E-9
IONS	1.64E-9	1.64E-9	1.0E-9	8.04E-10	1.5E-9

For the MEA system, the important thermodynamic parameters are the carbamate stability of MEA, the pK_a of the amine and the Henry's Law constant. These parameters have been estimated by Dang (2001) by fitting the experimental data of Jou et al. (1994). All equilibrium constants used in this work are summarized in table 7.5.

A direct extension of the MEA system is the PZ/MEA system. The thermodynamics of this system are defined by using the equilibrium constants

extracted from the aqueous work in chapter 4 of this work and combining them with the equilibrium constants for MEA of Dang (2001).

The thermodynamics of the PZ/MDEA system are discussed in chapter 5 of this work. This system is studied in more detail than the other systems and includes Gibbs excess free energy models for the liquid phase non-idealities (Electrolyte NRTL model: Chen et al., 1982) and a cubic equation of state to describe gas phase non-idealities (SRK EOS, Soave, 1972).

The potassium carbonate system at 2.2 M was studied by Tosh et al. (1959). They show that the equilibrium can be defined using one global equilibrium constant defined as

$$K_{eq} = \frac{[HCO_3^-]^2}{[CO_3^{=}]P^*_{CO_2}} \quad (7.11)$$

Their data covers the range of 70°C to 140°C and the value of K is found to be constant for a given temperature at 30 wt% K₂CO₃. We extrapolate their results to 60°C for use in this work. We arbitrarily set the Henry's law constant to the same value for water and set the bicarbonate equilibrium constant to the value reported by Posey (1996). The carbonate equilibrium constant, therefore, is adjusted to match equation 7.11. The equilibrium constants for all piperazine species reactions from chapter 4 of this work are used to define the PZ/K₂CO₃ system.

AMP is modeled like aqueous MDEA since its carbamate formation is not important. The data of Tontiwachwuthikul et al. (1991) is considered in this work. We adjust the amine pK_a (K_a=5.53E-12 on a mole fraction basis) to match their data at 3M and 60°C.

The rate constants used in this work are all taken from the literature reviewed in chapter 2 of this work. The rate constant expression of Hikita et al. (1977) is used for MEA. The rate constants of PZ and PZCOO⁻ determined in chapter 4 and chapter 5 of this work are used along with estimates of the MEA

enhanced carbamate and dicarbamate formation. The MEA enhanced carbamate formation rate constant (Eq. 7.5) was found to be $1.67\text{E}5 \text{ L}^2/\text{mol}^2 \text{ s}$ using the data of Dang at 0.6M PZ, 4.4M MEA at low loading and 60°C. This value is less than the corresponding value for MDEA which is surprising since Littel et al. (1992) would expect it to increase with pK_a . The data of Dang (2001) is highly gas film controlled (>70%) and therefore, we cannot expect this number to be highly accurate. For the data available, however, this is the best approximation that can be made. The MEA enhanced formation of dicarbamate rate constant is estimated by assuming the same ratio of MEA catalyzed carbamate formation to carbamate formation.

The rate constant of Xu et al. (1996) is used for AMP. Although they find the zwitterion mechanism to be important, we use an approximate value calculated using their expression at 3.5M AMP and 60°C. We have assumed second order behavior.

The aqueous rate constants measured in chapter 4 and 5 of this work for the carbamate and dicarbamate formation are used when considering the K_2CO_3 system. We do not account for the proton extraction of the piperazine mono and di-carbamate zwitterions by carbonate due to a lack of data. This may significantly increase the kinetics of this system. Rate constants used in this work are summarized in table 7.4. Equilibrium constants used in this work are summarized in table 7.5.

Table 7.4 Rate constants at 60°C used in this work along with their sources.

Rate Constant	Value at 60°C	Source
MEA	33700 (L/mol s)	Hikita et al. (1977)
AMP	1946 (L/mol s)	Xu et al. (1996)
$\text{PZ} \rightarrow \text{PZCOO}^-$	$2.23\text{E}5$ (L/mol s)	This Work – Chapter 4
$\text{PZ} + \text{MEA} \rightarrow \text{PZCOO}^-$	$1.70\text{E}5$ ($\text{L}^2/\text{mol}^2 \text{ s}$)	Estimated - data of Dang (2001)
$\text{PZCOO}^- \rightarrow \text{PZ}(\text{COO}^-)_2$	$1.9\text{E}5$ (L/mol s)	This Work – Chapter 4
$\text{PZCOO}^- + \text{MEA} \rightarrow \text{PZ}(\text{COO}^-)_2$	$1.5\text{E}5$ ($\text{L}^2/\text{mol}^2 \text{ s}$)	Estimated - data of Dang (2001)
MDEA	39.8 (L/mol s)	Littel (1992)

Table 7.5 Summary of equilibrium constants used in this work. Values are mole fraction based at 60°C.

Equilibrium Constant	Value at 60°C	Source
$\frac{x_{PZ} x_{H3O^+}}{x_{H2O} x_{PZH^+}}$	1.42E-11	Pagano et al. (1960)
$\frac{x_{H3O^+} x_{PZCOO^-}}{x_{PZ} x_{CO2} x_{H2O}}$	3.93E-6	This work – Chapter 4
$\frac{x_{H3O^+} x_{-OOC PZCOO^-}}{x_{PZCOO^-} x_{CO2} x_{H2O}}$	9.02E-7	This work – Chapter 4
$\frac{x_{PZCOO^-} x_{H3O^+}}{x_{H^+} x_{PZCOO^-} x_{H2O}}$	3.47E-11	This work – Chapter 4
$\frac{x_{H3O^+} x_{MEACOO^-}}{x_{MEA} x_{CO2} x_{H2O}}$	5.71E-6	Dang (2001)
$\frac{x_{MEA} x_{H3O^+}}{x_{H2O} x_{MEAH^+}}$	6.90E-12	Dang (2001)
$\frac{x_{AMP} x_{H3O^+}}{x_{H2O} x_{AMPH^+}}$	5.53E-12	This work – estimated from Xu et al. (1996) data
$\frac{x_{HCO3^-} x_{H3O^+}}{x_{CO2} x_{H2O}^2}$	9.14E-9*	Tosh et al. (1959) renormalized for mole fraction.
$\frac{x_{H3O^+} x_{CO3^{2-}}}{x_{HCO3^-} x_{H2O}}$	2.17E-12*	Tosh et al. (1959) renormalized for mole fraction.

* These constants are only used for the potassium carbonate case. They are set to the values outlined in chapter 4 for all other cases.

7.5 Results

Table 7.6 shows results that are a reflection of the physical system and the thermodynamics while table 7.7 shows results that quantify the effect of the chemical solvent. There is a large difference in the viscosity between solvents

with a high hydrocarbon content (MDEA, AMP) versus solvents with moderate hydrocarbon content (MEA, PZ / MEA, PZ / K₂CO₃). The effect of the viscosity on diffusion coefficients is the main difference why there is a large difference in liquid film mass transfer coefficients. The large difference in liquid phase mass transfer coefficients makes it difficult to compare enhancement factors directly and, therefore we compare the total volume of packing per transfer unit.

Table 7.6 Physical and thermodynamic results. 60°C, 10% CO₂ in, 1% CO₂ out, 33% approach to equilibrium in both rich and lean solvent.

Parameter	MEA	PZ/MEA	PZ/MDEA	AMP	PZ / K ₂ CO ₃
$k_l^o * 10^4$	2.82	2.82	0.61	0.70	2.03
$k_g^o * 10^4$	1.25	1.25	0.83	0.99	0.96
$a_w \text{ m}^2/\text{m}^3$	141	142	139	144	136
$L/V \text{ kg/kg}$	6.7	5.6	10.1	3.9	6.9
Lean Loading	0.345	0.343	0.046	0.105	0.256
Rich Loading	0.458	0.473	0.129	0.288	0.438

Table 7.7 Results demonstrating performance of the chemical solvent. 60°C, 10% CO₂ in, 1% CO₂ out, 33% approach to equilibrium in both rich and lean solvent.

System	Total Packed Height (m)	E^{PFO}		E		$K_g * 10^5 \text{ kmol/m}^2 \text{ s atm}$		$H_{OG} \text{ (m)}$		$V \text{ (m}^3 \text{ m}^2 \text{ s/kmol)}$	
		L	R	L	R	L	R	L	R	L	R
MEA	12.2	40	25	39	20	14.6	8.0	3.4	6.8	49	88
PZ/MEA	6.6	85	54	81	40	27.0	14.7	1.8	3.7	26	48
PZ/MDEA	6.1	471	408	245	106	1.7	8.4	1.6	3.7	42	86
AMP	35.9	38	33	38	32	3.3	2.8	11	14	212	250
PZ/K ₂ CO ₃	11.1	59	40	57	29	12.1	6.7	2.9	5.8	61	110

Thermodynamic results shown in table 7.6 show that there is not a high loading change across the absorber for the base case system (5M MEA). This trend is also apparent in the PZ/MDEA and the PZ/MEA system. The AMP system retains its capacity more than the MEA system and, therefore, the change in loading across the absorber is larger. The change in loading across the absorber

is directly related to the L/V ratio. We can see that the use of the hindered amine greatly reduces the amount of solvent that needs to be circulated. The PZ/MDEA system is not competitive with the MEA system in terms of liquid circulation rate. Figure 7.1 shows the gas phase resistance as a function of CO₂ partial pressure in the gas phase. For almost all systems except the PZ/MEA and the PZ/MDEA system, the gas phase mass transfer resistance is not significant.

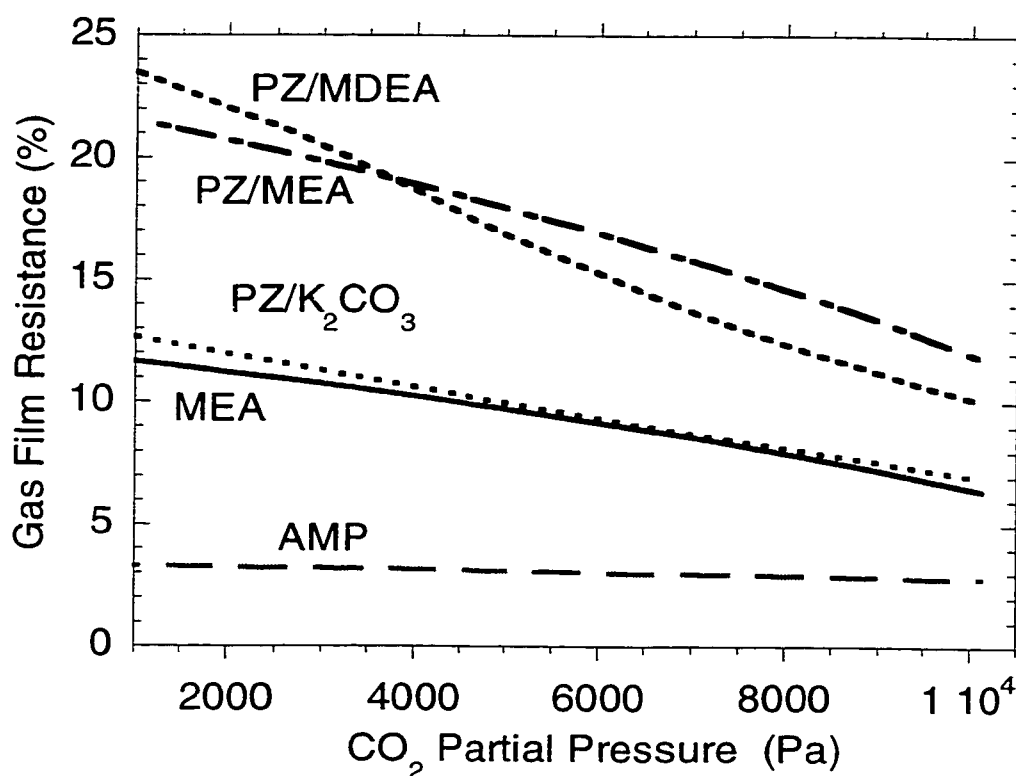


Figure 7.1 Effect of gas phase resistance for case studies examined in this Work. All calculations at 60°C, $P^{\text{TOT}} = 1$ atm, 10% CO₂ in, 1% CO₂ out, 33% approach to equilibrium in both rich and lean solvent.

The gas phase resistance for the PZ/MEA system is higher because of the increased rate of the liquid phase process compared to the base case. The gas

phase limitations of the PZ/MDEA system are higher than the base case because of the lower gas film mass transfer coefficient due to column hydraulics.

Table 7.7 shows results related to the performance of the chemical solvent. Comparing the lean and rich enhancement factors, we see that there is a consistent drop of a factor of two in the enhancement factor across the column due to the depletion of the solvent. This effect is not seen in the AMP system, showing that the hindered amine retains its rate capacity more than the other systems. We also see that the pseudo first order assumption is a good assumption at the lean end for all solvents except PZ/MDEA. The rich end sees significant deviation from pseudo first order behavior for PZ/MDEA, PZ/MEA and PZ/K₂CO₃ because of the piperazine reactions approaching instantaneous behavior.

Since the gas rate per area is different for each solvent, we compare the volume per transfer unit instead of the height per transfer unit. This is shown in table 7.7 and figure 7.2. In terms of total amount of packing, the PZ/MEA system appears to be best. The PZ/MDEA system is competitive with the base case of 5M MEA while the hindered amine (AMP) and the promoted potassium carbonate system have less mass transfer capability. The estimate of the PZ/MEA and the PZ/K₂CO₃ systems are conservative since there is not enough data to consider the total effect of the zwitterion mechanism on the reaction kinetics. A proper estimate of these interactions may make each of these options significantly more attractive.

The use of 0.6M PZ in a 4.4M MEA solvent can reduce the amount of packing and the size of the absorber by a factor of two, making significant difference in the capital cost of this equipment.

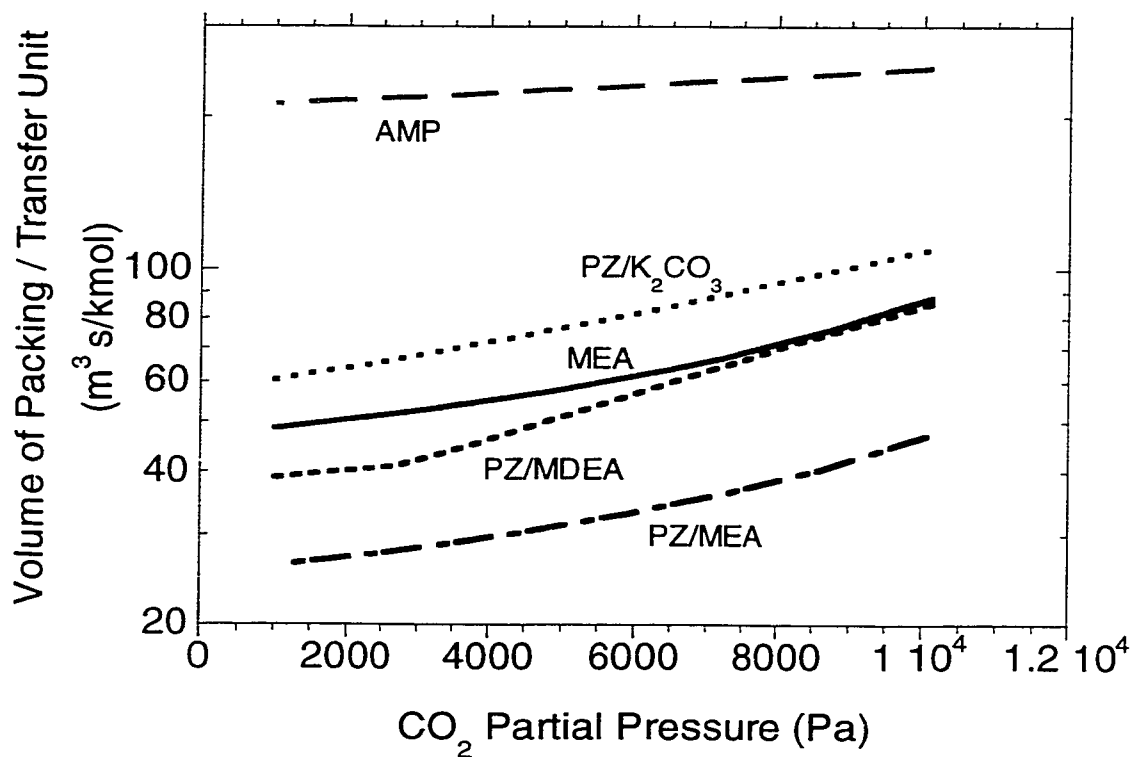


Figure 7.2 Volume of packing per transfer unit for case studies examined in this work. All calculations at 60°C, $P^{\text{TOT}} = 1 \text{ atm}$, 10% CO₂ in, 1% CO₂ out, 33% approach to equilibrium in both rich and lean solvent.

The use of less packing will also affect the operating cost by reducing the size of the blower needed to drive the flue gas through the packed tower. From the height of a transfer unit and the overall integrated height of the contactor, we see that the overall pressure drop can be reduced by a factor of 2 by using the PZ/MEA or the PZ/MDEA system.

7.6 Conclusions and Recommendations

Comparison of the volume of packing parameter indicates which solvent reduces the capital cost the most. For minimizing the amount of packing, the

PZ/MEA blend is the best option. Minimization of the operating costs are more complicated and will be a function of three things: the liquid rate, the combined heat of absorption and reaction and the total packed height. The liquid rate is directly proportional to the amount of sensible heat needed to raise the solvent temperature from absorber to stripper conditions. The hindered amine is clearly the option that will minimize this the most since it maintains its capacity more when loaded with carbon dioxide. In terms of pressure drop across the absorber, the hindered amine appears to require too much contact area.

Recommendations

Further study of the effect of the zwitterion mechanism on piperazine in the presence of MEA and K_2CO_3 will help define what we can expect from these solvents in terms of packed height. The deprotonation due to carbonate and MEA may show that these solvents are more effective than suggested in this work. We recommend that the chemistry of these reactions be studied in greater detail.

An optimization of packed height and total packing volume should be conducted since the columns may be designed with different aspect ratio for the different solvents. This will have an effect on the packed height and therefore, the pressure drop across the packed bed for the same overall amount of packing.

Chapter 8

Conclusions and Recommendations

8.1 Summary

Our study of PZ activated MDEA solvents for CO₂ removal started by examining aqueous CO₂/H₂O/PZ system. Equilibrium partial pressure and absorption data for CO₂ in aqueous PZ solvents were obtained in a wetted wall column. Proton and ¹³C NMR data were acquired for the PZ/D₂O/CO₂ system. The NMR data were combined with CO₂ solubility data, ionic conductivity data and the pH data of Kaganoi (1997) to determine the important ionic reaction products in the CO₂/PZ/H₂O system. The absorption data in aqueous PZ were used to obtain a second order rate constant for the PZ/CO₂ reaction to form mono-carbamate.

Equilibrium partial pressure, NMR and absorption data were also acquired for the PZ/MDEA blend. The thermodynamics of this system were modeled using the electrolyte NRTL model and the SRK equation of state along with the equilibrium constants obtained from the aqueous work. The absorption data were analyzed using a rigorous boundary layer model based on eddy diffusivity theory. This model was used to make predictions for the performance of PZ activated MDEA blends at industrially significant conditions. Calculations for PZ/MDEA are compared to MEA and DEA blends with MDEA.

8.2 Conclusions

8.2.1 Thermodynamic Interactions of PZ/CO₂

Proton and ¹³C NMR data have conclusively shown that CO₂ reacts with PZ to form a variety of reaction products. Both nitrogens play a significant role in the absorption of CO₂. A mono-carbamate was expected and found while a protonated carbamate and a di-carbamate were also seen to exist. The second pK_a of piperazine is low enough that a di-protonated species need not be included when considering CO₂ absorption.

The mono-carbamate stability constant was found comparable to other secondary amines such as DEA in both its absolute value and its temperature dependence. The second carbamate is an order of magnitude less stable than the first. The pK_a of the second nitrogen when the first nitrogen has been carbamated was found to decrease. This is consistent with theory, which suggests that the carbamate acts as an electron withdrawing group, thus making it harder to protonate the second nitrogen.

At low loading in the CO₂/H₂O/PZ system, the main reaction product is PZ mono-carbamate. This is replaced by protonated carbamate at high loading. The dicarbamate is never seen to be the dominant reaction species.

In the PZ/MDEA blend, the mono-carbamate is the dominant reaction product at low loading. The main reaction product at high loading is again the protonated carbamate. The main difference between the blend and PZ alone is that there is much more di-carbamate in the blended system. This was attributed to the large amount of bicarbonate present in the blend.

CO₂ solubility in PZ/MDEA blends was found to be greater than DEA/MDEA blends but lower than MEA/MDEA blends.

8.2.2 Kinetics of PZ/CO₂

The second order rate constant of PZ with CO₂ to form mono-carbamate has been experimentally determined to be 10 times higher than MEA even though

the pK_a is comparable. It is hypothesized that this large increase in the rate constant is due to the reduced hindrance around the nitrogen caused by the cyclic nature of the PZ molecule. The PZ concentration was varied from 0.2M to 0.6M in the absence of MDEA. The measured rate constant of PZ was found to be first order in PZ across this concentration range. Due to gas phase resistance and solubility limitations, it was not possible to study higher concentrations in the aqueous system.

Rate of absorption into blends of MDEA/PZ show that PZ kinetics increase significantly in the presence of another amine at high concentration. This behavior is consistent with the zwitterion mechanism. Furthermore, data at moderate loading cannot be fit without considering the reaction of mono-carbamate to di-carbamate as a finite rate reaction. The inability to observe the zwitterion mechanism in the absence of MDEA suggests that the water deprotonation is dominant in the $CO_2/H_2O/PZ$ system while the tertiary amine deprotonation is dominant in the more concentrated, blended system.

8.2.3 New Solvents for Flue Gas Treating

There is potential to reduce the capital and operational expenses involved in removing CO_2 from flue gas by changing the solvent used. The use of PZ/MEA can reduce the total packing required by a factor of two while the study conducted with AMP suggests that a hindered amine may have significant effect on the solvent circulation rate and, therefore, the steam requirement.

8.3 Recommendations

8.3.1 Data acquisition

The acquisition of further data for the PZ/MDEA system will increase our understanding of its interactions when absorbing CO_2 from process gas. NMR data at higher temperature will help quantify the temperature dependence of the di-

carbamate stability constant. The NMR experiment can be slowed down to make the ^{13}C response quantitative helping us obtain information about the amount of PZ species with respect to carbonate species in the blended system.

One of the largest questions in the thermodynamics of this system remains the activity coefficient of piperazine in aqueous solutions and in MDEA blends. Attempts to measure the activity coefficient of piperazine by measuring the equilibrium partial pressure of PZ above these solutions failed. The use of freezing point depression and calorimetry do not look promising because of the limited solubility of PZ. We recommend studying the equilibrium partial pressure of PZ above aqueous solutions using FT/IR. We recommend heating the gas lines and sample chamber of the FT/IR analyzer instead of the dilution technique attempted in this work.

The absorption of CO_2 into partially loaded solution of PZ/MDEA should be studied at conditions between this work and the work of Kaganoi (1997). The future work should emphasize a large percent removal from the gas phase to determine fluxes with high confidence. This may be achieved in the current apparatus by increasing the reservoir size such that large driving forces may be used without loading the solvent too fast. The measurement of flux at a constant loading and a variety of driving forces will provide insight into the interaction of PZ carbamate and MDEA. Specifically, we wish to determine whether the only interaction between the piperazine carbamate species and MDEA is the reversion of the carbamate to carbon dioxide and the consequent reaction with MDEA. If the measured flux is consistently higher than the model predicts, this will suggest that there is a direct interaction between MDEA and the carbamate.

It appears that the only reason PZ is run at low concentrations is because the protonated carbamate is not soluble at high concentrations. We suggest measuring the solubility of the protonated carbamate by loading PZ solutions of various strength and observing the precipitation of the carbamate.

The measurement of PZ kinetics in the presence of MEA and K_2CO_3 will show whether these solvents have increased potential as solvents for CO_2 removal from flue gas. These experiments will have to be conducted with a large k_g or a low temperature since their fast kinetics results in significant gas film resistance.

8.3.2 Model performance

The current model is rigorous enough for most applications of carbon dioxide removal using aqueous amines. There are several improvements that increase the speed of the model, but will have no impact on the ultimate results. The speed of the model will be important when using the model for rigorous absorber calculations or when performing a parameter estimation run.

The current model employs a Newton Raphson technique to solve all equations. This method uses Gaussian elimination using scaled partial pivoting to solve the associated linear equations. The introduction of a LU factorization technique or a band solver will significantly increase the speed of the solution.

The full rank Jacobian is calculated in this work. For further optimization of the computation speed, only the important, diagonal elements of the Jacobian need to be considered.

This work has used enough nodes with fine enough spacing to achieve the level of detail desired for PZ based amines. No attempt was made, however to optimize the number of nodes needed. A decrease in the number of nodes used in each section of the finite difference scheme will significantly reduce the number of equations to be solved and will increase computation time.

8.3.3 Overall Absorber modeling

The rigorous modeling of an absorber for bulk CO_2 removal from process gas is possible with modern computational capabilities. Incorporation of the

routines developed in this work with an enthalpy model will make it possible to model the entire absorber. The enthalpy model should be generated to account for the heat of absorption of carbon dioxide into the solution as well as the cooling of the solvent which occurs when water is transferred from the solvent to the gas phase. The enthalpy model should also accurately predict the associated temperature increase of the solvent due to the heat of absorption and evaporation.

Based on the results of this work, it is possible to initially ignore the rigorous model and calculate the enhancement factor using the approximation:

$$\frac{1}{E_{TOT}} = \frac{1}{E_{INST}} + \frac{1}{E_{PFO}} \quad (8.1)$$

Initializing the column this way should only require a few iterations of the rigorous model in order to achieve convergence of the absorber.

Appendix A

Analytical Solutions for Mass Transfer with Chemical Reaction

A.1 Pseudo First Order Cases

A.1.1 First Order Irreversible Reactions

Film Theory

When the reaction is first order overall and irreversible, the material balance for CO_2 with associated boundary conditions become:

$$D_{CO_2} \frac{\partial [CO_2]}{\partial X} - k_1 [CO_2] = 0 \quad (A.1)$$

$$\begin{aligned} [CO_2] &= [CO_2]_i @ X = 0 \\ [CO_2] &= 0 @ X = \delta \end{aligned} \quad (A.2)$$

Here, δ is the film thickness. Rearranging this differential equation into normal form, we obtain:

$$\frac{\partial [CO_2]}{\partial X} - \frac{k_1}{D_{CO_2}} [CO_2] = 0 \quad (A.3)$$

For which the general solution is:

$$[CO_2] = C_1 \cosh\left(\sqrt{\frac{k_1}{D_{CO_2}}} X\right) + C_2 \sinh\left(\sqrt{\frac{k_1}{D_{CO_2}}} X\right) \quad (A.4)$$

Here, C_1 and C_2 are constants of integration. Solving for the condition at $X=0$ is trivial. The result for C_1 is:

$$C_1 = [CO_2]_i \quad (A.5)$$

We substitute the film theory liquid mass transfer coefficient for the film thickness δ when evaluating the condition at $X=\delta$. Notice that the argument for the hyperbolic trigonometric expressions can change to the Hatta number:

$$\sqrt{\frac{k_1}{D_{CO_2}}} \cdot \delta = \sqrt{\frac{k_1 D_{CO_2}}{k_l^o}} = \sqrt{M} \quad (A.6)$$

The second integration constant then becomes:

$$C_2 = -\frac{[CO_2]_i}{\tanh \sqrt{Ha}} \quad (A.7)$$

We obtain expression 2.11 for the concentration of CO₂ in the liquid film.

$$[CO_2] = \frac{1}{\sinh \sqrt{M}} \left[[CO_2]_B \sinh \left(x \sqrt{\frac{k_1}{D_{CO_2}}} \right) + [CO_2]_i \sinh \left(\frac{D_{CO_2}}{k_l^o} - x \right) \sqrt{\frac{k_1}{D_{CO_2}}} \right] \quad (A.8)$$

Surface Renewal Theory

For a single first order irreversible reaction, the CO₂ material balance becomes:

$$D_{CO_2} \frac{\partial^2 [CO_2]}{\partial X^2} = \frac{\partial [CO_2]}{\partial t} + k_1 [CO_2] \quad (A.9)$$

$$[CO_2] = [CO_2]_i @ X = 0$$

$$[CO_2] = 0 @ X = \infty$$

$$[CO_2] = 0 @ t = 0$$

We take the Laplace transform of each term in equation A.9 to obtain:

$$L\left\{D_{co2} \frac{\partial^2 [CO_2]}{\partial X^2}\right\} = D_{co2} \frac{1}{s} \frac{\partial^2 \overline{[CO_2]}}{\partial X^2} \quad (A.10)$$

$$L\left\{\frac{\partial [CO_2]}{\partial t}\right\} = s[CO_2] - [CO_2]_{t=0} = s[CO_2] \quad (A.11)$$

$$L\{k_1 [CO_2]\} = k_1 \overline{[CO_2]} \quad (A.12)$$

Combining all terms and rearranging, we obtain :

$$D_{co2} \frac{\partial^2 \overline{[CO_2]}}{\partial X^2} = \overline{[CO_2]}(k_1 + s) \quad (A.13)$$

The general solution of this linear problem is:

$$\overline{[CO_2]} = C_1 \exp\left(\sqrt{\frac{k_1 + s}{D_{co2}}} X\right) + C_2 \exp\left(-\sqrt{\frac{k_1 + s}{D_{co2}}} X\right) \quad (A.14)$$

A necessary condition for this expression to remain finite throughout all X is that $C_1=0$. Solving for C_2 we obtain:

$$C_2 = [CO_2]_i \quad (A.15)$$

Substituting into equation A.14 along with the definition of the liquid film mass transfer coefficient using surface renewal theory, we obtain the concentration profile of CO_2 in the liquid.

$$\overline{[CO_2]} = [CO_2]_i \exp\left(-X \frac{k_l}{D_{co2}} \sqrt{1 + \frac{k_1 D_{co2}}{k_l^2}}\right) \quad (A.16)$$

Applying Fick's law to this expression we obtain the following expression for the flux.

$$N_{CO_2} = k_l \sqrt{1 + \frac{k_1 D_{CO_2}}{k^2_l}} [CO_2]_i \quad (A.17)$$

A.1.2 First Order Reversible Reactions

We first rearrange the reaction expression for CO₂ (equation 2.?) by substituting the definition of the equilibrium constant. Here, [CO₂]* is the concentration of CO₂ in equilibrium with the concentration of CO₂ product.

$$r_{CO_2} = k_1 ([CO_2] - [CO_2]^*) \quad (A.18)$$

Substitution of this reaction expression into the CO₂ material balance leads to the following modification of the irreversible equation.

$$D_{CO_2} \frac{\partial^2 [CO_2]}{\partial X^2} = \frac{\partial [CO_2]}{\partial t} + k_1 ([CO_2]_i - [CO_2]^*) \quad (A.19)$$

Boundary conditions for this problem are:

$$\begin{aligned} [CO_2] &= [CO_2]_i @ X = 0 \\ [CO_2] &= [CO_2]^* @ X = \infty \\ [CO_2] &= [CO_2]^* @ t = 0 \end{aligned} \quad (A.20)$$

We take the Laplace transform of this equation to eliminate the time variable and obtain:

$$D_{CO_2} \frac{\partial^2 \overline{[CO_2]}}{\partial X^2} = s(\overline{[CO_2]} - [CO_2]^*) + k_1(\overline{[CO_2]} - [CO_2]^*) \quad (A.21)$$

Since this is a linear, non-homogeneous equation, we solve for the general solution of the related homogeneous equation and add a particular solution. The combined general and particular solution for this problem is:

$$\overline{[CO_2]} = C_1 \exp\left(\sqrt{\frac{k_1 + s}{D_{CO_2}}} X\right) + C_2 \exp\left(-\sqrt{\frac{k_1 + s}{D_{CO_2}}} X\right) + [CO_2]^* \quad (A.22)$$

Evaluation of the boundary conditions yields the integration constants. Again, we find that C_1 must be zero in order for the concentration to be finite over all positive X . For C_2 we find:

$$C_2 = [CO_2]_i - [CO_2]^* \quad (A.23)$$

The concentration profile is a slight modification of the irreversible case which accounts for the equilibrium concentration of CO_2 in the bulk liquid.

$$\overline{[CO_2]} = ([CO_2]_i - [CO_2]^*) \exp\left(-X \frac{k_l}{D_{CO_2}} \sqrt{1 + \frac{k_1 D_{CO_2}}{k_l^2}}\right) \quad (A.24)$$

Using Fick's Law, we obtain an expression for the flux that is a slight modification of the irreversible case.

$$N_{CO_2} = k_l \sqrt{1 + \frac{k_1 D_{CO_2}}{k_l^2}} ([CO_2]_i - [CO_2]^*) \quad (A.25)$$

A.2 Instantaneous Reactions

With instantaneous reactions, all the reaction takes place at the interface. The only phenomenon occurring through the liquid boundary layer, then, is the physical mass transfer of total CO₂ species. We can express this as:

$$N_{CO_2} = k_{l,PROD}^o \left([CO_2]^i_T - [CO_2]^B_T \right) \quad (A.26)$$

Where

$k_{l,PROD}^o$ = Mass Transfer Coefficient for CO₂ Products

$[CO_2]^i_T$ = Total CO₂ at the interface

$[CO_2]^B_T$ = Total CO₂ in the bulk solution

The reaction is in equilibrium at the interface and the CO₂ at the interface is in equilibrium with the gas phase. For this reason, we can replace the interfacial concentration of CO₂ with the equilibrium concentration of CO₂. The bulk liquid phase concentration of CO₂ is in equilibrium with the bulk gas phase. Therefore, the total CO₂ concentration in the bulk can be replaced with the total CO₂ concentration in equilibrium with the bulk phase partial pressure of CO₂.

$$N_{CO_2} = k_{l,PROD}^o \left([CO_2]^{*i}_T - [CO_2]^{*B}_T \right) \quad (A.27)$$

A.2.1 Instantaneous Reactions / Small Driving Force

A specific case of instantaneous reactions is when small driving forces are used. In this instance, an extremely useful extension of equation ? can be derived. We divide equation ? By the total amine concentration. The driving force is then equal to the change in effective solution loading across the boundary layer. As the driving force is reduced to infinitely small values, the difference in loading across the boundary layer becomes a differential. Dividing by the derivative of the equilibrium partial pressure with respect to loading, we obtain equation 2.22.

$$N_{CO_2} = k_l^o \frac{[Am]_T}{\frac{\partial P_{CO_2}^*}{\partial \alpha}} [P_{CO_2,i} - P_{CO_2,B}^*] \quad (A.28)$$

A.3 Pseudo First Order / Instantaneous Reaction with Small Driving Force

CO₂ absorption into fast amine solutions may result in an instance where the reactions approach instantaneous behavior. A very useful expression can be derived for the case of series resistance where the initial portion of the boundary layer acts like pseudo first order and the rest of the boundary layer acts like instantaneous reactions with small driving forces.

$$N_{CO_2} = k_l^o E^{1st} \left([CO_2]_i - [CO_2]^*_i \right) \quad (A.29)$$

$$N_{CO_2} = k_l^o E^{Inst} \left([CO_2]^*_i - [CO_2]^*_B \right) \quad (A.30)$$

First we solve equation A.29 for the CO₂ concentration at equilibrium at the interface. This expression is then substituted into equation A.30 to come up with the following expression for the flux.

$$N_{CO_2} = k_l^o \left(\frac{1}{\frac{1}{E^{Inst}} + \frac{1}{E^{1st}}} \right) \left([CO_2]_i - [CO_2]^*_B \right) \quad (A.31)$$

Appendix B

Additional NMR data not tabulated in Chapter 4 & 5

Unloaded 3 M MDEA

¹ H Peak			¹³ C Peak	
δ (ppm)	Height	Species	δ (ppm)	Species
3.462	54.3	Methylene H's Adjacent to Alcohol	58.729	Methylene C's Adjacent to Alcohol
3.460	56.9		58.483	Methylene C's Adjacent to Amine
3.449	81.4	Methylene H's Adjacent to Amine	42.039	Methyl C
3.446	105.8			
3.434	79.9			
2.388	54			
2.386	55.3	Methyl H's		
2.373	98			
2.360	73			
2.041	122.6			

3 M MDEA, Loading = 0.34

¹ H Peak			¹³ C Peak	
δ (ppm)	Height	Species	δ (ppm)	Species
3.435	66.2	Methylene H's Adjacent to Alcohol	161.36	Carbonate / Bicarbonate
3.423	96.5		158.95	
3.411	78.2	Methylene H's Adjacent to Amine	58.055	Methylene C's Adjacent to Alcohol
2.538	63.8		57.43	Methylene C's Adjacent to Amine
2.525	91.9		41.43	Methyl C
2.513	71.9			
2.166	113.4	Methyl H's		

Unloaded 1 M PZ / 3 M MDEA

¹ H Peak			¹³ C Peak	
δ (ppm)	Intensity	Species	δ (ppm)	Species
3.506	7.70	Methylene H's Adjacent to Alcohol	58.306	Methylene C's Adjacent to Alcohol in MDEA
3.493	11.41			
3.480	7.18		58.184	Methylene C's Adjacent to Amine in MDEA
2.555	11.92	H's in PZ ring	44.71	C's in PZ ring
2.434	7.20	Methylene H's Adjacent to Amine	41.73	C's in MDEA Methyl Group
2.424	10.43			
2.411	6.38			
2.098	13.00	Methyl H's		

Appendix C

Program Documentation

Simplified Equilibrium Program

A complete program listing for the predictive model used in Chapter 4 follows. This simplified VLE model speciates the PZ / MDEA / H₂O / CO₂ system and calculates CO₂ equilibrium partial pressure assuming ideal solution.

```
program test
C
C   THIS PROGRAM CALCULATES EQUILIBRIUM FOR THE PZ/MDEA
C   /H2O/CO2 SYSTEM. MODEL INPUTS ARE FORMATTED IN TEST
C   EQUILIBRIUM CALCULATIONS ARE PERFORMED IN
C   SUBROUTINE BLENDVLE.
C
C   PROGRAM IS WRITTEN BY SANJAY BISHNOI (1998 AND 1999)
C   COPYRIGHT – THE UNIVERSITY OF TEXAS AT AUSTIN
C
  real *8 temp,alpha,xmdeat,xpzt,xdegt,pco2,par(6)
c
c   ENTER PARAMETER VALUES
C
  par(1)=1.0
  par(2)=1.0
  par(3)=1.00
  par(4)=1.00
  par(5)=-30.777
c
c   ENTER CONDITIONS TO EVALUATE MODEL
C
  temp=313.15
  alpha=0.32
  xmdeat=1.0e-10
  xpzt=0.0113
  xdegt=0.0
C
C   FOLLOWING DO LOOP ALLOWS CALCULATION AT ONE POINT
C   OR SEVERAL.
```

```

C
c      do 10 i=1,100
            call blendvle(temp,alpha,xmdeat,xpzt,xdegt,par,pcO2)
            xpzt=0.0113
            xmdeat=1.0e-10
            xdegt=0.0
c      write (*,*) pco2,alpha
            alpha=alpha+0.01
10      continue
      end
CCCCCCCCCCCCCCCCCCCCCCCCCCCCCCCCCCCCCCCCCCCCCCCCCCCCCCCCCCCC
C
subroutine blendvle(temp,alpha,xmdeat,xpzt,xdegt,par,pcO2)
C
C      THIS PROGRAM LINEARIZES EQUILIBRIUM RELATIONSHIPS
C      AND SPECIATES SOLUTION FOR CO2/MDEA/PZ/H2O SYSTEM
C      USING NEWTON'S METHOD FOR NONLINEAR SETS OF EQNS
C
C      PROGRAM WRITTEN BY SANJAY BISHNOI 6/15/98
C
C      COPYRIGHT, THE UNIVERSITY OF TEXAS, 1999
C
implicit real*8 (a-h, o-z)
real*8 k(8), x(13), f(13), j(13,13),xdx(13),fdx(13)
real*8 p(13),s(13),hco2,temp,cco2,cpz,mw,par(6)
integer n,ia,icount,lo(13)
n=13
ia=n
C
C      DICTIONARY OF VECTORS
C
C      X(1): X CO2
C      X(2): X H2O
C      X(3): X PZ
C      X(4): X MDEA
C      X(5): X MDEAH+
C      X(6): X PZH+
C      X(7): X H3O+
C      X(8): X HCO3-
C      X(9): X CO3=
C      X(10): X OH-
C      X(11): X PZCOO-

```



```

C      X(12): X H+PZCOO-
C      X(13): X -OOC PZCOO-
C      F(N): VECTOR OF EQUATIONS ALL=0 AT CONVERGENCE
C      J(N,N): JACOBIAN MATRIX
C      ALPHA: LOADING OF SOLUTION
C      XCO2T: TOTAL CO2 CONCENTRATION
C      XMDEAT: TOTAL MDEA CONCENTRATION
C      XPZT: TOTAL PZ CONCENTRATION
C      XH2OT: TOTAL WATER CONCENTRATION
C      K: EQUILIBRIUM CONSTANTS
C      HCO2: HENRY'S LAW CONSTANT FOR CO2 (Pa/molefrac)
C
C      READ LOADING, AMINE STRENGTHS, AND EQM CONSTANTS
C
      icount=0
      k(1)=exp(231.465-12092.1/temp-36.7816*log(temp))
      k(2)=exp(216.049-12431.7/temp-35.4819*log(temp))
      k(3)=exp(-56.2-4044.8/temp +7.848*log(temp))
      k(4)=exp(132.899-13445.9/temp-22.4773*log(temp))
      k(5)=exp(-11.91-4350.6/temp)
      k(6)=exp(-29.308*par(1)+5614.64*par(2)/temp)
      k(7)=exp(-8.212*par(3)-5285.94*par(4)/temp)
      k(8)=exp(par(5)+5614.64/temp)
      hco2=2.3e8
C
C      RENORMALIZE MOLEFRACTIONS IN THE LOADED SOLN
C
      xamine=xpzt+xmdeat
      xco2t=alpha*xamine
      xh2ot=1.0-xamine-xdegt
      totmol=xco2t+xh2ot+xamine+xdegt
      mw=(xco2t*44.01+xmdeat*119.17+xpzt*86.13+xdegt*106.14+xh2ot*18.02)/tot
      mol
      xco2t=xco2t/totmol
      xpzt=xpzt/totmol
      xmdeat=xmdeat/totmol
      xh2ot=xh2ot/totmol
C      write (*,*) 'total initial molefrac:', (xh2ot+xmdeat+xpzt+xco2t)
C      write (*,*) 'co2,mdea,pz,h2o,deg',xco2t,xmdeat,xpzt,xh2ot,xdegt
C
C      ENTER INITIAL GUESSES FOR MOLEFRACTIONS
C

```

```

x(1)=2.0e-3
x(2)=xh2ot
x(3)=(1.0-alpha)*xpzt
x(4)=(1.0-alpha)*xmdeat
x(5)=alpha*xmdeat
x(6)=0.3*alpha*xpzt
x(7)=1.0e-7
x(8)=x(5)+x(6)
x(9)=0.00001*x(8)
x(10)=1.0e-7
x(11)=0.5*alpha*xpzt
x(12)=0.5*alpha*xpzt
x(13)=1.0e-10
l      continue
icount=icount+1
c      write(*,*) 'icount= ',icount
c
C      EVALUATE FUNCTION VALUES
C

```

```

call eq(n,x,xco2t,xmdeat,xpzt,k,f)

```

```

c
C      CALCULATE THE JACOBIAN MATRIX
C
do 30 i=1,n
    do 40 l=1,n
        xdx(l)=x(l)
40    continue
        xdx(i)=1.04*x(i)
        call eq(n,xdx,xco2t,xmdeat,xpzt,k,fdx)
        do 50 m=1,n
            j(m,i)=(fdx(m)-f(m))/(xdx(i)-x(i))
50        continue
30    continue
C
C      USE GAUSSIAN ELIMINATION TO GET THE NEXT GUESS
C      FIRST CALL GAUSS FOR FORWARD ELIMINATION THEN
C      CALL SOLVE FOR BACK SUBSTITUTION
C
call gauss(n,j,ia,lo,s)

```

```

c
call solve(n,j,ia,lo,-f,p)
do 60 i=1,n
    x(i)=x(i)+p(i)
60    continue
do 70 i=1,n
    if (abs(p(i)/x(i)).gt.1.0e-8) then
        goto 1
    else
        continue
    endif
70    continue
write (*,*) ''

c
C    write (*,*) ''
C    write (*,*) f(1),f(2),f(3)
C    write (*,*) f(4),f(5),f(6)
C    write (*,*) f(7),f(8),f(9)
C    write (*,*) f(10),f(11),f(12)
C    write (*,*) f(13)

c
c    write (*,*) ' check material balances: '
c    write (*,*) 'total molefractions:'
c    write (*,*) xco2t,xmdeat,xpzt,xh2ot
c    write (*,*) 'CO2: ', xco2t-x(1)-x(8)-x(9)-x(11)-x(12)
c    write (*,*) 'MDEA: ',xmdeat-x(4)-x(5)
c    write (*,*) 'PZ: ',xpzt-x(3)-x(6)-x(11)-x(12)
c    write (*,*) 'CHARGE: ', 2*x(9)+x(8)+x(10)+x(11)-x(7)-x(5)-x(6)

c
c    write (*,*) 'CONVERGED IN ',ICOUNT,' ITERATIONS.'

c
c    USE MOLEFRACTIONS TO CALCULATE CONCENTRATIONS
C
c    tot=0.0
c    do 10 i=1,n
c        write(*,*) 'X(' ,i,')=' ,x(i), 'F(' ,i,')=' ,f(i)
c        tot=tot+x(i)
10    continue
cco2=x(1)/mw
cpz=x(4)/mw
cmdea=x(3)/mw

```

```

c      write (*,*) ''
c      write (*,*) 'Temp (K)= ',temp
c      write (*,*) 'Sum of molefractions= ',tot
pco2=x(1)*hco2
c      write (*,*)'CO2 Partial Pressure (Pa): ', pco2
open (unit=10, file='pred1.txt', status='new')
open (unit=11, file='pred2.txt', status='new')
open (unit=12, file='pred3.txt', status='new')
open (unit=13, file='pred4.txt', status='new')
open (unit=14, file='pred5.txt', status='new')
write (10,*) pco2,alpha,x(1)
write (11,*) x(2),x(3),x(4)
      write (12,*) x(5),x(6),x(7)
write (13,*) x(8),x(9),x(10)
write (14,*) x(11),x(12),x(13)
      end

```

```

CCCCCCCCCCCCCCCCCCCCCCCCCCCCCCCCCCCCCCCCCCCCCCCCCCCCCCCC
CCCCCCCCCCCC

```

```

C
C      THIS SUBROUTINE CALCULATES THE FUNCTION VALUES
C      SOLUTION HAS BEEN ACHIEVED WHEN EACH OF THESE F
C      FUNCTIONS EQUALS 0
C

```

```

      subroutine eq(n,x,xco2t,xmdeat,xpzt,k,f)
real*8 k(7), x(n), f(n),xco2t,xmdeat,xpzt
C
f(1)=x(2)*x(2)*x(1)*k(1)-x(8)*x(7)
f(2)=x(2)*x(8)*k(2)-x(9)*x(7)
f(3)=x(2)*x(5)*k(3)-x(7)*x(4)
f(4)=x(2)*x(2)*k(4)-x(7)*x(10)
f(5)=x(6)*x(2)*k(5)-x(3)*x(7)
f(6)=x(3)*x(1)*x(2)*k(6)-x(7)*x(11)
f(7)=x(12)*x(2)*k(7)-x(7)*x(11)
f(8)=x(1)*x(2)*x(11)*k(8)-x(7)*x(13)
f(9)=x(1)+x(8)+x(9)+x(11)+x(12)+2.0*x(13)-xco2t
f(10)=x(4)+x(5)-xmdeat
f(11)=x(3)+x(6)+x(11)+x(12)+x(13)-xpzt
f(13)=2.0*x(9)+x(8)+x(10)+x(11)+2.0*x(13)-x(7)-x(5)-x(6)
f(12)=1.0-x(1)-x(2)-x(3)-x(4)-x(5)-x(6)-x(7)-x(8)-x(9)-x(10)
&      -x(11)-x(12)-x(13)

```

```

C

```

```

return
end
C
CCCCCCCCCCCCCCCCCCCCCCCCCCCCCCCCCCCCCCCCCCCCCCCCCCCCCCCC
CCCCCCCCCCCCCCCC
C
C   THIS SUBROUTINE PERFORMS THE FORWARD ELIMINATION
C   PROCESS FOR GAUSSIAN ELIMINATION WITH SCALED PARTIAL
C   PIVOTING FOR N EQUATIONS. IT IS BASED ON THE BOOK
C   'NUMERICAL MATHEMATICS AND COMPUTING' BY CHENEY
C   AND KINCAID.SECOND EDITION.CHAP6 SEC 2
C
C   SUBROUTINE WRITTEN BY SANJAY BISHNOI 1998
C
subroutine gauss(n,a,ia,l,s)
real*8 a(ia,n), s(n)
integer i,j,k,l(n)
c
c   FIRST TWO DO LOOPS INITIALIZE L INDEX VECTOR AND FIND
C   SCALING VECTOR S.
C
do 3 i=1,n
    l(i)=i
    smax=0.0
    do 2 j=1,n
        if (abs(a(i,j)).gt.smax) smax=abs(a(i,j))
2       continue
    s(i)=smax
3   continue
C
C   NOW PERFORM FORWARD ELIMINATION STEP AND PLACE
C   MULTIPLIERS WHERE ZEROES WOULD BE FOR REDUCED
C   EQUATIONS.
C
do 7 k=1,n-1
    rmax=0.0
    do 4 i=k,n
        r=abs(a(l(i),k))/s(l(i))
        if(r.le.rmax) goto 4
        j=i
        rmax=r
4       continue

```

```

lk=l(j)
l(j)=l(k)
l(k)=lk
do 6 i=k+1,n
    xmult=a(l(i),k) / a(lk,k)
    do 5 j=k+1,n
        a(l(i),j)=a(l(i),j)-xmult*a(lk,j)
5        continue
    a(l(i),k)=xmult
6    continue
7    continue
return
end

CCCCCCCCCCCCCCCCCCCCCCCCCCCCCCCCCCCCCCCCCCCCCCCCCCCCCCCC
CCCCCCCCCCCCCCCCCCCC
C
C    THIS SUBROUTINE PERFORMS THE BACKWARD SUBSTITUTION
C    PROCESSFOR GAUSSIAN ELIMINATION WITH SCALED PARTIAL
C    PIVOTING FOR N EQUATIONS. IT IS BASED ON THE BOOK
C    'NUMERICAL MATHEMATICS AND COMPUTING' BY CHENEY
C    AND KINCAID.SECOND EDITION.CHAP6 SEC 2
C
C    SUBROUTINE WRITTEN BY SANJAY BISHNOI 1998
C
subroutine solve(n,a,ia,l,b,x)
real*8 a(ia,n),b(n),x(n)
integer n,l(n),i,k,j
C
C    CORRECT THE MATRIX B BY MULTIPLIERS FOUND IN
C    FORWARDELIMINATION AND PLACED IN MATRIX A WHERE O
C    TERMS ARE ENCOUNTERED
C
do 3 k=1,n-1
    do 2 i=k+1,n
        b(l(i))=b(l(i))-a(l(i),k)*b(l(k))
2        continue
3    continue
C
C    SOLVE FOR THE UNKNOWN X VECTOR
C
x(n)=b(l(n))/a(l(n),n)

```

```

do 5 i=n-1,1,-1
    sum=b(l(i))
    do 4 j=i+1,n
        sum=sum-a(l(i),j)*x(j)
4      continue
    x(i)=sum/a(l(i),i)
5    continue
C
C    RETURN TO MAIN PROGRAM
C
return
end

```

Rigorous Rate Model for PZ / MDEA

An excerpt of the rigorous rate model is shown below. Since a list of the whole program would be too long, we only show the equations that must be solved for one grid size. The equation solver is the same as in the simplified VLE program listed above and therefore it is not listed. The rigorous VLE follows the model of Austgen (1989) and is too long to be listed here. Extension of these equations to other grid sizes is trivial.

```

C    VARIABLES DICTIONARY:
C
C    SCALARS:
C
C    n: NUMBER OF NODES
C    H1: STEPSIZE FOR GRID SIZE ONE
C    R: DIMENSIONLESS DISTANCE FROM INTERFACE
C    I: INTEGER COUNTER, IDENTIFIED NODE NUMBER
C    C: COSINE OF  $\pi/2r$  AT R
C    S: SINE OF  $\pi/2r$  AT R
C    T: TAN OF  $\pi/2r$  AT R
C    T1: TERM ONE IN MATERIAL BALANCE EQUATIONS – SEE
C    APPENDIX E
C    T2: TERM 2
C    T3: TERM 3

```

```

C      T4: TERM 4
C
C      VECTORS
C
C      Dr(l)=DERIVATIVE OF SPECIES L
C      D2r(l)=SECOND DERIVATIVE OF SPECIES L
C      RR: VECTOR OF FINITE RATE REACTIONS
C      1:      CO2+OH- → HCO3-
C      2:      CO2+MDEA → HCO3-+MDEAH+
C      6:      CO2+PZ+H2O → PZCOO- + H3O+
C      7:      CO2+PZ+MDEA → PZCOO- + MDEAH+
C      9:      CO2+PZCOO- + MDEA → PZ(COO-)2 + MDEAH+
C      10:     CO2+PZCOO- + H2O → PZ(COO-)2 + H3O+
C      DELTA(n)=RESIDUALS: THESE ARE ALL 0 AT SOLUTION.
C      Y(n*11): VECTOR OF MOLEFRACTIONS. AT A GIVEN NODE,
C      SPECIES COME IN THE FOLLOWING ORDER
C      1:      CO2
C      2:      PZ
C      3:      MDEA
C      4:      MDEAH+
C      5:      PZH+
C      6:      HCO3-
C      7:      CO3-
C      8:      OH-
C      9:      PZCOO-
C      10:     H+PZCOO-
C      11:     PZ(COO-)2
C      KF:     FORWARD REACTION RATE CONSTANTS, SEE RR FOR
C      REACTION NUMBERS
C      K;      EQUILIBRIUM CONSTANTS: NUMBERS ARE SAME AS RR.
C      IN ADDITION:
C      3:      HCO3- + OH- → CO3= + H2O
C      4:      MDEA → MDEAH+ + H2O
C      5:      PZ → PZH+ + H2O
C      8:      PZCOO- → H+PZCOO- + H2O
C      11:     H2O → H3O+ + OH-
C
C
C      CALCULATE RESIDUALS FROM NODES 1 TO N1 USING GRIDSIZE
C      H1
C
do 10 i = 1,n1-1

```



```

C      r=real(i)*h1
C
C      CALCULATE FIRST AND SECOND DERIVATIVES FOR ALL
C      SPECIES AT EACH NODE
C
C      do 20 l=1,11
C      Dr(l)=1.0/(2.0*h1)*(-y(11*(i-1)+l) + y(11*(i+1)+l))
C      Dr2(l)=1.0/(h1*h1)*(y(11*(i-1)+l) -2.0*y(11*i+l) + y(11*(i+1)+l))
20    continue
C      write (12,*) 'First Derivatives'
C      write (12,*) Dr
C      write (12,*) 'Second Derivatives'
C      write (12,*) Dr2
C
C      CALCULATE THE REACTION RATES FOR FINITE RATE
C      REACTIONS
C
C      RR(1)=kf(1)*y(11*i+1)*y(11*i+3) - kf(1)/K(1)*y(11*i+4)*y(11*i+6)
C      RR(2)=kf(2)*y(11*i+1)*y(11*i+8) - kf(2)/K(2)*y(11*i+6)
C      RR(6)=kf(6)*y(11*i+1)*y(11*i+2)
C      *      - kf(6)/K(6)*y(11*i+9)*K(11)/y(11*i+8)
C      RR(7)=kf(7)*y(11*i+1)*y(11*i+2)*y(11*i+3)
C      *      - kf(7)/K(7)*y(11*i+9)*y(11*i+4)
C      RR(9)=kf(9)*y(11*i+1)*y(11*i+3)*y(11*i+9)
C      *      - kf(9)/K(9)*y(11*i+4)*y(11*i+11)
C      RR(10)=kf(10)*y(11*i+1)*y(11*i+9)
C      *      - kf(10)/K(10)*y(11*i+11)*K(11)/y(11*i+8)
C
C      write (12,*) 'Reaction Rates'
C      write (12,*) RR
C
C      CALCULATE TRIG FUNCTIONS AT R
C
C      c=cos(pi/2.0*r)
C      s=sin(pi/2.0*r)
C      ta=tan(pi/2.0*r)
C
C      CALCULATE LEADING TERMS
C
C      t1=4.0*e/(pi*pi)*s*s*c*c
C      t2=4.0/(pi*pi)*c*c*c*c*e/D(1)
C      t3=-4.0/pi*e*s*s*s*c + 4.0/pi*e*ta*c*c

```

```

t4=-4.0/pi*e/D(1)*c*c*c*s
c write (12,*) 'Term 1 and 2'
c write (12,*) t1,t2
c write (12,*) 'Term 3 and 4'
c write (12,*) t3,t4
C
C RESIDUALS CORRESPONDING TO THE PIPERAZINE MATERIAL
C BALANCE
C
delta(11*i+1)=(t1+D(2)*t2)*Dr2(2) + (t3+D(2)*t4)*Dr(2)
* + (t1+D(9)*t2)*Dr2(9) + (t3+D(9)*t4)*Dr(9)
* + (t1+D(10)*t2)*Dr2(10) + (t3+D(10)*t4)*Dr(10)
* + (t1+D(5)*t2)*Dr2(5) + (t3+D(5)*t4)*Dr(5)
* + (t1+D(11)*t2)*Dr2(11) + (t3+D(11)*t4)*Dr(11)
C
C RESIDUALS CORRESPONDING TO THE MDEA MATERIAL
C BALANCE
C
delta(11*i+2)=(t1+D(3)*t2)*Dr2(3) + (t3+D(3)*t4)*Dr(3)
* + (t1+D(4)*t2)*Dr2(4) + (t3+D(4)*t4)*Dr(4)
C
C RESIDUALS CORRESPONDING TO TOTAL CARBON BALANCE
C
delta(11*i+3)=(t1+D(1)*t2)*Dr2(1) + (t3+D(1)*t4)*Dr(1)
* + (t1+D(6)*t2)*Dr2(6) + (t3+D(6)*t4)*Dr(6)
* + (t1+D(7)*t2)*Dr2(7) + (t3+D(7)*t4)*Dr(7)
* + (t1+D(9)*t2)*Dr2(9) + (t3+D(9)*t4)*Dr(9)
* + (t1+D(10)*t2)*Dr2(10) + (t3+D(10)*t4)*Dr(10)
* + 2.0*((t1+D(11)*t2)*Dr2(11) + (t3+D(11)*t4)*Dr(11))
C
C RESIDUAL CORRESPONDING TO MDEA / MDEAH+ EQUILIBRIUM
C
delta(11*i+4)=K(4)*y(11*i+3) - y(11*i+4)*y(11*i+8)
C
C RESIDUAL CORRESPONDING TO PZ/PZH+ EQUILIBRIUM
C
delta(11*i+5)=K(5)*y(11*i+2) - y(11*i+5)*y(11*i+8)
C
C RESIDUAL CORRESPONDING TO H+PZCOO- / PZCOO- EQM
C
delta(11*i+6)=K(8)*y(11*i+9) - y(11*i+10)*y(11*i+8)
C

```

```

C   RESIDUAL CORRESPONDING TO CARBON DIOXIDE MATERIAL
C   BALANCE
C
      delta(11*i+7)=(t1+D(1)*t2)*Dr2(1) + (t3+D(1)*t4)*Dr(1)
      *      - RR(1) - RR(2) - RR(6) - RR(7) - RR(9) - RR(10)
C
C   RESIDUAL CORRESPONDING TO CO3= / HCO3- EQUILIBRIUM
C
      delta(11*i+8)=K(3)*y(11*i+6)*y(11*i+8) - y(11*i+7)
C
C   RESIDUAL CORRESPONDING TO CARBAMATE BUFFER SYSTEM
C   BALANCE
C
      delta(11*i+9)=(t1+D(9)*t2)*Dr2(9) + (t3+D(9)*t4)*Dr(9)
      *      + (t1+D(10)*t2)*Dr2(10) + (t3+D(10)*t4)*Dr(10)
      *      + RR(7) + RR(6) - RR(9)      - RR(10)
C
C   RESIDUAL CORRESPONDING TO DICARBAMATE MATERIAL
C   BALANCE
C
      delta(11*i+10)=(t1+D(11)*t2)*Dr2(11) + (t3+D(11)*t4)*Dr(11)
      *      + RR(9)      + RR(10)
C
C   RESIDUAL CORRESPONDING TO ELECTRONEUTRALITY
C
      delta(11*i+11) = y(11*i+4) + y(11*i+5)
      * - (y(11*i+6)+2.0*y(11*i+7)+y(11*i+8)+y(11*i+9)+2.0*y(11*i+11))
c
c   WRITE RESIDUALS FOR NODE I
c
c   write (12,*) 'Residuals at Node ',i
c   do 30 l=1,11
c       write (12,*) delta(11*i+l)
c30  continue
C
c   FINISH CALCULATIONS AT NODE I
10  CONTINUE

```

Appendix D

Predictions of other PZ/MDEA data using the models of this work

CO₂ Solubility Predictions

Predictions for the data of Xu et al. (1998) and Liu et al. (1999)

[PZ] M	[MDEA] M	T (K)	Loading	P* _{CO2} Meas(Pa)	P* _{CO2} Pred (Pa)
Data of Xu et al. (1998)					
0.000	4.280	343	0.04	4263	4030
0.000	4.280	343	0.09	14455	11649
0.000	4.280	343	0.17	35259	30863
0.000	4.280	343	0.20	55414	40285
0.000	4.280	343	0.23	76701	50611
0.257	4.280	343	0.12	14058	15382
0.257	4.280	343	0.20	36859	38247
0.257	4.280	343	0.25	76770	62017
0.103	4.280	343	0.05	3835	4260
0.103	4.280	343	0.08	13074	9149
0.103	4.280	343	0.16	35951	27587
0.103	4.280	343	0.20	54509	41816
0.103	4.280	343	0.24	76770	54354
0.515	4.280	343	0.15	11365	20942
0.515	4.280	343	0.20	32254	39649
0.515	4.280	343	0.29	76574	83945
Data of Liu et al. (1999)					
0.17	1.53	323	0.468	21180	24531
0.17	1.53	323	0.589	44000	45012
0.17	1.53	323	0.696	89440	76488
0.17	1.53	323	0.851	271900	189668
0.17	1.53	323	0.98	669400	575799
0.17	1.53	343	0.387	35430	39851
0.17	1.53	343	0.492	71290	71335
0.17	1.53	343	0.641	148800	148752
0.17	1.53	343	0.811	418800	362181
0.17	1.53	343	0.876	688800	540926
0.35	1.35	323	0.5	17780	24106
0.35	1.35	323	0.609	41140	44329
0.35	1.35	323	0.707	89430	75048

0.35	1.35	323	0.936	509400	361498
0.35	1.35	323	0.955	586900	432960
0.35	1.35	343	0.349	17600	22739
0.35	1.35	343	0.427	32070	40321
0.35	1.35	343	0.558	71260	87785
0.35	1.35	343	0.759	243800	256262
0.35	1.35	343	0.79	296300	305557
0.35	3.15	303	0.477	16730	12436
0.35	3.15	303	0.642	54240	27160
0.35	3.15	303	0.714	97470	39296
0.35	3.15	303	0.812	247500	71407
0.35	3.15	303	0.842	407500	89082
0.35	3.15	323	0.377	23950	23004
0.35	3.15	323	0.455	42970	34942
0.35	3.15	323	0.573	90110	61341
0.35	3.15	323	0.665	200100	95658
0.35	3.15	323	0.75	422600	151481
0.35	3.15	343	0.287	33860	42642
0.35	3.15	343	0.324	48080	55372
0.35	3.15	343	0.47	178000	125234
0.35	3.15	343	0.591	368000	222576
0.35	3.15	343	0.691	573000	363203
0.35	3.15	363	0.147	19880	63615
0.35	3.15	363	0.191	37540	97465
0.35	3.15	363	0.247	82540	149726
0.35	3.15	363	0.407	312500	373111
0.35	3.15	363	0.49	482500	555913
0.7	2.8	303	0.506	15600	14097
0.7	2.8	303	0.647	48430	29458
0.7	2.8	303	0.733	97450	46715
0.7	2.8	303	0.793	202500	67221
0.7	2.8	303	0.88	460000	131293
0.7	2.8	323	0.41	18980	23266
0.7	2.8	323	0.54	49600	49713
0.7	2.8	323	0.617	90170	73452
0.7	2.8	323	0.694	195100	108947
0.7	2.8	323	0.768	380100	165057
0.7	2.8	343	0.274	19240	25910
0.7	2.8	343	0.366	52640	57683
0.7	2.8	343	0.41	73140	78096
0.7	2.8	343	0.541	177800	163645
0.7	2.8	343	0.766	935300	522580
0.7	2.8	363	0.198	17370	104079
0.7	2.8	363	0.221	25370	127102

0.7	2.8	363	0.254	37190	164288
0.7	2.8	363	0.401	157200	402947
0.7	2.8	363	0.54	412200	802237
0.53	4.77	323	0.318	42510	36246
0.53	4.77	323	0.415	91150	67153
0.53	4.77	323	0.649	326200	224618
0.53	4.77	323	0.706	508700	311311
0.53	4.77	323	0.76	753700	440771
0.53	4.77	343	0.193	35830	56600
0.53	4.77	343	0.252	75610	99457
0.53	4.77	343	0.396	203100	257907
0.53	4.77	343	0.529	460600	501105
0.53	4.77	343	0.592	713100	678482
1.55	3.75	323	0.349	14340	18597
1.55	3.75	323	0.454	46490	51777
1.55	3.75	323	0.525	91150	84079
1.55	3.75	323	0.65	278300	170096
1.55	3.75	323	0.746	678300	294769
1.55	3.75	343	0.247	13160	33447
1.55	3.75	343	0.323	37350	75260
1.55	3.75	343	0.544	224700	361189
1.55	3.75	343	0.635	479700	576914
1.55	3.75	343	0.665	667200	672138

Rate Predictions

Model predictions of CO₂ absorption in PZ / MDEA solutions (Data of Xu et al., 1992).

Temp (K)	k_1^o (m/s)	P_{CO_2} (Pa)	Loading Mol CO ₂ / mol Am	[MDEA] mol/L	[PZ] mol/L	Flux*10 ⁷ (mol/cm ² s)	
						Meas	Predicted
303	1.50E-5	98930	0.104	4.21	0.1	3.64	3.38
303	1.50E-5	98930	0.144	4.21	0.1	3.34	3.2
303	1.50E-5	98930	0.178	4.21	0.1	3.10	3.09
303	1.50E-5	98930	0.225	4.21	0.1	2.79	2.96
303	1.50E-5	98930	0.303	4.21	0.1	2.36	2.76
303	1.50E-5	98930	0.496	4.21	0.1	1.33	2.19
313	2.05E-5	96260	0.128	4.21	0.1	4.26	4.77
313	2.05E-5	96260	0.161	4.21	0.1	3.89	4.58
313	2.05E-5	96260	0.19	4.21	0.1	3.57	4.43
313	2.05E-5	96260	0.23	4.21	0.1	3.13	4.22
313	2.05E-5	96260	0.266	4.21	0.1	2.90	4.03
313	2.05E-5	96260	0.294	4.21	0.1	2.61	3.88

313	2.05E-5	96260	0.348	4.21	0.1	2.17	3.56
313	2.05E-5	96260	0.406	4.21	0.1	1.75	3.18
313	2.05E-5	96260	0.495	4.21	0.1	1.08	2.52
328	3.02E-5	88800	0.144	4.21	0.1	4.33	7.08
328	3.02E-5	88800	0.159	4.21	0.1	4.01	6.81
328	3.02E-5	88800	0.186	4.21	0.1	3.58	6.32
328	3.02E-5	88800	0.208	4.21	0.1	3.21	5.92
328	3.02E-5	88800	0.236	4.21	0.1	2.79	5.41
328	3.02E-5	88800	0.266	4.21	0.1	2.36	4.86
328	3.02E-5	88800	0.284	4.21	0.1	2.08	4.53
328	3.02E-5	88800	0.324	4.21	0.1	1.46	3.79
328	3.02E-5	88800	0.360	4.21	0.1	0.08	3.12
343	4.26E-5	74660	0.088	4.21	0.1	5.39	8.23
343	4.26E-5	74660	0.104	4.21	0.1	4.52	7.57
343	4.26E-5	74660	0.129	4.21	0.1	3.43	6.54
343	4.26E-5	74660	0.139	4.21	0.1	2.97	6.12
343	4.26E-5	74660	0.156	4.21	0.1	2.11	5.42
343	4.26E-5	74660	0.175	4.21	0.1	1.65	4.64
328	3.02E-5	88800	0.133	4.21	0.041	3.98	5.49
328	3.02E-5	88800	0.151	4.21	0.041	3.67	5.28
328	3.02E-5	88800	0.167	4.21	0.041	3.42	5.09
328	3.02E-5	88800	0.194	4.21	0.041	3.02	4.76
328	3.02E-5	88800	0.216	4.21	0.041	2.72	4.49
328	3.02E-5	88800	0.242	4.21	0.041	2.38	4.16
328	3.02E-5	88800	0.266	4.21	0.041	2.08	3.85
328	3.02E-5	88800	0.319	4.21	0.041	1.43	3.14
328	3.02E-5	88800	0.371	4.21	0.041	0.63	2.42
328	3.02E-5	88800	0.176	4.21	0.21	4.47	8.58
328	3.02E-5	88800	0.192	4.21	0.21	4.09	8.13
328	3.02E-5	88800	0.206	4.21	0.21	3.84	7.74
328	3.02E-5	88800	0.231	4.21	0.21	3.36	7.06
328	3.02E-5	88800	0.251	4.21	0.21	2.98	6.52
328	3.02E-5	88800	0.269	4.21	0.21	2.66	6.04
328	3.02E-5	88800	0.293	4.21	0.21	2.28	5.42
328	3.02E-5	88800	0.332	4.21	0.21	1.41	4.43
313	3.38E-5	95460	0.168	3.04	0.1	5.57	5.56
313	3.38E-5	95460	0.199	3.04	0.1	5.18	5.36
313	3.38E-5	95460	0.228	3.04	0.1	4.86	5.17
313	3.38E-5	95460	0.280	3.04	0.1	4.35	4.83
313	3.38E-5	95460	0.327	3.04	0.1	3.94	4.51
313	3.38E-5	95460	0.369	3.04	0.1	3.55	4.22
313	3.38E-5	95460	0.407	3.04	0.1	3.10	3.93
313	3.38E-5	95460	0.441	3.04	0.1	2.73	3.67
313	3.38E-5	95460	0.471	3.04	0.1	2.51	3.42
313	3.38E-5	95460	0.499	3.04	0.1	2.26	3.18
313	3.38E-5	95460	0.524	3.04	0.1	2.21	2.96

Appendix E

Derivation of mass transfer equations using eddy diffusivity theory

We transform the material balance from x space to r space. The material balance in x space for a species A is:

$$\frac{\partial}{\partial x} \left[(D_A + \epsilon x^2) \frac{\partial [A]}{\partial x} \right] - R_A = 0 \quad (\text{E.1})$$

Expanding the derivative using the product rule, we obtain the following expression:

$$2\epsilon x \frac{\partial [A]}{\partial x} + D_A \frac{\partial^2 [A]}{\partial x^2} + \epsilon x^2 \frac{\partial^2 [A]}{\partial x^2} - R_A = 0 \quad (\text{E.2})$$

The relationship between x and r space is given by the following two relationships.

$$r = \frac{2}{\pi} \tan^{-1} \left(x \sqrt{\frac{\epsilon}{D}} \right) \quad (\text{E.3})$$

$$x = \sqrt{\frac{D}{\epsilon}} \tan \left(\frac{\pi}{2} r \right) \quad (\text{E.4})$$

We wish to express the first and second derivatives in terms of r instead of x

First Derivative

$$\frac{\partial [A]}{\partial x} = \frac{\partial [A]}{\partial r} \frac{\partial r}{\partial x} = \frac{\partial [A]}{\partial r} \frac{\partial}{\partial x} \left[\frac{2}{\pi} \tan^{-1} \left(x \sqrt{\frac{\epsilon}{D_A}} \right) \right] \quad (\text{E.5})$$

Evaluating the derivative, we obtain:

$$\frac{\partial [A]}{\partial x} = \frac{2}{\pi} \frac{D_A}{D_A + x^2 \epsilon} \sqrt{\frac{\epsilon}{D_A}} \frac{\partial [A]}{\partial r} \quad (\text{E.6})$$

We substitute the definition of x in terms of r (eq E.3) into this expression to obtain:

$$\frac{\partial [A]}{\partial x} = \frac{2}{\pi} \cos^2\left(\frac{\pi r}{2}\right) \sqrt{\frac{\epsilon}{D_A}} \frac{\partial [A]}{\partial r} \quad (\text{E.7})$$

Second Derivative

By Chain Rule differentiation,

$$\frac{\partial^2 [A]}{\partial^2 x} = \frac{\partial}{\partial x} \left[\frac{\partial [A]}{\partial x} \right] = \frac{\partial}{\partial r} \left[\frac{\partial [A]}{\partial r} \frac{\partial r}{\partial x} \right] \frac{\partial r}{\partial x} \quad (\text{E.8})$$

Substituting the first derivatives that we evaluated above, we obtain:

$$\frac{\partial^2 [A]}{\partial^2 x} = \frac{\partial}{\partial r} \left[\left(\frac{2}{\pi} \cos^2\left(\frac{\pi r}{2}\right) \sqrt{\frac{\epsilon}{D_A}} \right) \frac{\partial [A]}{\partial r} \right] \left(\frac{2}{\pi} \cos^2\left(\frac{\pi r}{2}\right) \sqrt{\frac{\epsilon}{D_A}} \right) \quad (\text{E.9})$$

Evaluating the derivative with respect to r , we obtain a final expression for the second derivative:

$$\frac{\partial^2 [A]}{\partial^2 x} = \left(\frac{2}{\pi} \cos^2\left(\frac{\pi r}{2}\right) \sqrt{\frac{\epsilon}{D_A}} \right)^2 \frac{\partial^2 [A]}{\partial r^2} - \frac{4}{\pi} \frac{\epsilon}{D_A} \cos^3\left(\frac{\pi r}{2}\right) \sin\left(\frac{\pi r}{2}\right) \frac{\partial [A]}{\partial r} \quad (\text{E.10})$$

We substitute the expressions for x , along with the first and second derivatives into equation E.2 to obtain the final expression for the material balance of CO_2 through the liquid using eddy diffusivity theory.

Final Expression

$$\begin{aligned} & \left[\frac{4\varepsilon}{\pi^2} \sin^2\left(\frac{\pi}{2}r\right) \cos^2\left(\frac{\pi}{2}r\right) + \frac{4D_A}{\pi^2} \frac{\varepsilon}{D_A} \cos^4\left(\frac{\pi}{2}r\right) \right] \frac{\partial^2 [A]}{\partial r^2} \\ & - \left[\frac{4\varepsilon}{\pi} \sin^3\left(\frac{\pi}{2}r\right) \cos\left(\frac{\pi}{2}r\right) + \frac{4D_A}{\pi} \frac{\varepsilon}{D_A} \cos^3\left(\frac{\pi}{2}r\right) \sin\left(\frac{\pi}{2}r\right) - \frac{4}{\pi} \varepsilon \tan\left(\frac{\pi}{2}r\right) \cos^2\left(\frac{\pi}{2}r\right) \right] \frac{\partial [A]}{\partial r} \quad (\text{E.11}) \\ & - RA = 0 \end{aligned}$$

In many instances it may appear that this expression can be further simplified by canceling D_A . This work is consistent with the treatment of Glasscock (1990) who states that we can use the CO_2 diffusion coefficient in all cases where the ratio of D/ε appears. This allows us to use the same expressions for each component. With this substitution, the final material balance can be expressed as:

$$[T_1 + T_2 D_A] \frac{\partial^2 [A]}{\partial r^2} + [T_3 + T_4 D_A] \frac{\partial [A]}{\partial r} - RA = 0 \quad (\text{E.12})$$

Where

$$\begin{aligned} T_1 &= \frac{4\varepsilon}{\pi^2} \sin^2\left(\frac{\pi}{2}r\right) \cos^2\left(\frac{\pi}{2}r\right) \\ T_2 &= \frac{4}{\pi^2} \frac{\varepsilon}{D_A} \cos^4\left(\frac{\pi}{2}r\right) \\ T_3 &= -\frac{4\varepsilon}{\pi} \sin^3\left(\frac{\pi}{2}r\right) \cos\left(\frac{\pi}{2}r\right) + \frac{4}{\pi} \varepsilon \tan\left(\frac{\pi}{2}r\right) \cos^2\left(\frac{\pi}{2}r\right) \\ T_4 &= -\frac{4D_A}{\pi} \frac{\varepsilon}{D_A} \cos^3\left(\frac{\pi}{2}r\right) \sin\left(\frac{\pi}{2}r\right) \end{aligned} \quad (\text{E.13})$$

Appendix F

Detailed Simulation Output at Conditions of Data in 0.6 M PZ / 4M MDEA

Data Point PZ/MDEA 8-2

Data Conditions

T (K)	Bulk Gas P _{CO2} (Pa)	k _g *10 ⁵ (moles/(atm cm ² s))	k _l *10 ⁵ (m/s)	Loading (mol CO ₂ / mol amine)	Flux *10 ⁷ (mol / cm ² s)	
					Measured	Predicted
313	5250	1.43	2.87	0.095	3.61	3.09

Calculated Physical Properties

P [*] _{CO2} (Pa)	μ (cP)	H _{CO2} atm L/mol	ρ (g/cc)	Diffusion Coefficient (m/s) *10 ⁹			
				CO2	MDEA	PZ	IONS
431	5.48	52.64	1.04	0.69	0.43	0.52	0.52

Thermodynamic Results

Species	Equilibrium Molefraction (Liquid)	Activity Coefficient
CO2	1.37E-06	1.34E+00
H2O	8.49E-01	1.01E+00
PZ	5.81E-03	1.34E-01
MDEA	1.20E-01	3.51E-01
PZH+	4.71E-03	2.58E-01
MDEAH+	8.02E-03	3.63E-01
H3O+	2.30E-11	2.81E-01
PZCOO-	4.90E-03	2.60E-01
HCO3-	4.76E-03	4.01E-01
CO3=	2.14E-04	1.28E+00
OH-	1.39E-06	7.70E-01
H+PZCOO-	1.37E-03	1.01E+00
PZ(COO-)2	1.32E-03	6.98E-02

Rate Results

r - Dimensionless Distance from Interface	Concentration (Mol / L)					
	CO ₂	PZ	MDEA	MDEAH ⁺	PZH ⁺	HCO ₃ ⁻
0.0E+00	5.7E-04	1.2E-01	3.6E+00	3.5E-01	1.5E-01	1.5E-01
1.0E-04	5.6E-04	1.2E-01	3.6E+00	3.5E-01	1.5E-01	1.5E-01
2.0E-04	5.5E-04	1.2E-01	3.6E+00	3.5E-01	1.5E-01	1.5E-01
3.0E-04	5.4E-04	1.2E-01	3.6E+00	3.5E-01	1.5E-01	1.5E-01
4.0E-04	5.3E-04	1.2E-01	3.6E+00	3.5E-01	1.5E-01	1.5E-01
5.0E-04	5.2E-04	1.2E-01	3.6E+00	3.5E-01	1.5E-01	1.5E-01
6.0E-04	5.1E-04	1.2E-01	3.6E+00	3.5E-01	1.5E-01	1.5E-01
7.0E-04	5.0E-04	1.2E-01	3.6E+00	3.5E-01	1.5E-01	1.5E-01
8.0E-04	5.0E-04	1.2E-01	3.6E+00	3.5E-01	1.5E-01	1.5E-01
9.0E-04	4.9E-04	1.2E-01	3.6E+00	3.5E-01	1.5E-01	1.5E-01
1.0E-03	4.8E-04	1.2E-01	3.6E+00	3.5E-01	1.5E-01	1.5E-01
2.0E-03	4.1E-04	1.2E-01	3.6E+00	3.5E-01	1.5E-01	1.5E-01
3.0E-03	3.5E-04	1.2E-01	3.6E+00	3.5E-01	1.5E-01	1.5E-01
4.0E-03	3.1E-04	1.2E-01	3.6E+00	3.5E-01	1.5E-01	1.5E-01
5.0E-03	2.8E-04	1.2E-01	3.6E+00	3.5E-01	1.5E-01	1.5E-01
6.0E-03	2.6E-04	1.2E-01	3.6E+00	3.5E-01	1.5E-01	1.5E-01
7.0E-03	2.5E-04	1.2E-01	3.6E+00	3.5E-01	1.5E-01	1.5E-01
8.0E-03	2.3E-04	1.2E-01	3.6E+00	3.5E-01	1.5E-01	1.5E-01
9.0E-03	2.3E-04	1.2E-01	3.6E+00	3.5E-01	1.5E-01	1.5E-01
1.0E-02	2.2E-04	1.3E-01	3.6E+00	3.5E-01	1.5E-01	1.5E-01
2.0E-02	2.0E-04	1.3E-01	3.6E+00	3.5E-01	1.5E-01	1.5E-01
3.0E-02	1.9E-04	1.3E-01	3.6E+00	3.5E-01	1.5E-01	1.5E-01
4.0E-02	1.9E-04	1.3E-01	3.6E+00	3.5E-01	1.5E-01	1.5E-01
5.0E-02	1.9E-04	1.3E-01	3.6E+00	3.5E-01	1.5E-01	1.5E-01
6.0E-02	1.9E-04	1.3E-01	3.6E+00	3.4E-01	1.5E-01	1.5E-01
7.0E-02	1.8E-04	1.3E-01	3.6E+00	3.4E-01	1.5E-01	1.5E-01
8.0E-02	1.8E-04	1.3E-01	3.6E+00	3.4E-01	1.5E-01	1.5E-01
9.0E-02	1.8E-04	1.3E-01	3.6E+00	3.4E-01	1.5E-01	1.5E-01
1.0E-01	1.8E-04	1.3E-01	3.6E+00	3.4E-01	1.5E-01	1.5E-01
2.0E-01	1.6E-04	1.4E-01	3.7E+00	3.3E-01	1.5E-01	1.5E-01
3.0E-01	1.4E-04	1.5E-01	3.7E+00	3.1E-01	1.5E-01	1.5E-01
4.0E-01	1.3E-04	1.5E-01	3.7E+00	3.0E-01	1.5E-01	1.5E-01
5.0E-01	1.2E-04	1.6E-01	3.7E+00	2.9E-01	1.5E-01	1.5E-01
6.0E-01	1.1E-04	1.7E-01	3.7E+00	2.8E-01	1.6E-01	1.5E-01
7.0E-01	9.7E-05	1.8E-01	3.7E+00	2.7E-01	1.6E-01	1.4E-01
8.0E-01	8.8E-05	1.8E-01	3.7E+00	2.6E-01	1.6E-01	1.4E-01
9.0E-01	8.0E-05	1.9E-01	3.7E+00	2.5E-01	1.6E-01	1.4E-01
1.0E+00	7.3E-05	2.0E-01	3.7E+00	2.4E-01	1.6E-01	1.4E-01

r-Dimensionless Distance from Interface	Concentration (Mol / L)				
	$\text{CO}_3^{=}$	OH^-	PZCOO^-	H^+PZCOO^-	$\text{PZ}(\text{COO}^-)_2$
0.0E+00	6.7E-03	3.2E-05	1.7E-01	7.1E-02	8.2E-02
1.0E-04	6.7E-03	3.2E-05	1.7E-01	7.1E-02	8.2E-02
2.0E-04	6.7E-03	3.2E-05	1.7E-01	7.1E-02	8.2E-02
3.0E-04	6.7E-03	3.2E-05	1.7E-01	7.1E-02	8.2E-02
4.0E-04	6.7E-03	3.2E-05	1.7E-01	7.1E-02	8.2E-02
5.0E-04	6.7E-03	3.2E-05	1.7E-01	7.1E-02	8.2E-02
6.0E-04	6.7E-03	3.2E-05	1.7E-01	7.1E-02	8.2E-02
7.0E-04	6.7E-03	3.2E-05	1.7E-01	7.1E-02	8.2E-02
8.0E-04	6.7E-03	3.2E-05	1.7E-01	7.1E-02	8.2E-02
9.0E-04	6.7E-03	3.2E-05	1.7E-01	7.1E-02	8.2E-02
1.0E-03	6.7E-03	3.2E-05	1.7E-01	7.1E-02	8.2E-02
2.0E-03	6.7E-03	3.2E-05	1.7E-01	7.1E-02	8.2E-02
3.0E-03	6.7E-03	3.2E-05	1.7E-01	7.1E-02	8.2E-02
4.0E-03	6.7E-03	3.2E-05	1.7E-01	7.1E-02	8.2E-02
5.0E-03	6.7E-03	3.2E-05	1.7E-01	7.1E-02	8.2E-02
6.0E-03	6.7E-03	3.2E-05	1.7E-01	7.1E-02	8.2E-02
7.0E-03	6.7E-03	3.2E-05	1.7E-01	7.1E-02	8.2E-02
8.0E-03	6.7E-03	3.2E-05	1.7E-01	7.1E-02	8.2E-02
9.0E-03	6.7E-03	3.2E-05	1.7E-01	7.1E-02	8.1E-02
1.0E-02	6.7E-03	3.2E-05	1.7E-01	7.1E-02	8.1E-02
2.0E-02	6.8E-03	3.2E-05	1.7E-01	7.1E-02	8.1E-02
3.0E-02	6.8E-03	3.2E-05	1.7E-01	7.0E-02	8.0E-02
4.0E-02	6.8E-03	3.2E-05	1.7E-01	7.0E-02	7.9E-02
5.0E-02	6.9E-03	3.3E-05	1.7E-01	7.0E-02	7.9E-02
6.0E-02	6.9E-03	3.3E-05	1.8E-01	7.0E-02	7.8E-02
7.0E-02	6.9E-03	3.3E-05	1.8E-01	6.9E-02	7.7E-02
8.0E-02	6.9E-03	3.3E-05	1.8E-01	6.9E-02	7.7E-02
9.0E-02	7.0E-03	3.3E-05	1.8E-01	6.9E-02	7.6E-02
1.0E-01	7.0E-03	3.3E-05	1.8E-01	6.9E-02	7.5E-02
2.0E-01	7.3E-03	3.5E-05	1.7E-01	6.5E-02	7.0E-02
3.0E-01	7.6E-03	3.6E-05	1.7E-01	6.2E-02	6.5E-02
4.0E-01	7.9E-03	3.8E-05	1.7E-01	5.9E-02	6.1E-02
5.0E-01	8.2E-03	3.9E-05	1.7E-01	5.6E-02	5.7E-02
6.0E-01	8.5E-03	4.1E-05	1.7E-01	5.4E-02	5.3E-02
7.0E-01	8.8E-03	4.3E-05	1.7E-01	5.1E-02	4.9E-02
8.0E-01	9.1E-03	4.4E-05	1.6E-01	4.8E-02	4.6E-02
9.0E-01	9.4E-03	4.6E-05	1.6E-01	4.6E-02	4.3E-02
1.0E+00	9.7E-03	4.8E-05	1.6E-01	4.4E-02	4.0E-02

Data Point PZ/MDEA 8-5

Data Conditions

T (K)	Bulk Gas P _{CO2} (Pa)	k _g *10 ⁵ (moles/(atm cm ² s))	k _i *10 ⁵ (m/s)	Loading (mol CO ₂ / mol amine)	Flux *10 ⁷ (mol / cm ² s)	
					Measured	Predicted
313	3530	2.36	2.89	0.140	2.19	1.52

Calculated Physical Properties

P* _{CO2} (Pa)	μ (cP)	H _{CO2} atm L/mol	ρ (g/cc)	Diffusion Coefficient (m/s) *10 ⁹			
				CO2	MDEA	PZ	IONS
1129	5.48	52.64	1.04	0.69	0.43	0.52	0.52

Thermodynamic Results

Species	Equilibrium Molefraction (Liquid)	Activity Coefficient
CO ₂	3.60E-06	1.34E+00
H ₂ O	8.49E-01	1.02E+00
PZ	3.31E-03	1.66E-01
MDEA	1.13E-01	3.41E-01
PZH+	5.49E-03	2.70E-01
MDEAH+	1.23E-02	3.75E-01
H ₃ O+	3.92E-11	2.85E-01
PZCOO-	5.04E-03	2.69E-01
HCO ₃ -	7.55E-03	3.84E-01
CO ₃ =	1.32E-04	1.82E+00
OH-	6.90E-07	9.00E-01
H+PZCOO-	2.51E-03	1.01E+00
PZ(COO-) ₂	2.45E-03	6.06E-02

Rate Data

r - Dimensionless

Distance from

Interface	CO ₂	PZ	MDEA	MDEAH ⁺	PZH ⁺	HCO ₃ ⁻
0.0E+00	5.4E-04	8.1E-02	3.5E+00	4.5E-01	1.6E-01	2.4E-01
1.0E-04	5.3E-04	8.1E-02	3.5E+00	4.5E-01	1.6E-01	2.4E-01
2.0E-04	5.3E-04	8.1E-02	3.5E+00	4.5E-01	1.6E-01	2.4E-01
3.0E-04	5.2E-04	8.1E-02	3.5E+00	4.5E-01	1.6E-01	2.4E-01
4.0E-04	5.2E-04	8.1E-02	3.5E+00	4.5E-01	1.6E-01	2.4E-01
5.0E-04	5.1E-04	8.1E-02	3.5E+00	4.5E-01	1.6E-01	2.4E-01
6.0E-04	5.1E-04	8.1E-02	3.5E+00	4.5E-01	1.6E-01	2.4E-01
7.0E-04	5.1E-04	8.1E-02	3.5E+00	4.5E-01	1.6E-01	2.4E-01
8.0E-04	5.0E-04	8.1E-02	3.5E+00	4.5E-01	1.6E-01	2.4E-01
9.0E-04	5.0E-04	8.1E-02	3.5E+00	4.5E-01	1.6E-01	2.4E-01
1.0E-03	4.9E-04	8.1E-02	3.5E+00	4.5E-01	1.6E-01	2.4E-01
2.0E-03	4.5E-04	8.1E-02	3.5E+00	4.5E-01	1.6E-01	2.4E-01
3.0E-03	4.3E-04	8.1E-02	3.5E+00	4.5E-01	1.6E-01	2.4E-01
4.0E-03	4.0E-04	8.1E-02	3.5E+00	4.5E-01	1.6E-01	2.4E-01
5.0E-03	3.9E-04	8.1E-02	3.5E+00	4.5E-01	1.6E-01	2.4E-01
6.0E-03	3.7E-04	8.1E-02	3.5E+00	4.5E-01	1.6E-01	2.4E-01
7.0E-03	3.6E-04	8.1E-02	3.5E+00	4.5E-01	1.6E-01	2.4E-01
8.0E-03	3.6E-04	8.1E-02	3.5E+00	4.5E-01	1.6E-01	2.4E-01
9.0E-03	3.5E-04	8.1E-02	3.5E+00	4.5E-01	1.6E-01	2.4E-01
1.0E-02	3.5E-04	8.1E-02	3.5E+00	4.5E-01	1.6E-01	2.4E-01
2.0E-02	3.3E-04	8.2E-02	3.5E+00	4.5E-01	1.6E-01	2.4E-01
3.0E-02	3.2E-04	8.2E-02	3.5E+00	4.5E-01	1.6E-01	2.4E-01
4.0E-02	3.2E-04	8.2E-02	3.5E+00	4.5E-01	1.6E-01	2.4E-01
5.0E-02	3.2E-04	8.2E-02	3.5E+00	4.5E-01	1.6E-01	2.4E-01
6.0E-02	3.2E-04	8.2E-02	3.5E+00	4.5E-01	1.6E-01	2.4E-01
7.0E-02	3.2E-04	8.3E-02	3.5E+00	4.4E-01	1.6E-01	2.4E-01
8.0E-02	3.1E-04	8.3E-02	3.5E+00	4.4E-01	1.6E-01	2.4E-01
9.0E-02	3.1E-04	8.3E-02	3.5E+00	4.4E-01	1.6E-01	2.4E-01
1.0E-01	3.1E-04	8.3E-02	3.5E+00	4.4E-01	1.6E-01	2.4E-01
2.0E-01	3.0E-04	8.6E-02	3.5E+00	4.3E-01	1.6E-01	2.4E-01
3.0E-01	2.8E-04	8.8E-02	3.5E+00	4.3E-01	1.6E-01	2.4E-01
4.0E-01	2.7E-04	9.1E-02	3.5E+00	4.2E-01	1.7E-01	2.4E-01
5.0E-01	2.6E-04	9.3E-02	3.5E+00	4.2E-01	1.7E-01	2.4E-01
6.0E-01	2.5E-04	9.6E-02	3.5E+00	4.1E-01	1.7E-01	2.4E-01
7.0E-01	2.4E-04	9.8E-02	3.5E+00	4.0E-01	1.7E-01	2.4E-01
8.0E-01	2.3E-04	1.0E-01	3.5E+00	4.0E-01	1.7E-01	2.4E-01
9.0E-01	2.2E-04	1.0E-01	3.6E+00	3.9E-01	1.7E-01	2.4E-01
1.0E+00	2.1E-04	1.0E-01	3.6E+00	3.9E-01	1.7E-01	2.4E-01

r-Dimensionless Distance from Interface	CO ₃ ⁼	OH ⁻	PZCOO ⁻	H ⁺ PZCOO ⁻	PZ(COO ⁻) ₂
0.0E+00	3.56E-03	1.84E-05	1.58E-01	9.33E-02	1.02E-01
1.0E-04	3.56E-03	1.84E-05	1.58E-01	9.33E-02	1.02E-01
2.0E-04	3.56E-03	1.84E-05	1.58E-01	9.33E-02	1.02E-01
3.0E-04	3.56E-03	1.84E-05	1.58E-01	9.33E-02	1.02E-01
4.0E-04	3.56E-03	1.84E-05	1.58E-01	9.33E-02	1.02E-01
5.0E-04	3.56E-03	1.84E-05	1.58E-01	9.33E-02	1.02E-01
6.0E-04	3.56E-03	1.84E-05	1.58E-01	9.33E-02	1.02E-01
7.0E-04	3.56E-03	1.84E-05	1.58E-01	9.33E-02	1.02E-01
8.0E-04	3.56E-03	1.84E-05	1.58E-01	9.33E-02	1.02E-01
9.0E-04	3.56E-03	1.84E-05	1.58E-01	9.33E-02	1.02E-01
1.0E-03	3.56E-03	1.84E-05	1.58E-01	9.33E-02	1.02E-01
2.0E-03	3.56E-03	1.84E-05	1.58E-01	9.33E-02	1.02E-01
3.0E-03	3.56E-03	1.84E-05	1.58E-01	9.32E-02	1.02E-01
4.0E-03	3.56E-03	1.84E-05	1.58E-01	9.32E-02	1.02E-01
5.0E-03	3.56E-03	1.84E-05	1.58E-01	9.32E-02	1.01E-01
6.0E-03	3.56E-03	1.84E-05	1.58E-01	9.32E-02	1.01E-01
7.0E-03	3.56E-03	1.84E-05	1.58E-01	9.32E-02	1.01E-01
8.0E-03	3.56E-03	1.84E-05	1.58E-01	9.32E-02	1.01E-01
9.0E-03	3.56E-03	1.84E-05	1.58E-01	9.32E-02	1.01E-01
1.0E-02	3.57E-03	1.84E-05	1.58E-01	9.32E-02	1.01E-01
2.0E-02	3.57E-03	1.85E-05	1.58E-01	9.32E-02	1.01E-01
3.0E-02	3.58E-03	1.85E-05	1.59E-01	9.31E-02	1.00E-01
4.0E-02	3.59E-03	1.85E-05	1.59E-01	9.30E-02	1.00E-01
5.0E-02	3.59E-03	1.86E-05	1.59E-01	9.29E-02	9.97E-02
6.0E-02	3.60E-03	1.86E-05	1.59E-01	9.28E-02	9.93E-02
7.0E-02	3.61E-03	1.86E-05	1.59E-01	9.26E-02	9.90E-02
8.0E-02	3.61E-03	1.87E-05	1.59E-01	9.25E-02	9.86E-02
9.0E-02	3.62E-03	1.87E-05	1.59E-01	9.24E-02	9.83E-02
1.0E-01	3.63E-03	1.88E-05	1.59E-01	9.22E-02	9.80E-02
2.0E-01	3.69E-03	1.91E-05	1.60E-01	9.07E-02	9.50E-02
3.0E-01	3.76E-03	1.95E-05	1.60E-01	8.91E-02	9.23E-02
4.0E-01	3.83E-03	1.98E-05	1.60E-01	8.76E-02	8.98E-02
5.0E-01	3.89E-03	2.02E-05	1.60E-01	8.61E-02	8.74E-02
6.0E-01	3.95E-03	2.05E-05	1.60E-01	8.46E-02	8.52E-02
7.0E-01	4.01E-03	2.08E-05	1.60E-01	8.33E-02	8.31E-02
8.0E-01	4.07E-03	2.11E-05	1.60E-01	8.19E-02	8.11E-02
9.0E-01	4.12E-03	2.15E-05	1.59E-01	8.06E-02	7.91E-02
1.0E+00	4.18E-03	2.18E-05	1.59E-01	7.93E-02	7.73E-02

Data Point PZ/MDEA 9-2

Data Conditions

T (K)	Bulk Gas P _{CO2} (Pa)	k _g *10 ⁵ (moles/(atm cm ² s))	k _l *10 ⁵ (m/s)	Loading (mol CO ₂ / mol amine)	Flux *10 ⁷ (mol / cm ² s)	
					Measured	Predicted
313	9040	2.85	2.87	0.185	2.60	2.85

Calculated Physical Properties

P _{CO2} (Pa)	μ (cP)	H _{CO2} atm L/mol	ρ (g/cc)	Diffusion Coefficient (m/s) *10 ⁹			
				CO2	MDEA	PZ	IONS
2564	5.48	52.64	1.04	0.69	0.43	0.52	0.52

Thermodynamic Results

Species	Equilibrium Molefraction (Liquid)	Activity Coefficient
CO ₂	8.07E-06	1.36E+00
H ₂ O	8.45E-01	1.02E+00
PZ	1.77E-03	2.00E-01
MDEA	1.07E-01	3.35E-01
PZH+	5.34E-03	2.81E-01
MDEAH+	1.77E-02	3.83E-01
H ₃ O+	6.04E-11	2.91E-01
PZCOO-	4.51E-03	2.80E-01
HCO ₃ -	1.13E-02	3.69E-01
CO ₃ =	6.00E-05	3.68E+00
OH-	3.53E-07	1.12E+00
H+PZCOO-	3.66E-03	1.01E+00
PZ(COO-)2	3.52E-03	5.66E-02

Rate Results

r - Dimensionless

Distance from

Interface

	CO ₂	PZ	MDEA	MDEAH ⁺	PZH ⁺	HCO ₃ ⁻
0.0E+00	1.5E-03	3.3E-02	3.2E+00	6.9E-01	1.3E-01	3.6E-01
1.0E-04	1.5E-03	3.3E-02	3.2E+00	6.9E-01	1.3E-01	3.6E-01
2.0E-04	1.5E-03	3.3E-02	3.2E+00	6.9E-01	1.3E-01	3.6E-01
3.0E-04	1.5E-03	3.3E-02	3.2E+00	6.9E-01	1.3E-01	3.6E-01
4.0E-04	1.5E-03	3.3E-02	3.2E+00	6.9E-01	1.3E-01	3.6E-01
5.0E-04	1.5E-03	3.3E-02	3.2E+00	6.9E-01	1.3E-01	3.6E-01
6.0E-04	1.4E-03	3.3E-02	3.2E+00	6.9E-01	1.3E-01	3.6E-01
7.0E-04	1.4E-03	3.3E-02	3.2E+00	6.9E-01	1.3E-01	3.6E-01
8.0E-04	1.4E-03	3.3E-02	3.2E+00	6.9E-01	1.3E-01	3.6E-01
9.0E-04	1.4E-03	3.3E-02	3.2E+00	6.9E-01	1.3E-01	3.6E-01
1.0E-03	1.4E-03	3.3E-02	3.2E+00	6.9E-01	1.3E-01	3.6E-01
2.0E-03	1.3E-03	3.3E-02	3.2E+00	6.9E-01	1.3E-01	3.6E-01
3.0E-03	1.3E-03	3.3E-02	3.2E+00	6.9E-01	1.3E-01	3.6E-01
4.0E-03	1.2E-03	3.3E-02	3.2E+00	6.9E-01	1.3E-01	3.6E-01
5.0E-03	1.2E-03	3.3E-02	3.2E+00	6.9E-01	1.3E-01	3.6E-01
6.0E-03	1.1E-03	3.3E-02	3.2E+00	6.9E-01	1.3E-01	3.6E-01
7.0E-03	1.1E-03	3.3E-02	3.2E+00	6.9E-01	1.3E-01	3.6E-01
8.0E-03	1.1E-03	3.3E-02	3.2E+00	6.9E-01	1.3E-01	3.6E-01
9.0E-03	1.1E-03	3.3E-02	3.2E+00	6.9E-01	1.3E-01	3.6E-01
1.0E-02	1.1E-03	3.3E-02	3.2E+00	6.9E-01	1.3E-01	3.6E-01
2.0E-02	1.0E-03	3.3E-02	3.2E+00	6.8E-01	1.3E-01	3.6E-01
3.0E-02	9.8E-04	3.3E-02	3.2E+00	6.8E-01	1.3E-01	3.6E-01
4.0E-02	9.7E-04	3.4E-02	3.2E+00	6.8E-01	1.3E-01	3.6E-01
5.0E-02	9.6E-04	3.4E-02	3.2E+00	6.8E-01	1.3E-01	3.6E-01
6.0E-02	9.5E-04	3.4E-02	3.2E+00	6.8E-01	1.3E-01	3.6E-01
7.0E-02	9.4E-04	3.4E-02	3.2E+00	6.8E-01	1.3E-01	3.6E-01
8.0E-02	9.3E-04	3.4E-02	3.2E+00	6.8E-01	1.3E-01	3.6E-01
9.0E-02	9.2E-04	3.5E-02	3.2E+00	6.7E-01	1.3E-01	3.6E-01
1.0E-01	9.1E-04	3.5E-02	3.2E+00	6.7E-01	1.3E-01	3.6E-01
2.0E-01	8.4E-04	3.7E-02	3.3E+00	6.6E-01	1.4E-01	3.6E-01
3.0E-01	7.7E-04	3.9E-02	3.3E+00	6.4E-01	1.4E-01	3.6E-01
4.0E-01	7.2E-04	4.2E-02	3.3E+00	6.3E-01	1.5E-01	3.6E-01
5.0E-01	6.7E-04	4.4E-02	3.3E+00	6.1E-01	1.5E-01	3.6E-01
6.0E-01	6.2E-04	4.6E-02	3.3E+00	6.0E-01	1.5E-01	3.6E-01
7.0E-01	5.8E-04	4.9E-02	3.3E+00	5.9E-01	1.6E-01	3.6E-01
8.0E-01	5.5E-04	5.1E-02	3.3E+00	5.8E-01	1.6E-01	3.6E-01
9.0E-01	5.1E-04	5.3E-02	3.3E+00	5.6E-01	1.6E-01	3.6E-01
1.0E+00	4.8E-04	5.5E-02	3.4E+00	5.5E-01	1.7E-01	3.5E-01

r-Dimensionless Distance from Interface	CO ₃ ²⁻	OH ⁻	PZCOO ⁻	H ⁺ PZCOO ⁻	PZ(COO) ₂
0.0E+00	1.5E-03	8.5E-06	1.3E-01	1.4E-01	1.6E-01
1.0E-04	1.5E-03	8.5E-06	1.3E-01	1.4E-01	1.6E-01
2.0E-04	1.5E-03	8.5E-06	1.3E-01	1.4E-01	1.6E-01
3.0E-04	1.5E-03	8.5E-06	1.3E-01	1.4E-01	1.6E-01
4.0E-04	1.5E-03	8.5E-06	1.3E-01	1.4E-01	1.6E-01
5.0E-04	1.5E-03	8.5E-06	1.3E-01	1.4E-01	1.6E-01
6.0E-04	1.5E-03	8.5E-06	1.3E-01	1.4E-01	1.6E-01
7.0E-04	1.5E-03	8.5E-06	1.3E-01	1.4E-01	1.6E-01
8.0E-04	1.5E-03	8.5E-06	1.3E-01	1.4E-01	1.6E-01
9.0E-04	1.5E-03	8.5E-06	1.3E-01	1.4E-01	1.6E-01
1.0E-03	1.5E-03	8.5E-06	1.3E-01	1.4E-01	1.6E-01
2.0E-03	1.5E-03	8.5E-06	1.3E-01	1.4E-01	1.6E-01
3.0E-03	1.5E-03	8.5E-06	1.3E-01	1.4E-01	1.6E-01
4.0E-03	1.5E-03	8.5E-06	1.3E-01	1.4E-01	1.6E-01
5.0E-03	1.5E-03	8.5E-06	1.3E-01	1.4E-01	1.6E-01
6.0E-03	1.5E-03	8.5E-06	1.3E-01	1.4E-01	1.6E-01
7.0E-03	1.5E-03	8.5E-06	1.3E-01	1.4E-01	1.6E-01
8.0E-03	1.5E-03	8.5E-06	1.3E-01	1.4E-01	1.6E-01
9.0E-03	1.5E-03	8.5E-06	1.3E-01	1.4E-01	1.6E-01
1.0E-02	1.5E-03	8.5E-06	1.3E-01	1.4E-01	1.6E-01
2.0E-02	1.5E-03	8.5E-06	1.3E-01	1.4E-01	1.6E-01
3.0E-02	1.5E-03	8.6E-06	1.3E-01	1.4E-01	1.6E-01
4.0E-02	1.5E-03	8.6E-06	1.3E-01	1.4E-01	1.6E-01
5.0E-02	1.5E-03	8.6E-06	1.3E-01	1.4E-01	1.6E-01
6.0E-02	1.5E-03	8.6E-06	1.3E-01	1.4E-01	1.6E-01
7.0E-02	1.5E-03	8.7E-06	1.3E-01	1.4E-01	1.6E-01
8.0E-02	1.5E-03	8.7E-06	1.3E-01	1.4E-01	1.6E-01
9.0E-02	1.5E-03	8.7E-06	1.3E-01	1.4E-01	1.6E-01
1.0E-01	1.5E-03	8.8E-06	1.3E-01	1.3E-01	1.5E-01
2.0E-01	1.6E-03	9.0E-06	1.3E-01	1.3E-01	1.5E-01
3.0E-01	1.6E-03	9.3E-06	1.4E-01	1.3E-01	1.4E-01
4.0E-01	1.6E-03	9.5E-06	1.4E-01	1.3E-01	1.4E-01
5.0E-01	1.7E-03	9.8E-06	1.4E-01	1.3E-01	1.3E-01
6.0E-01	1.7E-03	1.0E-05	1.4E-01	1.2E-01	1.3E-01
7.0E-01	1.8E-03	1.0E-05	1.4E-01	1.2E-01	1.2E-01
8.0E-01	1.8E-03	1.1E-05	1.4E-01	1.2E-01	1.2E-01
9.0E-01	1.8E-03	1.1E-05	1.4E-01	1.2E-01	1.1E-01
1.0E+00	1.9E-03	1.1E-05	1.4E-01	1.1E-01	1.1E-01

Data Point PZ / MDEA 9-5

Data Conditions

T (K)	Bulk Gas P _{CO2} (Pa)	k _g *10 ⁵ (moles/(atm cm ² s))	k _l *10 ⁵ (m/s)	Loading (mol CO ₂ / mol amine)	Flux *10 ⁷ (mol / cm ² s)	
					Measured	Predicted
313	27300	1.19	2.87	0.311	4.02	2.87

Calculated Physical Properties

P _{CO2} (Pa)	μ (cP)	H _{CO2} atm L/mol	ρ (g/cc)	Diffusion Coefficient (m/s) *10 ⁹			
				CO2	MDEA	PZ	IONS
10920	5.48	52.64	1.04	0.69	0.43	0.52	0.52

Thermodynamic Results

Species	Equilibrium Molefraction (Liquid)	Activity Coefficient
CO ₂	3.23E-05	1.45E+00
H ₂ O	8.31E-01	1.03E+00
PZ	4.25E-04	3.24E-01
MDEA	9.06E-02	3.22E-01
PZH+	4.21E-03	3.11E-01
MDEAH+	3.44E-02	3.58E-01
H ₃ O+	1.25E-10	3.15E-01
PZCOO-	2.99E-03	3.11E-01
HCO ₃ -	2.52E-02	3.13E-01
CO ₃ =	4.29E-05	4.31E+00
OH-	9.33E-08	1.87E+00
H+PZCOO-	6.00E-03	1.02E+00
PZ(COO-)2	5.18E-03	5.37E-02

Rate Results

r - Dimensionless

Distance from

Interface

	CO ₂	PZ	MDEA	MDEAH ⁺	PZH ⁺	HCO ₃ ⁻
0.0E+00	3.99E-03	8.41E-03	2.6413944	1.1692223	9.71E-02	7.82E-01
1.0E-04	3.98E-03	8.41E-03	2.6413945	1.1692221	9.71E-02	7.82E-01
2.0E-04	3.98E-03	8.41E-03	2.6413949	1.1692218	9.71E-02	7.82E-01
3.0E-04	3.97E-03	8.41E-03	2.6413956	1.1692213	9.71E-02	7.82E-01
4.0E-04	3.96E-03	8.41E-03	2.6413965	1.1692205	9.71E-02	7.82E-01
5.0E-04	3.95E-03	8.41E-03	2.6413977	1.1692195	9.71E-02	7.82E-01
6.0E-04	3.95E-03	8.41E-03	2.6413991	1.1692183	9.71E-02	7.82E-01
7.0E-04	3.94E-03	8.41E-03	2.6414008	1.1692169	9.71E-02	7.82E-01
8.0E-04	3.93E-03	8.41E-03	2.6414028	1.1692153	9.71E-02	7.82E-01
9.0E-04	3.92E-03	8.41E-03	2.6414049	1.1692134	9.71E-02	7.82E-01
1.0E-03	3.92E-03	8.41E-03	2.6414074	1.1692114	9.71E-02	7.82E-01
2.0E-03	3.85E-03	8.41E-03	2.641444	1.1691809	9.71E-02	7.82E-01
3.0E-03	3.79E-03	8.41E-03	2.641501	1.1691334	9.71E-02	7.82E-01
4.0E-03	3.74E-03	8.42E-03	2.6415757	1.1690712	9.71E-02	7.82E-01
5.0E-03	3.70E-03	8.42E-03	2.6416657	1.1689962	9.71E-02	7.82E-01
6.0E-03	3.66E-03	8.42E-03	2.6417689	1.1689102	9.71E-02	7.82E-01
7.0E-03	3.63E-03	8.42E-03	2.6418836	1.1688146	9.71E-02	7.82E-01
8.0E-03	3.60E-03	8.42E-03	2.6420083	1.1687107	9.71E-02	7.82E-01
9.0E-03	3.57E-03	8.42E-03	2.6421416	1.1685996	9.71E-02	7.82E-01
1.0E-02	3.55E-03	8.43E-03	2.6422824	1.1684822	9.71E-02	7.82E-01
2.0E-02	3.42E-03	8.45E-03	2.6438951	1.1671381	9.73E-02	7.82E-01
3.0E-02	3.37E-03	8.49E-03	2.6456633	1.165664	9.75E-02	7.82E-01
4.0E-02	3.33E-03	8.52E-03	2.6474575	1.1641676	9.77E-02	7.82E-01
5.0E-02	3.30E-03	8.56E-03	2.6492453	1.1626757	9.79E-02	7.82E-01
6.0E-02	3.28E-03	8.60E-03	2.6510193	1.1611944	9.82E-02	7.82E-01
7.0E-02	3.25E-03	8.64E-03	2.6527785	1.1597244	9.85E-02	7.82E-01
8.0E-02	3.23E-03	8.69E-03	2.6545233	1.158265	9.88E-02	7.82E-01
9.0E-02	3.20E-03	8.73E-03	2.6562544	1.1568156	9.92E-02	7.82E-01
1.0E-01	3.18E-03	8.78E-03	2.6579724	1.1553755	9.95E-02	7.82E-01
2.0E-01	2.98E-03	9.28E-03	2.6745338	1.1413691	1.03E-01	7.81E-01
3.0E-01	2.81E-03	9.79E-03	2.6899547	1.1280281	1.07E-01	7.80E-01
4.0E-01	2.66E-03	1.03E-02	2.7041936	1.115356	1.11E-01	7.79E-01
5.0E-01	2.53E-03	1.08E-02	2.7172826	1.1033568	1.14E-01	7.78E-01
6.0E-01	2.41E-03	1.13E-02	2.729339	1.0919945	1.17E-01	7.77E-01
7.0E-01	2.31E-03	1.17E-02	2.7405291	1.0811983	1.20E-01	7.75E-01
8.0E-01	2.21E-03	1.22E-02	2.7510326	1.070879	1.23E-01	7.73E-01
9.0E-01	2.13E-03	1.26E-02	2.7610148	1.0609513	1.26E-01	7.71E-01
1.0E+00	2.05E-03	1.30E-02	2.770569	1.0513905	1.29E-01	7.69E-01

r-Dimensionless Distance from Interface	CO ₃ ⁼	OH ⁻	PZCOO ⁻	H ⁺ PZCOO ⁻	PZ(COO ⁻) ₂
0.0E+00	1.14E-03	2.45E-06	8.03E-02	1.88E-01	2.01E-01
1.0E-04	1.14E-03	2.45E-06	8.03E-02	1.88E-01	2.01E-01
2.0E-04	1.14E-03	2.45E-06	8.03E-02	1.88E-01	2.01E-01
3.0E-04	1.14E-03	2.45E-06	8.03E-02	1.88E-01	2.01E-01
4.0E-04	1.14E-03	2.45E-06	8.03E-02	1.88E-01	2.01E-01
5.0E-04	1.14E-03	2.45E-06	8.03E-02	1.88E-01	2.01E-01
6.0E-04	1.14E-03	2.45E-06	8.03E-02	1.88E-01	2.01E-01
7.0E-04	1.14E-03	2.45E-06	8.03E-02	1.88E-01	2.01E-01
8.0E-04	1.14E-03	2.45E-06	8.03E-02	1.88E-01	2.01E-01
9.0E-04	1.14E-03	2.45E-06	8.03E-02	1.88E-01	2.01E-01
1.0E-03	1.14E-03	2.45E-06	8.03E-02	1.88E-01	2.01E-01
2.0E-03	1.14E-03	2.45E-06	8.04E-02	1.88E-01	2.01E-01
3.0E-03	1.14E-03	2.45E-06	8.04E-02	1.88E-01	2.01E-01
4.0E-03	1.14E-03	2.45E-06	8.04E-02	1.88E-01	2.01E-01
5.0E-03	1.14E-03	2.45E-06	8.04E-02	1.88E-01	2.01E-01
6.0E-03	1.14E-03	2.45E-06	8.04E-02	1.88E-01	2.01E-01
7.0E-03	1.14E-03	2.45E-06	8.04E-02	1.88E-01	2.01E-01
8.0E-03	1.14E-03	2.45E-06	8.05E-02	1.88E-01	2.01E-01
9.0E-03	1.14E-03	2.45E-06	8.05E-02	1.88E-01	2.01E-01
1.0E-02	1.14E-03	2.45E-06	8.05E-02	1.88E-01	2.01E-01
2.0E-02	1.15E-03	2.45E-06	8.08E-02	1.89E-01	2.00E-01
3.0E-02	1.15E-03	2.46E-06	8.10E-02	1.89E-01	1.99E-01
4.0E-02	1.15E-03	2.46E-06	8.13E-02	1.89E-01	1.98E-01
5.0E-02	1.15E-03	2.47E-06	8.16E-02	1.89E-01	1.98E-01
6.0E-02	1.15E-03	2.47E-06	8.18E-02	1.89E-01	1.97E-01
7.0E-02	1.16E-03	2.48E-06	8.20E-02	1.90E-01	1.96E-01
8.0E-02	1.16E-03	2.48E-06	8.22E-02	1.90E-01	1.95E-01
9.0E-02	1.16E-03	2.49E-06	8.24E-02	1.90E-01	1.95E-01
1.0E-01	1.16E-03	2.49E-06	8.26E-02	1.90E-01	1.94E-01
2.0E-01	1.18E-03	2.54E-06	8.41E-02	1.90E-01	1.89E-01
3.0E-01	1.20E-03	2.58E-06	8.53E-02	1.89E-01	1.84E-01
4.0E-01	1.22E-03	2.63E-06	8.64E-02	1.88E-01	1.79E-01
5.0E-01	1.24E-03	2.67E-06	8.74E-02	1.88E-01	1.75E-01
6.0E-01	1.26E-03	2.71E-06	8.83E-02	1.87E-01	1.71E-01
7.0E-01	1.27E-03	2.75E-06	8.92E-02	1.86E-01	1.67E-01
8.0E-01	1.29E-03	2.78E-06	9.00E-02	1.85E-01	1.64E-01
9.0E-01	1.30E-03	2.82E-06	9.07E-02	1.84E-01	1.61E-01
1.0E+00	1.31E-03	2.85E-06	9.14E-02	1.83E-01	1.58E-01

Data Point PZ / MDEA 5-11

Data Conditions

T (K)	Bulk Gas P _{CO2} (Pa)	k _g *10 ⁵ (moles/(atm cm ² s))	k _l *10 ⁵ (m/s)	Loading (mol CO ₂ / mol amine)	Flux *10 ⁷ (mol / cm ² s)	
					Measured	Predicted
343	4440	3.44	6.14	0.038	5.02	3.10

Calculated Physical Properties

P _{CO2} (Pa)	μ (cP)	H _{CO2} atm L/mol	ρ (g/cc)	Diffusion Coefficient (m/s) *10 ⁹			
				CO2	MDEA	PZ	IONS
962	2.15	77.0	1.02	1.2	0.79	0.95	0.95

Thermodynamic Results

Species	Equilibrium Molefraction (Liquid)	Activity Coefficient
CO ₂	1.94E-06	1.25E+00
H ₂ O	8.52E-01	1.05E+00
PZ	1.50E-02	1.75E-01
MDEA	1.22E-01	4.19E-01
PZH+	2.41E-03	1.84E-01
MDEAH+	3.19E-03	5.56E-01
H ₃ O+	6.61E-11	1.66E-01
PZCOO-	1.26E-03	2.02E-01
HCO ₃ -	3.72E-03	4.30E-01
CO ₃ =	2.73E-04	6.42E-01
OH-	9.48E-06	3.90E-01
H+PZCOO-	1.49E-04	1.00E+00
PZ(COO-) ₂	3.11E-05	3.52E-02

Rate Results

r - Dimensionless

Distance from

Interface

	CO ₂	PZ	MDEA	MDEAH ⁺	PZH ⁺	HCO ₃ ⁻
0.0E+00	4.52E-04	4.10E-01	3.8320228	1.39E-01	9.12E-02	1.28E-01
1.0E-04	4.46E-04	4.10E-01	3.832023	1.39E-01	9.12E-02	1.28E-01
2.0E-04	4.41E-04	4.10E-01	3.8320237	1.39E-01	9.12E-02	1.28E-01
3.0E-04	4.37E-04	4.10E-01	3.8320247	1.39E-01	9.12E-02	1.28E-01
4.0E-04	4.33E-04	4.10E-01	3.8320261	1.39E-01	9.12E-02	1.28E-01
5.0E-04	4.29E-04	4.10E-01	3.8320278	1.39E-01	9.12E-02	1.28E-01
6.0E-04	4.26E-04	4.10E-01	3.8320298	1.39E-01	9.12E-02	1.28E-01
7.0E-04	4.23E-04	4.10E-01	3.8320321	1.39E-01	9.12E-02	1.28E-01
8.0E-04	4.20E-04	4.10E-01	3.8320347	1.39E-01	9.12E-02	1.28E-01
9.0E-04	4.17E-04	4.10E-01	3.8320375	1.39E-01	9.12E-02	1.28E-01
1.0E-03	4.15E-04	4.10E-01	3.8320404	1.39E-01	9.12E-02	1.28E-01
2.0E-03	3.99E-04	4.10E-01	3.8320782	1.39E-01	9.12E-02	1.28E-01
3.0E-03	3.92E-04	4.10E-01	3.8321241	1.39E-01	9.12E-02	1.28E-01
4.0E-03	3.89E-04	4.11E-01	3.8321735	1.38E-01	9.12E-02	1.28E-01
5.0E-03	3.88E-04	4.11E-01	3.8322243	1.38E-01	9.12E-02	1.28E-01
6.0E-03	3.87E-04	4.11E-01	3.8322757	1.38E-01	9.12E-02	1.28E-01
7.0E-03	3.86E-04	4.11E-01	3.8323274	1.38E-01	9.12E-02	1.28E-01
8.0E-03	3.86E-04	4.11E-01	3.8323791	1.38E-01	9.11E-02	1.28E-01
9.0E-03	3.85E-04	4.11E-01	3.8324309	1.38E-01	9.11E-02	1.28E-01
1.0E-02	3.85E-04	4.11E-01	3.8324827	1.38E-01	9.11E-02	1.28E-01
2.0E-02	3.81E-04	4.12E-01	3.833	1.38E-01	9.10E-02	1.28E-01
3.0E-02	3.76E-04	4.12E-01	3.8335163	1.37E-01	9.09E-02	1.28E-01
4.0E-02	3.72E-04	4.13E-01	3.8340317	1.37E-01	9.07E-02	1.28E-01
5.0E-02	3.68E-04	4.14E-01	3.8345463	1.37E-01	9.06E-02	1.28E-01
6.0E-02	3.64E-04	4.15E-01	3.8350598	1.36E-01	9.05E-02	1.28E-01
7.0E-02	3.60E-04	4.16E-01	3.8355722	1.36E-01	9.03E-02	1.28E-01
8.0E-02	3.56E-04	4.16E-01	3.8360833	1.35E-01	9.02E-02	1.28E-01
9.0E-02	3.52E-04	4.17E-01	3.8365931	1.35E-01	9.01E-02	1.28E-01
1.0E-01	3.48E-04	4.18E-01	3.8371013	1.34E-01	8.99E-02	1.28E-01
2.0E-01	3.11E-04	4.25E-01	3.8420781	1.30E-01	8.86E-02	1.27E-01
3.0E-01	2.78E-04	4.32E-01	3.8468046	1.26E-01	8.71E-02	1.27E-01
4.0E-01	2.48E-04	4.39E-01	3.8512332	1.22E-01	8.57E-02	1.26E-01
5.0E-01	2.21E-04	4.46E-01	3.8553582	1.18E-01	8.42E-02	1.25E-01
6.0E-01	1.97E-04	4.52E-01	3.8592051	1.15E-01	8.27E-02	1.24E-01
7.0E-01	1.75E-04	4.59E-01	3.8628176	1.11E-01	8.12E-02	1.23E-01
8.0E-01	1.56E-04	4.64E-01	3.8662486	1.08E-01	7.97E-02	1.21E-01
9.0E-01	1.39E-04	4.70E-01	3.8695544	1.05E-01	7.81E-02	1.20E-01
1.0E+00	1.23E-04	4.75E-01	3.8727939	1.01E-01	7.65E-02	1.18E-01

r-Dimensionless Distance from Interface	CO ₃ ⁼	OH ⁻	PZCOO ⁻	H ⁺ PZCOO ⁻	PZ(COO ⁻) ₂
0.0E+00	6.80E-03	2.18E-04	7.88E-02	1.29E-02	4.48E-03
1.0E-04	6.80E-03	2.18E-04	7.88E-02	1.29E-02	4.48E-03
2.0E-04	6.80E-03	2.18E-04	7.88E-02	1.29E-02	4.48E-03
3.0E-04	6.80E-03	2.18E-04	7.88E-02	1.29E-02	4.48E-03
4.0E-04	6.80E-03	2.18E-04	7.88E-02	1.29E-02	4.47E-03
5.0E-04	6.80E-03	2.18E-04	7.88E-02	1.29E-02	4.47E-03
6.0E-04	6.80E-03	2.18E-04	7.88E-02	1.29E-02	4.47E-03
7.0E-04	6.80E-03	2.18E-04	7.88E-02	1.29E-02	4.47E-03
8.0E-04	6.80E-03	2.18E-04	7.88E-02	1.29E-02	4.47E-03
9.0E-04	6.80E-03	2.18E-04	7.88E-02	1.29E-02	4.47E-03
1.0E-03	6.80E-03	2.18E-04	7.88E-02	1.29E-02	4.47E-03
2.0E-03	6.81E-03	2.18E-04	7.88E-02	1.29E-02	4.47E-03
3.0E-03	6.81E-03	2.18E-04	7.87E-02	1.29E-02	4.46E-03
4.0E-03	6.81E-03	2.18E-04	7.87E-02	1.28E-02	4.45E-03
5.0E-03	6.81E-03	2.18E-04	7.86E-02	1.28E-02	4.44E-03
6.0E-03	6.81E-03	2.18E-04	7.86E-02	1.28E-02	4.43E-03
7.0E-03	6.82E-03	2.19E-04	7.86E-02	1.28E-02	4.43E-03
8.0E-03	6.82E-03	2.19E-04	7.85E-02	1.28E-02	4.42E-03
9.0E-03	6.82E-03	2.19E-04	7.85E-02	1.28E-02	4.41E-03
1.0E-02	6.82E-03	2.19E-04	7.84E-02	1.28E-02	4.40E-03
2.0E-02	6.84E-03	2.19E-04	7.80E-02	1.27E-02	4.34E-03
3.0E-02	6.86E-03	2.20E-04	7.75E-02	1.25E-02	4.27E-03
4.0E-02	6.88E-03	2.21E-04	7.71E-02	1.24E-02	4.22E-03
5.0E-02	6.91E-03	2.22E-04	7.66E-02	1.23E-02	4.16E-03
6.0E-02	6.93E-03	2.22E-04	7.62E-02	1.22E-02	4.10E-03
7.0E-02	6.95E-03	2.23E-04	7.57E-02	1.21E-02	4.04E-03
8.0E-02	6.97E-03	2.24E-04	7.53E-02	1.20E-02	3.99E-03
9.0E-02	6.99E-03	2.25E-04	7.48E-02	1.19E-02	3.93E-03
1.0E-01	7.01E-03	2.25E-04	7.44E-02	1.18E-02	3.88E-03
2.0E-01	7.22E-03	2.33E-04	6.99E-02	1.07E-02	3.37E-03
3.0E-01	7.42E-03	2.41E-04	6.56E-02	9.70E-03	2.91E-03
4.0E-01	7.62E-03	2.49E-04	6.14E-02	8.79E-03	2.51E-03
5.0E-01	7.81E-03	2.57E-04	5.74E-02	7.96E-03	2.16E-03
6.0E-01	8.00E-03	2.65E-04	5.35E-02	7.19E-03	1.86E-03
7.0E-01	8.18E-03	2.74E-04	4.99E-02	6.49E-03	1.59E-03
8.0E-01	8.35E-03	2.83E-04	4.64E-02	5.85E-03	1.36E-03
9.0E-01	8.52E-03	2.92E-04	4.31E-02	5.26E-03	1.16E-03
1.0E+00	8.66E-03	3.01E-04	4.01E-02	4.74E-03	9.90E-04

Kaganoi Point PZ / MDEA # 2

Data Conditions

T (K)	Bulk Gas P _{CO2} (Pa)	k _g *10 ⁵ (moles/(atm cm ² s))	k _l *10 ⁵ (m/s)	Loading (mol CO ₂ / mol amine)	Flux *10 ⁷ (mol / cm ² s)	
					Measured	Predicted
313	97000	0.94	3.44	0.244	1.93	1.24

Calculated Physical Properties

P _{CO2} (Pa)	μ (cP)	H _{CO2} atm L/mol	ρ (g/cc)	Diffusion Coefficient (m/s) *10 ⁹			
				CO2	MDEA	PZ	IONS
5724	5.48	52.6	1.04	0.7	0.43	0.52	0.52

Thermodynamic Results

Species	Equilibrium Molefraction (Liquid)	Activity Coefficient
CO ₂	1.76E-05	1.40E+00
H ₂ O	8.39E-01	1.02E+00
PZ	8.46E-04	2.53E-01
MDEA	9.96E-02	3.28E-01
PZH+	4.79E-03	2.96E-01
MDEAH+	2.54E-02	3.77E-01
H ₃ O+	9.08E-11	3.02E-01
PZCOO-	3.71E-03	2.95E-01
HCO ₃ -	1.73E-02	3.44E-01
CO ₃ =	3.73E-05	5.40E+00
OH-	1.74E-07	1.45E+00
H+PZCOO-	4.93E-03	1.02E+00
PZ(COO-) ₂	4.53E-03	5.45E-02

Rate Results

r - Dimensionless

Distance from

Interface

	CO ₂	PZ	MDEA	MDEAH ⁺	PZH ⁺	HCO ₃ ⁻
0.0E+00	1.57E-02	2.75E-03	2.5043167	1.314296	3.21E-02	5.91E-01
1.0E-04	1.57E-02	2.75E-03	2.5043171	1.3142957	3.21E-02	5.91E-01
2.0E-04	1.56E-02	2.75E-03	2.5043183	1.3142947	3.21E-02	5.91E-01
3.0E-04	1.56E-02	2.75E-03	2.5043203	1.314293	3.21E-02	5.91E-01
4.0E-04	1.56E-02	2.75E-03	2.504323	1.3142907	3.21E-02	5.91E-01
5.0E-04	1.55E-02	2.75E-03	2.5043266	1.3142878	3.21E-02	5.91E-01
6.0E-04	1.55E-02	2.75E-03	2.5043309	1.3142842	3.21E-02	5.91E-01
7.0E-04	1.55E-02	2.75E-03	2.5043359	1.31428	3.21E-02	5.91E-01
8.0E-04	1.54E-02	2.75E-03	2.5043417	1.3142752	3.21E-02	5.91E-01
9.0E-04	1.54E-02	2.75E-03	2.5043483	1.3142697	3.21E-02	5.91E-01
1.0E-03	1.54E-02	2.75E-03	2.5043556	1.3142636	3.21E-02	5.91E-01
2.0E-03	1.50E-02	2.75E-03	2.5044673	1.3141705	3.21E-02	5.91E-01
3.0E-03	1.47E-02	2.76E-03	2.504645	1.3140224	3.21E-02	5.91E-01
4.0E-03	1.45E-02	2.76E-03	2.5048826	1.3138244	3.21E-02	5.91E-01
5.0E-03	1.42E-02	2.76E-03	2.5051745	1.3135812	3.21E-02	5.91E-01
6.0E-03	1.40E-02	2.76E-03	2.5055156	1.3132969	3.22E-02	5.91E-01
7.0E-03	1.38E-02	2.76E-03	2.5059015	1.3129754	3.22E-02	5.91E-01
8.0E-03	1.36E-02	2.77E-03	2.5063279	1.31262	3.22E-02	5.91E-01
9.0E-03	1.34E-02	2.77E-03	2.5067912	1.3122339	3.22E-02	5.91E-01
1.0E-02	1.32E-02	2.77E-03	2.507288	1.3118198	3.22E-02	5.91E-01
2.0E-02	1.20E-02	2.82E-03	2.5134331	1.3066981	3.26E-02	5.91E-01
3.0E-02	1.13E-02	2.88E-03	2.5207434	1.3006037	3.31E-02	5.91E-01
4.0E-02	1.07E-02	2.96E-03	2.5284853	1.2941468	3.37E-02	5.91E-01
5.0E-02	1.03E-02	3.05E-03	2.5363741	1.287564	3.43E-02	5.90E-01
6.0E-02	9.93E-03	3.14E-03	2.5442992	1.2809466	3.51E-02	5.90E-01
7.0E-02	9.58E-03	3.24E-03	2.5522177	1.2743295	3.59E-02	5.90E-01
8.0E-02	9.26E-03	3.34E-03	2.5601123	1.2677264	3.68E-02	5.90E-01
9.0E-02	8.95E-03	3.46E-03	2.567976	1.2611424	3.77E-02	5.90E-01
1.0E-01	8.65E-03	3.57E-03	2.5758051	1.2545798	3.87E-02	5.89E-01
2.0E-01	6.33E-03	4.97E-03	2.6518373	1.1902726	4.95E-02	5.86E-01
3.0E-01	4.78E-03	6.70E-03	2.7227588	1.1289125	6.17E-02	5.82E-01
4.0E-01	3.69E-03	8.72E-03	2.78784	1.070988	7.44E-02	5.77E-01
5.0E-01	2.91E-03	1.10E-02	2.8471512	1.0166099	8.72E-02	5.72E-01
6.0E-01	2.34E-03	1.35E-02	2.9012952	9.66E-01	1.00E-01	5.66E-01
7.0E-01	1.90E-03	1.63E-02	2.9511303	9.17E-01	1.13E-01	5.59E-01
8.0E-01	1.56E-03	1.93E-02	2.9975796	8.72E-01	1.25E-01	5.53E-01
9.0E-01	1.29E-03	2.26E-02	3.0415188	8.28E-01	1.37E-01	5.45E-01
1.0E+00	1.08E-03	2.62E-02	3.0836528	7.86E-01	1.48E-01	5.37E-01

r-Dimensionless

Distance from

Interface	CO ₃ ⁼	OH ⁻	PZCOO ⁻	H ⁺ PZCOO ⁻	PZ(COO ⁻) ₂
0.0E+00	6.18E-04	2.61E-06	5.25E-02	1.44E-01	3.51E-01
1.0E-04	6.18E-04	2.61E-06	5.25E-02	1.44E-01	3.51E-01
2.0E-04	6.18E-04	2.61E-06	5.25E-02	1.44E-01	3.51E-01
3.0E-04	6.18E-04	2.61E-06	5.25E-02	1.44E-01	3.51E-01
4.0E-04	6.18E-04	2.61E-06	5.25E-02	1.44E-01	3.51E-01
5.0E-04	6.18E-04	2.61E-06	5.25E-02	1.44E-01	3.51E-01
6.0E-04	6.18E-04	2.61E-06	5.25E-02	1.44E-01	3.51E-01
7.0E-04	6.18E-04	2.61E-06	5.25E-02	1.44E-01	3.51E-01
8.0E-04	6.18E-04	2.61E-06	5.25E-02	1.44E-01	3.51E-01
9.0E-04	6.18E-04	2.61E-06	5.25E-02	1.44E-01	3.51E-01
1.0E-03	6.18E-04	2.61E-06	5.25E-02	1.44E-01	3.51E-01
2.0E-03	6.18E-04	2.61E-06	5.26E-02	1.44E-01	3.51E-01
3.0E-03	6.18E-04	2.61E-06	5.26E-02	1.44E-01	3.51E-01
4.0E-03	6.18E-04	2.61E-06	5.26E-02	1.44E-01	3.51E-01
5.0E-03	6.18E-04	2.61E-06	5.27E-02	1.44E-01	3.51E-01
6.0E-03	6.19E-04	2.61E-06	5.27E-02	1.44E-01	3.50E-01
7.0E-03	6.19E-04	2.62E-06	5.28E-02	1.44E-01	3.50E-01
8.0E-03	6.19E-04	2.62E-06	5.28E-02	1.44E-01	3.50E-01
9.0E-03	6.19E-04	2.62E-06	5.29E-02	1.44E-01	3.50E-01
1.0E-02	6.20E-04	2.62E-06	5.30E-02	1.44E-01	3.50E-01
2.0E-02	6.24E-04	2.64E-06	5.39E-02	1.46E-01	3.47E-01
3.0E-02	6.28E-04	2.66E-06	5.49E-02	1.48E-01	3.43E-01
4.0E-02	6.33E-04	2.68E-06	5.60E-02	1.49E-01	3.40E-01
5.0E-02	6.38E-04	2.70E-06	5.71E-02	1.51E-01	3.37E-01
6.0E-02	6.43E-04	2.72E-06	5.81E-02	1.52E-01	3.33E-01
7.0E-02	6.49E-04	2.74E-06	5.91E-02	1.54E-01	3.30E-01
8.0E-02	6.54E-04	2.77E-06	6.01E-02	1.55E-01	3.27E-01
9.0E-02	6.59E-04	2.79E-06	6.11E-02	1.56E-01	3.23E-01
1.0E-01	6.64E-04	2.81E-06	6.21E-02	1.57E-01	3.20E-01
2.0E-01	7.17E-04	3.05E-06	7.10E-02	1.66E-01	2.90E-01
3.0E-01	7.71E-04	3.31E-06	7.90E-02	1.71E-01	2.64E-01
4.0E-01	8.25E-04	3.57E-06	8.62E-02	1.73E-01	2.40E-01
5.0E-01	8.79E-04	3.84E-06	9.26E-02	1.72E-01	2.19E-01
6.0E-01	9.33E-04	4.12E-06	9.83E-02	1.70E-01	2.00E-01
7.0E-01	9.88E-04	4.41E-06	1.03E-01	1.67E-01	1.83E-01
8.0E-01	1.04E-03	4.71E-06	1.08E-01	1.63E-01	1.67E-01
9.0E-01	1.10E-03	5.03E-06	1.11E-01	1.58E-01	1.53E-01
1.0E+00	1.16E-03	5.38E-06	1.15E-01	1.52E-01	1.40E-01

Appendix G

Rate Constants for PZ Derivatives

***The work presented in this section is based on work performed during the summer of 1999 at the Specialty Alkanolamines group of the Dow Chemical Company at Freeport, Texas. It is reproduced with permission of the Dow Chemical Company. The aid of Dr. Steve Bedell, Clare Worley and Jenny Seagraves in construction, operation and data analysis is greatly appreciated.**

We study the kinetics of several derivatives of PZ using a stirred cell reactor. Second order rate constants are extracted. All measurements are made at 30oC and at low amine concentration around 0.1M.

G.1 Description of Equipment

A schematic of the apparatus is shown in figure G.1. The general principle of operation is to send a known concentration of CO₂ and a known total flow rate of gas to a stirred cell reactor where it is contacted with the amine solution being studied. The exit gas from the reactor is analyzed for CO₂ concentration, thereby determining the amount of CO₂ removed.

The inlet CO₂ is delivered from a gas cylinder containing 1% CO₂ in N₂ mixture. Oxygen free bottled N₂ was used for all experiments. All cylinders were provided by Trigas Inc. of Freeport, Texas. Flow of all gases was controlled using 2 Brooks mass flow controllers. The CO₂ mixture flow rate was controlled using a 0-100 sccm mass flow controller while the N₂ flow rate was controlled with a 0-1000 sccm mass flow controller.

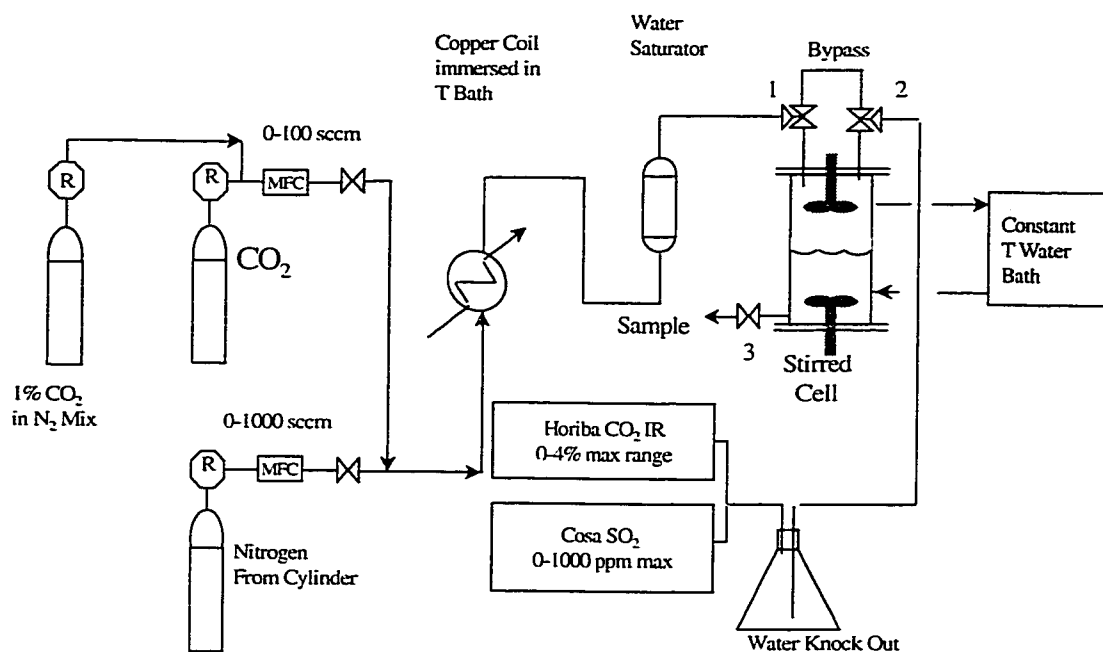


Figure G.1 Overall Flowsheet of Stirred Cell Reactor

The gas streams were combined and sent to a preheater which was composed of a copper coil submersed in a constant water bath (Neslab model RTE-100). The heated gas was then sent to a sample bomb that was half filled with water and also submersed in the constant temperature water bath. By contacting the heated gas with water, the gas was saturated with water so that it did not strip water from the amine solution when introduced into the reactor.

Details of the reactor are shown in figure G.2. The reactor and both head assemblies were constructed by SG&P machine and glass shop in Freeport, Texas. The reactor is composed of a jacketed glass wall with two polypropylene heads. The inside shell has a 10 cm inside diameter and the jacket has a 13.5 cm outside

diameter. Four baffles extend from the bottom of the glass to the midpoint and are meant to aid the agitation of the liquid phase. The top head assembly is 3.2 cm thick and has the same outside diameter as the glass assembly. There is a 24/40 glass neck that has been inserted into the center of the top head by drilling a hole through the polyethylene and fixing the neck in the hole with silicone. There are four ¼ inch NPT holes drilled into the head such that fittings can be attached to the top and bottom of the head. Two holes are equipped with the gas inlet and outlets respectively. A pressure gauge is and a pressure relief valve is attached to the third hole while a thermocouple is inserted into the final hole. An O-ring groove houses an O-ring which squeezes between another O-ring groove on the glass, sealing the reactor when the head is clamped to the glass.

A ground glass fitting is seated in the 24/40 glass neck of the top head assembly. This fitting allows for a 10 mm ground glass shaft to turn inside the fitting while sealing the gas space. Two glass impellers with 4 blades each are attached to the bottom of the glass shaft with reverse pitch (ie pushing the gas downward). The impeller are 70 mm in diameter and 100 mm in width. The top of the glass shaft is clamped to a 3" piece of rubber hose whose other end is consequently clamped to a metal bit. The bit is fixed to a Lightnin Labmaster SI Mixer with variable rotational speed.

The bottom head assembly consists of two disks, one which clamps the glass to the head similar to the top head. The second clamps the entire reactor assembly to the table. The shaft is attached to the head assembly using the bearing box from a Waring Blender. The shaft is threaded on the inside of the reactor to allow a teflon impeller to be attached to the shaft as well as a skimmer which ensures a smooth liquid / vapor interface even at moderate impeller speeds (200 rpm)

A Lightnin mixer similar to the one used on the gas side is used for liquid agitation. There are two holes drilled in the bottom head assembly: one for taking a liquid sample and the other houses a thermocouple.

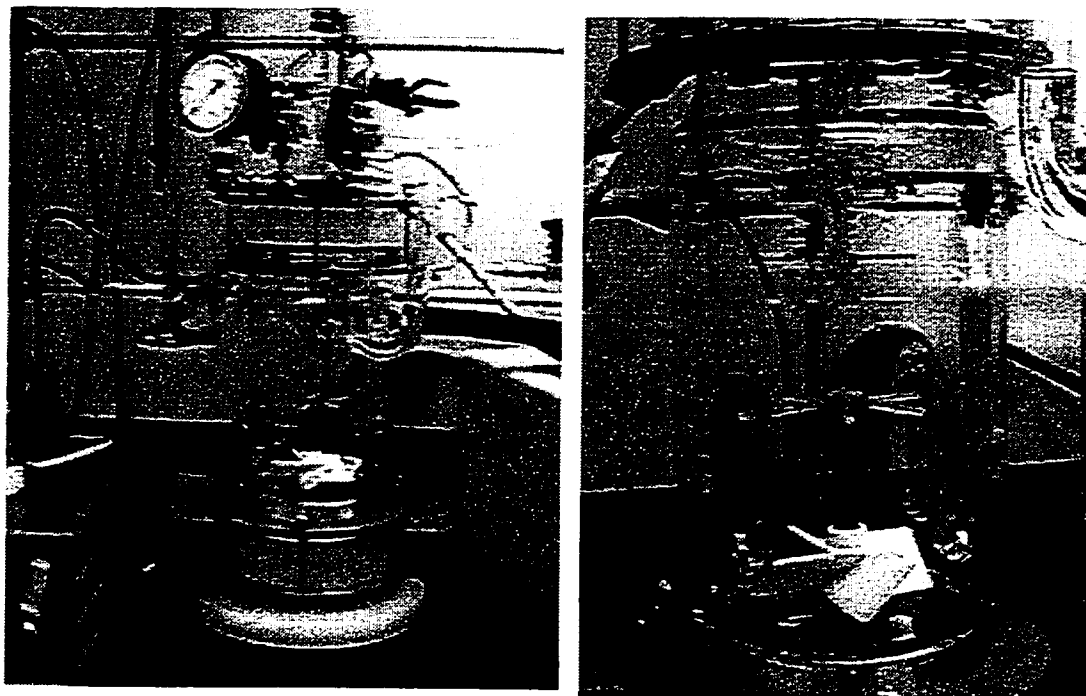
The reactor effluent gases are then sent on to an erlenmeyer flask which sits in a bucket of dry ice. Here the gas is cooled and water is knocked out before it is sent to an infrared analyzer which measures CO₂ concentrations in 4 different ranges: 0-2000 ppm, 0-4000 ppm, 0-2 %, 0-4%. The analyzer is a Horiba series 510 that measures IR absorption around 2400 cm⁻¹. An analog, 1 Volt signal is sent to a chart recorder where data is logged as a function of time.

G.2 Procedures

While flux comparison experiments are effective in comparing one amine to another, the existing apparatus may also be run to extract the rate constant of the amine. In these experiments, the full range of the analyzer is calibrated and several data points are taken at different partial pressures. The procedures are similar to those for flux comparison experiments and are listed below.

1. The reactor is cleaned and put together with the amine to be studied charged into the reactor. amine concentrations studied by this method were much lower than flux comparison experiments (around 0.1M).

Figure G.2 – Details of the Reactor



2. 3-way valves 1 and 2 on figure G.1 are turned such that the reactor is being bypassed. The nitrogen flow controller is turned on (usually to a high value around 98-99%).
3. The chart recorder is turned on and the analyzer is set for the desired range (usually these experiments were run with the 2000 ppm range). At this point, sometimes the reactor was tested to see if it was holding pressure. This was done by closing the output valve of the reactor and flowing gas to the reactor until it

had a positive pressure. Flow was then shut down and the pressure was observed over time. No significant pressure drop was usually seen over a period of 10 minutes or so.

4. When the analyzer lines out to zero, the CO₂ valve was turned on to various levels (100,80,60,40,20,10%). At each level, steady state was waited for by watching the chart recorder. When steady state was achieved, an analyzer reading was taken. By knowing the mass flow controller output, a linear correlation was obtained between concentration at the analyzer and the analyzer output.
5. The N₂ valve is opened approximately to 85% of full scale and the CO₂ valve is adjusted to several different levels (100,70,50). At each level, steady state is achieved and the following readings are taken: Gas temperature, liquid temperature, pressure, liquid and gas agitator RPM, CO₂ controller setting, N₂ controller setting.
6. At this time, a sample may be withdrawn using valve 3 and this sample may be analyzed for pH and / or solution loading. For most experiments, the pH was too low to significantly affect rates and the solution loading was estimated by material balance of the gas phase. The solution loading was essentially constant at zero throughout the course of a typical experiment.

The flux was determined for each of the controller settings and the data were analyzed using the pseudo first order assumption for mass transfer accompanied with chemical reaction in an agitated vessel. Through this treatment, the second order rate constant of the amine was extracted. This analysis will be provided in section 4.

G.2 Reactor Characterization

Gas Phase Resistance

An estimate was made of the gas phase mass transfer coefficients for the reactor by decreasing the liquid phase resistance as far as possible. This was done by studying absorption of carbon dioxide into a very fast amine (piperazine) at very high concentrations (2M). The measured flux of CO₂ can be expressed as:

$$N_{CO_2} = K_G (P_{CO_2}^{Bulk, Gas} - P_{CO_2}^*) \quad (G.1)$$

Here, the driving force is the difference between the bulk gas phase partial pressure of CO₂ and the equilibrium partial pressure of CO₂. Since these experiments were run with fresh solution at very low loading, the equilibrium partial pressure approached zero. The overall resistance to mass transfer (1/K_G) could then be easily expressed as:

$$\frac{1}{K_G} = \frac{N_{CO_2}}{P_{CO_2}^{Bulk, Gas}} \quad (G.2)$$

The total liquid phase resistance to mass transfer was obtained since we know the kinetic rate constant of piperazine. From equation 21, the gas phase resistance was estimated as:

$$\frac{1}{kg} = \frac{1}{K_G} - \frac{H}{EK_l} \quad (G.3)$$

Although an estimate of the gas phase mass transfer coefficients were made in this work, most of the data used to make this estimation were 50% gas film controlled

or less. A better estimation could be obtained by absorbing SO₂ into NaOH solutions which would be completely gas film controlled. It was not pursued further since this did not interfere with the ability of the apparatus to distinguish one amine from another. The measured gas phase mass transfer coefficients are listed in table G.1.

Table G.1 Gas Film Mass Transfer Coefficients at 30°C

Gas Phase RPM	kg (mol / s cm ² atm) *10 ⁵
50	1.36
100	1.01
200	1.53
300	1.88
400	2.14
500	2.40
700	2.81
1000	3.36
1300	3.75

Liquid Phase Resistance

The desorption of carbon dioxide from water is completely liquid film controlled and was studied to determine the liquid phase mass transfer resistance. In these experiments, water was saturated with carbon dioxide by sparging for approximately one hour. The liquid agitator was set at one speed and then pure nitrogen was flowed through the reactor and the outlet CO₂ concentration was measured as a function of time.

Performing a material balance on the CO₂ in the reactor as a function of time, we have: Rate of change of total CO₂ in reactor = Rate of removal of CO₂ by mass transfer. Numerically,

$$V_L \frac{d[CO_2]_o^L}{dt} = \frac{k_L a}{H_{CO_2}} (P_{CO_2}^{Interface} - P_{CO_2}^*) \quad (G.4)$$

Here, V_L is the liquid volume of the reactor and [CO₂]_o^L is the bulk liquid concentration of carbon dioxide. Equation 30 can be simplified by realizing that the partial pressure of CO₂ at the interface approaches the bulk gas partial pressure since there is negligible gas phase resistance. We can also use the ideal gas law to rewrite the partial pressure of carbon dioxide in the gas phase in terms of molar concentration. Equation 30 then becomes,

$$V_L \frac{d[CO_2]_o^L}{dt} = \frac{k_L a}{H_{CO_2}} (RT[CO_2]_o^g - H_{CO_2}[CO_2]_o^L) \quad (G.5)$$

In equation 31 the only term that we don't directly measure is the bulk liquid concentration of CO₂ as a function of time and, therefore we perform a material balance on the gas phase in order to express the bulk liquid concentration of CO₂ in terms of measurable properties.

$$k_L^o a ([CO_2]_i^L - [CO_2]_o^L) = G ([CO_2]^{g,in} - [CO_2]^{g,out}) \quad (G.6)$$

G is the vapor volumetric flowrate and the subscript g,in and g,out refer to the concentrations of CO₂ into and out of the reactor gas phase. Pure nitrogen was flowed to the reactor and, therefore, the inlet concentration is zero. Equation 32 is

then solved for the bulk liquid CO₂ concentration and inserted into equation 31
The result is

$$\frac{d[CO_2]^{g.out}}{dt} = - \frac{G}{V_L \left\{ \frac{G}{k_L a} + \frac{RT}{H_{CO_2}} \right\}} [CO_2]^{g.out} \quad (G.7)$$

This equation can be integrated easily by separation of variables from t=0 (at some arbitrary time) to a given time t. The result is an expression that results in a straight line when the outlet gas concentration is plotted against time.

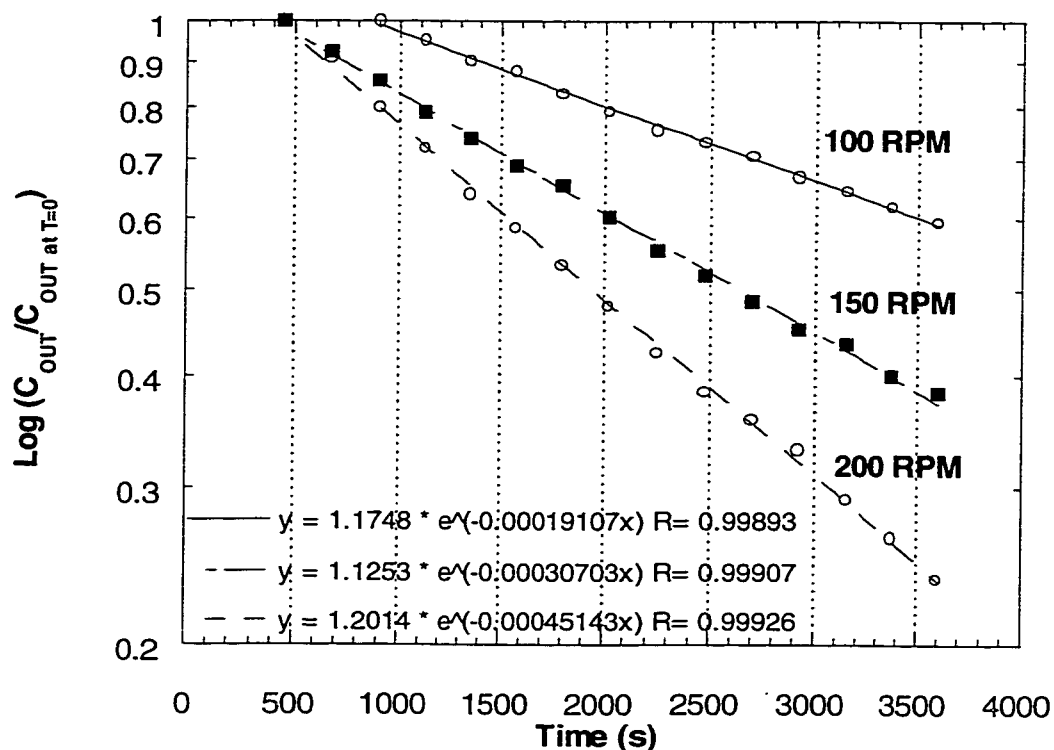
$$\ln \left\{ \frac{[CO_2]^{g.out}(t)}{[CO_2]^{g.out}(t=0)} \right\} = - \frac{G}{V_L \left\{ \frac{G}{k_L a} + \frac{RT}{H_{CO_2}} \right\}} t \quad (G.8)$$

From the slope of the line, the liquid film mass transfer coefficient can be obtained. Figure G.3 summarizes the experimental results of these calculations. The liquid film mass transfer coefficients are also reported in table G.2.

Table G.2 : Liquid Film Mass Transfer Coefficients at 30°C

Liquid RPM	kl (cm/s) *10 ³
100	2.27
150	3.31
200	4.51

Figure G.3: Determination of Liquid Phase Mass Transfer Coefficients at 30°C



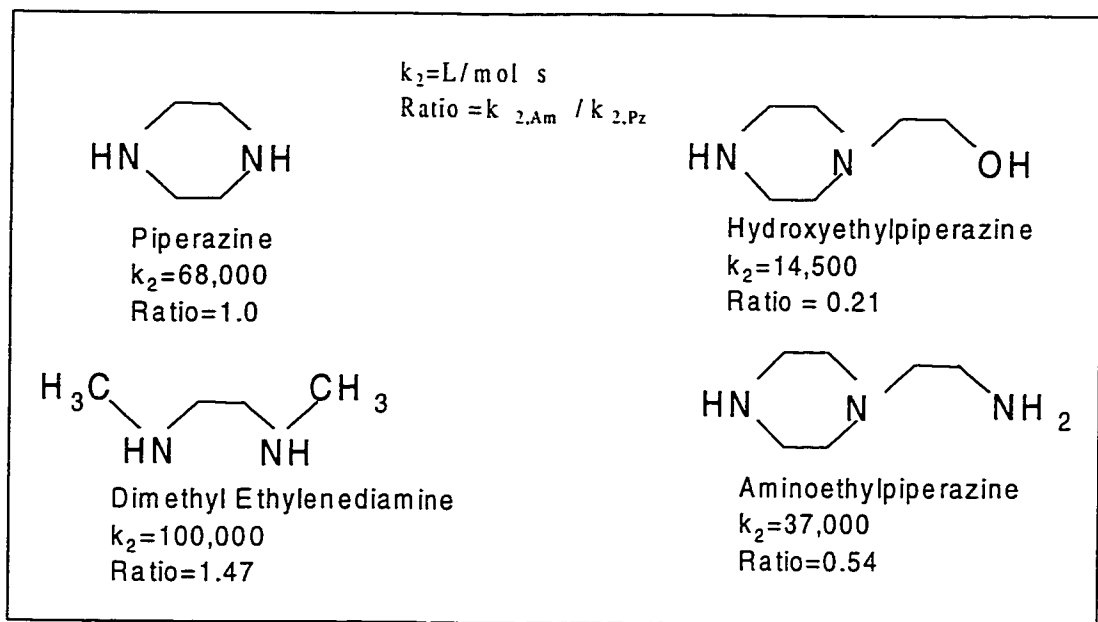
Piperazine Related Promoters

A study was conducted to measure the rate of absorption into amines that closely resemble piperazine. This was done in order to further understand why piperazine activated MDEA is such an effective solvent. These solvents have found wide spread use in ammonia and hydrogen plants.

A series of molecules similar to piperazine were studied in order to understand the importance of each of these issues. Figure G.4 shows the structures

of amines studied. The rate constants of each of these amines was obtained at 30°C.

Figure G.4: Piperazine Related Molecules and Their Relative Kinetics



Glossary

Chemical Species

Molecular

PZ	Piperazine
H ₂ O	Water
CO ₂	Carbon Dioxide
MDEA	Methyldiethanolamine
AMP	2-Amino-2-methyl Propanol
K ₂ CO ₃	Potassium Carbonate
MEA	Monoethanolamine

Cations

H ₃ O ⁺	Hydronium Ion
MDEAH ⁺	Protonated Methyldiethanolamine
PZH ⁺	Protonated Piperazine
AMPH ⁺	Protonated 2-Amino-2-methyl Propanol
K ₂ ²⁺	Potassium Ion
MEAH ⁺	Protonated Monoethanolamine

Anions

PZCOO ⁻	Piperazine mono-carbamate
H+PZCOO ⁻	Protonated piperazine carbamate
PZ(COO ⁻) ₂	Piperazine di-carbamate
MEACOO ⁻	Monoethanolamine carbamate
CO ₃ ⁼	Carbonate
HCO ₃ ⁻	Bicarbonate
OH ⁻	Hydroxide

Symbols

a	Dry specific contact area (m^2/m^3)
a	Wetted specific contact area (m^2/m^3)
a_i	Activity of species i
D_i	Diffusion coefficient of species i (m^2/s)
E	Enhancement Factor
E^{PFO}	Pseudo first order enhancement factor
$E^{\text{PZ.INST}}$	Enhancement factor: small driving force, all PZ reactions are instantaneous
$E^{\text{GLBL.INST}}$	Enhancement factor: small driving force, all reactions are instantaneous
$E^{1.05 \cdot P^*}$	Enhancement factor calculated at interfacial partial pressure 1.05* the equilibrium value.
$[i]$	Concentration of species i (mol / L)
$[i]^i$	Concentration of species i (mol / L) at gas/liquid interface
$[i]^B$	Concentration of species i (mol / L) in bulk solution
$[i]^*$	Concentration of species i (mol / L) at equilibrium
f	Fugacity
G_M	Gas rate per area ($\text{Kg} / \text{m}^2 \text{ s}$)
G	Gibbs free energy
H_i	Henry's constant for species i ($\text{L atm} / \text{mol}$)
ΔH_R	Heat of reaction (kJ/kmol)
H_{OG}	Height of transfer unit (m)
k_2	Second order rate constant (L/mol s)
k_1	First order rate constant (L/mol s)
k_1^0	Liquid film mass transfer coefficient (m/s)
k_g	Gas film mass transfer coefficient ($\text{kmol/m}^2 \text{ atm s}$)
K	Equilibrium constant
K_G	Overall gas phase mass transfer coefficient ($\text{kmol/m}^2 \text{ atm s}$)
L	Liquid rate per unit area ($\text{kg/m}^2 \text{ s}$)

M	Hatta number ($k_1 D_{CO_2} / (k^0_i)^2$)
N_{CO_2}	Flux of CO ₂ (moles / cm ² s)
P	Pressure (Pa, kPa, atm)
$P^*_{CO_2}$	Equilibrium partial pressure of CO ₂ (Pa)
$P^i_{CO_2}$	Interfacial partial pressure of CO ₂ (Pa)
Q_L	Liquid flow rate (cm ³ /s)
R	Universal gas constant (8.314 J/mol K)
R_{CO_2}	Rate of reaction of CO ₂ (moles/s m ³)
Re	Reynolds number ($\rho V D / \mu$)
r	Dimensionless distance from the interface
s	time constant for surface renewal theory (1/s)
Sh	Sherwood number ($k_g d / D_i$)
T	Temperature (K)
t	time (s)
u_{surf}	Velocity of surface fluid in the wetted wall (cm/s)
V	Volume of packing per transfer unit (m ³ s/kmol)
W	Wetted perimeter of the wetted wall
X	Distance from interface (m)
x_i	liquid mole fraction of i
y_i	gas mole fraction of i
Z_{TOT}	Total packed bed height (m)

Greek Symbols

α	Loading (mols CO ₂ / mol Amine)
δ	liquid mass transfer boundary layer thickness for film theory
δ	Wetted wall film thickness
ε	Eddy diffusivity mass transfer parameter (1/s)
ϕ	Fugacity coefficient
γ	Activity coefficient
η	Mass transfer coefficient parameter
λ	Lagrangian multiplier
μ	solution viscosity (cP)
μ	chemical potential
ν	stoichiometric coefficient
π	pi (3.14159)
ρ	density (g/cc)
σ	surface tension (dyne/cm)
τ	electrolyte NRTL parameters (interaction energy)
τ	surface exposure time in wetted wall.
θ	Mass transfer coefficient parameter.

Bibliography

Al-Ghawas, H.A., Hagewiesche, D.P., Ruiz-Ibanez, G. Sandall, O.C.,
"Physicochemical Properties Important for Carbon Dioxide Absorption in
Aqueous Methyldiethanolamine," *Journal of Chemical and Engineering Data*, 34,
385-391, 1989

Alper, E., "Reaction Mechanism and Kinetics of Aqueous Solutions of 2-Amino-
2-methyl-1-propanol and carbon dioxide," *Ind. Eng. Chem. Res.*, 29, 1725-1728,
1990.

Alper, E., "Kinetics of Reactions of Carbon Dioxide with Diglycolamine and
Morpholine," *Chem. Eng. J.*, 44, 107-111, 1990.

Alvarez-Fuster, C., N. Midoux, A. Laurent, and J.C. Charpentier, "Chemical
Kinetics of the Reaction of Carbon Dioxide with Amines in Pseudo m-nth Order
Conditions in Aqueous and Organic Solutions," *Chem. Eng. Sci.*, 35, 1717-1723,
1980.

Appl, M., Wagner, U., Henrici, H.J., Kuessner, K., Volkamer, F, Ernst Neust, N.
(1982). Removal of CO₂ and/or H₂S and/or COS From Gases Containing These
Constituents. U.S. Patent 4336233.

Astarita, G., "Carbon Dioxide Absorption in Aqueous Monoethanolamine
Solutions," *Chem. Eng. Sci.*, 16, 202, 1961.

Astarita, G., D.W. Savage, and A. Bisio, *Gas Treating with Chemical Solvents*,
John Wiley and Sons, New York, 1983.

Austgen, D.M., A Model for Vapor-Liquid Equilibrium for Acid gas-
Alkanolamine-Water Systems. Ph.D. Dissertation, The University of Texas at
Austin, 1989.

Austgen, D.M., Rochelle, G.T., Chen, C.C., "A Model of Vapor-Liquid Equilibria
for Aqueous Acid Gas-Alkanolamine Systems Using the Electrolyte-NRTL
Equation," *Ind Eng. Chem. Res.*, 28(7), 1060, 1989

Austgen, D.M., Rochelle, G.T., Chen, C.C., "A Model of Vapor-Liquid Equilibria
for Aqueous Acid Gas-Alkanolamine Systems. 2. Representation of H₂S and CO₂

Solubility in Aqueous MDEA and CO₂ Solubility in Aqueous Mixtures of MDEA with MEA or DEA," *Ind.Eng. Chem. Res.*, 30, 543-555, 1991.

Barth, D., Tondre, C., and Delpuech, J.J., "Kinetics and Mechanisms of the Reactions of Carbon Dioxide with Alkanolamines: A Discussion Concerning the Cases of MDEA and DEA," *Chem. Eng. Sci.*, 39(12), 1753, 1984.

Barth, D., C. Tondre, and J. J. Delpuech, "Stopped-Flow Investigations of the Reaction Kinetics of Carbon Dioxide with Some Primary and Secondary Alkanolamines in Aqueous Solutions," *Int. J. Chem. Kinetics*, 18, 445, 1986.

Bird, R.B., Stewart, W.E., Lightfoot, E.N., *Transport Phenomena.*, John Wiley and Sons, Inc., New York, 1960.

Bishnoi, S., Rochelle, G.T., "Physical and Chemical Solubility of Carbon Dioxide in Aqueous Methyldiethanolamine," *Fluid Phase Equilibria*, 168, 241-258, 2000.

Bishnoi, S., Physical and Chemical solubility of carbon dioxide in aqueous methyldiethanolamine. Masters Report, The University of Texas at Austin, 1998.

Bishnoi, S., Bedell, S., Worley, C., Seagraves, J., Work performed for the Dow Chemical Company. See Appendix G of this work.

Bishnoi, S., Rochelle, G.T., "Absorption of carbon dioxide into aqueous piperazine: reaction kinetics, solubility and mass transfer," *Chem. Eng. Sci.*, 55, 5531-5543, 2000.

Bhairi, A., Experimental Equilibrium Between Acid Gases and Ethanolamine Solutions. Ph.D. Dissertation, Oklahoma State University, 1984.

Bosch, H., Versteeg, G.F., van Swaaij, W.P.M., "Gas liquid mass transfer with parallel reversible reactions III. Absorption of CO₂ into solutions of blends of amines," *Chem. Eng. Sci.*, 44, 11, 2745-2750, 1989.

Bosch, H., G.F. Versteeg and W.P.M. van Swaaij, "Kinetics of the Reaction of CO₂ with the Sterically Hindered Amine 2-amino-2-methylpropanol at 298K," *Chem. Engg. Sci.*, 45, 1167-1173, 1990.

Brelvi, S.W., O'Connell, J.P., "Corresponding States Correlations for Liquid Compressibility and Partial Molal Volumes of Gases at Infinite Dilution in Liquids," *AIChE J.*, 18(6), 1239-1242, 1972.

Blanc, C. and G. Demarais, *Entropie*, 102, 53 (1981).

Blauwhoff, P.M.M., G.F. Versteeg, and W.P.M. Van Swaaij, "A Study on the Reaction Between CO₂ and Alkanolamines in Aqueous Solutions," *Chem. Eng. Sci.*, 39, 2, 207, 1984.

Caplow, M., "Kinetics of Carbamate Formation and Breakdown," *J. Am. Chem. Soc.*, 90, 6795, 1968.

Caracotsios, M., Model Parametric Sensitivity Analysis and Nonlinear Parameter Estimation. Theory and Applications. Ph.D. Dissertation, The University of Wisconsin – Madison, 1986.

Carey, T.R., Rate-Based Modeling of Acid Gas Absorption and Stripping Using Aqueous Alkanolamine Solutions, M.S. Thesis, The University of Texas at Austin, 1990.

Chakraborty, A.K., Astarita, G., Bischoff, K.B., "CO₂ Absorption in aqueous solutions of hindered amines," *Chem. Eng. Sci.*, 41(4), 997-1003, 1986.

Chakravarty, T., Phukan, U.K., Weiland, R.H., "Reaction of acid gas with mixtures of amines," *Chem. Eng. Prog.*, 32-36, 1995.

Chakravarty, S., Absorption of carbon dioxide in aqueous blends of diethanolamine and methyldiethanolamine, M.S. Thesis, University of Texas at Austin, 1992.

Chang, H.T.; Posey, M.L.; Rochelle, G.T.; "Thermodynamics of alkanolamine-water solutions from freezing point depression measurements," *Ind. Eng. Chem. Res.*, 32, 2324-2335, 1993.

Chapel, D., Ernst, J., Mariz, C., "Recovery of CO₂ from flue gases: Commercial Trends," Presented at 49th annual CSChE conference, Paper 340 Session 67; Saskatoon, Saskatchewan; October 3-6, 1999.

Chen, C.C., Britt, H.I., Boston, J.F., Evans, L.B. "Extension and Application of the Pitzer Equation for Vapor-Liquid Equilibrium of Aqueous Electrolyte Systems with Molecular Solutes," *AIChE J.*, 25(5), 820, 1979.

Chen, C.C. and Evans, L.B. "A Local Composition Model for the Excess Gibbs Energy of Aqueous Electrolyte Systems," *AIChE J.*, 32(3), 444-454, 1986.

Chen, C.C. Britt, H.I., Boston, J.F., Evans, L.B. "Local Composition Model for Excess Gibbs Energy of Electrolyte Systems, Part I: Single Solvent, Single Completely Dissociated Electrolyte," *AIChE J.*, 28(4), 588-596, 1982.

Cheney, W., Kincaid, D., Numerical mathematics and computing, Brooks / Cole publishing company., Pacific Grove, California, 1985.

Chisholm, P.N., Dry absorption of hydrogen chloride and sulfur dioxide by calcium based sorbents from humidified flue gas. Ph.D. Dissertation, The University of Texas at Austin, 1999.

Clarke, J.K.A., "Kinetics of Absorption of Carbon Dioxide in Monoethanolamine Solutions at Short Contact Times," *I & EC Fundamentals* 3(3), 239-245, 1964.

Coldrey, P.W., and I.J.Harris, "Kinetics of the Liquid Phase Reaction Between Carbon Dioxide and Diethanolamine," *Can. J. Chem. Eng.*, 51, 566-571, 1976.

Correia, R.J., Kestin, J., Khalifa, H.E., "Viscosity and density of aqueous Na_2CO_3 and K_2CO_3 solutions in the temperature range 20-90°C and the pressure range 0-30 Mpa," *J. Chem. Eng. Data*, 25, 201-206, 1980.

Critchfield, J. E. and G. T. Rochelle, "CO₂ Absorption into Aqueous MDEA and MDEA/MEA Solutions," Presented at the AIChE National Meeting, Paper No. 43e, Houston, TX, March, 1987.

Critchfield, J.E., CO₂ Absorption/Desorption in Methyldiethanolamine Solutions Promoted With Monoethanolamine and Diethanolamine: Mass Transfer and Reaction Kinetics. Ph.D. Dissertation, The University of Texas at Austin., 1988.

Crooks, J.E., Donnellan, J.P., "Kinetics and mechanism of the reaction between carbon dioxide and amines in aqueous solutions," *J. Chem. Soc. Perkin. Trans. II*, 331, 1989.

Danckwerts, P.V., "Significance of liquid film coefficients in gas absorption," *Ind. Eng. Chem.*, 43, 1460-1467, 1951.

Danckwerts, P.V., Sharma, M.M., "The Absorption of Carbon Dioxide into Solutions of Alkalis and Amines," *Chemical Engineer*, 10, CE244, 1966.

Danckwerts, P.V. (1970). Gas Liquid Reactions. McGraw Hill, NY

Danckwerts, P.V., "The Reaction of CO₂ with Ethanolamines," *Chem. Eng. Sci.*, 34, 443, 1979

Davis, R.A., Sandall, O.C., "Kinetics of the reaction of carbon dioxide with secondary amines in polyethylene glycol," *Chem. Eng. Sci.*, 48(18), 3187-3193, 1993.

Dang, H. Master's Thesis, The University of Texas at Austin, 2001.

Dohnal, V., Roux, A.H., Hynek, V., "Limiting partial molar excess enthalpies by flow calorimetry: Some organic solvents in water," *Journal of Solution Chemistry*, 23, 889-900, 1994.

Donaldson, T.L., and Y.N. Nguyen, "Carbon Dioxide Reaction Kinetics and Transport in Aqueous Amine Membranes," *Ind. Eng. Chem. Fundam.*, 19, 260 1980.

Eckert, J.S., "Selecting the proper distillation column packing," *Chem. Eng. Progress.*, 66, 3, 1970.

Fleyfel, F., Song, K.Y., Ward, A., Kobayashi, R., Chapman, W., Martin, R. (1993). Acid Gas Treating with Aqueous Alkanolamines. GRI/GPA Annual Report, GPA Grant No. 5091-260-2284.

Glasscock, D.A., Rochelle, G.T., "Numerical simulation of theories for gas absorption with chemical reaction," *AIChE Journal*, 35, 8, 1271-1281, 1989.

Glasscock, D.A. (1990). Modelling and experimental study of carbon dioxide absorption into aqueous alkanolamines. Ph.D. Dissertation, The University of Texas at Austin.

Glasscock, D.A.; Critchfield, J.E.; Rochelle, G.T., "CO₂ absorption/desorption in mixtures of methyldiethanolamine with monoethanolamine and diethanolamine," *Chem. Eng. Sci.*, 46(11), 2829-2845, 1991.

Gmehling, J.; Li, J.; Schiller, M.; "A modified UNIFAC model. 2. Present parameter matrix and results for different thermodynamic properties," *Ind. Eng. Chem. Res.*, 32, 178-193, 1993.

Groothuis, H., *de Ingenieur*, 78, CH9, 1966.

Haimour, N., A. Bidarian, and O.C. Sandall, "Kinetics of the Reaction Between Carbon Dioxide and Methyldiethanolamine," *Chem. Eng. Sci.*, 42(6), 1393, 1987.

Hendrickson, Cram and Hammond. Organic Chemistry. (3rd Edition), McGraw Hill, New York., 1970.

Hefner, W., Meissner, H., Davis, J., "Revamping of CO₂ removal systems by Activated MDEA Process," 1992 AIChE Ammonia Symposium, San Antonio, Texas, September 27-30, 1992.

Hikita, H., S. Asai, H. Ishikawa, and M. Honda, "The Kinetics of Reactions of Carbon Dioxide with Monoethanolamine, Diethanolamine, and Triethanolamine by a Rapid Mixing Method," *Chem. Eng. J.*, 13, 7-12, 1977.

Hikita, H., S. Asai, H. Ishikawa, and M. Honda, "The Kinetics of Reactions of Carbon Dioxide with Monoisopropanolamine, Diglycolamine, and Ethylenediamine by a Rapid Mixing Method," *Chem. Eng. J.*, 14, 27-30, 1977.

Hikita, H., Asai, S., Katsu, Y., Ikuno, S., "Absorption of Carbon Dioxide into Aqueous Monoethanolamine Solutions," *AIChE Journal*, 25,5,793, 1979.

Higbie, R., "The rate of absorption of a pure gas into a still liquid during short period of exposure," *Trans. Am. Inst. Chem. Eng.*, 31,7,1977.

Ho, B. and Eguren, R. (1988). "Solubility of Acidic Gases in Aqueous DEA and MDEA Solutions," Presented at the 1988 AIChE Spring National Meeting. March 6-10., 1988.

Jensen, A., Jorgensen, E., Faurholt, C., "Reactions between carbon dioxide and amino alcohols. I. Monoethanolamine and Diethanolamine," *Acta Chemica Scandinavica*, 8, 1137-1140, 1954.

Jorgensen, E., "Reactions between Carbon Dioxide and Amino Alcohols III. Diethanolamine," *Acta Chemica Scandinavica*, 10, 747, 1956.

Jou, F.Y., Mather, A.E., Otto, F.D., "Solubility of H₂S and CO₂ in Aqueous Methyldiethanolamine Solutions," *Ind. Eng. Chem. Process. Des. Dev.*, 21, 539-544., 1982.

Jou, F.Y. Carroll, J.J., Mather, A.E., Otto, F.D., "The Solubility of Carbon Dioxide and Hydrogen Sulfide in a 35 wt% Aqueous Solution of Methyldiethanolamine," *The Canadian Journal of Chemical Engineering*, 71, 264-268, 1993.

Jou, F.Y., Mather, A.E., Otto, F.D., "The solubility of CO₂ in a 30 mass percent monoethanolamine solution," *Can. J. Chem. Eng.*, 73, 140-147, 1995.

Jou, F.Y., Otto, F.D., Mather, A.E., "Vapor-Liquid Equilibrium of Carbon Dioxide in Aqueous Mixtures of Monoethanolamine and Methyldiethanolamine," *Ind. Eng. Chem. And Eng. Data*, 29, 309, 1984.

Kaganoi, S., Carbon Dioxide Absorption in Methyldiethanolamine with Piperazine or Diethanolamine: Thermodynamics and Rate Measurements. M.S. Thesis, The University of Texas at Austin, 1997.

Kent, R.L., Eisenberg, B., "Better Data for Amine Treating" *Hydrocarbon Processing*, February, 87-90, 1976.

King, C.J., "Turbulent liquid phase mass transfer at a free gas-liquid interface," *Ind. Eng. Chem. Fund.*, 5,1,1-8, 1966.

Laddha, S.S. and P.V. Danckwerts, *Chem. Eng. Sci.*, 37, 475, 1982.

Leder, F., "The Absorption of CO₂ into Chemically Reactive Solutions at High Temperatures," *Chem. Eng. Sci.* 26, 1381-1390, 1971.

Lewis, W.K., Whitman, W.G., "Principles of gas absorption," *Ind. Eng. Chem.*, 16,12, 1924.

Littel, R.J., W.P.M. van Swaaij, and G.F. Versteeg, "The Kinetics of Carbon Dioxide with Tertiary Amines in Aqueous Solution," Presented at the AIChE Spring National Meeting, Orlando, FL, March 1990.

Littel, R.J., "Selective carbonyl sulfide removal in acid gas treating processes," Ph.D. Dissertation, Twente University, 1991.

Littel, R.J., Versteeg, G.F., Van Swaaij, W.P.M., "Kinetics of CO₂ with primary and secondary amines in aqueous solutions –I. Zwitterion deprotonation kinetics for DEA and DIPA in aqueous blends of alkanolamines," *Chem. Eng. Sci.*, 47(8), 2027-2035, 1992.

Littel, R.J., Versteeg, G.F., Van Swaaij, W.P.M., "Kinetics of CO₂ with primary and secondary amines in aqueous solutions –II. Influence of temperature on zwitterion formation and deprotonation rates," *Chem. Eng. Sci.* 47(8), 2037-2045, 1992.

- Liu, J., Pope, G., Sepehrnoori, K., "A high resolution finite difference scheme for non-uniform grids," *Appl. Math. Modelling*, 19, 162-172, 1995.
- Liu, H.-B.; Zhang, C.-F.; Xu, G.-W. "A study on equilibrium solubility for carbon dioxide in methyldiethanolamine-piperazine-water solution," *Ind. Eng. Chem. Res.*, 38, 4032, 1999.
- Mock, B., Evans, L.B., Chen, C.C., "Thermodynamic Representation of Phase Equilibria of Mixed-Solvent Electrolyte Systems," *AIChE J.*, 32(10), 1655-1664, 1986.
- Mshewa, M.M. Carbon Dioxide Desorption / Absorption with Aqueous Mixtures of Methyldiethanolamine and Diethanolamine at 40 to 120°C. Ph.D. Dissertation, The University of Texas at Austin, 1995
- Onda, K., Takeuchi, H., Okumoto, Y., "Mass transfer coefficients between gas and liquid phases in packed columns," *Journal of Chemical Engineering of Japan*, 56,1, 1968.
- Posey, M.L. Thermodynamic model for acid gas loaded aqueous alkanolamine solutions. Ph.D. Dissertation, The University of Texas at Austin, 1996.
- Posey, M.L., Rochelle, G.T. "A Thermodynamic Model of Methyldiethanolamine-CO₂-H₂S-Water," *Industrial and Engineering Chemistry Research*, 36, 3944-3958, 1997.
- Pacheco, M.A., Mass Transfer, Kinetics and Rate-Based Modeling of Reactive Absorption. Ph.D. Dissertation, The University of Texas at Austin., 1998.
- Pacheco, M.A., Kaganoi, S., Rochelle, G.T., "CO₂ Absorption into Aqueous Mixtures of Diglycolamine[®] and Methyldiethanolamine," *Chemical Engineering Science*, 55, 5125-5140, 2000.
- Pagano, J.M., Goldberg, D.E., Fernelius, W.C., "A Thermodynamic Study of Homopiperazine, Piperazine, and N-(2-Aminoethyl)-Piperazine and Their Complexes with Copper(II) Ion," *Journal of Physical Chemistry*, 65, 1062, 1961.
- Pani, F, Gaunand, A., Cadours, R, Bouallou, C., Richon, D., "Kinetics of absorption of CO₂ in concentrated aqueous methyldiethanolamine solutions in the range 296-343K," *J.Chem. Eng. Data*, 42, 353-359, 1997.

Penny, D.E., and T.J.Ritter, "Kinetic Study of the Reaction between Carbon Dioxide and Primary Amines," *J.Chem.Soc.*, Faraday Trans.79, 2103-2109, 1983.

Pigford, R.L. Counter-Diffusion in a Wetted Wall Column. Ph.D. Dissertation, The University of Illinois/Urbana., 1941.

Pinsent, B.R., Pearson, L., Roughton, F.J.W., "The kinetics of combination of carbon dioxide with hydroxide ions," *Trans. Faraday Soc.*, 52,1512, 1956.

Prasher, B.D., Fricke, A.L., "Mass transfer at a free gas liquid interface in turbulent thin films," *Ind. Eng. Chem. Process Des. Dev.*, 13,4,336-340, 1974

Rangwala, R.A., Morrell, B.R., Mather, A.E., Otto, F.D., "Absorption of CO₂ into aqueous tertiary amine/MEA solutions," *Can. J. Chem. Eng.*, 70, 482-490, 1992.

Renon, H. Prausnitz, J.M. "Local Compositions in Thermodynamics Excess Functions for Liquid Mixtures. *AIChE J.*, 14(1), 135, 1968.

Rinker, E.B., Ashour, S.S., Sandall, O.C., "Kinetics and modeling of carbon dioxide absorption into aqueous solutions of N-methyldiethanolamine," *Chem. Eng. Sci.*, 50(5), 755-768, 1995.

Rinker, E.B., Ashour, S.S., Sandall, O.C., "Kinetics and modeling of carbon dioxide absorption into aqueous solutions of diethanolamine," *Ind. Eng. Chem. Res.*, 35, 1107-1114, 1996.

Rinker, E.B. Ashour, S.S. Sandall O.C., Acid Gas Treating with Aqueous Alkanolamines: Part I, II, and III. GRI / GPA Research Report RR-158. GPA Project 911, GRI Contract #5092-260-2345, 1997.

Rochelle, G.T., Bishnoi, S., Chi, S., Dang, H., "Research needs for CO₂ capture from flue gas by aqueous absorption/stripping," Final report, U.S. Dept. of Energy, Federal Energy Technology Center, P.O. No. DE-AF26-99FT01029, 2000.

Rowley, R.L., Diffusion coefficients in aqueous alkanolamines., GRI/GPA Research Report RR-163. GPA Project 911, GRI Contract #5092-260-2356., 1999.

Rowley, R.L.; Wilding, W.V.; Oscarson, J.L., Adams, M.E.; Marshall, T.L., Physical and thermodynamic properties of pure chemicals.

Sada, E., Kumazawa, H., Butt, M., "Gas Absorption with Consecutive Chemical Reaction: Absorption of Carbon Dioxide into Aqueous Amine Solutions," *AIChE Journal*, 54, 421-424, 1976.

Sada, E., H. Kumazawa, and M.A. Butt, "Gas Absorption with Consecutive Chemical Reaction: Absorption of Carbon Dioxide into Aqueous Amine Solutions," *Can. J. Chem. Eng.*, 54, 421, 1976.

Sada, E., Kumazawa, H., Han, Z.Q., "Kinetics of reaction between carbon dioxide and ethylenediamine in nonaqueous solvents," *Chem. Eng. J.*, 31, 109-115, 1985.

Saha, A.K., Bandyopadhyay, S.S., Biswas, A.K., "Kinetics of absorption of CO₂ into aqueous solutions of 2-amino-2-methyl-1-propanol," *Chem. Eng. Sci.* 50(22), 3587-3598, 1995.

Sartori, G., Savage, D.W., "Sterically Hindered Amines for CO₂ Removal from Gases," *Industrial and Engineering Chemistry Fundamentals*, 22, 239, 1983.

Scaufaire, P., Richards, D., and Chen, C.C., "Ionic Activity Coefficients of Mixed-Solvent Electrolyte Systems," *AIChE J.*, submitted (1989).

Schwarzenbach, D., "Structure of piperazine hexahydrate," *J. Chem. Phys.*, 48, 9, 4134-4140, 1968.

Seo, D.J., Hong, W.H., "Effect of piperazine on the kinetics of carbon dioxide with aqueous solutions of 2-amino-2-methyl-1-propanol," *Ind. Eng. Chem. Res.*, 39, 2062, 2000

Sharma, M.M., Thesis, Cambridge University (1964).

Sharma, M.M., "Kinetics on Reactions of Carbonyl Sulphide and Carbon Dioxide with Amines and Catalysis by Bronsted Bases of the Hydrolysis of COS," *Transactions of the Faraday Society*, 61, 681-687, 1965.

Sherwood, T.K., R.L. Pigford, and C.R. Wilke, *Mass Transfer*, McGraw-Hill, New York (1975).

Smith, W.R. Missen, R.W., "Strategies for Solving The Chemical Equilibrium Problem and an Efficient Microcomputer Based Algorithm," *Can. J. Chem. Eng.*, 66, 591, 1988.

Smith, J. M., Van Ness, H.C., Introduction to chemical engineering thermodynamics. McGraw Hill Book Company, New York, 1975.

Snijder, E.D., te Riele, M.J.M., Versteeg, G.F., van Swaaij, W.P.M., "Diffusion coefficients of several aqueous alkanolamine solutions," *J. Chem. Eng. Data*, 38, 475, 1993.

Soave, G., "Equilibrium Constants from a Modified Redlich-Kwong Equation of State," *Chem. Eng. Sci.*, 27, 1197, 1972.

Stephenson, R.M., Malanowski, S., *Handbook of the thermodynamics of organic compounds*, Elsevier Science Publishing Co., New York, 1987.

Toman, J.J., Draft Ph.D. Dissertation, The University of Texas at Austin, 1990.

Toman, J.J., and G.T. Rochelle, "Carbon Dioxide Absorption Rates and Physical Solubility in 50% Aqueous Methyldiethanolamine Partially Neutralized with Sulfuric Acid," Presented at the AIChE Spring National Meeting, Houston, TX, 1989.

Tomcej, R.A., and F.D. Otto, "Absorption of CO₂ and N₂O into Aqueous Solutions of Methyldiethanolamine," *AIChE J.*, 35(5), 861, 1989.

Tontiwachwuthikul, P., Meisen, A., Lim, C.J., "Solubility of CO₂ in 2-Amino-2-methyl-1-propanol solutions," *J. Chem. Eng. Data*, 36, 130-133, 1991.

Tosh, J.S., Field, J.H., Benson, H.E., Haynes, W.P., "Equilibrium study of the system potassium carbonate, potassium bicarbonate, carbon dioxide, water," United States Department of the Interior, Bureau of Mines Report of Investigation 5484, 1959.

Vazquez, G., Alvarez, E., Navaza, J.M., Rendo, R., Romero, E., "Surface tension of binary mixtures of water+monoethanolamine and water + 2-amino-2-methyl-1-propanol and tertiary mixtures of these amines with water from 25°C to 50°C," *J. Chem. Eng. Data*, 42, 57-59, 1997.

Van Krevelen, D.W., and P.J.Hoftijzer, "Kinetics and Simultaneous Absorption and Chemical Reaction," *Chem.Eng.Prog.*, 44, 7, 529-536, 1948.

Versteeg, G.F., Mass Transfer and Chemical Reaction Kinetics in Acid Gas Treating Processes. Ph.D. Dissertation, Twente University, 1987.

Versteeg, G.F., van Swaaij, W.P.M., "Solubility and Diffusivity of Acid Gases (CO₂, N₂O) in Aqueous Alkanolamine Solutions," *Journal of Chemical and Engineering Data*, 33,29, 1988.

Versteeg, G.F., and W.P.M. van Swaaij, "On the Kinetics Between CO₂ and Alkanolamines both in Aqueous and Non-aqueous Solutions. Part I: -Primary and Secondary Amines," *Chem. Eng. Sci.*, 43(3), 573, 1988.

Versteeg, G.F., and W.P.M. van Swaaij, "On the Kinetics Between CO₂ and Alkanolamines both in Aqueous and Non-aqueous Solutions. Part II: -Tertiary Amines," *Chem. Eng. Sci.*, 43(3), 587, 1988.

Wagner, I., Stichlmair, J., Fair, J.R., "Mass transfer in beds of modern, high efficiency random packings," *Ind. Eng. Chem. Res.*, 36, 227-237, 1997.

Wammes, W.; Meissner, H.; Hefner, W., "Activated MDEA Process: a flexible process for acid gas removal from natural gas," Conference Preprint, Presented at 73rd Annual GPA convention, March 7-9, 1994, New Orleans, Louisiana.

Weiland, R.H., "Physical properties of MEA, DEA, MDEA and MDEA based blends loaded with CO₂," GRI/GPA Research Report RR-152. GPA project 911, 1996.

Weiland, R.H., "Reaction kinetics of CO₂ with MEA, DEA and MDEA in MDEA based blends," GPA / GRI research report, GPA project number 911, 1996.

Weiland, R.H., Trass, O., "Absorption of Carbon Dioxide in Ethylenediamine Solutions I. Absorption Kinetics and Equilibrium," *Can. J. Chem. Eng.*, 49, 767, 1971.

Wilson, and Wilding, Data gathered for the DIPPR project., 1994.

Xu, S., Wang, Y.W., Otto, F., Mather, A.E., "Kinetics of the reaction of carbon dioxide with 2-amino-2-methyl-1-propanol solutions," *Chem. Eng. Sci.*, 51(6), 841-850, 1996.

Xu, S., Otto, F.D., Mather, A.E., "Physical properties of aqueous AMP solutions," *J. Chem. Eng. Data*, 36, 71-75, 1991.

Xu, G-W. Zhang, C-F. Qin, S-J. Wang, Y-W., "Kinetics Study on Absorption of Carbon Dioxide into Solutions of Activated Methyldiethanolamine," *Industrial and Engineering Chemistry Research*, 31, 921-927., 1992.

Xu, G-W. Zhang, C-F. Qin, S-J. Zhu, B-C., "Desorption of CO₂ from MDEA and Activated MDEA Solutions," *Industrial and Engineering Chemistry Research*, 34, 874-880., 1995.

Xu, G-W. Zhang, C-F. Qin, S-J. Gao, W-H. Liu, H-B., "Gas-Liquid Equilibrium in a CO₂-MDEA-H₂O System and the Effect of Piperazine on It," *Industrial and Engineering Chemistry Research*, 37, 1473-1477, 1998.

Yih, S.M., Shen, K.P.; "Kinetics of carbon dioxide reaction with sterically hindered 2-amino-2-methyl-1propanol aqueous solutions," *Ind. Eng. Chem. Res.*, 27, 2237-2241, 1988.

Yu, W. C., G. Astarita, and D.W. Savage, "Kinetics of Carbon Dioxide Absorption in Solutions of Methyldiethanolamine," *Chem. Eng. Sci.*, 40(8), 1585, 1985.

Vita

Sanjay Bishnoi was born on October 27, 1973 in Edmonton, Alberta, Canada the son of Dr. Prithwi Raj and Urmila Bishnoi. He graduated from Sir Winston Churchill High School in Calgary, Alberta, Canada in 1991. After matriculating in 1991 at The University of Calgary, he was awarded the degree of Bachelor of Science in Chemical Engineering with Distinction in 1995. He worked for Imperial Oil Resources Ltd. as a reservoir engineer for conventional and heavy oil properties during 1995 and 1996. He entered the graduate school of Chemical Engineering at the University of Texas at Austin in 1996. He was awarded the degree of Master of Science in Chemical Engineering from the University of Texas at Austin in 1998. In the summer of 1999 he worked in the research labs of the Specialty Alkanolamines group at the Dow Chemical Company in Freeport, Texas.

Full time employment has been accepted with The Boston Consulting Group after graduation in Dallas, Texas.

Permanent Address: 712 Varsity Estates Place N.W., Calgary, Alberta, Canada
T3B 4R2

This dissertation was typed by the author.